

TECHNISCHE UNIVERSITÄT MÜNCHEN

Ingenieur fakultät Bau Geo Umwelt

Precast Ultra-Thin Whitetopping (PUTW) in Singapore and its Application for Electrified Roadways

Nen Nguyen Dinh

Vollständiger Abdruck der von der Ingenieur fakultät Bau Geo Umwelt der Technischen Universität München zur Erlangung des akademischen Grades eines

Doktor-Ingenieurs

genehmigten Dissertation.

Vorsitzender: Univ.-Prof. Dr. Rolf Moeckel

Prüfer der Dissertation:

1. Univ.-Prof. Dr.-Ing. Stephan Freudenstein
2. Asst.-Prof. En-Hua Yang, Ph.D.

Die Dissertation wurde am 04.04.2016 bei der Technischen Universität München eingereicht und durch die Ingenieur fakultät Bau Geo Umwelt am 28.09.2016 angenommen.

Table of Contents

Zusammenfassung	v
Abstract	vi
1 Introduction.....	1
1.1 Background.....	1
1.2 Research scopes	2
1.3 Research approach and thesis organization	2
2 Pavement system in Singapore	3
2.1 Introduction.....	3
2.2 Pavement Management System (PMS) in Singapore	3
2.2.1 Traffic loading – Equivalent single axle loads (ESALS).....	4
2.2.2 Environmental loading.....	5
2.3 Pavement structures	6
2.3.1 Flexible Pavements	6
2.3.2 Rigid Pavements	7
2.4 Properties of pavement material	7
2.4.1 Asphalt.....	7
2.4.2 Concrete	9
2.4.3 Unbound materials for base, sub-base and sub-grade layers	10
2.5 Performance of asphalt pavement in Singapore.....	10
2.6 Performance of rigid pavement in Singapore	11
2.7 User delay cost due to rigid pavement rehabilitation.....	12
2.7.1 Traffic simulation using VISSIM software.....	13
2.7.2 The value of travel time and delay cost	15
2.8 Summary.....	16
3 Electrified roadways	18
3.1 Introduction.....	18
3.2 Electrified roadways concept.....	18
3.2.1 Introduction.....	18
3.2.2 Electrified Roadway for EVs.....	18
3.3 Power supply components of OLEV electrified roadways and their pavements.....	27
3.4 Requirements of pavement for electrified roadways	30
3.5 Summary.....	30
4 Precast Ultra-Thin Whitetopping (PUTW) concept.....	32
4.1 Introduction.....	32
4.2 Precast Concrete Pavement (PCP) technology	32

4.2.1	Prestressed precast concrete pavement (PPCP)	32
4.2.2	Jointed precast concrete pavement (JPrCP)	33
4.2.3	Performance of precast concrete pavement	34
4.3	Ultra-thin Whitetopping (UTW)	35
4.4	Precast Ultra-Thin Whitetopping (PUTW) concept.....	36
4.5	Research on the Precast Ultra-Thin Whitetopping (PUTW)	38
5	Engineered Cementitious Composite (ECC) material for Precast Ultra-Thin Whitetopping (PUTW)	39
5.1	Introduction.....	39
5.2	ECC in transportation related applications	40
5.3	ECC for structural layer of PUTW	40
5.4	Verification of ECC material model in ANSYS	43
5.5	ECC for pavement surface.....	44
5.5.1	Introduction.....	44
5.5.2	Skid resistance measurement methods.....	45
5.5.3	Requirement values for skid resistance.....	45
5.5.4	Developing a new version ECC for pavement surface	46
5.5.5	Lab tests on skid resistance for pavement surface made of ECC with corundum	47
5.6	Compatibility of ECC material to wireless power transfer.....	50
5.7	Conclusion	51
6	Interface bonding in Precast Ultra-Thin Whitetopping (PUTW).....	52
6.1	Introduction.....	52
6.2	Calculation of horizontal interface shear stresses in PUTW.....	52
6.2.1	Reference pavement structure.....	52
6.2.2	Shear stresses under vertical load	53
6.2.3	Horizontal shear stresses under horizontal load.....	56
6.2.4	Horizontal shear bond strength requirement for PUTW	58
6.3	Calculation of vertical interface split stress in PUTW due to temperature change	59
6.4	Method to improve interface bonding.....	60
6.4.1	Bond between grout and asphalt	60
6.4.2	Bond between PUTW slab and grout.....	60
6.5	Laboratory tests on interface bond strength.....	61
6.5.1	Introduction.....	61
6.5.2	Testing concept.....	62
6.5.3	Sample preparation	62
6.5.4	Direct shear test	63
6.5.5	Pull-off test	64
6.5.6	Result and discussion.....	64

6.6	Conclusion	66
7	Design of Precast Ultra-Thin Whitetopping (PUTW)	67
7.1	Introduction.....	67
7.2	Calculation of traffic-induced stress in PUTW.....	67
7.2.1	Westergaad’s closed-form formulas	67
7.2.2	Calculation method for multilayer systems	68
7.2.3	Calculation of vertical shear stress in asphalt at PUTW joint.....	70
7.2.4	Finite element models (FEMs).....	70
7.3	Calculation of environment-induced stress in PUTW	72
7.3.1	Introduction.....	72
7.3.2	Warping stress.....	72
7.3.3	Curling stress	73
7.4	Slab dimension design	74
7.4.1	Introduction.....	74
7.4.2	Stresses and deformation of the PUTW slab in construction phase.....	76
7.4.3	The influence of slab dimension on traffic and environmental induced stress	79
7.5	Parameters study	86
7.5.1	Changing of composite thickness and support layers’ equivalent modulus (E_{v2})	86
7.5.2	Changing of interface bonding condition (debonding)	88
7.6	Conclusion	90
8	Life Cycle Cost Analysis (LCCA) of Precast Ultra-Thin Whitetopping (PUTW)	91
8.1	Introduction.....	91
8.2	Life cycle cost analysis (LCCA) of PUTW	91
8.2.1	Life cycle cost analysis	91
8.2.2	Activity timing of alternative pavements.....	91
8.3	User delay cost.....	92
8.4	Initial cost and rehabilitation cost	92
8.5	LCCA Summary	93
8.6	The cost of electrified roadways	94
8.7	Conclusion	95
9	Precast Ultra-Thin Whitetopping (PUTW) Process – Guideline for PUTW Application	96
9.1	Introduction.....	96
9.2	Pavement evaluation	96
9.3	PUTW as a candidate.....	97
9.4	Pavement design	97
9.5	Three dimensional (3D) geometrical design for PUTW (PUTW3D)	97
9.6	Fabrication of PUTW slab	99

9.6.1	Introduction.....	99
9.6.2	Panel formwork and hardware	99
9.6.3	ECC mixtures.....	101
9.6.4	ECC placement	101
9.6.5	Formwork stripping and panel finishing details	101
9.6.6	QA/QC activities.....	101
9.7	Installation of PUTW pavement	102
9.7.1	Introduction.....	102
9.7.2	Installation staging and lane closures	102
9.7.3	Asphalt pavement preparation	102
9.7.4	Panel placement, levelling and grouting.....	103
9.8	Monitoring and maintenance of PUTW.....	105
9.9	Summary.....	106
10	Conclusion	107
	Bibliography	112
	List of figures.....	120
	List of tables	123
	List of Abbreviations	125
	List of Symbols.....	127
A.	Appendix.....	129
A. 1.	Summary of skid resistance measurement and improvement methods	129
A. 2.	Calculation of environment-induced stress in PUTW	137
A. 3.	PUTW3D - User manual.....	141

Zusammenfassung

Eine über einen längeren Zeitraum andauernde Straßensperre zum Zwecke des Straßenunterhalts an Betonfahrbahnen und zur Sanierung an stark befahrenen Straßenabschnitten führt in Singapur zu einem erheblich höheren volkswirtschaftlichen Kosten. Eine elektrifizierte Fahrbahn, die das Laden eines Elektrofahrzeugs (EV) während der Fahrt, durch Verwendung induktiver Energieübertragung, ermöglicht, hat ein großes Potenzial in naher Zukunft flächendeckend eingesetzt zu werden. Darüber hinaus ist sie ein vielversprechender Ansatz, für einen Paradigmenwechsel herkömmlicher Antriebstechnik mit fossilen Brennstoffen, zukünftig hin zu elektrischen Antrieben. Zurzeit ist die Forschung immer noch auf der Suche nach einer geeigneten Straßenbefestigung zur großflächigen Umsetzung elektrifizierter Fahrbahnen. Die Forschung konzentriert sich daher auf die Entwicklung eines hochleistungsfähigen und wirtschaftlichen Fahrbahnsystems, genannt Precast Ultra-Thin Whitetopping (PUTW). Das PUTW ist ein innovatives Fahrbahnsystem, welches die Konstruktionsmerkmale der schnell herzustellenden Fertigteilmontage auf die Bauweise mit ultradünnem Whitetopping überträgt. Erforscht wird die strukturelle und funktionale Leistungsfähigkeit sowie wirtschaftliche Faktoren mit Hilfe einer breiten Palette von theoretischen Simulationen und Labortests. Die geplante Lebensdauer von 25 Jahre einer Betonfahrbahn in Singapur wird auch als Lebensdauer für ein PUTW angesetzt.

Das konstruktive Verhalten eines PUTW hängt von den Materialparametern, dem Schichtenverbund, den Abmessungen und der Fugenkonstruktion ab. Eine Weiterentwicklung des Engineered Cementitious Composite (ECC) wurde mit Zusätzen, die in Singapur einfach zu bekommen sind, entwickelt. Dieses ECC hat eine sehr hohe Biegezugfestigkeit und zeigte im Dauerschwingversuch sehr gute Ergebnisse. Laborversuche zum Schichtenverbund zeigten, dass die geforderte Verbundfestigkeit eingehalten wurde. Ein kalibriertes FE-Modell mit nicht-linearem Materialverhalten wurde zur Dimensionierung des PUTW genutzt. Das angedachte PUTW und PUTW mit Aussparung zur Implementierung der Elektrifizierung der Fahrbahn (Plattengröße von 3600 mm x 2400 mm und hexagonale Platten mit 1800 mm Innendurchmesser) bieten eine lange Lebensdauer. Die Lebensdauer kann so um 25 %, trotz der „nur“ 50 mm Plattenstärke, verlängert werden.

Die Funktionsfähigkeit eines PUTW wird durch die Oberflächenrauheit und Griffigkeit bestimmt. Die Rauheit von PUTW ist durch das vorgeschlagene Herstellungs- und Montageverfahren erreichbar. Die Verwendung von Korund als Zuschlag in einer ECC-Mischung erhöht die Oberflächengriffigkeit signifikant. Die extrapolierten Ergebnisse aus einer 5- bis 10-jährigen äquivalenten Verkehrsbelastung zeigten, dass die Anforderung an die Oberflächenrauheit in Singapur für die gesamte Lebensdauer der Fahrbahn ohne weitere Eingriffe erfüllt ist.

Die Lebenszykluskosten (LCC) des Fahrbahnsystems wurden mit Hilfe eines mikroskopischen Verkehrssimulationstools analysiert. PUTW zeigt anfangs höhere Baukosten, aber weitaus niedrigere volkswirtschaftliche Kosten als Ortbetonfahrbahnen. Die LCC von PUTW können bis zu 2,15-mal niedriger sein, als eine alternative Bauweise im Untersuchungsgebiet. Die LCC variieren jedoch je nach Baustellenstandort und Verkehrsaufkommen.

Leitlinien für PUTW-Anwendung wurden im Rahmen dieser Forschung erörtert, welche die Fahrbahnbewertung, Auswahl des Fahrbahntyps, die Fahrbahnausbildung, die Plattenanordnung, die Plattenherstellung, den Platteneinbau und die Wartung umfassen.

Zusammenfassend konzentrierte sich die Forschungsarbeit auf die Entwicklung des PUTW-systems für Fahrbahnen unter Verwendung lokaler Bedingungen für Singapur. Hierfür dienten z.B. Verkehrsbedingungen, Umweltbedingungen, Materialverfügbarkeit und Fahrbahnstrukturen, als Eingangsgrößen der Fallstudie. Das PUTW ist ein kostengünstiges, schnell konstruiertes und robustes Fahrbahnsystem, welches helfen kann, die aktuellen Probleme einer langen Fahrstreifensperre an hoch belasteten Verkehrsknotenpunkten anzugehen und elektrifizierte Fahrbahnen in das Straßenmanagementsystem einzuführen.

Abstract

Extended road closure for rigid pavement maintenance and rehabilitation at heavy traffic road sections in Singapore leads to a significantly high user delay cost. Also, an electrified roadway, which allows charging of EVs while they are in operation using inductive power transfer, has good potential to be widely adopted in the near future and is an attractive approach to switch mobility from conventional fossil fuel traction to future electric traction. However, research is still ongoing to find an applicable road pavement for the broad implementation of the electrified roadways. Therefore, this research focuses on developing a high performance and economic pavement system called Precast Ultra-Thin Whitetopping (PUTW). PUTW is an innovative pavement system that applies the very fast construction characteristic of the precast concrete pavement for the ultra-thin whitetopping. The research considered pavement structural and functional performance, and economic factors with the help of a wide range of theoretical simulations and laboratory tests. Singapore rigid pavement structural performance of 25 years is the targeted design life for PUTW.

The structural performance of PUTW pavement system depends on material properties, interface bonding in composite layer, slabs dimensions and joint performance. A new version of Engineered Cementitious Composite (ECC) with ingredients that can be easily obtained in Singapore locally was developed. This ECC has a very high flexural strength and performs very well under fatigue tests. The laboratory tests of interface bond strength indicated that the required bond strengths are fulfilled. The design of PUTW was studied using calibrated non-linear finite element models. The proposed PUTW and PUTW with integrated culvert for electrified roadways with slab sizes of 3600 mm x 2400 mm and hexagon slab (1800 mm internal diameter) provide long service life that exceeds the targeted design life by 25% even with just 50 mm thick slab.

The functional performance of PUTW is decided by the surface roughness and skid resistance. The roughness of PUTW is achievable by the proposed manufacture and installation process. The use of corundum aggregate in ECC mixture significantly increases surface skid resistance. The extrapolated results from a 5 to 10 years of equivalent traffic simulation indicated that the Singapore skid resistance requirement is fulfilled for the whole pavement lifetime without any further intervention.

The Life cycle cost (LCC) of the pavement system was analysed with the help of a microscopic traffic simulation tool. PUTW has higher initial construction cost, but far less user delay cost than cast-in-place concrete pavement. The LCC of PUTW can be up to 2.15 times lower than the alternative pavement at the study area. However, the LCC varies according to construction site locations and traffic volume.

Guidelines for PUTW application was discussed in this research, which involves pavement evaluation, pavement type selection, pavement design, slab arrangement design, slab fabrication, slabs installation and maintenance.

In summary, the research focused on developing the PUTW pavement system using Singapore local conditions such as traffic conditions, environmental condition, material availability, and pavement structures as a case study. The PUTW is a cost effective, quickly constructed and durable pavement system that can help to tackle the current issues about long lane closure time at heavy traffic junctions and implement electrified roadways into the road management system.

1 Introduction

1.1 Background

The rigid pavement in Singapore is used at junctions and bus stops instead of asphalt pavement to prevent severe rutting due to heavy stop and go vehicles (see Figure 1-1). However, there are big concerns about extended road closure during rigid pavement maintenance and rehabilitation process at heavy traffic road sections. Longer road closure can adversely affect road users' satisfactory. More importantly, it can lead to a very expensive user delay cost. Additionally, using rigid pavement at junction results in a rather complicated pavement structure at the transition area between concrete and asphalt pavement (see Figure 1-2). The supporting layers of concrete pavement, asphalt pavement and transition area pavement are also different, which interrupts the construction work for supporting layers spot by spot.

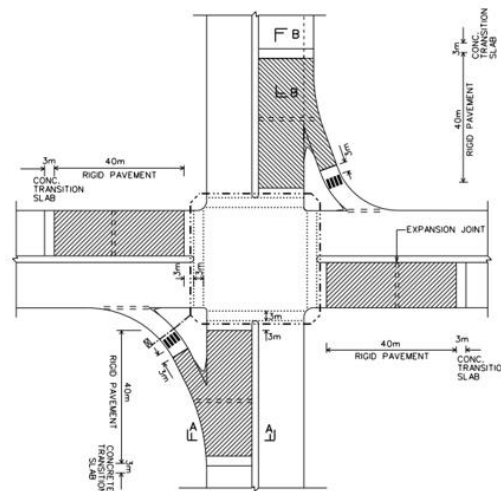


Figure 1-1: Typical section of rigid pavement at junction in Singapore (LTA, 2015)

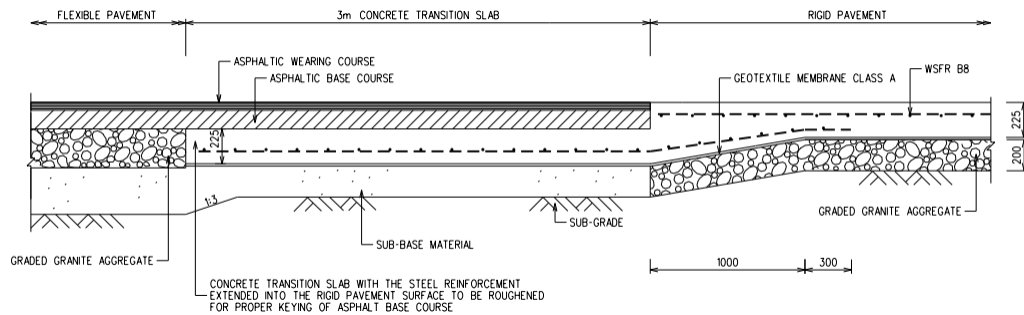


Figure 1-2: Rigid pavement structure at junctions and the connection with flexible pavement (LTA, 2015)

In addition, to reduce the dependence on the scarce petroleum supply in the near future and to decrease greenhouse gases emissions, electric vehicles (EVs) are being introduced worldwide. However, the adoption of EVs remains low mainly because of its battery related problems including a high price, heavy weight and limited range. An electrified roadway (see Figure 1-3), which allows charging of EVs while they are in operation (moving or stationary), is an innovative technology to overcome these battery related issues. There have been huge developments in inductive power transfer (IPT) for electrified roadways since the 1890s (NguyenDinh & Lechner, 2013) (NguyenDinh, et al., 2014). However, it is still unclear about an applicable road pavement which can help to implement broadly electrified roadways into a road management system.

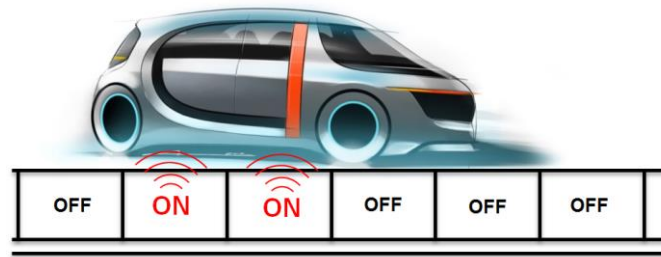


Figure 1-3: Electrified Roadway concept (Wu, et al., 2011)

Interestingly, the potential locations for electrified roadways are exactly the locations of current rigid pavement in Singapore. Unfortunately, the pavement that can overcome the aforementioned issues has not yet existed in Singapore context. Therefore, the overall objective of this research is to develop a high performance, and economical pavement system that can be an alternative for Singapore rigid pavement at heavy traffic junctions and bus stops where extended road closure is an issue, and can be used for electrified roadways. The applicable pavement should have a lifetime at least matching the current rigid pavement.

1.2 Research scopes

This research has two overall scopes:

- Identifying requirements of the new pavement system
- Developing a pavement system that fulfils the requirements. The development of this pavement considers pavement material, pavement design, construction, maintenance, as well as life cycle cost analysis.

1.3 Research approach and thesis organization

After the overall introduction in Chapter 1, the requirements for the new pavement system are determined by reviewing and analysing Singapore pavement systems and electrified roadways concept in Chapter 2 and Chapter 3. The proposed pavement concept called precast ultra-thin whitetopping (PUTW) will be presented in Chapter 4.

Chapter 5 will focus on developing new versions of engineered cementitious composite (ECC) material for PUTW slab's structural and functional layer. The properties of the new versions of ECC will be determined by laboratory tests. The skid resistance performance of the ECC for pavement functional layer will be also evaluated by laboratory tests. The performance of the structural ECC in the PUTW pavement structure will be evaluated in the later chapters.

The interface bonding of the composite pavement PUTW will be studied in Chapter 6. Theories on calculating horizontal interface shear stress will be reviewed and used to calibrate the finite element models (FEMs). The required interface bond strength will be calculated using the calibrated FEMs. The laboratory experiments will be done to study actual interface bond strength in the PUTW pavement.

The dimensional design of PUTW is the focus of Chapter 7. The stress calculation theories that can be applied for PUTW will be reviewed and used to calibrate the FEMs, which will be used later for designing PUTW.

The life cycle cost of PUTW will be analysed in Chapter 8 with the help of a microscopic traffic simulation.

Chapter 9 will focus on the guideline for PUTW application from survey until construction and maintenance.

The overall conclusion will be presented in Chapter 10.

2 Pavement system in Singapore

2.1 Introduction

This chapter focuses on reviewing and analysing pavement system in Singapore to determine requirements for a new pavement as well as provide comprehensive input for developing the new pavement. The chapter will start with the introduction of Pavement Management System in Singapore, then follow by reviewing traffic loading, environmental loading, pavement structure, and pavement materials. The performance of asphalt and concrete pavement will be analysed. Most importantly, the user delay cost due to the rehabilitation of rigid pavement will be estimated for a case study area with the help of microscopic traffic simulation tool.

2.2 Pavement Management System (PMS) in Singapore

Road pavements in Singapore are managed by Land Transportation Authority (LTA), a statutory board under the Ministry of Transportation, Singapore. LTA is responsible for the planning, constructing, operating, and maintaining Singapore's land transport infrastructure and systems.

According to (LTA, 2012), PMS aims to maintain road network at the acceptable level of service with optimum expenditure and to analyse automatically the collected information of road conditions. PMS can define standards for maintenance (intervention level) then evaluate various methods of treatments. Using PMS, maintenance activities can be planned and prioritized based on the available funds. The system is also capable of developing the long-term ten years' budget plans.

Sufficient and detailed road network condition information is collected using Deflectograph, Multifunction road monitor and Sideway-force coefficient routine investigation Machine (SCRIM). Deflectograph (see Figure 2-1) is used to measure pavement structural performance (pavement deflection). The pavement structural survey is done at all expressways, major arterial and collector roads mostly in the night time with the speed of 2.5 km/h. SCRIM (see Figure 2-2) measures wet road skid resistance at all expressways, major arterial roads, collectors and some local access roads with the speed of 50 km/h. Multifunction road monitor (see Figure 2-3) measures longitudinal and transverse profile, gradient, cross fall, macrotexture, rut depth, radius of curvature of almost all roads to determine road riding quality.



Figure 2-1: Deflectograph (LTA, 2012)



Figure 2-2: Sideway-force coefficient routine investigation machine (SCRIM) (LTA, 2012)



Figure 2-3: Multifunction road monitor (LTA, 2012) Traffic loading and environment loading

2.2.1 Traffic loading – Equivalent single axle loads (ESALS)

Singapore is an extremely dense country with a vehicle population of nearly 1 million. The vehicle population in the last ten years is presented in Figure 2-4. The average annual growth rate is close to 3% in the whole decade period. Possibly, due to changes in quota premium price of Certificate of Entitlement (COE) since 2010-2011, the annual vehicle population growth rate is lowered to 0.5% for the last three years. And it is almost 0% since 2013.

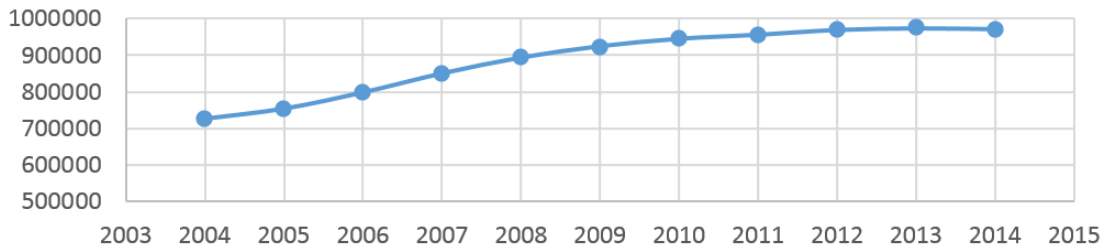


Figure 2-4: Total motor vehicle population (LTA, 2015)

Sufficient traffic information on the road network Singapore is still absent in the PMS. Therefore, within this research, a survey has been done to collect important traffic data for calculating of ESALS at some key corridors in the network. The average daily traffic (ADT) was extracted from the data captured by the traffic cameras, which are managed by LTA's Intelligent Transportation System (ITS) Center for traffic control purpose. ADT data from LTA's cameras was extrapolated to get the yearly traffic volume. However, the proportion of different axle configuration vehicles, which is required for ESAL's calculation, cannot be extracted from the cameras' data. This proportion was collected manually by 30-minute video recording individually at some locations around the network as shown in Figure 2-5. Videos were recorded in the morning peak hours. Vehicular compositions from the videos were used to calculate the proportion of different axle configuration for all the vehicles in all lanes.

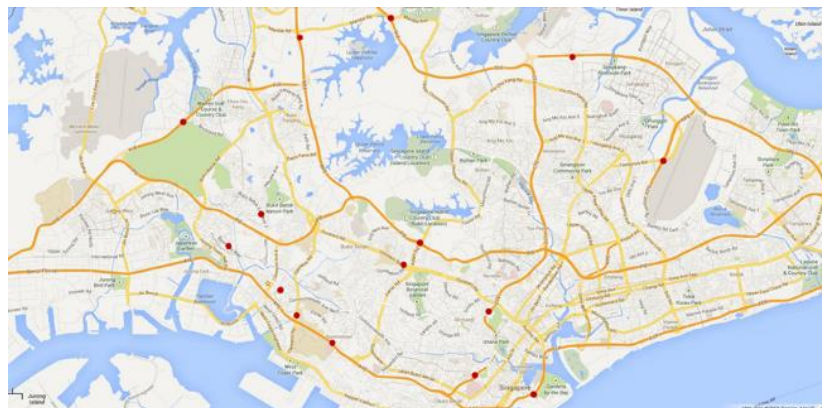


Figure 2-5: Locations for manual video recording (Google Maps, 2013)

The ESALS using in this research is the 80 kN (18kips) ESAL according to (AASHTO, 1993) with structural number (SN) and Terminal serviceability number (p_t) as shown in Table 2-1. It is important to notice that the total number ESALS of 80 kN (18 kips) is about 2.15-2.41 times higher (accordingly to p_t) than the ESALS of 100 kN (10 ton or 22.05 kips) with the same number of traffic count. The ESALS (for the year 2013) in the design lane of the selected roads are summarized in Figure 2-6. The ESALS values presented in Figure 2-6 are the flexible ESALS. For concrete pavement or concrete overlay over an asphalt pavement, the ESALS will be multiplied by a factor 1.5 according to the recommendation of AASHTO design guide in Part III, Chapter 5, Paragraph 5.2.3 (AASHTO, 1993).

Table 2-1 Structural Numbers and Terminal Serviceability assigned for different pavements

Pavement Type	Structural Number [SM]	Terminal Serviceability Number [p _t]
Expressways	6	3
Arterial Roads	5	2.5

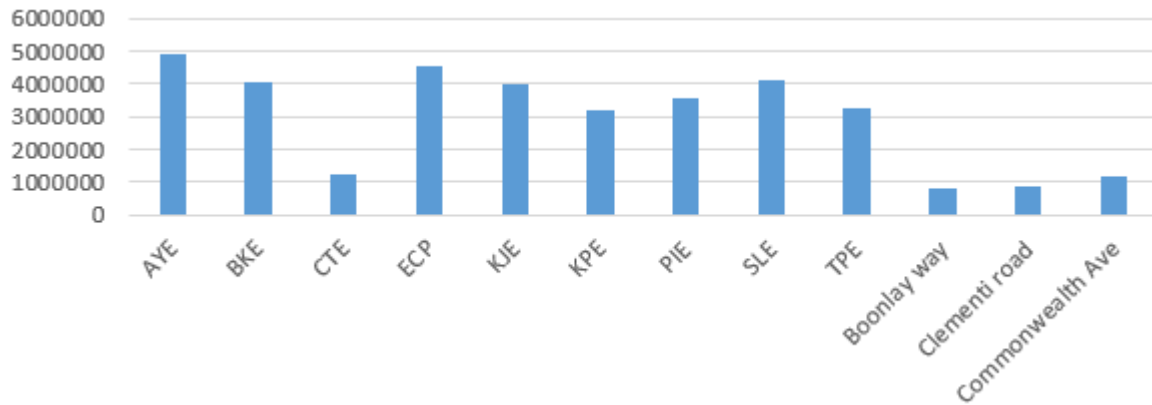


Figure 2-6: Flexible ESALS (80 kN or 18 kips) in design lane around Singapore road network

2.2.2 Environmental loading

Singapore is a tropical country where temperature and humidity are quite constant throughout the year. Daily temperature ranges from about 18 to 37°C with a mean humidity of 82-87% (NEA, 2015). The pavement surface temperatures mentioned by Tan and Fwa (1992) is presented in Figure 2-7. Asphalt pavement had a surface temperature of about 33°C in the morning, 57°C at noon and 40°C in the afternoon. For temperature in concrete pavement, Figure 2-8 presents day and night thermal gradients where the temperature at the bottom of a 200 mm slab is constant at 30°C throughout the day while the surface temperature changes from 25°C at night to maximum 48°C in the noon time (Lau, et al., 1994).

According to Figure 2-7 and Figure 2-8, the highest surface temperature registers in the pavement from about 11 am to 4 pm, which is about 25% of the day, and this repeats daily. Therefore, it can be assumed that 25% of traffic volume is distributed during the midday period, the rest of the day carries 75% of the traffic volume. This traffic volume distribution during the day will be later used for calculating the allowable load cycles of pavement in the next parts.

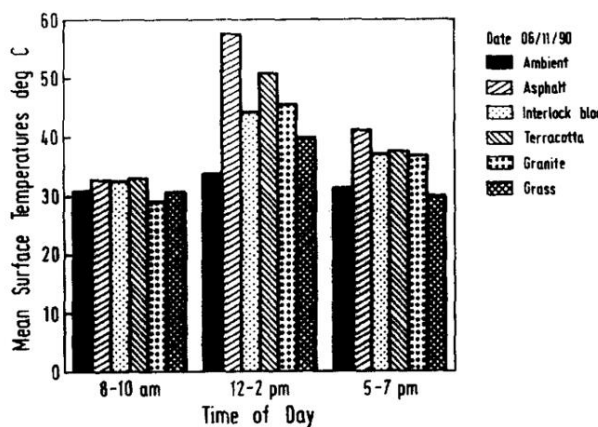


Figure 2-7: Mean surface temperatures of pavements in morning, midday and evening for 6/11/90 (Tan & Fwa, 1992)

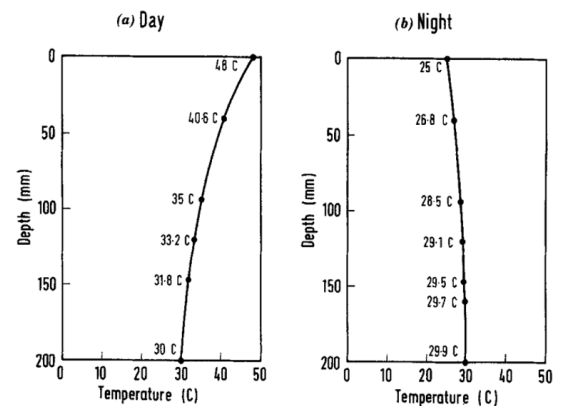


Figure 2-8: Day and night thermal gradients for concrete pavement in Singapore (Lau, et al., 1994)

2.3 Pavement structures

The total length of paved road surface in Singapore is about 3495 km (9232 lane-km). It consists of expressways, arterial roads, collector roads and local access roads (LTA, 2015).

Table 2-2: Paved road length in Singapore

Road category	Road Length (km)	Road Lane-Kilometres (lane-km)
Expressways	161	1059
Arterial Roads	652	3054
Collector Roads	561	1584
Local Access Roads	2051	3384

Asphalt pavements are intensively used throughout the road network, whereas rigid pavements are used limited at some traffic junctions and bus stops. There are in total 4685 bus stops (LTA, 2015).

Singapore pavements are designed based on the Standard Details of Road Element (SDRE) published by LTA (2015). There are four types of flexible pavement namely Type 1A, 1B, Type 2, Type 3 and Type 4. One rigid pavement structure is designed for junctions and another one for bus stops.

2.3.1 Flexible Pavements

Flexible pavement is a multi-layer structure containing five different layers and each layer has different material properties and thickness. The structure and details of this pavement, as specified in (LTA, 2015), are shown in Figure 2-9 and Table 2-3. The total asphalt thickness of pavement Type 1B is 170mm. This thickness is thinner compared to 220 – 260 mm according to German standard for 24-65 million ESALS (>10-32 million ESALS of 10 Ton) (Lechner & Freudenstein, 2010) or 195 mm according to Indonesian standard for 30-50 million ESALS (Ministry of Public Work Indonesia, 2012). However, the thickness comparison is just for reference because the support conditions of these pavements are different.

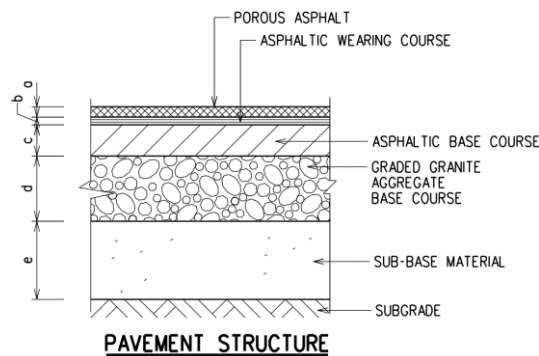


Figure 2-9: Flexible pavement structure (LTA, 2015)

Table 2-3: Thickness of flexible pavement layers (LTA, 2015)

Type of flexible pavement	Road type	Thickness (mm)				
		a	b	c	d	e
Type 1A (with porous asphalt)	Expressway Semi-expressway	40	30	120	250	300
Type 1B (without porous asphalt)	Arterial road Road in industrial area		50	120	250	300
Type 2	Primary access		40	90	200	300
Type 3	Local access		25	75	200	200

2.3.2 Rigid Pavements

The concrete slab is laid over a layer of graded granite which rests on the subgrade material. The design specified by LTA (LTA, 2015) for rigid pavements is shown in Figure 2-10. Rigid pavement is used to replace asphalt at many junctions and bus stops to prevent rutting due to high braking and acceleration forces as well as longer static loading time. The rigid pavement is the jointed reinforced concrete pavement that uses 225 mm thick slab. This type of rigid pavement is becoming less popular because of some performance issues related to the embedded steel. The embedded steel is incapable to hold together mid-panel cracking that results in erosion or faulting (ACPA, 2014).

There is a transition zone designed in between asphalt and concrete pavement. For bus bays, 105 mm thick of concrete layer extrudes 150 mm into asphalt pavement (see Figure 2-11). Whereas, the transition zone is rather complicated in the case of junctions. The two pavement types use different unbound support layers and in between the support layers are also different from the other two around.

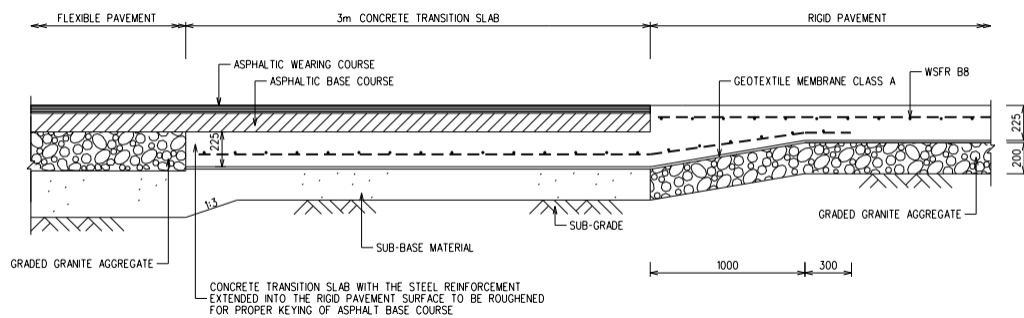


Figure 2-10: Rigid pavement structure at junctions and the connection with flexible pavement (LTA, 2015)

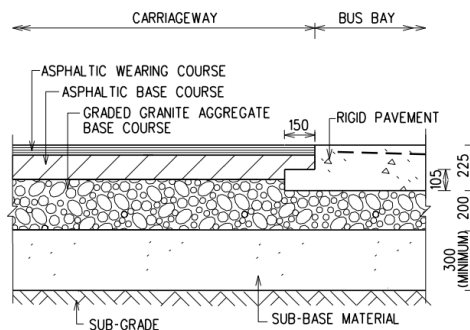


Figure 2-11: Rigid pavement structure at bus stops and the connection with flexible pavement (LTA, 2015)

2.4 Properties of pavement material

2.4.1 Asphalt

The first two layers are asphalt wearing course and asphalt binder course. The mix classification is B60/70 with a bitumen content of 4.5-5.5 % and 4.5-5.0 % for wearing course and binder course, respectively. The asphalt is laid using a mechanical spreader (LTA, 2010).

Asphalt has visco-elastic properties in combination with permanent deformation. These properties are very temperature dependence. Elastic property dominants at low temperature while at high temperature viscose deformation does. When the temperature is in-between low and high range, asphalt shows all two properties (Lechner & Freudenstein, 2010).

Modulus of elasticity of asphalt is influenced by loading time and temperature. Imam Aschuri (2003) studied the changes in mechanical properties of B60/70 asphalt in Indonesia, which is similar to Singapore. The stiffness modulus of the asphalt were 3783 MPa, 1066 MPa, and 319.9 MPa at 25°C, 37.5°C, and 50°C, respectively. These modulus values will be used as references for later analysis.

When asphalt is used in precast ultra-thin whitetopping (PUTW), which will be discussed in later chapters, there are two asphalt temperature values of interest: 39°C and 28°C according to the temperature distributed in pavement structure in Singapore as presented in Figure 2-8. These two asphalt temperature values are correspondent to the modulus values of 950 MPa and 2800 MPa, respectively.

Common fatigue performance criteria for asphalt is its tensile strain. A number of asphalt fatigue functions were summarized by Judycki (1997), Priest and Timm (2006). That included the formulas from French method, Nottingham University (United Kingdom), Road research center in Belgium, “2002 Design Guide”, California Department of Transport and Minnesota Department of Transport. The functions of The Asphalt Institute and Shell are presented here as examples.

Judycki (1997) cited Shook et al. (1982) about the Asphalt Institute fatigue function as follows:

$$N = 18.4 * C * \{6.167 * 10^{-5} * \varepsilon_t^{-3.291} * [E^*]^{-0.854}\} \quad 2-1$$

Where:

- N : Number of load cycles
- ε_t : Tensile strain in asphalt
- E^* : Dynamic modulus of asphalt mix, MPa
- C : function of volume of voids and volume of bitumen in the mix, equal to:

$$C = 10^M \quad 2-2$$

Where:

$$M = 4.84 * \left(\frac{V_B}{V_B + V_v} - 0.69 \right) \quad 2-3$$

- V_B : Volume of bitumen, %
- V_v : Volume of voids, %

Shell International Petroleum Company (1978) introduced the Shell fatigue transfer function as follow:

$$N_f = \left[\frac{6918 * (0.856 * V_B + 1.08)}{S_{mix}^{0.36} * \mu\varepsilon} \right]^5 \quad 2-4$$

Where:

- N_f : Number of load cycles
- $\mu\varepsilon$: Tensile microstrain in asphalt
- V_B : Volume of bitumen, %
- S_{mix} : stiffness modulus of asphalt mix, MPa

In a recent research done by Anthony P. Stubbs (2011), a series of fatigue tests with different strain levels, temperatures, and loading rates was done to characterise the behaviour of two typical structural asphalt B60/70 and B80/100. The equations 2-5 and 2-6 were formed by regression of the experimental fatigue response data. These equations were mentioned to agree well with previous research done in (Bodin, et al., 2010) (Deacon, et al., 1994) (Tayebali, et al., 1993) (Stubbs, 2011). The most recent

formula (Equation 2-5) is used later for roughly estimating the pavement life of asphalt pavement and PUTW in later sections and chapters

$$\mathbf{B60/70} \quad \ln N_f = (57.2623 - 0.8167 * T) - (7.924 - 0.1555 * T) * \ln \varepsilon_t \quad 2-5$$

$$\mathbf{B80/100} \quad \ln N_f = (47.28938 - 0.81668 * T) - (6.15559 - 0.15516 * T) * \ln \varepsilon_t \quad 2-6$$

Where:

- N_f = laboratory fatigue life (cycles)
- ε_t = applied tensile strain ($\mu\varepsilon$)
- T = asphalt temperature ($^{\circ}\text{C}$)

According to (Lechner & Freudenstein, 2010), due to the loading rate acting by actual traffic is much lower than the loading rate used in the laboratory. Therefore, the longer rest period between the load cycles by traffic generates an increase of the allowable load cycle by a factor of about 10 to 15 times. As a conservative approach, a factor of 15 is used for evaluation of current asphalt pavement structural performance while the factor of 10 is used for the proposed PUTW.

2.4.2 Concrete

Fatigue performance of concrete is characterized by the tensile stress. Eid (2012) summarized eleven different fatigue functions that were previously mentioned in (Rao & Roesler, 2004) (Cornelissen, 1984) (Tepfers, et al., 1984) and (Eisenmann & Leykauf, 2003). These fatigue curves are plotted in Figure 2-12 below.

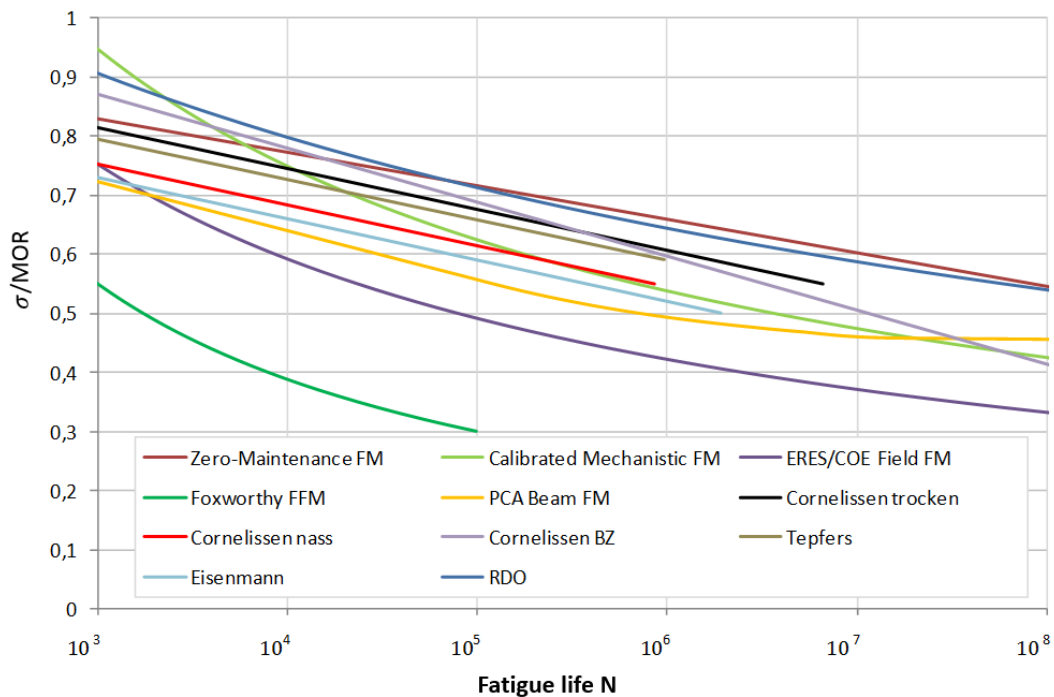


Figure 2-12: Summary of fatigue functions (Eid, 2012)

The zero-maintenance fatigue model is the function that was developed by Darter (1977) for jointed concrete pavements. Darter (1977) compiled the results of 140 fatigue beam tests into one least square regression equation, shown as 2-7.

$$\text{Log } N_f = 17.61 - 17.61 \cdot \left(\frac{\sigma}{MOR} \right) \quad 2-7$$

Where:

- N_f = Allowable loading cycles
- σ = flexural tensile Stress
- MOR = Modulus of Rupture

Concrete with different concrete mixtures performs differently. However, the concrete using for rigid pavement in Singapore is assumed to perform similarly to this zero-maintenance fatigue model as a conservative approach.

2.4.3 Unbound materials for base, sub-base and sub-grade layers

Base course material can be plant-mixed graded granite aggregate, coarse granite aggregate or recycled concrete aggregate. Base course layer is laid in two layers of 125mm thick. It must be compacted to minimum 98% of the maximum dry density using the modified AASHTO Compaction Test or Test 13 of BS 1377. The sub-base layer is made of granular material (e.g. natural sand, crushed rock, crushed concrete, or recycle aggregates). The layer must be compacted to minimum 95% of the maximum dry density and must have at least minimum soaked CBR of 30%. Soil material is used for the 500mm thick sub-grade layer. The sub-grade layer must be compacted to minimum 95% of the maximum dry density and must have at least minimum soaked CBR of 5% (LTA, 2014) (LTA, 2010).

2.5 Performance of asphalt pavement in Singapore

The structural performance of asphalt pavement is dominated by asphalt microstrain under traffic loading. The flexural microstrain in asphalt is calculated with the help of the commonly used BISAR software (Shell International Oil Products B.V., 1998). The input parameters for calculation are as follows:

Asphalt wearing course and asphalt base course:

- $E_1 = E_2 = 950$ MPa (for noon time) or 2800 MPa (for other time)
- $h_1 = 50$ mm
- $h_2 = 120$ mm
- $\mu_1 = \mu_2 = 0.35$

Unbound layers include three layers as follows:

- Graded granite: $E_{GG} = 250$ MPa; $h_{GG} = 250$ mm
- Subbase material: $E_{SB} = 150$ MPa; $h_{SB} = 300$ mm
- Subgrade material: $E_{GG} = 50$ MPa

The results are summary in Table 2-4 below.

Table 2-4: Microstrain in asphalt pavement under traffic loading

Asphalt Elastic modulus (MPa)	Microstrain ($\mu\epsilon$)
950	663
2800	313

The total damage of the pavement is calculated as equation 2-8. At the end of pavement service, D is equal to 1. Therefore, for calculation of allowable load cycles, D value is 1.

$$D = \sum_{i=1}^n \frac{ESALS_i}{Allowable\ ESALS_i} \quad 2-8$$

Traffic distribution for noon time is 25% and for the rest of the day is 75% as mentioned in section 2.2.2. Using the equation 2-8 and fatigue formulas 2-5 with a generous factor of 15 due to loading rate, the life time of asphalt pavement is close to 13 million load cycles. This allowable ESALS is equivalent to about 15 years for heavy traffic junctions (non-expressways). However, in expressways, the life time of this pavement structure is just about three years. Despite the fact that the ESALS number listed in Figure 2-6 is quite conservative, the asphalt structure is still considered relatively weak. If there is a chance for asphalt thickness increase, the performance of asphalt improves significantly (see Figure 2-13). Increase the total thickness of asphalt layers 3 cm, from 170 mm (Type 1B) to 200 mm, will improve the life time of asphalt pavement up to more than 75%.

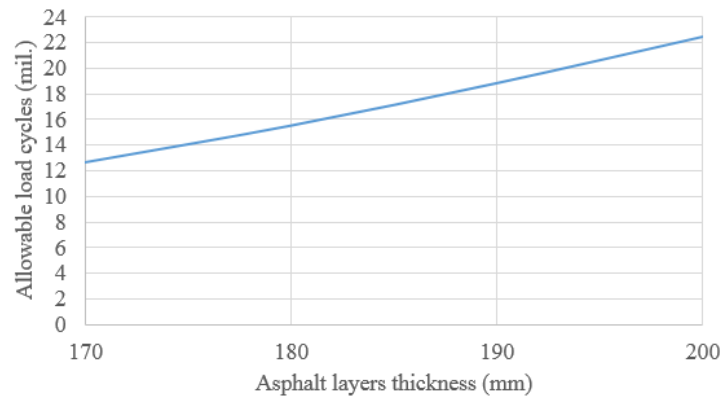


Figure 2-13: Allowable load cycles of asphalt pavement versus asphalt layers' thickness

2.6 Performance of rigid pavement in Singapore

A structure performance of Singapore rigid pavement is analysed to be used as a reference for developing the new pavement system. The jointed reinforced concrete pavement normally has mid-panel cracks at a typical average distance of 4.6 m (ACPA, 2014). The structural performance of this pavement is roughly estimated using three dimensional (3D) finite element model (FEM). An ANSYS 3D FEM is built to calculate stresses in a conventional concrete pavement. The concrete slab size is 3.6 m x 4.6 m. The support layers below the concrete slab are the granite base (thickness = 0.2 m) and subgrade (thickness = 0.5 m). Figure 2-14 illustrates the 3D FEM model with the load applied at the center of the concrete slab. The mesh is designed denser around the load applied area. For convergence in computation, negligible elastic supports are used at four sides of the FEM, while fixed supports are used at the bottom of the subgrade. The FEM is calibrated using Westergaad's closed-form formulas as to be presented in chapter 7. For the traffic loading, there are two scenarios: when the wheel load of 40 kN (axle load of 80 kN) is at the center or the edge of the slab. It is assumed that there is a good load transfer efficiency (LTE) between slabs. Based on the relation between the load applied at the edge of the slab and LTE, when LTE is 75%, the actual load applied to the loaded slab is 25 kN.

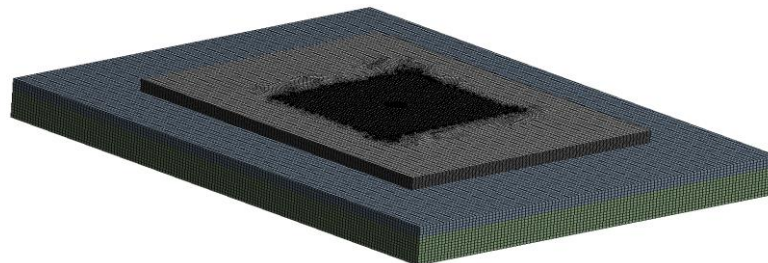


Figure 2-14: 3D FEM of rigid pavement

During the daily cycle of air temperature, there is an extreme temperature profile registered within a concrete pavement slab. The temperature at the bottom face of the pavement slab remain more or less

constant due to the large extent of the soil mass beneath the pavement structure produces a reservoir effect. In the afternoon when the air temperature is highest, the temperature of at the top of pavement surface will be higher than the bottom of the pavement slab. The situation is reversed at night time when the air temperate is lowest. The different in temperate at the top and bottom of the pavement slab creates warping and curling effects (Fwa, 2005). The four combinations of traffic loading and thermal loading accordingly to Figure 2-8 are presented in Table 2-5.

Table 2-5: Load cases applied on Singapore rigid pavement

Loading case	Mechanical loading		Thermal loading
	Loading point	Load value	Warping(W)/curling(C)
Case 1	Center	40 kN	W
Case 2	Edge	25 kN	C
Case 3	Center	40 kN	C
Case 4	Edge	25 kN	W

Table 2-6: Maximum flexural stresses in Singapore rigid pavement with different load cases

Maximum flexural stress in Concrete slab (MPa)			
Case 1	Case 2	Case 3	Case 4
3.15	0.88	0.57	3.01

The results from the FEM are summarized in Table 2-6. The stress in concrete pavement is highest in mid-day where the surface temperature is highest. The traffic volume distribution during midday is 25% and 75% for the rest of the day as mentioned earlier. Modulus of rupture (MOR) of Singapore pavement concrete is assumed to be about 5.2 MPa (Figure 5-3). The allowable load cycle of rigid pavement is calculated using the equations 2-7 and 2-8. The total life cycle of Singapore rigid pavement is about 35 million load cycles, which is equal to 23 million flexible ESALS or about 25 years for heavy traffic junctions (non-expressways). This number will be used as a reference for developing a new pavement system.

2.7 User delay cost due to rigid pavement rehabilitation

User delay cost represents the negative impact of roadwork on travellers by monetization of delay. The impact of work zone can be either inconvenience when traffic demand is relatively low or significant when the work zone capacity is not able to meet the demand (Smith & Walls III, 1998). According to LTA (2012), reconstruction of a cast-in-place rigid pavement requires at least ten days of lane closure as a common practise in Singapore. At heavy traffic junctions, this amount of lane closure time can result in a very high user delay cost. In this section, Clementi network in Singapore is used as a case study for estimating the user delay cost due to rigid pavement rehabilitation with the help of a microscopic traffic simulation tool.

User delay cost includes three components:

- *Time delay costs*: the cost caused by time increasing due to reduced speed or rerouting to other routes. This cost is one of the most controversial parameters as it is difficult to calculate by adding monetary value to the delay time of passengers and travellers (Smith & Walls III, 1998). The time delay costs are calculated by multiplying the estimated delays to of all types of vehicles (car, bus, HGV, LGV) caused by the work zone by the unit cost (\$/hr) of travel time.
- *Vehicle operating costs*: the cost resulted from fuel consumption, tyre wear and other costs related to vehicle operation and maintenance.
- *Accident costs*: the cost caused by vehicle damages, injuries and fatalities.

In this research, only time delay cost is analysed because of the data availability. Therefore, the delay caused by roadwork can be defined as the difference of travel time between the normal condition

without work zones and longer travel time in work zones. Three methods commonly used to estimate delay cost are macroscopic analytical approaches, macroscopic simulation approaches and microscopic simulation approaches (Weng & Meng, 2013). In this study, the microscopic traffic simulation using VISSIM software will be used to estimate the travel delay due to roadwork. This commercial tool can deliver reliable results.

2.7.1 Traffic simulation using VISSIM software

Microscopic simulation models are becoming important tools for modelling of transport systems. The main reason is that simulation is faster, safer and less expensive than field implementation and testing. First released in 1992, VISSIM is a microscopic, time step and behaviour based simulation model developed to model urban traffic and public transit operations. The tool has been used worldwide to simulate traffic control, driving behaviour and develop many scenarios for traffic operation. The microscopic simulation requires a huge amount of data (e.g. network data, traffic count, signal control, travel time and speed) as well as an adequate calibration and validation process. Regarding roadwork and incident simulation, many studies have used VISSIM as a reliable platform, generating plausible results for evaluation (Martin, et al., 2011). In Singapore context, VISSIM has been already used to simulate Singapore Queenstown network (Koh & Chin, 2007), SCATS operation along Bouna Vista street (Liu, 2013), bus priority schemes in the city (Quing, 2013), traffic light control for multi-junctions (Xian, 2014).

The purpose of this traffic simulation is to estimate the user cost generated during construction and maintenance of cast-in-place rigid pavement. Clementi network as shown in Figure 2-15 is chosen as a case study the roadwork is described as following:

- Work zone length = 50m at the intersection.
- The three-lane urban road in Clementi area and one lane will be close for rehabilitation.
- Vehicle mix: 85% cars, 10% buses and 5% trucks based on traffic count.
- Traffic volume collected from Land Transport Authority (LTA, 2012).

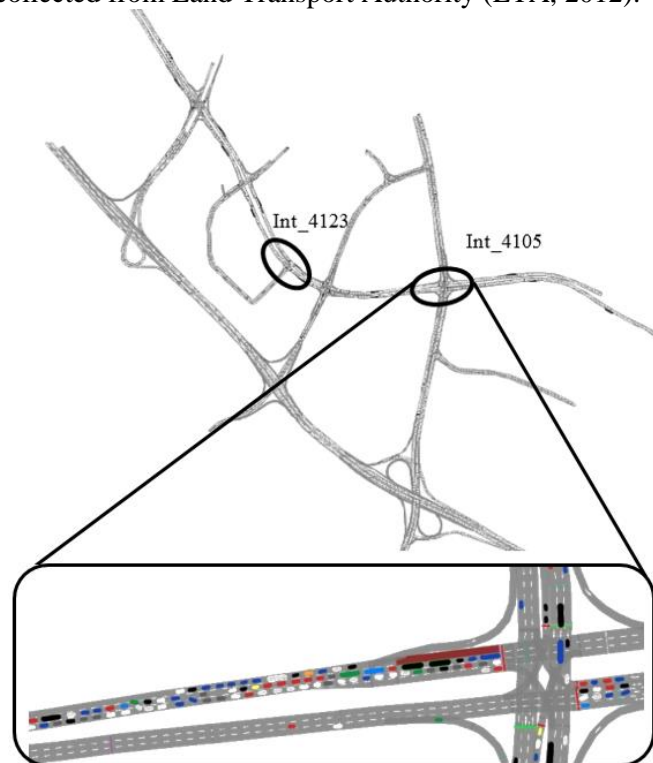


Figure 2-15: Clementi network and detail simulation of the roadwork at the intersection

In addition to the general scenario, it is assumed that the traffic diversion (VMS) is in three levels 0, 10%, and 30%. For calibration and validation purposes, travel time, travel speed and queue length are

collected from field measurement using video recording and the floating car method. The floating car method here is the method that uses a vehicle to run through the studied sections several times during peak hours. The roadwork is simulated by blocking one lane at the intersection approach for rehabilitation.

For calibration of the system performance, three goals are established as following (Dowling, et al., 2004):

Goal 1: Identification of AM peak period queuing.

Goal 2: Average travel time to be within 15 percent deviation from data collected by field measurement

Goal 3: Model link versus observed flows to meet the following criteria: link volumes for more than 85 percent of cases to be:

- Within 100 vehicles per hour (vph), for volumes less than 700 vph;
- Within 15 percent, for volumes between 700 vph and 2,700 vph;
- Within 400 vph, for volumes greater than 2,700 vph;

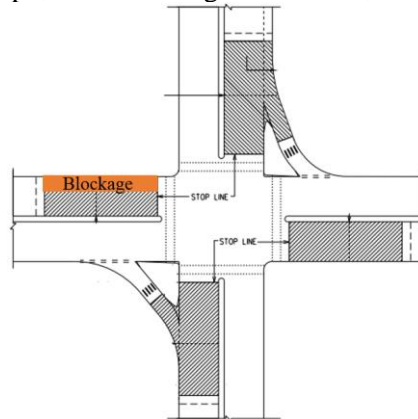


Figure 2-16: Define reduced speed road segment for construction simulation

The delay is measured for all vehicles passing through the construction work at the intersections (coded Int_4123 and Int_4105 according to LTA (see Figure 2-15). Travel delay at two intersections is shown in Figure 2-17.

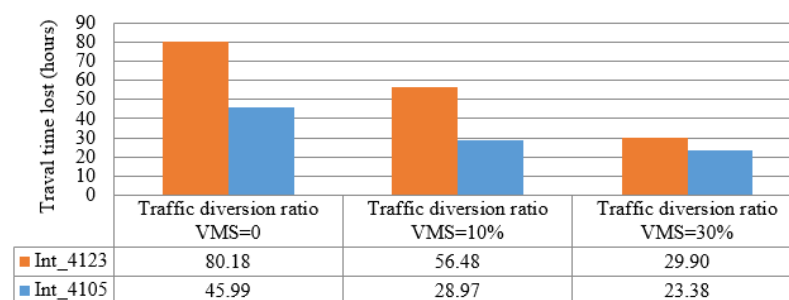


Figure 2-17: Travel time lost due to construction at intersections Int_4123 and Int_4105

Depending on the location and level of VMS, travel delay is different. At the intersection Int_4123 all three lanes are used for all types of vehicles, whereas at intersection Int_4105 one left lane is dedicated to buses. Therefore, closure of bus lane will cause less impact on traffic flow or lower travel delay compared to another case. It is well noted that when the level of VMS = 0, the travel delay is the most significant.

2.7.2 The value of travel time and delay cost

The unit value of time is quite different in various time and locations worldwide. Travel time value of trucks is always higher than that of passenger vehicles (1.3 to 2 times) (Smith & Walls III, 1998) (Scheving, 2011) (Mirzadeh, et al., 2014) (Salem, et al., 2013). The value of goods transported in these trucks is considered to be the main reason for the difference. Details are illustrated as the following Table 2-7.

Table 2-7: The value of travel time from different time and location worldwide

Locations	Unit cost converted to SGD/h/veh		Ratio (truck/car)	Source
	Car	Truck		
US (1998)	16.2	26-32.24	1.6-1.99	(Smith & Walls III, 1998)
Iceland (2011)	18.89	24.56	1.30	(Scheving, 2011)
Sweden (2011)	16-23.94	22.8-34.2	1.43	(Mirzadeh, et al., 2014)
Ohio (2006)	24.25	44.95	1.85	(Salem, et al., 2013)
New Jersey (2006)	21.7	36.17	1.67	(Salem, et al., 2013)

Travel time cost is dependent on a few factors: the number of each type of vehicle, the average occupancy rate for each type of vehicle and the average salary of occupants in each type of vehicle (Pawitra, 2002). There are mainly three types of vehicle: cars, buses and trucks (Heavy Goods Vehicle and Light Goods Vehicle). The average car occupancy in Singapore is 1.7. The maximum carrying capacity for a single decker bus is about 85 people, a double decker bus is 131 people and an articulated bus is 143 people (with seating is about 50, 90 and 53, respectively) (Menon & Kuang, 2006). The average bus occupancy is 55. In case of goods vehicles, this value is 1.62 (Pawitra, 2002).

The cost of travel time is calculated by the monetary loss of travellers going through the roadwork in one hour (Pawitra, 2002).

$$T = PV_{jk} \times AvSAL_j \quad 2-9$$

$$PV_{jk} = VT_{jk} \times OCC_{jk} \quad 2-10$$

$$AvSAL_j = \sum_{h=1}^{11} p_{ij} \times MGW_h \quad 2-11$$

Where:

- T = Value of Travel Time during hour k
- PV_{jk} = Total number of occupants in vehicle type j during hour k
- VT_{jk} = Number of each type of vehicle type j during hour k
- OCC_{jk} = Average occupancy of vehicle type j during hour k
- $AvSAL_j$ = Average salary of occupant in each type of vehicle
- p_{jh} = Proportion of travellers in occupation h in vehicle type j
- MGW_h = Mean Gross Wage of occupation h

There are eleven types of occupation according to Singapore Ministry of Manpower (MOM, 2014):

- (1) Managers & Administrators,
- (2) Working Proprietors,
- (3) Professionals,
- (4) Associate Professional & Technicians,
- (5) Clerical support workers, (6) Service & Sales Workers,
- (7) Craftsmen & Related Trades Workers,

- (8) Plan and Machine Operators & Assemblers,
- (9) Cleaners, Laborers & Related Workers,
- (10) Others, and
- (11) Unemployed.

The Mean Gross Wage and number of employment of each occupation are presented at Table 2-8

Table 2-8: Mean Gross Wage and number of employment of each occupation

	1	2	3	4	5	6	7	8	9	10	11
Mean Gross Wage (SGD)	10,000	3,250	6,974	4,060	2,630	2,100	2,495	1,976	1,265		0
Employment	349,052	156,352	372,252	646,503	421,607	412,707	238,507	302,707	322,307	227,107	81,700

The p_{jh} (proportion of travellers in occupation h in vehicle type j) value is collected from (Pawitra, 2002). Four types of travelers are divided by four salary ranges: below \$2000, \$2000-\$4999, \$5000 to over and no salary. The following Table 2-9 shows the $AvSAL$ calculated from p_{jh} and MGW_h data. The value of goods in the trucks is simplified to be involved in the $AvSAL$. Due to the fact that the unit cost of trucks is always higher than that of cars from 1.5-2 times, the $AvSALs$ of HGV and LGV are recalculated with a factor of 1.5 times of the cars value.

Table 2-9: Average delay cost of each type of vehicle per hour

	Cars	Buses	HGV	LGV
Average delay cost (SGD/h/per)	30.7	17.5	13.4	13.4
Modified average delay cost (SGD/h/per)	30.7	17.5	46.05	46.05

In total, travel delay cost at two intersections is estimated based on the travel delay and unit cost of travel then being aggregated into price per square meter as shown in Table 2-10 below. It is clear that the delay cost varies with construction site locations and traffic diversion ratio, which translates to traffic volume. In this case study, for the period of ten days, the travel delay cost for construction without traffic diversion of cast-in-place rigid pavement is about 890 and 510 (SGD/m²) at intersection Int_4123 and Int_4105, respectively. These costs are significantly high ranging from 1 up to 5 times more than the construction cost itself (roughly 185-250 SGD/m² (LTA, 2012)). Therefore, there is a demand for an alternative pavement that can be constructed quickly to reduce the user delay cost. This alternative pavement should have a performance similarly to the current rigid pavement.

Table 2-10: Travel delay cost estimation

Location	VMS=0		VMS=10%		VMS=30%	
	delay (h)	delay cost (SGD/m ²)	delay (h)	delay cost (SGD/m ²)	delay (h)	delay cost (SGD/m ²)
Int_4123	80.18	891.17	56.48	627.74	29.90	332.3
Int_4105	45.99	511.11	28.97	322.03	23.38	259.8

2.8 Summary

In this chapter, Singapore pavement systems have been reviewed. LTA is managing the whole Singapore road pavements. Deflectograph, Multifunction road monitor and SCRIM are used regularly to provide the PMS detailed information about road network condition. For traffic information, Singapore is an extremely dense country with a vehicle population is nearly 1 million. Within this project, important traffic data for calculating of 80 kN equivalent single axle loads (ESALS) was collected by a survey at some key corridors in the network. The ESALS is very high throughout the network especially along highways and secondary roads which are in average 3.6 million/year and 0.9 million/year, respectively. As a tropical country, the temperature registered in the pavement does not

vary significantly all year round. The temperature on concrete pavement surface changes from 25°C at night to maximum 48°C in the noon time daily.

The pavements are designed based on the Standard Details of Road Element (SDRE) published by LTA. For pavement structures, asphalt pavements are intensively used throughout the road network, whereas rigid pavements are used only at many traffic junctions and bus stops. There are four types of flexible pavement namely Type 1A, 1B, Type 2, Type 3 and Type 4. The total asphalt layer thickness of the most common asphalt pavement Type 1B for the expressway, semi-expressway, arterial road and road in the industrial area is 170 mm. The asphalt Type 1B thickness specified by SDRE is relatively thinner compared to German or Indonesia standard. One rigid pavement structure is designed for junctions and another one for bus stops. The rigid pavement is the jointed reinforced concrete pavement that uses 225 mm thick slab. Due to some performance issues, this type of rigid pavement is becoming less popular.

Properties of pavement materials, especially the asphalt and concrete performance, were reviewed to be used for evaluating the current pavement structural performance and providing intensive data for the new pavement development. Using a generous approach, the structural performance life time of asphalt and concrete pavement in Singapore are about 15 and 25 years for heavy traffic junctions (non-expressways), respectively.

With the help of the state of the art microscopic traffic simulation tool, user delay cost due to rigid pavement reconstruction was estimated for a selected case study area in Singapore. At heavy traffic junctions, the user delay cost at the study area can be up to 5 times of the construction cost itself, which is significantly high. Therefore, there is a need for an alternative pavement for the current rigid pavement at heavy traffic junctions. The alternative pavement should be constructed quickly but still have the performance of at least 25 years.

3 Electrified roadways

3.1 Introduction

This chapter will firstly introduce and summarize the state of the art of electrified roadways. The electrified roadways' power supply components, which are inside the pavement, will be studied in more detail. At the end, the requirements for an electrified roadways pavement will be identified.

3.2 Electrified roadways concept

3.2.1 Introduction

Transport accounts for around 19% of global energy use and 23% of energy-related carbon dioxide (CO₂) emissions. More interestingly, around 95% of that transport energy usage is petroleum (IEA, 2009). To reduce the dependence on the scarce petroleum supply in the near future and greenhouse gases emissions, electric vehicles (EVs) are being introduced worldwide. However, the adoption of EVs remains low mainly because of their battery related problems including price, weight and range limitation. The current price of the battery pack is about US\$700/KWh or even more (Suh, 2011). In the most optimistic scenario, the price is predicted to drop to US\$420/KWh in 2015 (as 2009) (Suh, 2011). But even in this case, the battery pack still costs as much as half of the car price. In addition to price, the battery occupies a large portion of vehicle weight (1/5th in Nissan Leaf (Wikipedia contributors, 2012)), which leads to more EVs' energy consumption to just carry the battery around. Moreover, limitation in battery capacity consequently leads to short range travelling that makes users feel very uncomfortable.

Charging infrastructure is one of the key elements to overcome battery related problems. Conductive and inductive charging stations level 2 or 3 (fast charging) can utilize EVs stopping time to charge the batteries while parking at public places such as office's parking lots, shopping centers, recreation centers. These public charging stations can address the range anxiety (Yilmaz & Krein, 2013) for well-planned and low daily mileage trips. For irregularly unplanned trips or fleet operators (like taxis or buses), an additional tool such as electrified roadway for range extension is needed. Electrified roadways have a good potential to solve not only the range anxiety but also the entire battery related problems.

3.2.2 Electrified Roadway for EVs

3.2.2.1 *Charging infrastructure as range extender for EVs*

According to (Yilmaz & Krein, 2013), there are three levels of charging power for EVs. Level 1 aims for charging at home or office using convenience outlet as a power supply. The expected power of level 1 is 1.9 kW (maximum), which means an empty battery of 24 kWh of Nissan Leaf can be fully charged in 13 hours. A higher power up to 19.2 kW can be found in charging level 2, which is the primary method for dedicated private or public facilities. Charging level 3 (also called fast charging) can provide very high power up to 50 kW or more. At this level, the Nissan Leaf's battery can be fully charged in about 30 minutes.

Conductive and inductive charging stations use level 2 or level 3 to charge EVs while the vehicles are parked at the office or public facilities (opportunity charging). EVs can be then charged more frequently instead of deep-cycling of the battery. For low daily mileage EVs and well-planned trip, these charging stations can overcome the range anxiety. Irregularly long trips, however, may often exist. In addition, trips of fleet operators such as taxis are somehow unpredictable and impossible to plan. In Singapore, for example, taxis account for just 3% of the vehicle population but contributing 18% of the total mileage (Hoster, 2012). Taxis are normally operating non-stop in 2 shifts with daily mileage of more than 500 km per vehicle (Hoster, 2012). With today's technology, it is almost impossible to produce a battery to fulfil this huge mileage demand in one or two charges otherwise very expensive and heavy. To overcome long daily mileage and to make EVs even more attractive to users, additional range

extenders are needed. Electrified roadways meet this requirement by offering charging while EVs are on the operation.

Electrified roadways are the roadways that have inductive charging components embedded inside. Therefore, they allow energy to transfer wirelessly to EVs and to charge the battery or to propel the engine when EVs are on the move (or stationary) using Inductive Power Transfer (IPT). Figure 3-1 demonstrates the concept of an electrified roadway. When EVs are on top of the electrified roadway, electrical components are triggered on automatically to transfer power to the vehicles wirelessly.

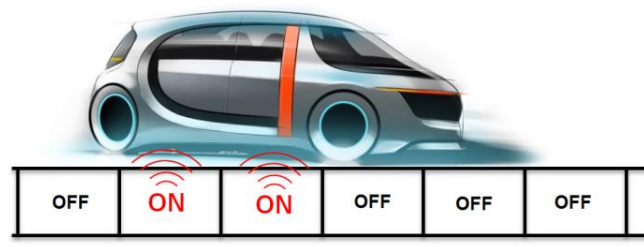


Figure 3-1: Electrified Roadway concept (Wu, et al., 2011)

Figure 3-2 illustrates a typical trip of an EV with very high daily mileage. The EV starts the trip with a fully charged (100%) battery on-board. If there is no charging infrastructure along the travel way, maximum distance this EV can travel continuously is about 80 km in this case. However, with electrified roadways, the EV can now be charged more regularly to overcome any long journey around the city. These charging locations can be at taxi stands where taxis are queuing and moving slowly in a couple of minutes or up to an hour at the airport to wait for their turn to pick up passengers. For buses, these locations can be at bus terminals or bus stops. Locations at traffic lights or some key sections of roads can also be part of an electrified roadway network. Interestingly, these potential charging points are the locations where the rigid pavement is normally used in Singapore.

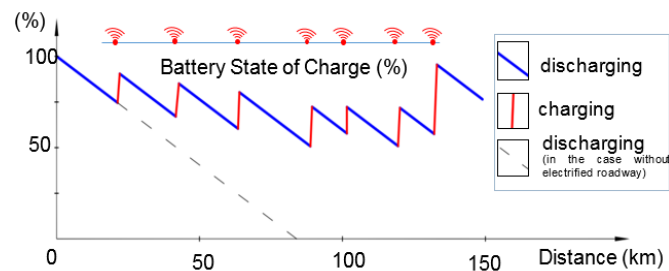


Figure 3-2: Battery state of charge of an electric vehicle using electrified roadways

A bus route of 12.5 km is used as an example to demonstrate the charging time, charging locations and energy collected from the electrified roadways. A daily bus operation involves 20 bus journeys or 250 km. The electrified roadways are placed at terminals, some selected bus stops, some key junctions and steep uphill sections (see Figure 3-3). Terminals are at the end of a bus journey. The first bus leaves terminal with a fully charged battery on-board. Every bus stops for 5 minutes between journeys (except for overnight parking) at terminals. With the bus stop spacing of about 400-500 m, there are 25-30 stops in a bus journey. Five key bus stops, where there are many passenger alighting and boarding (for example at shopping malls, schools or offices), are equipped with electrified roadways. The stopping time at each of these key bus stops is 20 seconds. There are about 12-20 junctions spacing at about 800-1 km along this 12.5 km bus route. Three of the junctions that have the longest red light time (normally at the crossing with higher hierarchy roads) are electrified. Buses may go through the junctions with or without stopping depending on traffic lights. The average duration that every bus spends on the

electrified roadways at these junctions is assumed to be 20 seconds. Other locations for electrified roadways are at a long, steep uphill road section or at a section where electrified roadways can be co-used by many other bus lines or EVs. Two charging lanes of 500 m are used in this example. With average bus speed of about 20 km/h, the duration of every bus on one charging lane is 90 seconds. The wireless power transfer is chosen to be 100 kW with the efficiency of 80%. The detail about daily energy collected from these charging infrastructures by one bus in this example is described in Table 3-1. With the availability of the charging infrastructure of 90%, the energy collected by one bus is about 250 kWh daily. Power consumption of electric buses depends on many factors such as type buses, occupancy rate, driver skills, road terrain, and air conditioner usage. If the power consumption of busses in this study route is 1.2 kWh/km, the total energy needs for the daily operation is 300 kWh. The electrified roadways provide 250 kW. With 50 kW buffer, buses operating in this bus route need only 100 kW on-board battery instead of 350 kW.

Table 3-1: Example of electrified roadways' locations along a bus line and the energy collected by one bus during its daily operation

Charging location	Charging duration (seconds)	Charging efficiency (%)	One bus journey (12.5 km)	Daily bus operation (20 journeys or 250 km)		
			Charging occurrence	Charging occurrence	Collected Energy (kWh)	
Terminal	300	80%	1	19	126.67	
Bus stops	20		5	100	44.44	
Junctions	20		3	60	26.67	
500 m - charging lane	90		2	40	80.00	
Total					277.78	
Total (90% of infrastructure availability)					250.00	

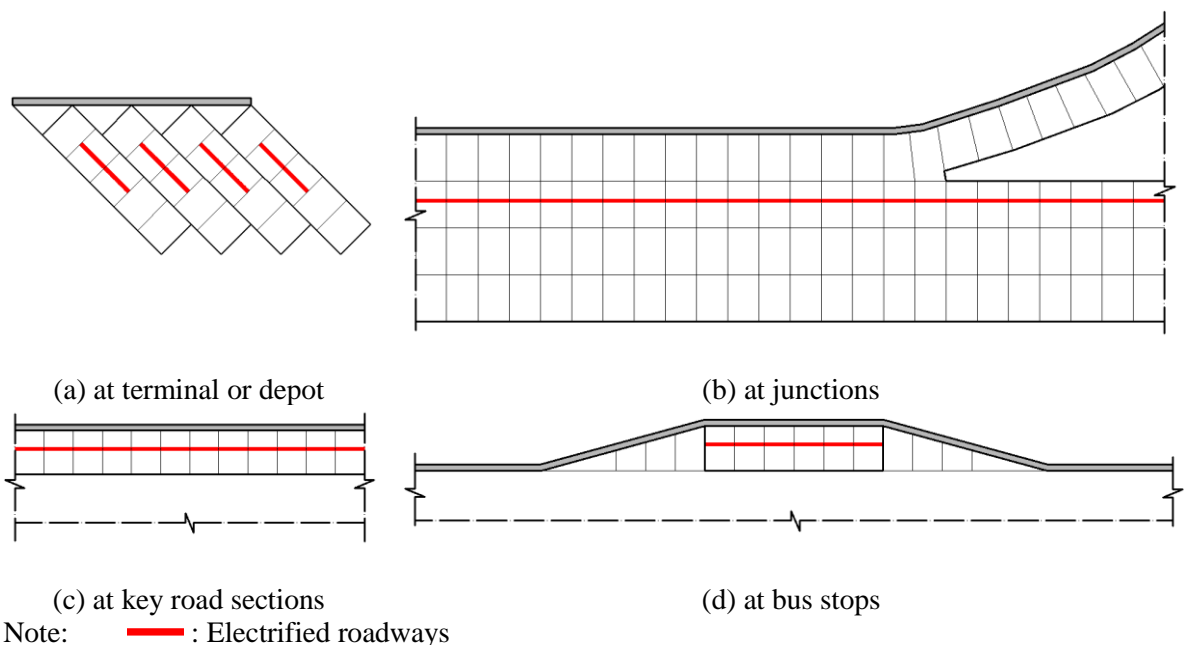


Figure 3-3: Potential locations of electrified roadways for bus application

In summary, if a city is installed with electrified roadways (or charging lanes) at the “right” locations where EVs could charge their battery whenever needed, there will be no more range limitation. In this case, the battery capacity could be reduced, which leads to the reduction of the battery weight, size and cost. In conclusion, electrified roadways can solve EVs’ battery related problems.

3.2.2.2 *The development of electrified roadway (Milestones)*

The concept of inductive wireless energy transfer using in transportation was first invented in railway application by Maurice Hutin and Maurice Leblanc (1894) in the early 1890s (see Figure 3-4). Even there was no application at the time, the idea was very important for the development of electrified roadways.

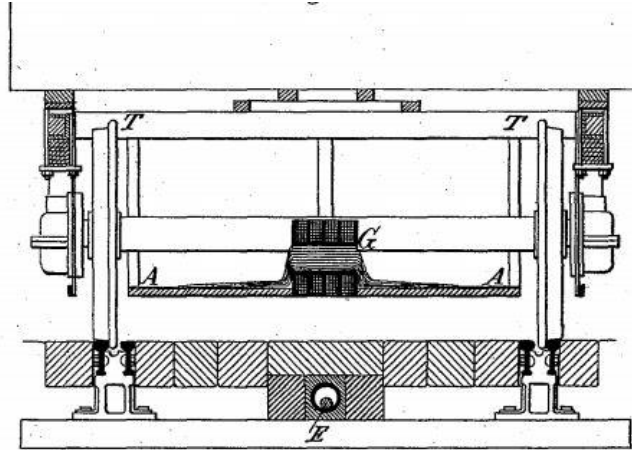


Figure 3-4: Inductive energy transfer for Tram (Hutin and Leblanc, 1894)

In order to reduce the dependence on fossil fuel during the oil crisis in the mid-1970s, the concept of inductive wireless energy transfer was again attractive. A 6 kW proof-of-concept system was fabricated and tested at Lawrence Berkeley and Lawrence Livermore National Laboratories. But “neither the vehicle nor roadway was suitable for an operational system” (Systems Control Technology, 1994).

In 1979, the Santa Barbara Electric Bus Project started with a planning and feasibility study, followed by preliminary engineering and prototype development and testing, but the technology used was still far from deployability (Shladover, 1992) (Systems Control Technology, 1994).

Following the Santa Barbara Electric Bus Project, at the end of the 1980s, California Partners for Advanced Transit and Highways (PATH), Institute of Transportation Studies, UC Berkeley introduced a project called “Roadway Powered Electric Vehicle project” (RPEV). RPEV was recorded as the first successful test in dynamic roadway power transfer (see Figure 3-5) (Risch, 2011).

Within the project, a 215 m (700-foot) roadway test track was designed and constructed at Richmond Field Station of University of California, Berkeley. The track consisted of two 60 m (200-foot) electrified segments with the layout shown in Figure 3-6. The vehicle used was a 35-passenger electric bus with a top speed of 64 km/h (40 miles per hours). It had “a conventional DC drive system with a 48 kW separately-excited traction motor capable of regenerative braking at the speed above 20 km/h (12 mph)” (Systems Control Technology, 1994).

The result of the test was very impressive. The system allowed up to 60 kW to transfer from the roadway to the electric bus on the move with the efficiency of up to 60% from AC power into the power conditioner to DC power out of the inductive coupling system (ICS). This made the full day bus operation possible instead of 2.5 hours based on battery only (400 km (250 miles) compared to 30 km (18 miles)) (Shladover, 1992).

Safety was one of the critical issues concerned. According to Shladover (1992), the introduction of field cancellation windings along outer edges of the roadway inductor led to reductions of magnetic flux density to about 1000 milligauss at the height of 0.3 m (1 ft) and about 100 milligauss at a height of 1.2 m (4 ft) above the center of the conductor slot. When these levels are compared with everyday expose levels of 1000 to 10000 milligauss while using electric shaver, 100 to 200 milligauss for electric blanket

or electric toaster users, 1 to 10 milligauss for sitting in the center of a typical living room”, it is clear that the magnetic fields of the roadway inductors were at “much lower levels than those commonly encountered in use of everyday electric appliances”. More interestingly, the exposure time of a person using an electric shaver or an electric blanket can be substantially longer than pedestrian walking across the powered roadway or walking along a sidewalk or waiting at a bus stop. Shladover (1992) confirmed that “there is no appreciable chance of producing a health hazard by this mechanism”.

The Playa Vista Project (next generation of RPEV system) for a G-VAN aimed to lower magnetic fields, lower acoustic noise, increase efficiency and lower cost. The deployment of RPEV was not successful because “it was not possible to develop an affordable design for the roadway inductor that was needed to supply power to the vehicles” (Shladover, 2006).



Figure 3-5: PATH Test track. Source: PATH

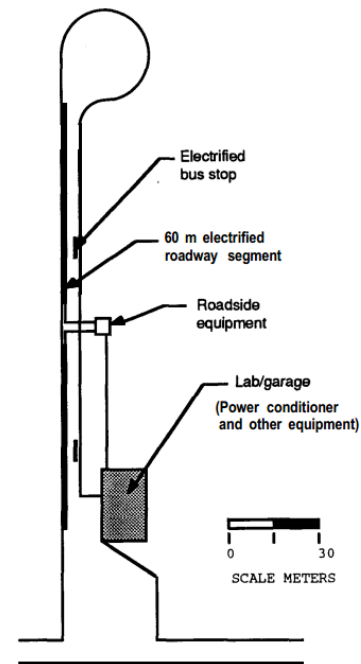


Figure 3-6: Test track layout (Systems Control Technology, 1994)

In 2009, Korea Advanced Institute of Science and Technology (KAIST) introduced on-line electric vehicle (OLEV). KAIST OLEV developed shaped magnetic field in resonance (SMFIR) to enable wireless electric power transmission while the vehicle is in motion. KAIST successfully demonstrated SMFIR in Seoul Grand Park. In this demonstration, three of six-segmented powered tracks, comprising five 24 m and one 2.5 m segments, were used. There were also two 2.5 m segmented powered tracks to allow charging the vehicle while waiting or idling. The total length of powered tracks was 372.5m which is approximately 17% of the travel way of one round trip (2.2km). The other test beds were also successfully demonstrated at the KAIST Munji campus, located in Daejeon, Korea (which is under operation) and at KAIST main campus (Figure 3-7) (Suh, 2011).

From the demonstrations, SMFIR showed very good performance with up to 20 cm airgap between the pavement surface and the pick-up installed under the vehicle with the efficiency of up to 80% (Huh & Rim, 2011).

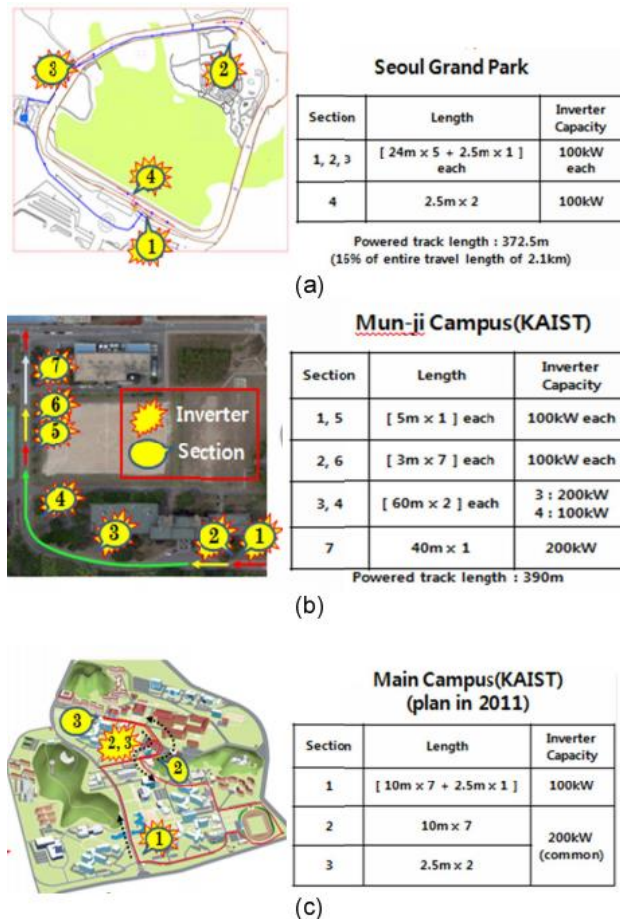


Figure 3-7: Demonstration projects with SMFIR technology (Suh, 2011)

Safety is one of the most important concerns. OLEV uses a method called reactive resonant current loop that generates a magnetic field to cancel the original magnetic field to minimize electro-magnetic field (EMF) noise. This reactive system interestingly uses magnetic field noise as a power source (Kim, et al., 2013).

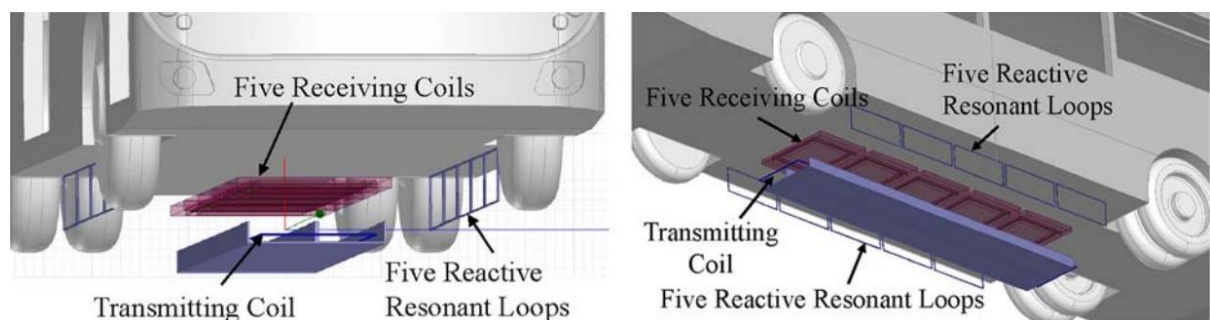


Figure 3-8: Application of reactive resonant current loop for an OLEV.

With the use of reactive resonant loops as shown in Figure 3-8, OLEV system meets the acceptable human exposure level to EMF requirement published by ICNIRP (International Commission on Non-Ionizing Radiation Protection) (Kim, et al., 2013).

It is interesting enough when Gumi-A South Korean city has begun testing an electrified roadway using OLEV technology (Figure 3-9). This is a 24 km bus route in the southern city of Gumi (Pentland, 2013).



Figure 3-9: OLEV system at a bus stop in Gumi (Pentland, 2013)

At about the same time with KAIST OLEV, in 2009, Bombardier introduced PRIMOVE. “Bombardier PRIMOVE is a game-changing e-mobility solution providing wireless power supply for all vehicles” (Walker, 2011). In September 2010, the first demonstration for tramway was installed at Augsburg trade fair site (Figure 3-10). The test bed was 600 m long, using the power supply of 750 VDC. The system could charge the tram with the power of 200 kW. An efficiency of 95% (Walker, 2011) shows the good performance of the wireless energy transfer.



Figure 3-10: Demonstration project for tramway in Augsburg trade fair site (Walker, 2011)

In October 2010, Bombardier demonstrated another test bed in Lommel (Belgium) for the bus application (Figure 3-11). The test track of 125 m on a public concrete road allowed charging the bus both statically and dynamically with a “very high” efficiency (Walker, 2011).

According to (Bombardier, 2015), PRIMOVE is confirmed to comply all regulations and requirements regarding EMF and compatibility (EMC).



Figure 3-11: Demonstration project for bus in Lommel (Bombardier, 2011)

And similar to OLEV, Bombardier has also just announced the first bus project for commercial operation. According to the announcement, this commercial bus project uses two buses operating on 12 km route in Braunschweig, Germany equipped with PRIMOVE technology (Bombardier, 2015).

Besides systems mentioned, there are many more other entities and suppliers that are working with wireless power transfer (static or dynamic charging or both) for EVs that were reviewed in (Highways England, 2015). These systems are listed in Table 3-2.

Table 3-2: Overview of WPT system (Highways England, 2015)

“Energy Dynamics Lab	Part of Utah State University. Still doing research but technology developed was spun out to Wave Inc. (see below)
Evatran	Marketed as ‘Plugless Power’. After market system for replacing current plug-in chargers with wireless system for residential charging only. Evatran has partnered with Yazaki to commercialise the system.
Fraunhofer Institute	A large German research organisation involved in a wide range of activities. Technology demonstrator only using inductive pads mounted on the front of the vehicle for residential charging. Uses smaller coils due to closer coupling and easier positioning. Not suitable for dynamic charging.
InovaLab	InovaLab was a spin off from the University of Padua which is now owned by SAET Group. InovaLab are participating in an EU funded programme called FABRIC (Feasibility analysis and development of on-road charging solutions for future electric vehicles). InovaLab are developing the primary infrastructure as part of FABRIC and aim to develop their own vehicle based components in order to be able to supply a complete DWPT system.
INTIS	INTIS (Integrated Infrastructure Solutions), subsidiary of the IABG group, developed an inductive energy transfer system for cars and buses. The system has been developed to operate as static or DWPT system. The project has been carried out in collaboration with Fraunhofer (Electromobility) plus a number of other companies and associated partners and it has been funded by the German Federal Ministry of Transport and Digital Infrastructure.
IPT Technology (sub-division of Conductix Wampfler)	Joint venture between Conductix Wampfler and PROOV B.V to develop applications in electric mobility. Long experience in the field due to parent company involvement. Concentrates on autonomous industrial system and bus applications for static charging, including eight buses on a route in Milton Keynes.
KAIST (Korea Advanced Institute of Science and Technology)	Korea Advanced Institute of Science and Technology. Magnetic resonance system which can operate over longer range than standard inductive charging systems. Currently fitted to demonstrator cars and buses. Technology licensed to OLEV Technologies (see below)
OLEV Technologies	Licenses technology from KAIST. Target markets are buses, port transportation, trucks.
ORNL (Oak Ridge National Laboratory)	American research institute which has laboratory based technology demonstrators for dynamic charging.
POLITO	Politecnico di Torino (POLITO) together with Centro Ricerche Fiat is working on the Charge While Driving (CWD) solution. The solution is being developed as part of a European Commission co-funded project FABRIC.
Primove	Primove is the e-mobility unit of Bombardier transportation who are a large supplier to the rail industry. Inductive charging system aimed at light rail, bus and automotive fleet operations. Concentrates on static charging, though claims dynamic charging capability as well.

Qualcomm Halo	Founded as Halo IPT by Arup using magnetic resonance technology originally developed by Auckland University. Halo IPT was purchased by Qualcomm in 2011 to found Qualcomm Halo. Currently working on a static charging system with ongoing research into dynamic charging. Also, part of the FABRIC project.
SEW Eurodrive	Offer industrial systems and electric bike systems only.
Siemens	Offer the Sivetec inductive charging system for static charging.
TDK	TDK Corporation made an intellectual property license agreement for the wireless power transfer technology developed by the MIT spin-off company WiTricity (see below). They aim to commercialise the static charging system, and to demonstrate a DWPT application.
Wave Inc.	This is a spin off from Utah State University (Energy Dynamics Lab) to market the technology. It concentrates on bus applications. They provide purely static charging systems situated at bus stops along the routes.
Witricity	Witricity have developed wireless charging systems based on magnetic resonance for static charging. The technology was originally developed at MIT.”

3.2.2.3 Summarize the performance of electrified roadways

To summarize the performance of operating parameters of different electrified roadway systems, the important factors are listed as follows (Wu, et al., 2011):

- Power level – this directly determines how fast it takes to charge the battery fully.
- Efficiency – the efficiency should be measured from AC mains (grid) to DC battery to be compared with plug-in charging systems
- Charging distance – is the distance between the primary and secondary windings (2 coils of IPT systems). Charging distance sometimes is represented by “Air gap” – the clearance between the pick-up installed under the vehicle to pavement surface (Charging distance = air gap + a thin layer of pavement covering coils)
- Charging tolerance – the relative ease of vertical and horizontal alignment for a normal driver when parking or driving over.

The summary is as follows (Huh & Rim, 2011) (Systems Control Technology, 1994) (Walker, 2011) (Kim, et al., 2013) (Choi, et al., 2015):

Table 3-3: Summary of the performance of electrified roadway

	PATH	PRIMOVE	OLEV
Year	1975-1996	2009-now	2009-now
Power level	60 kW	Up to 200 kW	Up to 200 kW
Efficiency	60 %	95% (max)	80%
Air-gap	Up to 7.6 cm	Not Given	Up to 20 cm
Tolerance	Max 10 cm	Not Given	10-30 cm
Safety	-	meet	ICNIRP

According to a recently published report about feasibility study of powering electric vehicles on England’s major roads (Highways England, 2015), a comprehensive evaluation has been done for the systems that are capable of dynamic wireless charging functionality in term of Technology Readiness Level (TRL) and Manufacturing Readiness Level (MRL) by the project team. OLEV and Primove are graded 8 and 7 for TRL and 7 and 5 for MRL, respectively. Detailed summaries are listed in Table 3-4.

Table 3-4: TRL and MRL of DWPT systems (Highways England, 2015)

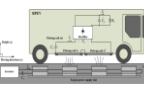
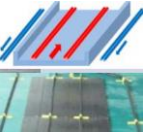
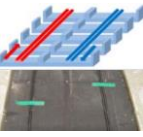
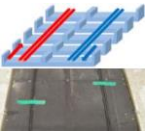
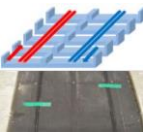
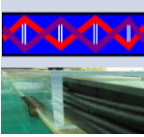
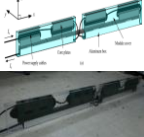
DWPT System Developer/Supplier	TRL	MRL
OLEV - KAIST	8	7
PRIMOVE –Bombardier	7	5
INTIS	6	4
ORNL	6	4
WiTricity / TDK	5	3
Polito	5	3
Qualcomm Halo	4	3
Saet	4	3

With very promising operating parameters especially from OLEV and PRIMOVE, electrified roadways confirmed their positions through the newly signed bus projects in Korea, Germany and United States. This technology is believed to be possible for the widely commercial adoption in very near future.

3.3 Power supply components of OLEV electrified roadways and their pavements

Only components and pavements from KAIST OLEV are mentioned here because published information about PRIMOVE system is yet very limited. Since 2009, the development of OLEV systems has gone through five generations (see Table 3-5). The improvement includes improving air-gap, efficiency, reducing EMF as well as construction feasibility.

Table 3-5: Five generations of KAIST OLEV (Huh & Rim, 2011) (Choi, et al., 2015)

	1 G (Car)	2 G (Bus)	3 G (SUV)	3+ G (Bus)	3+ G (Train)	4 G (Bus)	5 G
Date	Feb. 27, 2009	July 14, 2009	Aug. 14, 2009	Jan. 31, 2010	Mar. 9, 2010	2010~	
Vehicle							
System Spec.	Air-gap=1 cm Efficiency=80%	Air-gap=17 cm Efficiency=72%	Air-gap=17 cm Efficiency=71%	Air-gap=20 cm Efficiency=83%	Air-gap=12 cm Efficiency=74%	Air-gap=20 cm Efficiency=80%	Air-gap=20 cm Efficiency=80%
	All the efficiencies are measured by AC grid voltage to on-board battery terminals						
EMF	10 mG	51 mG	50 mG	50 mG	50 mG	<10 mG	<10 mG
Power Rail (width)	 20 cm	 140 cm	 80 cm	 80 cm	 80 cm	 10 cm	 4 cm
Power	3kW / pick-up	6kW / pick-up	15kW / pick-up	15kW / pick-up	15kW / pick-up	25kW / pick-up	22kW / pick-up

The first generations (1G) used 20 cm wide E-type cores. It delivered the overall system efficiency of 80% however the air-gap are limited at 1 cm only. The second generation (2G) was a great improvement from the 1G where the air-gap increased to 17 cm, which meets the road regulations (12 cm in Korea and 16 cm in Japan). The 2G used U-type power supply rail (Figure 3-12), which were 1.40 m wide. The third generation (3G) used 80 cm wide W-type power supply rail (Figure 3-13). A much narrower (10 cm) I-type power supply rail was developed in the fourth generation of OLEV (Figure 3-14). This I-type power supply rail is claimed to reduce the deployment cost significantly. The width of power supply rail is further reduced in the fifth generation, where 4 cm ultra slim core S-type is used (Figure 3-15) (Choi, et al., 2015) (Choi, et al., 2015).

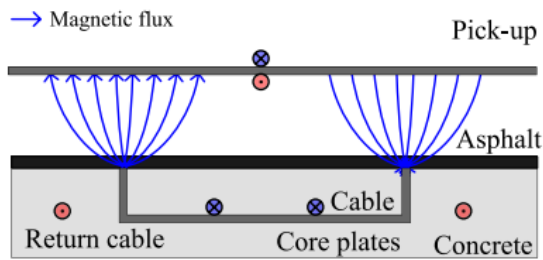


Figure 3-12: Cross section of U-type (2G) power supply rail

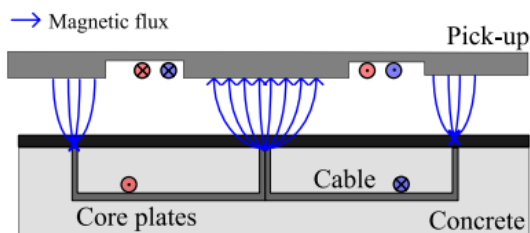


Figure 3-13: Cross section of W-type (3G) power supply rail

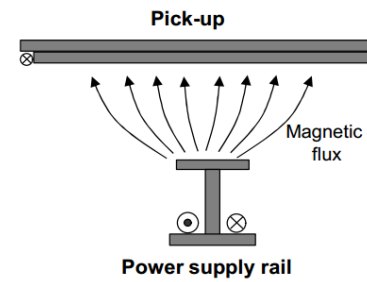


Figure 3-14: Cross section of I-type (4G) power supply rail

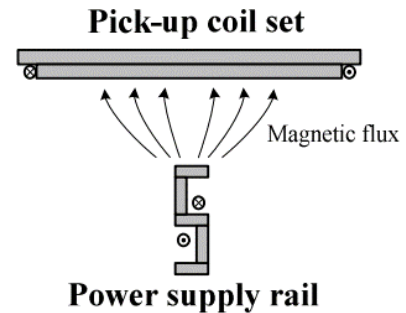


Figure 3-15: Cross section of S-type (5G) power supply rail

The pavement for the W-type power supply rail (3G) is presented in Figure 3-13, and Figure 3-16. The thick concrete layer is designed to protect the power supply rail. In construction, a wide strip is cut along asphalt pavement, then the power supply rails are installed and positioned in the slot. Concrete is later used for filling the slot. Using this design and construction method, there is a concern about load transfer between asphalt pavement and concrete pavement along the two longitudinal joints around the electrified pavement. Moreover, when construction and repair time are considered, besides the amount of time needed for electric installation, cast in place concrete pavement has its bad characteristic of longer delay to open to traffic due to concrete curing process. This delay leads to a higher user cost as detailed discussed in chapter 2.



Figure 3-16: The pavement for the W-type power supply rail (3G) (www.heise.de)

One of the initiations to narrow the power supply rail is for the construction feasibility. For system demonstration purpose, one way of the construction proposed in (Choi, et al., 2015) is presented in Figure 3-17 for I-type power supply rail. One slot in the middle of the pavement is milled. Prototype modules are slot into the pavement and back filled with asphalt or concrete. This is a good way to have fast electrified roadways constructed for demonstration. However, at a heavy traffic location, long term protection of the power supply modules, as well as long term performance of the pavement, might not be guaranteed.

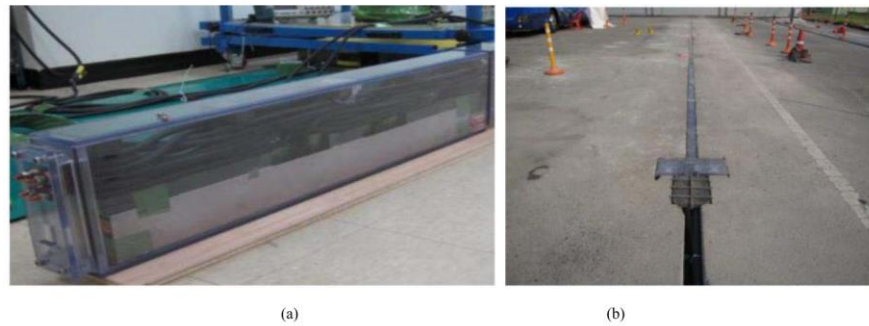


Figure 3-17: Deployment of I-type (4G) modules at 24 m test side. (a) Prototype module. (b) Deployed module (Choi, et al., 2015)

The newest S-type power supply rails (5G) are discussed more in detail in this section. The ultra-slim S-type power supply modules are foldable (Figure 3-18). The module includes power supply rails, transparent cover, an aluminium box for capacitor banks and better heat transfer to the ground. The pole width is just 3 cm adding up with the covers to the total width of 4 cm. The distance between poles is 20 cm, and the pole length is 30 cm, which contributes to the total length of the module to 1 m. The poles themselves are 14 cm high, together with aluminium box and the module cover high, the total module high should be around 20-25 cm. The modules are connected serially using 0.9 cm diameter power cables that are very flexible cables that allow modules to be folded easily. Therefore, all of the connection works between modules can be done off-site, which save construction time at the site (Choi, et al., 2015).



Figure 3-18: Foldable S-type power supply modules: (a) fully deployed case, (b) one-third folded case, (c) two-thirds folded case, (d) completely folded case (Choi, et al., 2015)

The operating temperature of the S-type power supply rails is relatively low at 35°C maximum when the ambient temperature is at 20°C with 50A output current (Figure 3-19) (Choi, et al., 2015). Inside pavement in Singapore, the ambient temperature can be different, which leads to the changes in maximum operating temperature.

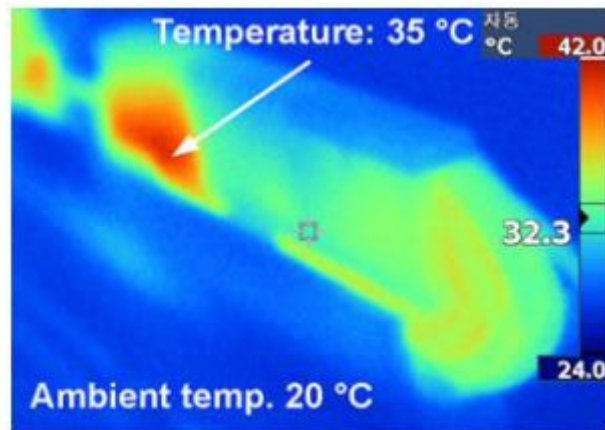


Figure 3-19: Measured the highest temperatures of the S-type power supply rail after 50 min operation in thermal equilibrium state (Choi, et al., 2015)

With the specifications mentioned above, the foldable ultraslim S-type power supply rails are able to achieve maximum efficiency (excluding the inverter) up to 91% at 22 kW, larger lateral displacement up to 30 cm at 20 cm air-gap, and it is estimated to have lower EMF because of narrower width (Choi, et al., 2015).

The S-type power supply rail with the modular concept can help to minimize construction time. However, if the same construction method for I-Type power supply rail is applied, there is still the same concern about long term protection of the power supply modules and long term performance of the pavement.

3.4 Requirements of pavement for electrified roadways

Pavement system for electrified roadways has to fulfil not only all requirements of a normal pavement but also requirements of an electrified roadway. Electrified roadways are normally installed at the heaviest traffic section to increase the usage efficiency. Therefore, almost all electrified roadways need to be installed and repaired quickly to reduce the down time and user cost due to road closure as well as to provide enough charging infrastructure that EVs need to operate. Moreover, pavement for electrified must be high performance and long lifespan along with electrical devices to compensate for the high initial investment cost. Electrified roadways have to be strictly protected under the pavement surface. In addition, the power supply rail must be close enough to the road surface to get the optimum efficiency in wireless power transfer. Because electrified roadways use the magnetic field for energy transfer, they work only when no metallic material is in between electrified roadway components including both roadside and on-vehicle components.

3.5 Summary

This chapter firstly summarized the state of the art of the electrified roadway. The electrified roadway has a good potential to be widely adopted in the near future and is an attractive approach to switch mobility from conventional fossil fuel traction to future electric traction. The electrified roadway provides a solution to address the most critical disadvantage of EVs, i.e. battery related problems and therefore increasing EVs' acceptance to the public. The concept of the electrified roadway was proposed and the first test track was demonstrated in the 1890s. In 2009, Bombardier introduced PRIMOVE and at about the same time Korea Advanced Institute of Science and Technology (KAIST) introduced on-line electric vehicle (OLEV). Bombardier and KAIST bring the electrified roadway to the next level regarding inductive power transfer (IPT) performance. These performance factors include higher efficiency (>80%), higher air-gaps and tolerances as well as safety factors (meet the standards).

Through five generations of the development, OLEV systems have improved the performance in terms of wireless power transfer, safety as well as the road construction feasibility. The pavements for the

power supply components have been proposed and constructed for demonstration purpose. However, there is still concerns about high user delay cost due to long construction time as well as long term protection of the power supply modules and long term performance of the pavement.

The requirements of electrified roadways pavement were identified. The main requirements include high performance, long lifespan, fast construction and maintenance. The power supply components have to be accurately positioned and well protected inside the pavement. Metallic material i.e. steel reinforcement and steel load transfer devices, is not allowed to be used in the pavement for electrified roadways.

4 Precast Ultra-Thin Whitetopping (PUTW) concept

4.1 Introduction

The target pavement's characteristics and requirements, which were identified in Chapter 2 and Chapter 3, are interestingly well aligned. Moreover, the locations that need a rigid pavement are also the most potential locations for electrified roadways. Two pavement types that partially fulfilled the requirements of the target pavement are precast concrete pavement (PCP) and ultra-thin whitetopping (UTW). These two pavement types will be reviewed in the following parts to be used as references for proposing the new pavement system.

4.2 Precast Concrete Pavement (PCP) technology

Precast concrete pavement (PCP) systems were introduced to provide durable, longer-lasting pavements that can be quickly repaired and constructed. PCP systems are the systems that “are essentially fabricated or assembled off-site, transported to the project site and installed on a prepared foundation” (Tayabji, et al., 2013). The process “fabricated off-site” of PCP will provide a durable and the best quality control concrete. Moreover, the concrete curing process is well controlled in the plant. Therefore, early age failures of concrete pavement like cracking due to high temperature change during this curing process (where concrete exhibits shrinkage and expansion) can be eliminated. Because there is no need for on-site concrete curing, weather condition has less impact and delay to open to traffic is minimized. PCP has been tested, improved and used widely for rapid intermittent repair and rehabilitation in Japan and United States of America (USA) in the last decades. In Japan, after improving the load transfer at joints and support condition, PCP has been used more intensive in the past 20 years ($>90,000 \text{ m}^2$), and their “very long service life can be expected” (Kitaguchi, et al., 2006). In the United States, more than $167,225 \text{ m}^2$ of PCP had been constructed in just 10 years from 2001 to 2011. PCP has two main systems: prestressed precast concrete pavement (PPCP) system and jointed systems.

4.2.1 Prestressed precast concrete pavement (PPCP)

Precast prestressed concrete pavement (PPCP) is formed by post-tensioning reinforced precast slabs panels into a 46-76m length section. These sections are by then connected with each other by expansion joints. The individual panel has the length of about 2.4 to 3 m for a multiple-lane panels and about 3 to 9 m or more for single-lane panels. Figure 4-1 illustrates three versions of PPCP. The original version (see Figure 4-1 (a)) comprises of base panels, central stressing panels and expansion joint panels. While second version (see Figure 4-1 (b)) includes base panels and expansion joint panels, and the third version (see Figure 4-1 (c)) uses base panels, end joint panels and expansion gap panels instead (Tayabji, et al., 2013).

The use of prestressed strain tendons and tongue-and-groove keyways helps to eliminate many joints related issues (for the joints inside the post-tensioned section). Moreover, the prestressed tendons also help to reduce slab thickness while maintaining the comparable performance as thicker slabs produced by a cast in place conventional method. PPCP was successfully installed in various states in the USA (Texas, California, Missouri, Iowa and Delaware) and Indonesia. Even though there are still some considerations about expansion joints and minor slab cracks, the tested data of installed PPCP show comparable performance to CIP pavement with service life expectation of 40 years (Tayabji, et al., 2013).

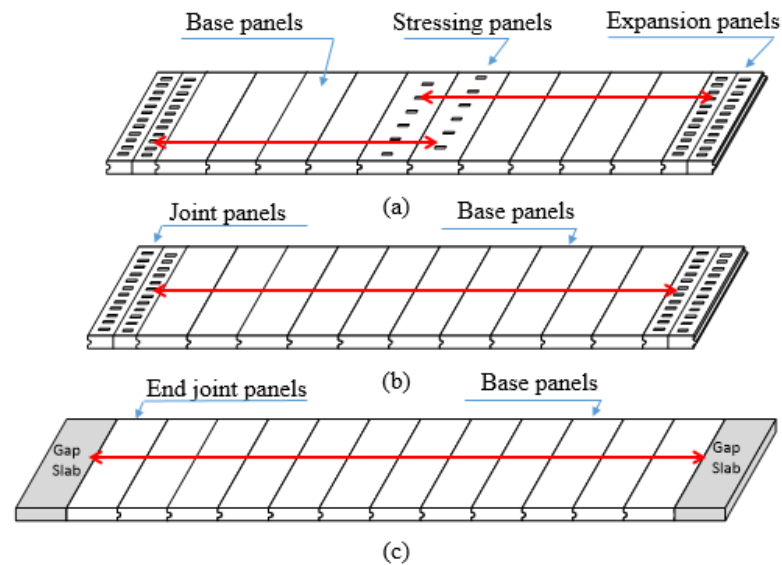


Figure 4-1: Types of Prestressed precast concrete pavement (PPCP) (Tayabji, et al., 2013)

4.2.2 Jointed precast concrete pavement (JPrCP)

Jointed precast concrete pavement (JPrCP) has been used widely in Russia and Japan since the 1970s (Tayabji, 2011) and in the USA since the last decade. Typically, JPrCP includes individual reinforced slabs, when installed, JPrCP acts like a normal jointed concrete pavement. There are many JPrCP systems that have been developed. And in general, the systems are quite similar to each other except the differences mainly in the support material/layer and the way slabs are connected to each other (joint and load transfer devices).

While the Japanese system is laid on an asphalt interlayer to prevent pumping at joints (KITAGUCHI, et al., 2006), systems developed in the USA like the Roman Road System (developed by the Roman Road Construction Company) is using polyurethane foam as bedding material (Tayabji, et al., 2013) or Super-slab (the most used system in USA and Canada, developed by Fort Miller Group) is recommended to use stone dust then fill with fast setting cementitious grout for supporting slabs.

Joint and load transfer devices are also the key factors that differentiate JPrCP systems. While Russian uses weld technique to connect panels together (see Figure 4-2), Japanese is using their own developed “horn” load transfer device, compression joint unit (see Figure 4-3 and Figure 4-4) and sliding dowel bar. In the USA, the most famous design was developed by Fort Miller for Super-slab system, where the dowel bar slot is at the bottom of the slab (see Figure 4-5). The gaps are by then filled with fast setting grout. There are also some other systems in the USA using other techniques like dowel bar retrofit (DBR) (Roman Road system) (see Figure 4-6), Kwik slab interlocking system (Kwik Slab system) (see Figure 4-7), Michigan method (resembles a DBR) (see Figure 4-8) and narrow-mouth surface dowel slot (see Figure 4-9) (Tayabji, et al., 2013).



Figure 4-2: Welded lift loop connection (Tayabji, 2011)



Figure 4-6: Installing dowel bars using DBR method (Buch, et al., 2012)

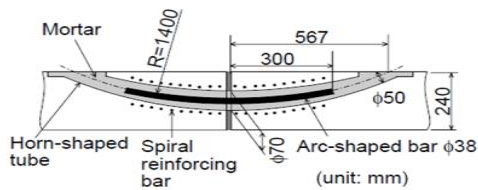


Figure 4-3: The "Horn" Load Transfer Device (Tayabji, 2011)



Figure 4-7: Kwik Slab joint interlocking system (Buch, et al., 2012)

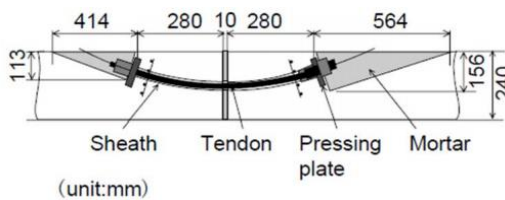


Figure 4-4: Compression Joint Unit (Tayabji, 2011)

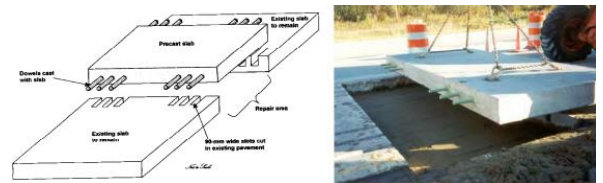


Figure 4-8: Michigan method (Buch, et al., 2012)



Figure 4-5: Dowel bar slot at the bottom of the slab (Buch, et al., 2012)



Figure 4-9: Narrow mouth surface dowel slot (Buch, et al., 2012)

4.2.3 Performance of precast concrete pavement

One study in Project R05 of the US Strategic Highway Research Program 2 was to obtain the field performance of the precast concrete pavement project constructed throughout the US. The study involved both structural and functional performance assessment. In general, the field performance data indicated that the well designed and installed PCP in the USA has a very high estimated service life of about 40 years, which is similar to the design life of a new cast-in-place concrete pavement. The majority of joints had load transfer efficiency of above 90%. However, there are still some minor issues

with the PCP. Some slabs showed tight cracking, which is not a big concern due to the present of reinforcement in each slab. In a PPCP project, there is spalling over the reinforcement, which suggested to redesign the reinforcement detail. Some extensive premature cracking and panel settlement were also observed. The causes of these issues were identified to be the low quality of the support condition or inadequate slab thickness (Tayabji, et al., 2013).

4.3 Ultra-thin Whitetopping (UTW)

UTW is a thin concrete overlay that is placed bonded to an existing asphalt pavement surface (see Figure 4-10). The existing asphalt pavement has to be in good condition with only minor surface distresses. Harrington and Fick (2014) mentioned that asphalt with some normal thermal cracks still can be used for UTW. However, it is not recommended due to the potential of reflective cracking. The bonding between concrete and asphalt in UTW creates a composite system where both concrete and asphalt are working together. Figure 4-11 illustrates the differences in load-induced stresses between a UTW and an unbonded overlay. The continuous asphalt base layer acts like a quasi-continuous support system that replaces the conventional dowels in conventional concrete pavement systems. Concrete layer protects the asphalt layer from the extreme temperature, and acts as a load distribution layer. Thus, it is no longer shear deformations in the asphalt. Conversely, asphalt acts as an erosion-resistant base layer and elastic support for the concrete layer. The different properties of the two materials must be considered when combining them together. Structure-temperature behavior is one of the formative differences between concrete and asphalt. The strength of concrete is independent of the temperature. However, strain changes when there are changes in temperature. For asphalt in a tropical country like Singapore, it is exactly the opposite, the relaxation due to temperature changes causes no stresses, and the stiffness decreases with increasing temperature. In a UTW system, the properties of concrete and asphalt positively complement. At high temperature, when the bearing capacity of asphalt decreases, the joints of the concrete are closed and the concrete slab system has the highest bearing capacity. Conversely, the bearing capacity of the asphalt is greatest when the joints of the concrete are open in a cooler temperature (Eid, 2012).

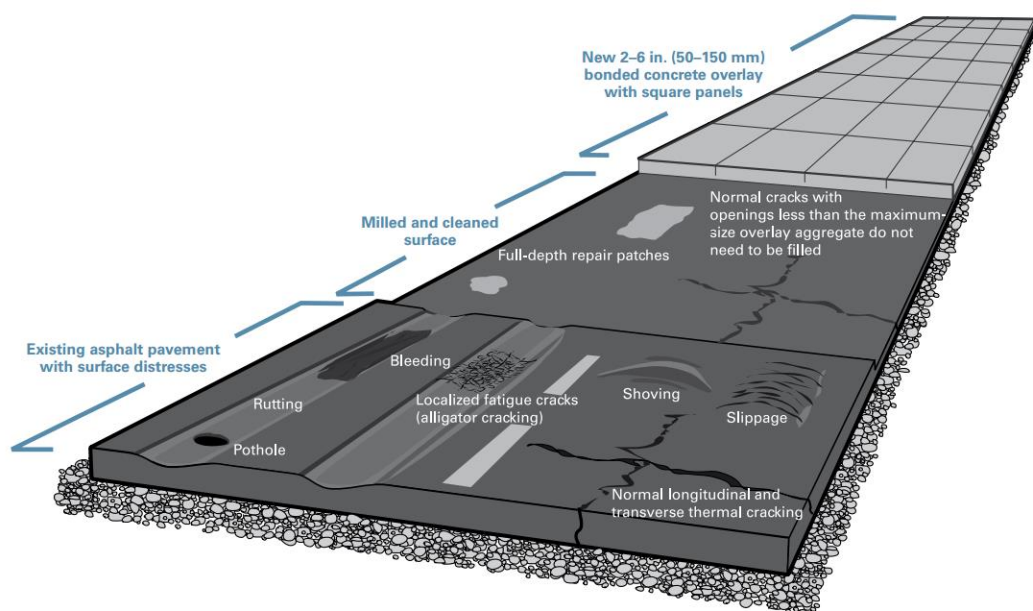


Figure 4-10: UTW on a fair or better asphalt pavement (still in good structural performance) with only minor surface distresses (Harrington & Fick, 2014)

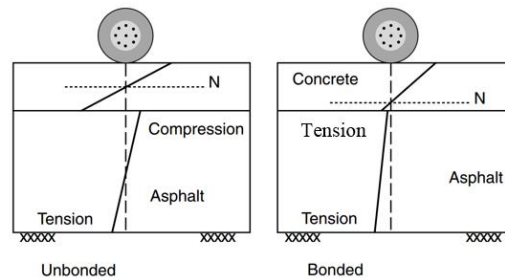


Figure 4-11: Effects of interface bonding (Fwa, 2005)

Whitetopping has its long history since 1918. However, until September 1991, the first test section of UTW was built in Louisville, Kentucky. ACPA has documented more than 300 UTW projects during 1992-2002. These projects have a size ranging from 170 to 58500 m². The average project size is 2500 m². The UTW project has not been only limited to the USA. Many others were also constructed at many locations worldwide including Europe (Belgium, Sweden, Austria and France), Asia (Japan, South Korea) and South America (Brazil) (Rasmussen & Rozycki, 2004).

UTW has been successfully used to rehabilitate existing HMA pavements (Rasmussen & Rozycki, 2004) (Eid, 2012) (Fwa, 2005) (Pereira, et al., 2006). The majority of UTW projects performed very well, however, some exhibited premature failure. The common factors which can cause failure of UTW are excessive stress in the concrete layer, excessive shear stress at the bonding between concrete and asphalt layer, wrong panel size and low quality or too thin remaining asphalt after milling.

4.4 Precast Ultra-Thin Whitetopping (PUTW) concept

Thin bonded concrete overlay over asphalt (or UTW) is a good solution for preventing rutting at heavy load locations, for example at junctions before the traffic lights or bus stops. However, due to its nature of using concrete, long road closure time for construction and concrete curing are still unavoidable. In the heavy traffic road network like Singapore, the long road closure time leads to a very high user delay cost as presented in Chapter 2. Accelerated mixtures are available. However, there are still concerns about long term durability of concrete due to excessive shrinkage, heat generation and poor microstructure (Harrington & Fick, 2014).

PCP can significantly reduce the road closure time while providing the high performance of a conventional rigid pavement. However, joint and load transfer devices in PCP are rather complicated and possibly expensive to manufactured and constructed. Moreover, due to the nature of construction, PCP slabs typically include two layers of steel reinforcement meshes to withstand the construction load (slab lifting). When electrified roadways are taken into account, metallic material used for reinforcement mesh, dowel bars, and tie bars are not possible because they will interfere the wireless power transfer via a magnetic field. Furthermore, using full-depth rigid pavement at junctions leads to a rather complicated pavement structure at the transition area between concrete and asphalt pavement (see Figure 2-10). The supporting layers are also different, which interrupts the construction of supporting layers spot by spot.

The target pavement should inherit the advantages of both PCP and UTW while overcoming their disadvantages. The proposed pavement is called Precast Ultra-thin Whitetopping (PUTW). PUTW is an innovative pavement system that applies the very fast construction characteristic of the precast concrete pavement (PCP) technology for Ultra-thin Whitetopping (UTW) (bonded concrete overlay). The main differences between a PUTW and a UTW are caused by the construction process. In UTW, fresh concrete is laid over a prepared asphalt surface while in PUTW, the concrete slabs are prefabricated in a plant, transported to the construction site and bonded over the prepared asphalt surface with the help of grouting. PUTW can be installed bonded on a milled old asphalt or newly paved asphalt. After installing, PUTW will behave similarly to a UTW pavement. PUTW overcomes the disadvantages

of UTW by inheriting the quick installation characteristic of a PCP. Moreover, due to the lack of dowel bars and tie bars, the PUTW fosters the construction process even faster, easier and is possibly cheaper than PCP.

Another unique feature of the proposed PUTW pavement system is the material used for PUTW slabs. PUTW is designed as a high performance precast pavement that can be used for heavy traffic junctions and bus stops as well as electrified roadways. Therefore, the pavement slab has to be very durable to handle heavy traffic and environmental loading as well as slab handling loading during construction without the help of any metallic reinforcement meshes due to the requirement of the electrified roadways. A very durable material called Engineered Cementitious Composite (ECC) is proposed for the PUTW slab. ECC is a unique type of high performance fiber-reinforced cementitious composite that has very high tensile ductility, which translates to a very high flexural strength.

The proposed PUTW pavement structures are presented in Figure 4-12. The main aim of PUTW is to provide an alternative for Singapore rigid pavement at heavy traffic junctions where extended road closure can be an issue and a pavement for electrified roadways. For simplicity of an uninterrupted pavement support layers' construction, the PUTW pavement structures are based on the popular flexible pavement Type 1B for expressway, semi-expressway, arterial road and road in industrial area in Singapore (See Figure 2-9 and Table 2-3). The total composite slab thickness, which includes ECC, grout and asphalt, is 170 mm. The purpose of the grout is to fill the gaps and create strong bonding between ECC slab and asphalt layer and to fill the gap between the unbound layers and the culvert in PUTW for electrified roadways. The thickness of the grout layer should be kept as thin as possible.

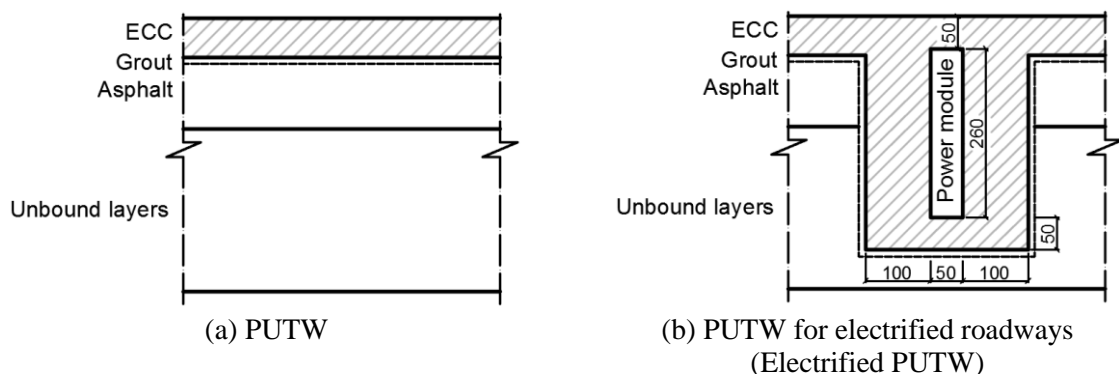


Figure 4-12: The proposed PUTW pavement structures

The structure PUTW for electrified roadways (electrified PUTW) is the same as normal PUTW except for the culvert to accommodate the S-Type power supply module of the latest KAIST OLEV system (5G). The purpose of the culvert is to protect and position the power supply modules precisely. The operating air-gap of the S-type power supply rails is 20 cm (Choi, et al., 2015). According to figure 4 in (Choi, et al., 2015), it is noticed that this air-gap is actually the gaps between power supply and pick-up coils. The actual air-gap is then 20 cm minus the pavement cover thickness over the power supply module. This air-gap needs to meet the road regulation for example 12cm in Korea and 16cm in Japan (Huh, et al., 2011). Therefore, 5 cm culvert's top cover thickness is proposed and this thickness is independent on the actual PUTW slab thickness. In operation, the power supply rails tend to generate heat (as discussed in section 3.3). Inside the pavement in Singapore as in Figure 4-12 (b), the ambient temperature around the power supply module varies from about 28 to 35°C, which might raise the saturated operating temperature to about 43-50°C. These temperatures will influence significantly the performance of asphalt if there is a direct contact. The culvert helps to separate the heat source away asphalt layers. With the thickness of 100 mm, the heat transferred from the power supply module to the asphalt is expected to be defused to a lower value than the heat transfer from the surface of the pavement. Moreover, there is a discontinuity in asphalt layer when there are electrified roadway components in the pavement. This creates weak edges in asphalt because of the similar effect to edge loading in

concrete pavement. The walls of the culvert are expected to behave like abutments, which help ECC slab bridging the gap better as well as reduce the load acting on asphalt layer.

In construction of PUTW for electrified roadways, PUTW slabs with the culvert will be installed first then followed by sliding the power supply modules into the culvert. At joints, the culvert can be sealed, for example by using epoxy or foam, to prevent mortar and aggregate coming into the culvert. Using this method, maintenance of the power supply modules later can be done easily. If the power supply modules need to be maintained not at the end of the pavement life, only a part of the pavement at the beginning of the electrified roadway needs to be opened and the power supply module will be slides out from there. Moreover, if a technical box for maintenance of the modules are available, PUTW pavement can remain untouched. The use of precast slab with the culvert also creates another advantage in implementation scheduling and planning for electrified roadways. Because road (and bus stop) pavements have to be repaired and rehabilitation from time to time. If a section of road or bus stop is planned to be electrified in the future, at the time of rehabilitation, PUTW slab with the culvert will be directly used (even without power modules) with a little additional cost compared to a normal PUTW. The power supply modules will be installed later to the channels when needed. Therefore, the implementation schedule of electrification of road network can somehow base on the maintenance and rehabilitation plan of the road pavement to save cost.

4.5 Research on the Precast Ultra-Thin Whitetopping (PUTW)

There are several research questions that need to be answered in order to develop the PUTW (including PUTW for electrified roadways) concept successfully:

- How is the structural performance of the PUTW pavement?
 - What are the pavement material's properties and performance?
 - Is there enough bond strength at the composite interface?
 - What is the design of the PUTW?
- How is the functional performance of the PUTW pavement?
- Is PUTW an economical solution?
- What are the guidelines for PUTW implementation?

5 Engineered Cementitious Composite (ECC) material for Precast Ultra-Thin Whitetopping (PUTW)

5.1 Introduction

Engineered Cementitious Composite (ECC) is a unique type of high performance fiber-reinforced cementitious composite. The most distinctive characteristic of ECC is high tensile ductility that is achieved by the formation of multiple microcracks. These cracks, which carry increasing load after formation, allow the material to exhibit strain-hardening similar to ductile metals (Li, et al., 2004). Figure 5-1 illustrates a typical uniaxial tensile stress-strain curve as well as crack width development of ECC. After matrix first cracking (at strain about 0.01%), early crack keeps opening to about 60-80 μm at about 1% strain. Further loading beyond this point, the straining is accommodated through the formation of additional multiple microcracks. The tensile strain capacity of ECC is several hundred times that of normal concrete. The crack width, however, is seized at a steady value of 60-80 μm . After saturation of multiple microcracks, ECC fails with a single localized crack and increased deformation (Li, et al., 2004) (Nawy, 2008).

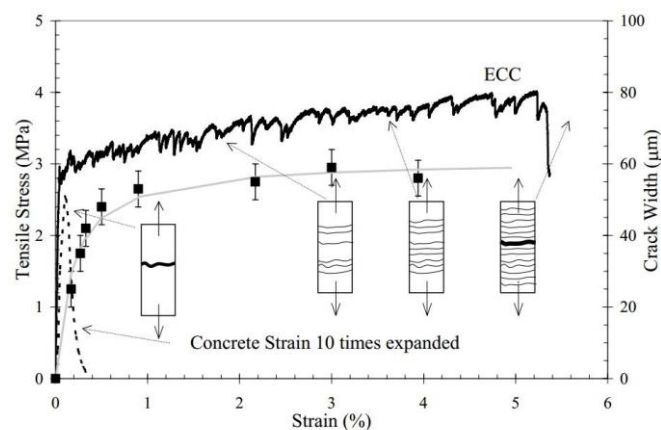


Figure 5-1: Typical uniaxial tensile stress-strain curve and crack width development of ECC material (Li et al., 2004)

The compression strength of ECC is quite similar to normal or high strength concrete (30 MPa to 90 MPa). Modulus of elasticity of ECC is about 20-25 GPa, which is slightly lower than that of normal concrete due to the absence of coarse aggregate in ECC mix design. The compressive strain capacity, on the other hand, is slightly higher than that of normal concrete (0.45-0.65%). ECC exhibits a very high flexural strength (modulus of rupture or MOR). An MOR of 10-15 MPa is “easily achievable and accompanied by a large extent of deflection hardening regime” by altering the brittle failure mode into a ductile failure mode under bending due to the high ductility of ECC material (Nawy, 2008).

PUTW uses very thin precast slabs. These slabs have to be durable enough to withstand the construction load (slabs lifting with all impact factors) as to be mentioned in chapter 7. The slabs are too thin that using reinforcement mesh is not an option. Moreover, metallic reinforcement mesh is not possible for PUTW for electrified roadways as presented in Chapter 3, because the metallic material will interfere with the electromagnetic field. Therefore, ECC material is chosen as a potential candidate for PUTW.

However, ECC is a cementitious material with typical fine aggregates in the mix design. So it may not provide enough grip on the surface. Therefore, surface treatments by using coarse aggregate in the ECC mixture and surface texture should be introduced to mitigate the negative impact of accidents by skidding.

Therefore, this chapter focuses on developing new versions for both ECC structural layer and ECC functional layer of PUTW. Firstly, the review about previous application of ECC in transportation will be done. A new version of ECC will be developed for the structural layer of PUTW slabs. The properties of this new version of ECC will be identified by laboratory monotonic (static) and fatigue tests. These material properties will be used to verify the material model in FEMs.

The chapter will continue by the introduction of skid resistance in pavement's surface, its requirements and measurement methods. Another version of ECC for the pavement surface will be also developed to fulfil the requirements for surface skid resistance. Lab testing will be designed to evaluate the surface performance of this new version of ECC.

5.2 ECC in transportation related applications

In transportation related applications, ECC has been used in a number of repair and rehabilitation projects. Two of these are a bridge deck patch repair and a bridge deck link slab application in Michigan, USA. For the bridge deck patch repair, a part of 7 m x 9 m patch work was casted with ECC and the remaining portion was casted with commercially available concrete repair material for comparison. After traffic reopening, the project was being well monitored over time. After four months, some microcracks of roughly 50 μm width appeared on ECC surface, while normal patch material showed cracks up to 2 mm and was surrounded by deteriorated and spalling concrete. After ten months, the concrete patch was severely damaged, while ECC still kept the cracks tight at 50 μm . The conclusion for this project was that, under the same loading condition, ECC outperforms concrete repair material (Li, et al., 2004). Bridge deck link slab application was another example of ECC used in transportation application. A link slab is 'a connector between two adjacent simple bridge spans, creating a continuous deck to prevent leaking while absorbing the thermal deformation of spans which are typically accommodated by expansion joints'. With the use of ECC, the need for heavy reinforcement, which is usually the case for the concrete link slab, can be significantly reduced or even eliminated. With low (or no) steel reinforcement and very high tensile capacity, ECC can form a very flexible link slab which is very desirable. Full scale laboratory testing of link slabs showed that ECC link slab had far superior performance over normal concrete slab under fatigue loading. After 100,000 loading cycles, ECC link slab maintained crack width at 50 μm while concrete link slab showed crack width up to 0.6 mm (Li, et al., 2004). There was no pavement surface treatment mentioned for the two applications.

5.3 ECC for structural layer of PUTW

In collaboration with Nanyang Technological University (NTU), a new version of ECC was developed for the project. A typical ECC (ECC-M45) mix design includes cement, coal fly ash, silica sand, water, high range water reducer and polyvinyl alcohol (PVA) fiber. Material such as coal fly ash and micro-silica sand were initially more difficult to obtain in Singapore locally. Therefore, the alternative is to use ground granulated blast-furnace slag (GGBS) and river sands instead of coal fly ash and micro-silica sand, respectively.

The raw materials of this version of ECC (called local ECC) include Type I OPC (CEM I 42.5), GGBS provided by Engro Co. Ltd, river sands sieved to below 600 μm in particle size, and PVA fibers from Kuraray Co. Ltd. The fibers are 12 mm in length and 39 μm in diameter, the nominal fiber strength is 1600 MPa. Superplasticizer (SP) was also included to ensure the workability of ECC.

Changing the content of supplementary cementitious materials like GGBS can greatly alter the mechanical properties of ECC (Chen, et al., 2013) (Yang, et al., 2007). In the current study, three different mix designs, which vary in the OPC replacement ratio by GGBS, were investigated. The details are shown in Table 5-1.

Table 5-1: Proportions of mix design in current study

Test No.	OPC (kg/m ³)	GGBS (kg/m ³)	Sand (kg/m ³)	Water (kg/m ³)	PVA fiber (kg/m ³)	SP (liter/m ³)	GGBS/ binder ratio	W/b ratio
GGBS0	1411	0	282	423	26	3.6	0%	0.30
GGBS30	976	418	279	418	26	3.0	30%	0.30
GGBS60	551	827	276	414	26	2.4	60%	0.30

The mixing of local ECC follows the typical ECC procedure. Firstly, aggregates including cement, sand, GGBS are mixed with a mixer for two minutes. Water and superplasticizer were slowly added to the mixture at a low mixing speed within one minute, followed by medium mixing speed for two minutes to assure the viscosity of the mixture. PVA fibers were then slowly added to the mixture at a low mixing speed within one minute, followed by medium mixing speed for three minutes. Finally, the fresh mixture was casted into different mould types for specific experimental purposes.

The dog-bone specimens (as recommended by (Kim, et al., 2007)) were used for monotonic (static) uniaxial tensile tests. Cube specimens (50×50×50 mm), coupon specimens (300×75×12 mm, depth = 12 mm), and prism specimens (280×70×50 mm, depth = 50 mm) were casted for compressive tests, four-point flexural tests, and fatigue four-point flexural tests, respectively. The samples were demoulded after one day and cured in the lab air temperature 20°C for a total of at least 28 days before the testing day.

Series of monotonic (static) tests, including uniaxial tensile tests, compressive tests, and four-point flexural tests, were conducted to characterize local ECC's mechanical properties. Displacement-controlled uniaxial tensile tests were conducted on dog-bone specimens with an Instron 5569 UTM machine, where two LVDTs were used to determine the extension of the middle uniform part of specimens. The loading rate of the tensile test was 0.04 mm/min. Load-controlled compressive tests were used to determine the compressive strength, where the loading rate was 0.25 MPa/s. Displacement-controlled four-point flexural tests were conducted on coupon specimens with the same Instron UTM machine, where the three spans were all 80mm. The loading rate of the flexural test was 0.7 mm/min.

Among the three mix designs, GGBS60 with highest MOR in monotonic (static) test was selected to verify the resistance against fatigue loads. In order to determine the fatigue performance of GGBS60 ECC, both monotonic and fatigue flexural tests were conducted. The Instron UTM testing equipment has a limited magnitude of deflection in fatigue tests. Therefore, prisms (280×70×50 mm) instead of coupon (300×75×12 mm) specimens were used to control the deflection within the testing machine's capacity in fatigue tests.

Modulus of rupture (MOR) of GGBS60 was determined by the monotonic (static) tests. These static tests were displacement-controlled and conducted in the same scheme as mentioned earlier except for a lower loading rate (0.2 mm/min). The fatigue tests were load-controlled and the loading scheme is described as follows: the load at valley was 0.20 MOR, while the load at peak ranging from 0.85 MOR to 0.95 MOR. Before the start of sinusoidal fatigue of 8 Hz, the load was increased monotonically to the medium value of the maximum and the minimum load within two minutes (Figure 5-2). The tests were stopped once the deflection reached 10 mm, at which the specimens would certainly fail according to the results of monotonic tests. The cycle numbers at failure were recorded for producing the fatigue curve.

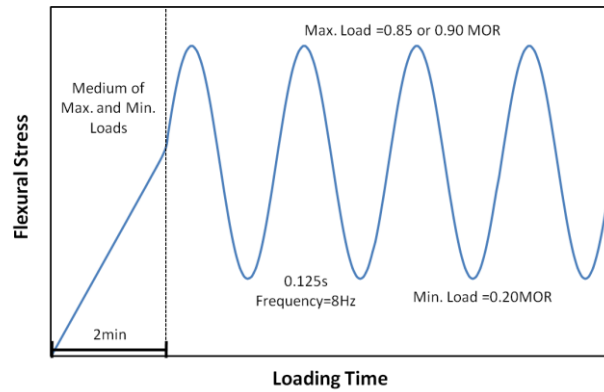


Figure 5-2: Loading scheme of fatigue test

Monotonic test results of GGBS0, 30, and 60 are summarized in Table 5-2. The values are the average of at least three specimens. Equivalent flexural stress was calculated with equation 5-1.

$$\text{Equivalent flexural stress} = 6M/bh^2 \quad 5-1$$

Where:

- M : are the moment at the middle span,
- b, h : coupon width, and coupon thickness, respectively.

Table 5-2: Summary of monotonic test results

Test No.	Tension		Compression	Four-point bending	
	Tensile strength (MPa)	Tensile ductility (%)	Compressive strength (MPa)	MOR (MPa)	Deflection at failure (mm)
GGBS0	4.25±0.48	1.12±0.36	63.1±3.8	10.77±0.98	7.57±2.51
GGBS30	4.40±0.19	1.05±0.07	66.3±3.7	10.56±1.80	9.58±3.31
GGBS60	4.88±0.62	1.26±0.28	70.8±1.8	12.90±0.66	18.93±1.19

It is seen from Table 5-2 that all of the three mix design achieved relatively high MOR (above 10 MPa), and the variation of GGBS content had a great impact on mechanical properties of ECC. GGBS60 showed the highest MOR, resulting from the highest tensile strength (about 5 MPa), moderate tensile ductility (above 1%), and sufficient compressive strength (about 70 MPa). The high tensile strength of GGBS60 resulted from the consumption of $\text{Ca}(\text{OH})_2$, the weakest part in the matrix, by the later hydration of GGBS (Neville, 2011).

Figure 5-3 shows the flexural stress-fatigue life (S-N) curve of conventional concrete (Byung Hwan Oh, 1991), PVA ECC-M45 (Qian, et al., 2013), and local ECC (GGBS60). It is clearly shown that with the same fatigue life, the fatigue strength by PVA ECC-M45 is about twice that of conventional concrete, and local ECC further enhances the fatigue strength. During fatigue load, multiple cracks gradually developed and fiber-bridging across crack surfaces helped to sustain the load. Due to fiber-bridging degradation, the fiber-bridging in one of these cracks eventually failed to sustain the load and result in specimen failure. Compared with PVA-ECC M45, the superior fatigue performance of local ECC resulted from aforementioned higher MOR as well as a slower decrease of flexural strength with increasing fatigue life, which implies that inclusion of GGBS or longer fibers (PVA fiber length in current study = 12 mm) may improve the fiber-bridging across crack surfaces under fatigue load.

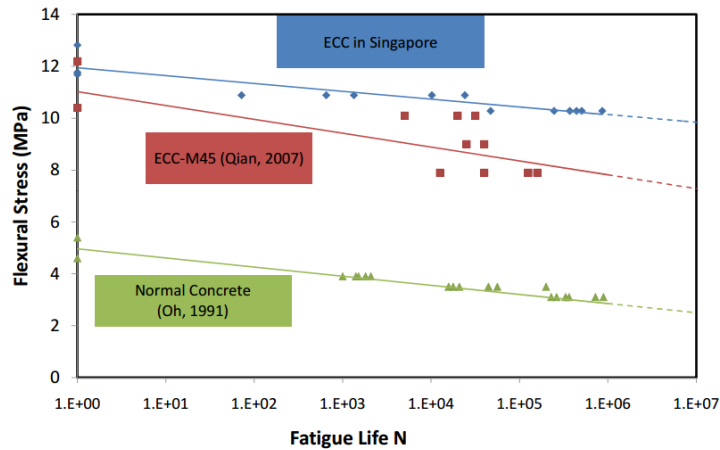


Figure 5-3: Fatigue response of ECC and normal concrete under four-point bending

5.4 Verification of ECC material model in ANSYS

When finite element analysis is taken into account, ECC is considered as a complicated non-linear material where behaviour in tension and compression are greatly different. Therefore, the material model has to be verified before using in a full pavement finite element model. A four-point bending finite element model is built based on laboratory test set up (Figure 5-4 and Figure 5-5). The non-linear behaviour of ECC is simplified into multi-linear stress-strain relation and modelled in ANSYS using CAST IRON plasticity material model. This material model allows inputting stress-strain relation in tension and compression separately. The input to the materials model is based on the uniaxial tensile test results and is summarized in Table 5-5



Figure 5-4: Four-point bending test setup
(Courtesy of Mr. Jishen Qiu, NTU)

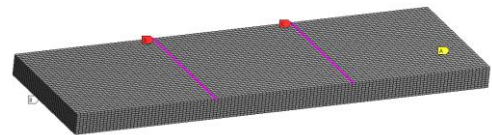


Figure 5-5: 3D FEM of Four-point bending test

Table 5-3: Input parameters to the materials model in ANSYS

	First transition point		Second transition point		Third transition point	
	ϵ	σ (MPa)	ϵ	σ (MPa)	ϵ	σ (MPa)
Tension	0.0125%	2.50	0.25%	2.55	3%	4.50
Compression	0.2%	40	0.25%	45	N.A.	N.A.

Figure 5-6 compares the simulated flexural stress-deflection response of four-point bending tests with the experimental results. As it can be seen, the cast-iron plasticity model can successfully capture the non-linearity of ECC and the flexural behavior of ECC can be accurately predicted.

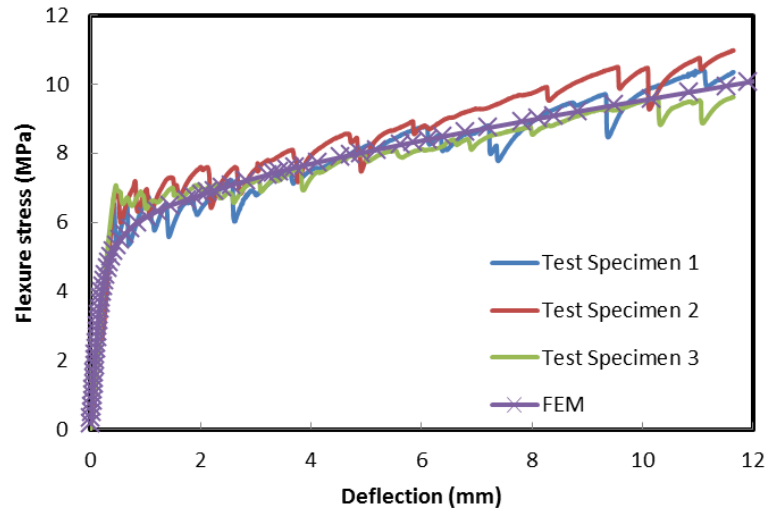


Figure 5-6: The verification of ECC material model for FEM

5.5 ECC for pavement surface

5.5.1 Introduction

ECC might not provide enough road grips due to the lack of large sand and larger size aggregates. This low skid resistance (friction) is a potential danger to road users. It is not an easy task to quantify the relationship between pavement surface friction and skidding accidents. However, several studies showed that the number of wet-skid accidents decreases as the pavement surface friction increases. Pavement friction was evaluated by Giles et al. (1962) at 120 sites, where skid-related crashes had occurred. The authors concluded that the risk of a skid-related crash was small for friction values (Skid Number - SN) above 60, but increased for SN below 50. Research done by Swedish National Road and Transport Research Institute concluded that there is a strong correlation between skid resistance and accident risk (Wallman & Astrom, 2001), as increasing pavement friction does reduce crash rates significantly. Therefore, surface treatments should be introduced to mitigate the negative impact of accidents by skidding.

There are several methods to improve skid resistance of concrete pavement surface. These include broom drag, turf drag, burlap drag, tining, grinding, etc (Hall, et al., 2009). Detail descriptions of these methods are listed in the Appendix A.1.

The skid resistance is provided by surface micro and macro textures (see Figure 5-7). The micro texture is provided by the aggregates. And the macro texture is normally provided by larger textures imprinted on the pavement surface by grinding for example.

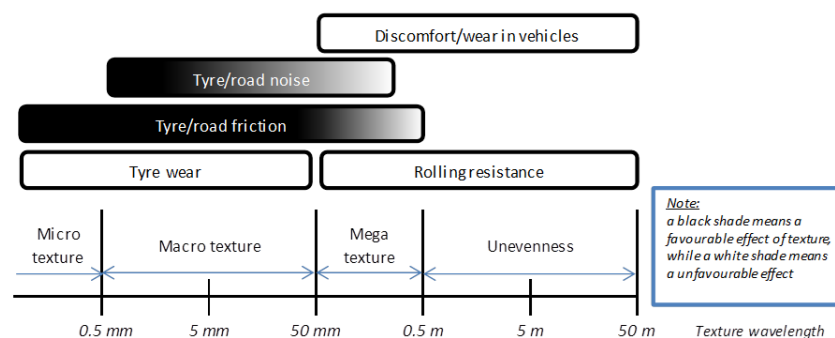


Figure 5-7: Type of pavement surface textures (Hall, et al., 2009)

This part focuses on developing a new version of ECC that can fulfil the Singapore skid resistance requirement for a new road.

5.5.2 Skid resistance measurement methods

There are two types of skid measurement equipment based on their mechanism, namely high-speed friction measurement equipment and low-speed or stationary that might require a lane closure. High-speed friction measurement equipment is commonly categorized into four types, i.e. locked wheel testers, side force devices, fixed slip devices and variable slip devices. Three low-speed measurement methods include stopping distance measurement, deceleration rate measurement and portable testers. The summary of skid resistance measurement testing methods are summarized in the Appendix A.1.

At the laboratory scale, the skid resistance measurements were done using British Pendulum Skid Resistance Tester (BPT), which is commonly used by many agencies. The macro texture is measured using sand patch method (SPM). Even though the test was mainly designed for in-situ test, but it can also apply to laboratory scale.

5.5.3 Requirement values for skid resistance

According to Code of Practice for Works on Public Streets (LTA, 2015) and Materials and Workmanship specification (LTA, 2010), skid resistance requirement for new concrete road surface is 65 BPN (British Pendulum Number). However, the intervention phase will be taken when the skid resistance value reaches 55 BPN for expressway and 45 BPN for both major and minor roads. The requirement values for skid resistance in Singapore as mentioned above are of the highest internationally as listed in Table 5-4 and Table 5-5 below:

Table 5-4: Standards of skid resistance for new road of many countries in BPN scale

Country	Method	Grade	Grade equivalent to BPN		
Singapore	British Pendulum Tester (BPT)	65	65		
Germany	μ SCRIM (SFC)	0.46	48 ¹⁾	50 ²⁾	60 ³⁾
UK (TRRL)	BPT	55	55		
Canada	Skid Number	40	52		
USA	Skid Number	40	52		

Table 5-5: Standards of skid resistance for the intervention level (in BPN scale) of major and minor roads

Country	Method	Grade	Grade equivalent to BPN		
Singapore	μ SCRIM (SFC)	0.35	37 ¹⁾	42 ²⁾	45 ³⁾
Germany	μ SCRIM (SFC)	0.4	42 ¹⁾	52 ²⁾	52 ³⁾
UK	μ SCRIM (SFC)	0.35	37 ¹⁾	42 ²⁾	45 ³⁾
Australia	μ SCRIM (SFC)	0.35	37 ¹⁾	42 ²⁾	45 ³⁾
New Zealand	μ SCRIM (SFC)	0.35	37 ¹⁾	42 ²⁾	45 ³⁾
USA	Skid Number	30	38.96		

1) Converted based on UK Highway Agency equations (UK Highway Agency, 2004)

2) Converted based on Chile HD equations (Hall, et al., 2009)

3) Converted based on Transit NZ equations (NZ Transport Agency, 2013)

5.5.4 Developing a new version ECC for pavement surface

Sahmaran et al. (2009) mentioned that the aggregate size might not affect the properties of ECC. During his research, he found that the flexural strength of ECC with gravel-sand with maximum aggregate size of 2.38 mm is high with 11.56 ± 1.35 MPa. Therefore, this research focuses on tailoring ECC by adopting larger aggregates in the mixture to fulfil the Singapore requirement on skid resistance. There are some aggregates that can be used for improving road grip, for example, granite, steel slag and corundum. Granite and steel slag have been used for surface treatments in Singapore. However, the results are still not impressive (Yurong, et al., 2001). Corundum is proposed to be used in this research.

Corundum is a crystalline form of aluminium oxide (Al_2O_3) and other substances as shown in Table 5-6. Corundum can be easily found locally in Asia. Corundum is extremely hard material, which is rated at nine on Mohs scale of mineral hardness (diamond rated as 10, while the most common mineral in aggregates, quartz, only rated as 7) that can scratch almost every other mineral (Tubey & Hosking, 1972). Application of surface treatment using corundum was reported to improve the skid resistance by Swiss experience. According to Rolf Werner et al. (2010), corundum material with the sizes of 1 to 3 mm has been applied to provide a high grip of the road surface by spraying an evaporative protection and followed by covering area with thermo mats. Moreover, corundum is well known for its abrasiveness and considered as one of the hardest material, it is expected to provide a long-term performance of skid resistance

Table 5-6: Chemical specification of Corundum

Chemical Specification (%)						
SiO ₂	Al ₂ O ₃	Fe ₂ O ₃	TiO ₂	CaO	MgO	FeO
14.61	61.80	12.25	8.14	N.A	N.A	N.A

Typical ECC (M45) mixture design in (Li, 2007) was adopted and modified to include corundum aggregate. In the versions of ECC with corundum, specific percentage (50%-100%) of fine sand in ECC-M45 was replaced with corundum as shown in Table 5-7.

Table 5-7: Mixture design of ECC and surface treatment of ECC mixed with Corundum

Test No.	OPC (kg/m ³)	Fly ash (kg/m ³)	Sand (kg/m ³)	Corundum (kg/m ³)	Water (kg/m ³)	PVA fiber (kg/m ³)	SP (Kg/m ³)	FA/C ratio	W/b ratio
ECC (M45)	559	671	447	0	327	26	2.3	1.2	0.27
ECC-Cor50	559	671	223.5	223.5	327	26	2.3	1.2	0.27
ECC-Cor60	559	671	178.8	268.2	327	26	2.3	1.2	0.27
ECC-Cor70	559	671	134.1	312.9	327	26	2.3	1.2	0.27
ECC-Cor80	559	671	89.4	357.6	327	26	2.3	1.2	0.27
ECC-Cor90	559	671	44.7	402.3	327	26	2.3	1.2	0.27
ECC-Cor100	559	671	0	447	327	26	2.3	1.2	0.27

The mixing of ECC with corundum followed the typical ECC mixing procedure as mentioned in section 5.3. There were three types of samples to be prepared: prism samples for flexural strength tests, slab samples with flat surface for skid resistance test, and slab samples with grooving (see Figure 5-8) for skid resistance test. The prism specimens had dimensions of 280×70×50 mm, depth = 50 mm. Slab specimens for skid resistance tests had dimensions of 206 x 206 x 10 mm. The casting process for slab samples was done using the bottom-up procedure. This was due to the reason that on the bottom face, it was relatively easier to make the surface flat by the mould's surface. All of the samples were demoulded after one day. The corundum aggregates on the slab surface were exposed using steel brush

right after demoulding. The exposing process had to be done as early as possible to assure the workability. That was because it took much more effort to expose the corundum when the surface was hardened for some more days.

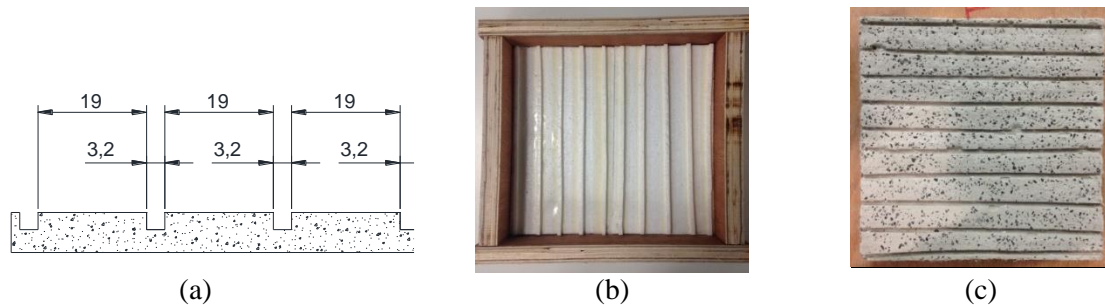


Figure 5-8: (a) Expected grooving on slab surface. (b) Mould with grooving plate. (c) Final slabs

The flexural strength of different ECC mixtures with corundum were tested using four-point bending tensile machine test in accordance with ASTM D 6272 (ASTM, 2010). Four specimens from each mixture with a dimension of 280 x 50 x 70 were tested.

The results of four-point bending tests are summarized in Figure 5-9. The flexural strength of all specimens remains very high. The amount of corundum within the matrix does not have a strong correlation with the flexural strength of ECC. The ECC-Cor60 has the highest mean and median values. Mixtures of ECC-Cor70 have the lowest flexural strength (mean and median values) among all the mixtures with an average of approximately 8.8 MPa. The lower flexure strength of ECC-Cor70 can be explained by the material segregation that was observed after mixing. This leads to a recommendation that even ECC with corundum is used for a functional layer, the mixing process of ECC with corundum has to be very well controlled to achieve high and consistent quality ECC.

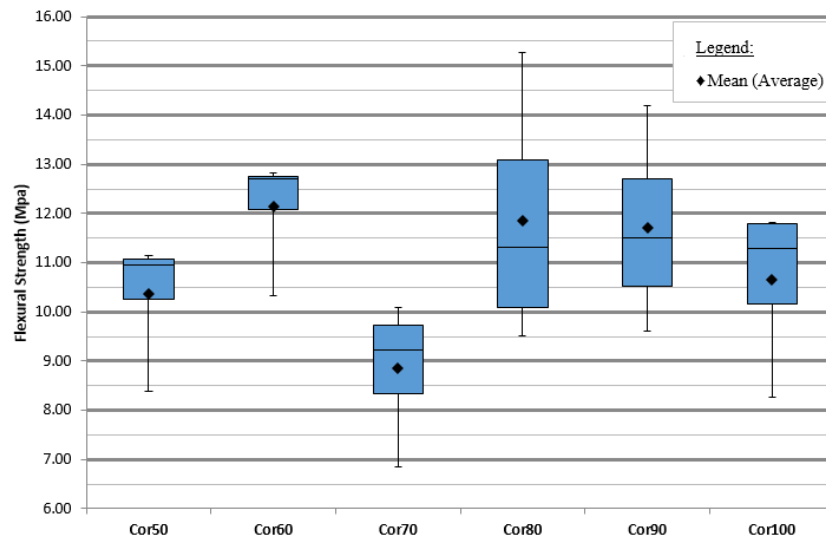


Figure 5-9: Flexural strength of ECC with corundum at 28 days

5.5.5 Lab tests on skid resistance for pavement surface made of ECC with corundum

In this research, three measurement methods were used: British Pendulum Tester (BPT), Sand Patch Method (SPM), and Wheel Tracking Machine (WTM). BPT was used for measuring skid resistance in BPN scale (see Figure 5-10). Measurements of skid resistance were assessed based on the standard ASTM E 303 (1993). SPM test has been conducted for determining macrotexture (see Figure 5-11). To measuring macrotexture depth, which is measured in Mean Texture Depth (MTD), the test using the volumetric technique which follows ASTM Standard E965 – 96 (2015). According to the standard, the macrotexture depth is the results of the application of a known volume of material (which is normally

using a specific size of glass beads or sands) on the surface and subsequent measurement of the total area covered. The Wheel Tracking Machine (WTM) was used to evaluate the long term durability of the surface treatments (see Figure 5-12). WTM consists of a rubber wheel that is able to rotate at 42 cycles per minute with an applying load of approximately 520 N. The trafficking simulation was executed with 100,000 wheel-passes. Woodward, et al. (2013) indicated that these 100,000 wheel-passes are equivalent to 5 to 10 years of real traffic. Due to lack of ability to apply braking or acceleration forces, this WTM is not the best method to evaluate the long-term performance of the surface treatment. However, it still gives a good indication about long term behaviour of the surface.



Figure 5-10: British Pendulum Tester (BPT)

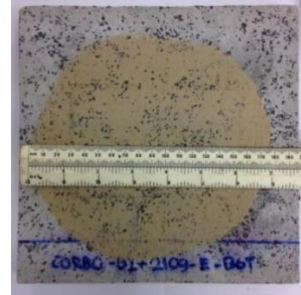


Figure 5-11: Sand Patch Method (SPM)



Figure 5-12: Wheel Tracking Machine

The results of BPT tests are plotted in Figure 5-13. ECC-M45 samples have pretty high PBN compared with exposed ECC with corundum in dry condition. This phenomenon happened because of the rough surface creating by fines and fibers that remained on the surface. However, fines were washed away during the test on wet condition. Therefore, the skid resistance of plain ECC-M45 drops significantly to an average of 52 BPN, which is much lower than requirement for new road in Singapore.

For the samples with corundum in the mixture, the general trend is that the BPN increases together with amount of corundum used. However, the changes are relative small. And most importantly, even with the least corundum used, ECC-Cor50 still fulfils the Singapore skid resistance requirement for new road.

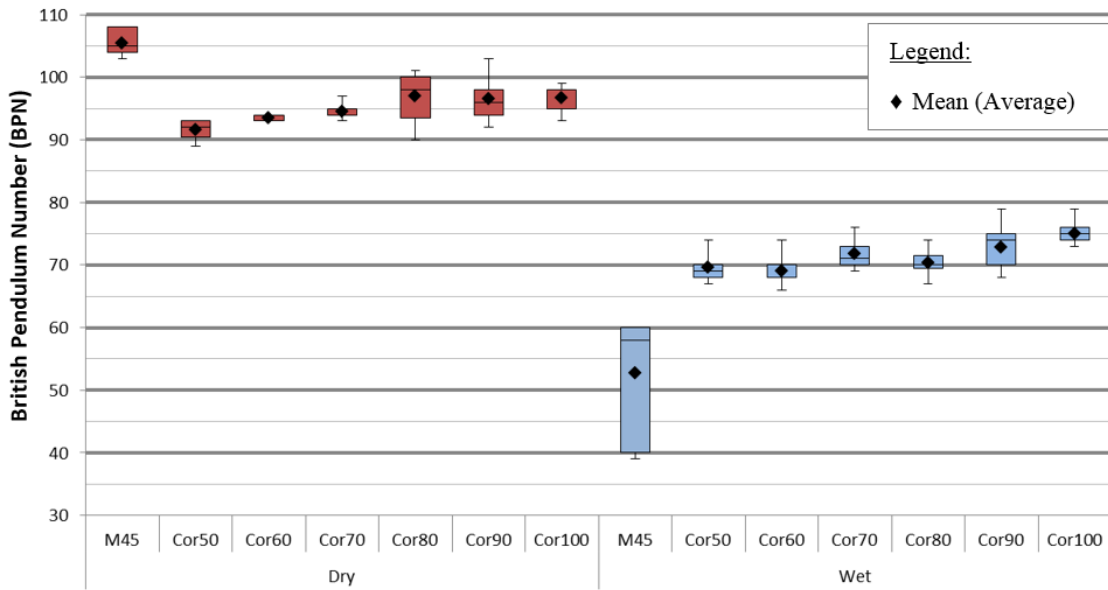


Figure 5-13: Skid resistance of exposed ECC with corundum versus typical ECC (M45)

Longitudinal textures on pavement surface are introduced to reduce road-tyre noise while transversal textures aim for higher skid resistance and better drainage. The influence of grooving textures on skid resistance of exposed ECC with corundum was studied. Figure 5-14 presents the influence of transversal and longitudinal grooving textures on BPN for ECC-Cor80 as an example. It can be clearly seen that transversal grooving textures improve the skid resistance significantly while longitudinal textures lower BPN slightly in wet condition. However, the average value of the samples with longitudinal textures still above the requirement of 65 BPN. In application, surface with transversal grooving at even distance is not recommended because it can increase road-tyre noise.

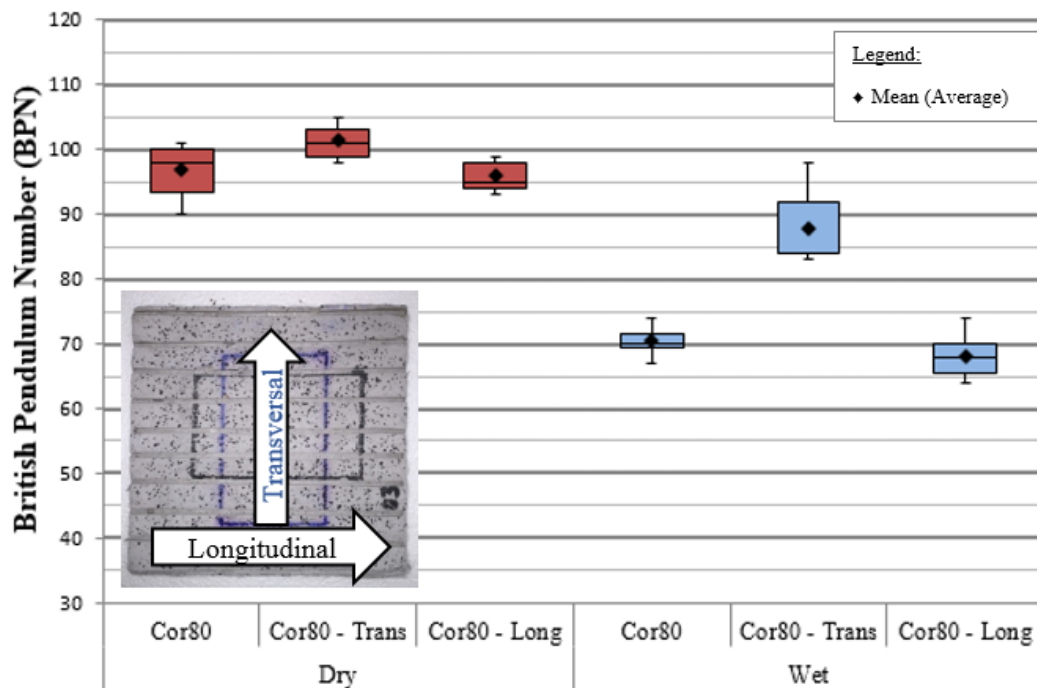


Figure 5-14: The influence of transversal and longitudinal grooving textures on skid resistance

Sand patch method (SPM) tests indicated that there were no significant macrotexture for ECC-M45. The Mean Texture Depth (MTD) results for these specimens were very low with only 0.09 to 0.10 mm.

While for exposed specimens of ECC with corundum, the MTDs were slightly higher with an average of 0.35. With the same test SPM, specimens with grooving textures produced the highest MTD with an average of 1.03 mm. It is clear that the bigger cross-section area of the groove, the smaller diameter of the area covered by the sands which are the higher MTD resulted. Even though there is no standard for the Mean Texture Depth (MTD), the results can be used as a reference because macro textures can help to avoid hydroplaning effect and they are responsible for road-tyre noise.

ECC-Cor50 and ECC-Cor100 were chosen for evaluation the long-term durability of the surface skid resistance using Wheel Tracking Machine (WTM) tests. During the traffic simulation, the tests were stopped in between to measure BPN. The results are summarized in Figure 5-15. Even after 100,000 of load cycles, which is equivalent to 5 to 10 years of traffic, the exposed surface of ECC with corundum still gives higher BPN than the requirement for a new road in Singapore (65 BPN). Moreover, if the trends continue in the same manner. The skid resistances are still above 60 BPNs, after 100 million load cycles. This value is much higher than the requirement for intervention level at 45 BPN. It can be concluded that the skid resistance can last until the end of the pavement life time without any further intervention.

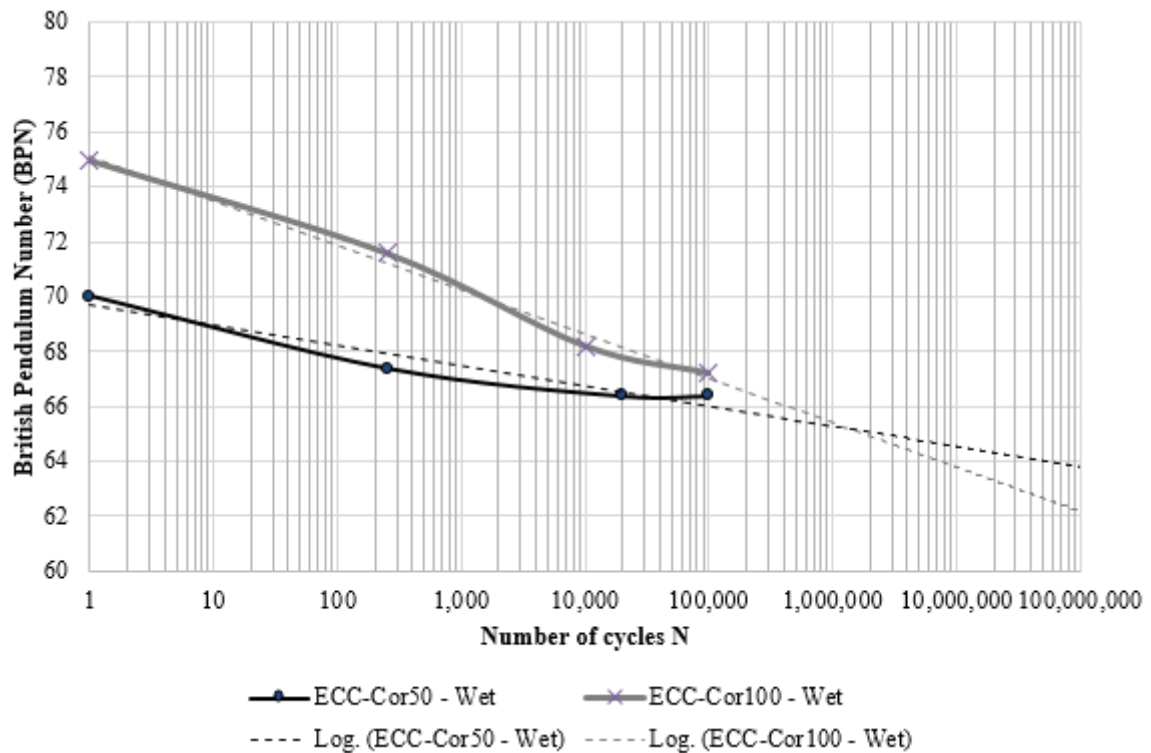


Figure 5-15: Long-term performance of ECC with corundum regarding skid resistance

5.6 Compatibility of ECC material to wireless power transfer

As stated in (OLEV Tech, 2015), concrete and asphalt are transparent to magnetic field at 20 kHz, which the OLEV system is using. In order to confirm that ECC is also transparent to the magnetic field, an effort to test the compatibility of ECC with a much smaller power transfer system has been done in collaboration with NTU. A coil with diameter of 30 cm, which has capability to transfer 2 kW power at the airgaps 16cm with efficiency of 80-90%, is casted into an ECC slab. Figure 5-16 (a) shows the coil set of the configuration and the slab which has coil embedded. Power transferred and efficiency were tested in the lab. And the conclusion from the electrical engineers was that the power transferred and efficiency remained the same and operated normally even when the coil was encased. Figure 5-16 (b) and (c) show the powered slab that can power the lamp and charge the EV. In summary, ECC is confirmed not to interfere the magnetic field.

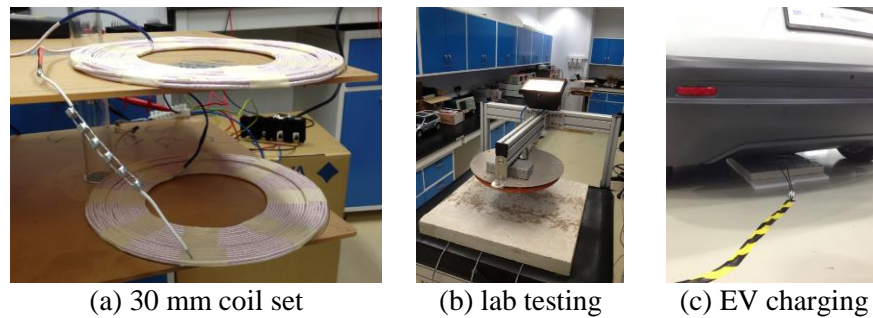


Figure 5-16: small scale testing of the transparency of ECC material to magnetic field

5.7 Conclusion

This chapter focused on developing new versions of ECC for PUTW pavement in both structural layer and surface functional layer. Firstly, the review about previous application of ECC in transportation was done. A new version of ECC was developed for structural layer of PUTW slabs. The new version of ECC for structural layer uses ground granulated blast-furnace slag (GGBS) and river sands instead of micro-silica sand and coal fly ash that are used in typical ECC. Three different mix designs, which vary in the OPC replacement ratio by GGBS, were investigated. The GGBS60 (called local ECC) showed the highest MOR, resulting from the highest tensile strength (about 5 MPa), moderate tensile ductility (above 1%). GGBS60 was chosen for further investigation in fatigue performance. The results from fatigue tests indicated that the local ECC has superior fatigue performance, which is even better than typical ECC-M45. Moreover, ECC material doesn't influence the electromagnetic fields. In addition, the non-linearity of ECC material model was also successfully calibrated in FEM for further application.

Skid resistance of pavement is a very important factor for road safety. Literature review on skid resistance regarding the importance of skid resistance, methods to improve skid resistance, methods for measurement of skid resistance, and requirement values for skid resistance in Singapore have been done. In this chapter, corundum aggregate, an extremely hard material, was successfully integrated in ECC mixture. The new version of ECC, with a certain percentage of sand replacement by corundum (50%-100%) in the mixture, still maintained very high flexural strength of a typical ECC. This new version of ECC, with exposed surface by steel brushing in one day after casting, significantly improved the skid resistance compared to a typical ECC-M45. With corundum in the mixture, ECC gave higher skid resistance than the requirement for a new road in Singapore (65 BPN) even after 100,000 load cycles, which is equivalent to 5 to 10 years of trafficking. And for the whole pavement lifetime, the skid resistance remains above 60 BPN, which is much higher than the Singapore requirement for intervention level at 55 BPN for expressway or 45 BPN for other roads. The skid resistance can be slightly compromised by using longitudinal grooving textures to reduce road-tyre noise. It can be concluded that the skid resistance can last until the end of the pavement life time without any further intervention.

6 Interface bonding in Precast Ultra-Thin Whitetopping (PUTW)

6.1 Introduction

The importance of bonding of the composite layer is a common issue in asphalt pavement research and engineering. The flexural stress in the asphalt wearing course layer in Construction Class 100 (BKL100) in Germany increase by 30% when there is no interconnection between asphalt layers. The poor bond between asphalt layers may lead to 35 to 40% greater rut depth with the same number of load cycles (Eisenmann, 1984) (Eisenmann & Neumann, 1993) (Eid, 2012)

In PUTW, concrete and asphalt layer are bonded together by grouting to form a composite layer. The good bonding strength is the foundation for a durable and long term performance of the system. In the absent of any load transfer devices (dowel bar or tie bar), bonding ensures the positions of PUTW slabs. If there is no bonding, the PUTW slab will drift or even endanger road users. And moreover, similar to UTW, the bonding is particularly important for the load transfer between slabs (Pereira, et al., 2006) (Eid, 2012).

This chapter will study whether there is a good and sufficient bond in PUTW pavement. Firstly, the methods for calculating horizontal interface shear stress under traffic loading will be presented. Together with calculation using formulas, a frequently used BISAR software (Shell International Oil Products B.V., 1998) will be also used to calibrate the FEMs. The ECC non-linear material model will be later inserted into the calibrated FEMs for calculating the required interface shear strength for PUTW. The chapter will follow with laboratory experiments to study actual interface bond strength.

6.2 Calculation of horizontal interface shear stresses in PUTW

6.2.1 Reference pavement structure

There are three methods used to calculate horizontal interface shear stresses presenting in this part. These methods include closed form formulas, BISAR software (Shell International Oil Products B.V., 1998) and FEM developed in ANSYS. For the purpose of calculating horizontal shear stresses at the composite interfaces in PUTW, a reference PUTW structure is proposed as Figure 6-1. In BISAR and FEM, ECC and grout are simulated as two individual layers bonded to each other. However, in the approximate solution using formulas, ECC and grout are simplified to be one homogeneous layer that has properties of ECC to reduce the calculation complicatedness. The non-linear properties of ECC are taken into account only in section 6.2.4.

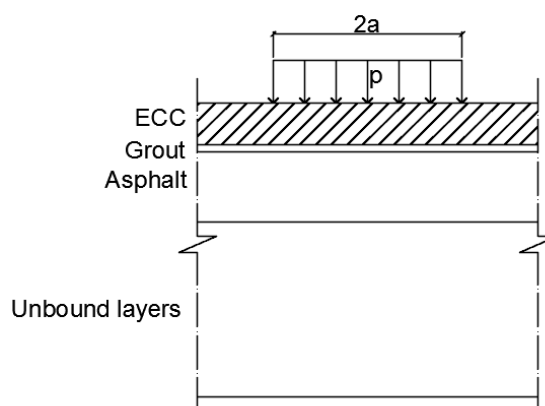


Figure 6-1 Reference PUTW system for interface shear stresses

Input parameters used for the reference system:

ECC and grout layer(s):

- $E_1 = 20000$ MPa
- $h_1 = 60$ mm (in BISAR and FEM, $h_{ECC} = 50$ mm, $h_{grout} = 10$ mm)
- $\mu_1 = 0.18$

Asphalt layer:

- $E_2 = 950$ MPa
- $h_2 = 110$ mm
- $\mu_2 = 0.35$

Unbound layers include three layers as follows:

- Graded granite: $E_{GG} = 250$ MPa; $h_{GG} = 250$ mm
- Subbase material: $E_{SB} = 150$ MPa; $h_{SB} = 300$ mm
- Subgrade material: $E_{GG} = 50$ MPa

a and p are the distributed load radius and pressure. p is equal to tire pressure of 7 bar or 0.7 MPa.

6.2.2 Shear stresses under vertical load

This part presents the calculation method for (horizontal-interface) shear stresses under vertical load that is summarized in (Eid, 2012) and applies it to calculate shear stress of the composite slab at different depths represented for the interface ECC slab–grout and grout–asphalt. Birmann (1981) presented an approximate solution to determine shear stresses in a thin slab for the load case in slab center. The shear stresses $\tau_{xz} = \tau_{zx}$ of a thin slab are distributed parabolically across the slab thickness and depend on the transverse force $q(x)$, the static moment $S_y(z)$ and the moment of inertia I_y .

$$\tau_{zx}(x, z) = \frac{q(x) \cdot S_y(z)}{I_y} \quad 6-1$$

The transverse force is biggest at the edge of a circular load (radius a , pressure p), it is:

$$q(x = a) = \frac{p \cdot a}{2} \quad 6-2$$

and it decreases hyperbolically with increasing distance from the load applied area.

Birmann's method (Birmann, 1981) will be used in combination with an equivalent T-beam model (Eisenmann & Leykauf, 2003) to calculate the horizontal shear stress in a two layer composite slab. Parameters of the T-beam are as follows: thickness of concrete layer h_1 , $\kappa = E_2/E_1$, $\beta = h_2/h_1$.

The T-beams can be described by the following variables:

$$i = [1 + \kappa\beta(4 + 6\beta + 4\beta^2 + \kappa\beta^3)] \frac{h_1^2}{12} \quad 6-3$$

$$e_o = \frac{h_1 \left(0,5 + \kappa\beta \left(1 + \frac{\beta}{2} \right) \right)}{1 + \kappa\beta} \quad 6-4$$

The moment of inertia of the T beam:

$$I_y = \frac{i \cdot h_1}{1 + \kappa\beta} \quad 6-5$$

Static moment $S_y(z)$:

$$S_y(z) = z_c F \quad 6-6$$

Where:

- F is the calculated area
- z_c is the center coordination of calculated area F

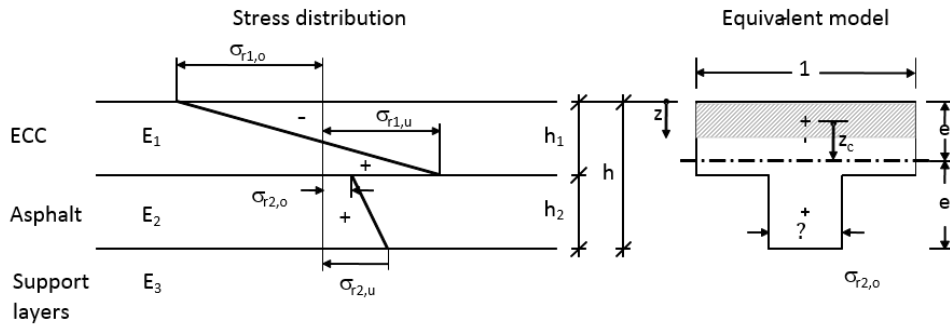


Figure 6-2: Equivalent model for calculating horizontal shear stress at different pavement depths

When $z \leq h_1$:

$$S_y(z) = e_0 z - 0,5z^2 \quad 6-7$$

When $z > h_1$:

$$S_y(z) = e_0 z - 0,5z^2 - \kappa(0,5z - e_0)(z - h_1) \quad 6-8$$

I_y calculated from equation 6-5 and $S_y(z)$ from equation 6-8 are used for calculating shear stresses at any depth within the composite of the pavement.

Especially, at the bottom of the grout layer ($z = h_1$), the shear flow is:

$$T(\kappa, \beta) = \frac{6 \cdot (1 + \beta)}{\frac{1}{\kappa\beta} + 4 + 6\beta + 4\beta^2 + \kappa\beta^3} \quad 6-9$$

Therefore, the shear stress over the cross section at the bottom of the grout layer is:

$$\tau_{zx}(z = h_1) = \frac{q(x) \cdot (e_0 h_1 - 0,5h_1^2)}{I_y} = \frac{q(x) \cdot T(\kappa, \beta)}{h_1} \quad 6-10$$

The formula above is used for a thin slab. For a thick slab, the shear stress at the bottom of concrete layer is smaller, and it is outside of the load area. Birmann (1981) took this into account by a factor V , which takes a load distribution at 45° to the main (neutral) axis $z = e_0$.

The maximum shear stress at the bottom of concrete layer under vertical load (Birmann, 1981) is then:

$$\max \tau_{zx} = p \cdot a \cdot \frac{T(\kappa, \beta)}{2 \cdot h_1 \cdot V} \quad 6-11$$

With:

$$V = 1 + h_1 \cdot \frac{(1 + \kappa\beta(2 + \beta))}{2a(1 + \kappa\beta)} = \frac{a + e_o}{a} \quad 6-12$$

The results of the specified Birmann's approximation method for an infinity slab will be compared with others. The solution of an infinity slab on a half space can also be calculated using BISAR – a calculation tool based on the multilayer theory. A numerical finite element model using ANSYS is created to compare the results with two above methods. For the purpose of comparison, the linear material model for ECC is used.

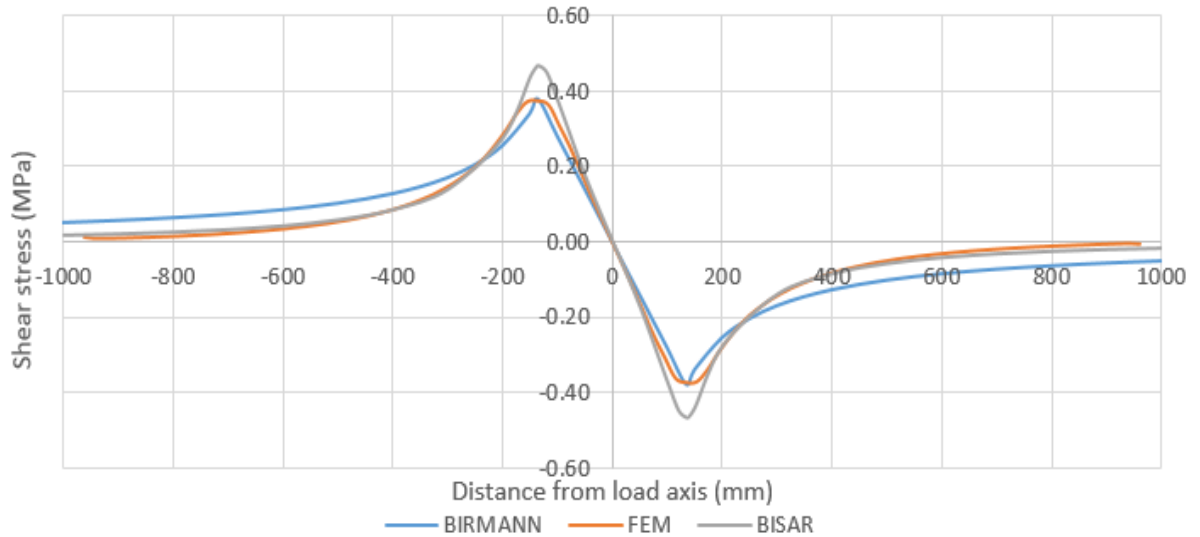


Figure 6-3: Horizontal shear stress under vertical load at the interface ECC-grout (at $h_1 = 5$ cm)

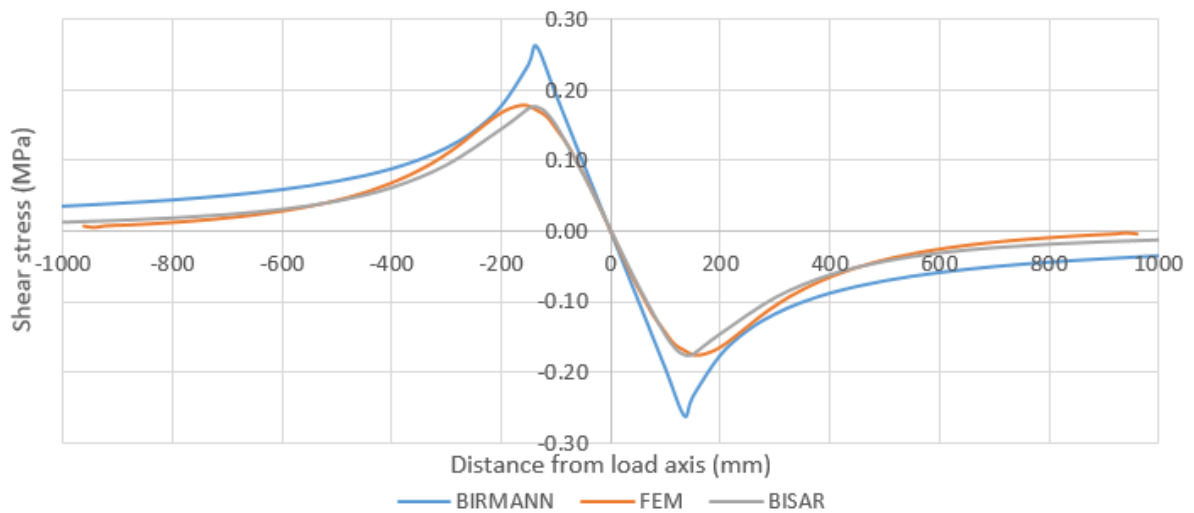


Figure 6-4: Horizontal shear stress under vertical load at the interface grout-asphalt (at $h_1 = 6$ cm)

The shear stresses at the interfaces under vertical load calculated using the above three calculation methods are plotted in Figure 6-3 and Figure 6-4. The trends of all three curves from different methods matched for each interface. Maximum interface shear stress values calculated by Birmann's and BISAR methods occur almost at the boundary of the load area ($x = 135$ mm) where values from FEM shifted just slightly out of load area. In Birmann's method, there is no grout intermediate layer. This is considered as an ideal case for bonding. Therefore, this can be the reason where the maximum shear

stress at 6 cm depth (interface between ECC and asphalt base course) here is the highest among the values from other methods. Maximum value from FEM matches well with the value from Birman's method at 5 cm and BISAR at 6 cm. It can be concluded that the FEM model is verified for the vertical load case.

6.2.3 Horizontal shear stresses under horizontal load

In addition to vertical traffic load, pavement layers are also strained under horizontal loads. These horizontal loads include acceleration, braking forces or centrifugal forces (when the vehicle is in the curve or cornering) or the combination of these forces.

The horizontal (braking or acceleration) force is actuated by vehicle weight and the friction coefficient between tyres and road surface. According to (Jones & Childers, 2001), the common friction coefficient is about 0.4 – 0.7 or up to 0.9. The friction coefficient more than 1.0 was also found (Villagra, et al., 2011), but it occurs only during emergency braking, which does not happen regularly on the road. Therefore, value 0.9 is taken into account for calculation. The horizontal force of a standard axle load 80 kN acting on the pavement is 36 kN per wheel. Lau et al. (1994) described a closed-form solution by Cerruti and Bousinesq for the displacement field in a homogeneous half-space under point load on the surface:

$$u = \frac{S}{4\pi\mu} \left(\frac{\lambda + 3\mu}{\lambda + \mu} \frac{1}{r} + \frac{x^2}{r^3} \right) - \frac{S}{2\pi(\lambda + \mu)} \frac{1}{r} + \frac{S}{4\pi(\lambda + \mu)} \left[\frac{1}{z + r} - \frac{x^2}{r(z + r)^2} \right] \quad 6-13$$

$$v = \frac{S}{4\pi\mu} \frac{xy}{r^3} - \frac{S}{4\pi(\lambda + \mu)} \frac{xy}{r(z + r)^2} \quad 6-14$$

$$w = \frac{S}{4\pi\mu} \frac{xy}{r^3} + \frac{S}{4\pi(\lambda + \mu)} \frac{x}{r(z + r)} \quad 6-15$$

$$\lambda = \frac{Ev}{(1 + \nu)(1 - 2\nu)} \quad 6-16$$

$$\mu = \frac{E}{2(1 + \nu)} \quad 6-17$$

$$r = \sqrt{x^2 + y^2 + z^2} \quad 6-18$$

Where:

- E : elastic modulus of the half-space
- ν : Poisson's ratio
- μ : shear stiffness
- u, v , and w : displacement in x -, y -, and z - directions.
- S : magnitude of the braking load acting in the positive x - direction.

The origin of the coordinate system is at the point of load application, and z is measured downward,

The horizontal shear stress τ_{xz} due to a surface point load is given by:

$$\tau_{xz} = \mu \left(\frac{\partial u}{\partial z} + \frac{\partial w}{\partial x} \right) \quad 6-19$$

The result from Cerruti's method is compared to the ones calculated from BISAR and FEM to verify FEM model.

Because the horizontal load due to braking is only active together with vertical load, a combined load case with both vertical and horizontal loads is used for calculation. For the method using closed form formulas, the shear stress portion caused by the vertical load is calculated by Birmann's method and the stress portion caused by the horizontal load is calculated by Cerruti's formulas. The results are summarized in Figure 6-5 and Figure 6-6 below.

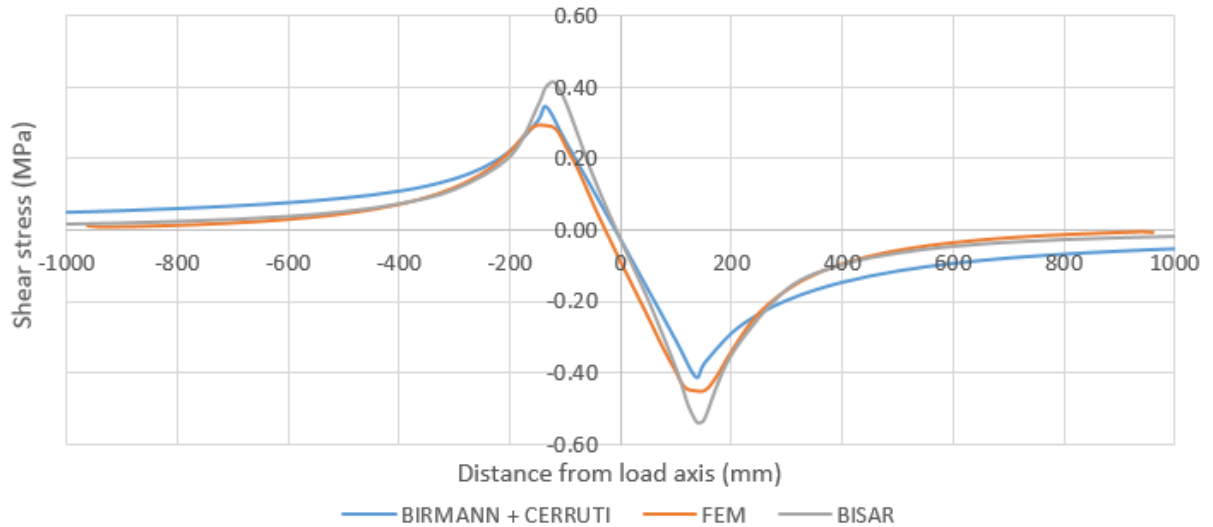


Figure 6-5: Horizontal shear stress under vertical and horizontal load at the interface ECC-grout (at $h_1 = 5$ cm)

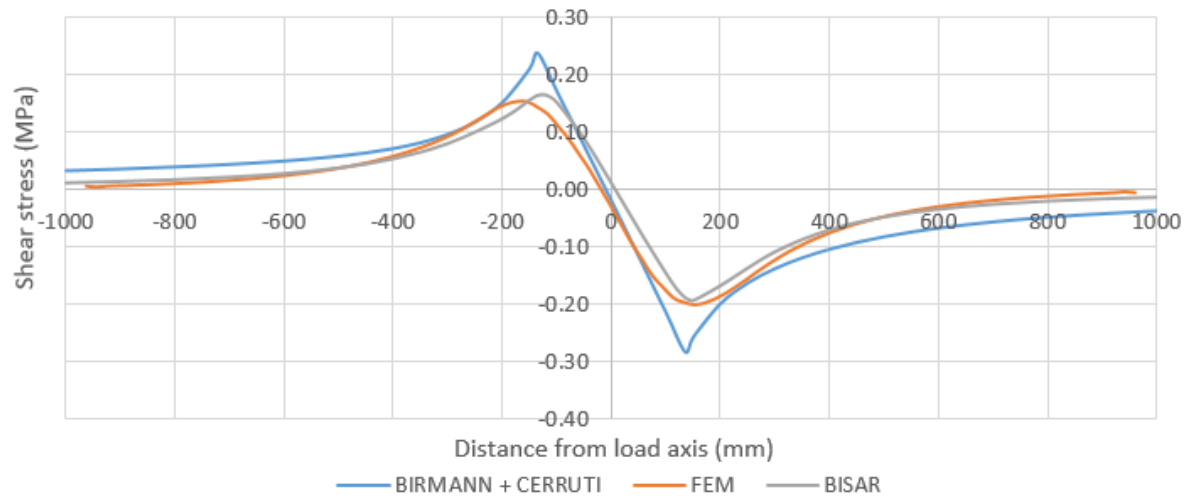


Figure 6-6: Horizontal shear stress under vertical and horizontal load at the interface grout-asphalt (at $h_1 = 6$ cm)

The shear stresses at the interfaces under the combined vertical and horizontal loads calculated from above three methods are plotted in Figure 6-5 and Figure 6-6. Similar to the case when only vertical load is applied, the trends of all three curves from different methods matched for each interface. Maximum interface shear stress values calculated using Birmann's method and BISAR also occur almost at the boundary of the load area ($x = 135$ mm) where the values from FEM shifted just slightly out of load area. Maximum values from FEM lie well in between values from other methods. It can be confirmed that the FEM model is verified for both horizontal and vertical load case.

6.2.4 Horizontal shear bond strength requirement for PUTW

In this part, the ECC non-linear material is inserted to the calibrated FEM for further analysis. Eisenmann and Leykauf (2003) suggested to use an additional factor 1.3 to 1.5 for designing a heavily loaded road and 1.2 for a less heavily loaded road when taking into account for driving at a curve, overtaking or dynamic wheel load fluctuations. Factor 1.5 is used for calculation as a conservative approach. The bonding at the interfaces are also subjected to fatigue. Eid (2012) suggested to use a factor of 2.0 for this effect. Therefore, in total the factor of 3.0 is used. Due to nonlinear behavior of ECC, the safety factor of 3.0 is applied directly to load apply (vertical and horizontal loads) on FEMs instead of using it for the final results.

The FEM will be inputted with a variation of parameters for analysing the effect of composite layer thickness, asphalt stiffness, and slab sizes:

- ECC, grout and asphalt thickness [mm]: (50, 10, 110), (60, 10, 100), (70; 10; 90), (80, 10, 80). The total thickness is always 170 mm as pavement Type 1B.
- Asphalt elastic modulus [MPa]: 950, 2800
- Slab size [mm x mm]: 900x900, 1800x1800, 3600x3600

The maximum shear stresses at interfaces ECC-grout and grout-asphalt taking into account the ECC non-linearity as well as safety factors of all combinations above are summarized in Table 6-1 and Table 6-2.

Table 6-1: Maximum horizontal shear stress at the interface ECC slab-grout

Asphalt E-Modulus (MPa)	Thickness combination (mm)	Maximum shear stress (MPa)		
		Slab size (mm x mm)		
		900x900	1800x1800	3600x3600
950	(50, 10, 110)	0.83	0.81	0.80
	(60, 10, 100)	0.81	0.79	0.82
	(70, 10, 90)	0.74	0.71	0.70
	(80, 10, 80)	0.66	0.64	0.64
2800	(50, 10, 110)	0.74	0.72	0.72
	(60, 10, 100)	0.76	0.74	0.73
	(70, 10, 90)	0.73	0.70	0.70
	(80, 10, 80)	0.71	0.68	0.68

Table 6-2: Maximum horizontal shear stress at the interface grout-asphalt

Asphalt E-Modulus (MPa)	Thickness combination (mm)	Maximum shear stress (MPa)		
		Slab size (mm ²)		
		900x900	1800x1800	3600x3600
950	(50, 10, 110)	0.45	0.44	0.44
	(60, 10, 100)	0.40	0.40	0.40
	(70, 10, 90)	0.37	0.36	0.36
	(80, 10, 80)	0.30	0.32	0.32
2800	(50, 10, 110)	0.57	0.55	0.55
	(60, 10, 100)	0.54	0.52	0.52
	(70, 10, 90)	0.49	0.48	0.48
	(80, 10, 80)	0.44	0.43	0.43

The differences in the maximum shear stresses of different thickness, length and asphalt combinations are relatively small. It can be concluded that changing in slab size has very little or almost no influence on the maximum shear stresses at both interfaces. Whereas, slab thickness has a bit more impact to the maximum shear stresses. Increasing the ECC thickness from 50 mm to 80 mm reduces about 20-30% of the maximum shear stresses at the interfaces. The asphalt elastic modulus has very slightly impact on the maximum shear stress. The maximum difference in shear stress is 0.09 MPa in the interface under ECC slab and 0.14 MPa on top of asphalt later.

The results in Table 6-1 and Table 6-2 are calculated for the grout thickness of 10 mm. In reality, the grout thickness can be slightly different from one location to another. The influence of the grout thickness to the maximum shear stress for the slab size 900x900x50 is presented in Figure 6-7. The slab size 900x900x50 is the slab where maximum values of horizontal shear stress at both interfaces ECC slab-grout and grout-asphalt are found at the grout layer thickness of 10 mm when asphalt elastic modulus is 950 and 2800 MPa, respectively (see Table 6-1 and Table 6-2). Figure 6-7 illustrates that the maximum horizontal shear stresses at both interface increase when grout thickness increases. The shear stress at the interface ECC-grout is more sensitive to the gout thickness.

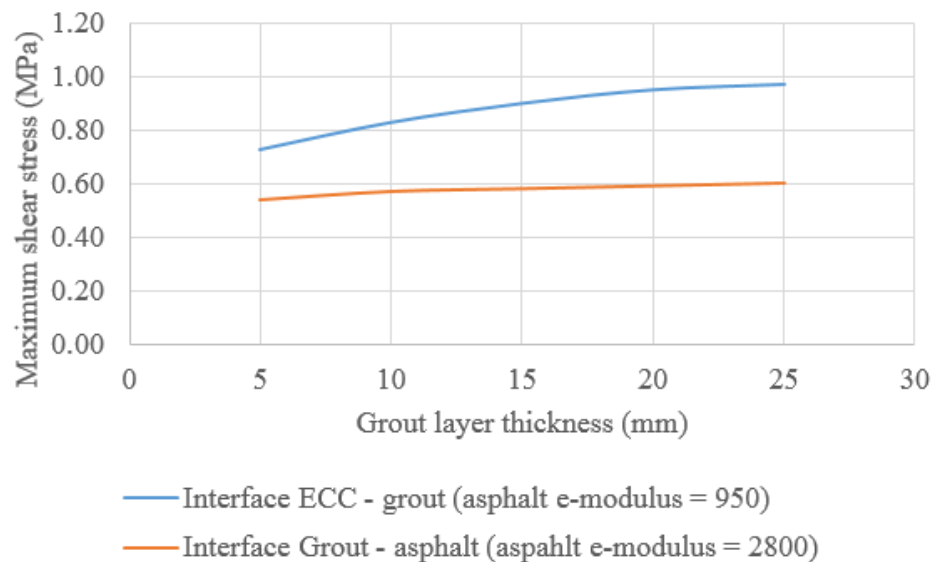


Figure 6-7: The influence of grout layer thickness to the maximum horizontal interface shear stresses (slab size: 900x900x50)

For simplicity, the required bond strengths of PUTW are the maximum values in Table 6-1, Table 6-2, and Figure 6-7, which are almost 1 MPa for the interface ECC slab–grout and 0.6 MPa for the interface grout–asphalt.

6.3 Calculation of vertical interface split stress in PUTW due to temperature change

The behaviour of the PUTW under temperature changes will be presented more detail in section 7.3. The temperature changes slowly during the day. Therefore, the deformation of the PUTW slab changes slowly. In the hot tropical environment like Singapore, asphalt is assumed to have no influence on the longitudinal movement and bending moment caused by constant temperature change and temperature gradient. When there is a complete bond between concrete and asphalt, asphalt follows the horizontal and vertical deformation of the PUTW slab. In this case, it is assumed that there is no horizontal shear stress at the composite interfaces and the vertical interface split stress in PUTW due to temperature change causes by only the asphalt (and grout) self-weight. If the asphalt and grout density is 2300 kg/m³, the vertical interface splitting stress is summarized in Table 6-3 below. With the assumption, the split stress is considered neglectable.

Table 6-3: Maximum vertical interface split stress in PUTW due to temperature change

Thickness combination (mm)	Maximum vertical interface split stress (MPa)	
	Interface ECC slab-grout	Interface grout-asphalt
(50, 10, 110)	2.76e-3	2.53e-3
(60, 10, 100)	2.53e-3	2.3e-3
(70, 10, 90)	2.3e-3	2.07e-3
(80, 10, 80)	2.07e-3	1.84e-3

6.4 Method to improve interface bonding

6.4.1 Bond between grout and asphalt

Eid (2012) did an intensive literature review about interface bonding in whitetopping. The effects of various pre-treatments on asphalt surface to the bond strength between concrete and asphalt have been studied. Some of the pre-treatments include: no pre-treatment, surface with drill hole grid, pre-treatment with bitumen emulsion as a bonding agent (wet on wet) and pre-treatment with bitumen emulsion (wet on dry), cleaning under low pressure with water and a bonding agent based on cement, cleaning with high pressure water jet, pre-treatment with cement slurry, cleaning with high pressure water jet, pre-treatment with mixture of cement slurry and plastic dispersion, cleaning with high pressure water jet, pre-treatment with plastic dispersion. The results show that milling and cleaning the old, or new asphalt provides best composite values (Steigenberger, 1998) (Tschegg, et al., 2007) (Eid, 2012).

There were two test sections constructed as parts of the research done by Eid (2012). In the test section Burghausen in Germany, the influence of asphalt surface cleanliness and the use of dispersion agent have been studied. The variations include the combination of using dispersion or without dispersion and the clean surface or dirty surface. The test results from cored samples are rather scattered. However, the average bond strength of all variations is about 1.2 MPa. In the test section Hengersberg in Germany, the effect of using dispersion on the milled and cleaned asphalt was studied. The results of cored samples from the site show the slight improvement of bond strength from 0.96 MPa to 1.14 MPa by using dispersion.

In PUTW, fresh self-levelling fast setting grout is used to fill the gap and create a bond between the PUTW slab and asphalt. Therefore, in principle, the bond between grout and asphalt is similar to the composite bond in bonded whitetopping overlay (fresh concrete on asphalt).

6.4.2 Bond between PUTW slab and grout

The bond between the PUTW slab and grout follows the concept of a fresh concrete on the substrate. The common practice is to firstly roughen the substrate surface. Surface roughening methods include concrete jacketing by jacket hammer, sand-blasting and water jetting, grinding, wire-brushing, and shot-blasting. A study was done by Júlio et al. (2004) to evaluate the effect of different surface treatment methods to the bond strength. The surface pre-treatments included: flat surface (against formwork when casting), surface prepared with steel brush, surface partial chipped, surface partial chipped plus water saturation 24h before concrete cast and surface with sand-blasting. The results from the slant shear tests and the pull-off tests showed that it was always an adhesive failure. When drilling the cores, all the samples with flat surface were de-bonded. There is not a significant effect of pre-wetting the substrate surface. The wire-brushed method resulted in about 40% more bond strength compare to the partially chipped method. And sand-blasting preparation method gave the best result (Júlio, et al., 2004).

Obata et al. (2007) investigated the interface bond strength between ultra-high strength fiber reinforcement concrete (UFC) panels to the fast setting grout. The irregularity of UFC panel's surface was provided by convex forming or by aggregate dispersion. The effect of surface irregularity was studied together with the effect of using primer. The results indicated that primer helped to increase the

bond strength in both pull-off and shear tests especially for the sample with a smooth surface. Surface irregularity improved the interface shear strength significantly.

6.5 Laboratory tests on interface bond strength

6.5.1 Introduction

There are two interfaces in the PUTW that need to be evaluated: grout-asphalt and PUTW slab–grout. For the bond between grout and asphalt, the requirement strength of 0.6 MPa according to the calculation in section 6.2.4 is expected to be achievable in good whitetopping practice as discussed in section 6.4.1. Moreover, the Chemilink SS-141, which is used for semi-rigid pavement in Singapore, is proposed to be used as a bedding grout in this research. Chemilink SS-141 is a polymer modified compound that is designed specifically for filling in gaps of porous asphalt to create semi-rigid pavement (Wu & Zhang, 2011). Therefore, it is expected to provide an excellent bond to asphalt layer.

This part focuses on evaluating the bond strength between PUTW slab and grout. The grout used for testing is Chemilink SS-141, which has properties shown in Table 6-4.

Table 6-4: Chemilink™ SS-141 technical data (Chemilink™, 2013)

Properties	Test Method	Chemilink™ SS-141
Flow value	JASS 15 M103	250~290 mm
Density	EN 12190	2100~2250 kg/m ³
1-day Compressive Strength*	EN 12190	55 ~80 MPa
7-day Compressive Strength	EN 12190	90 ~ 110 MPa
28-day Compressive Strength	EN 12190	120 ~ 140 MPa
28-day Flexural Strength	EN 196	7 ~ 15 MPa
Setting Time	EN 196 - 3	2~3h, 3~6h, 6~8h
*24 hours from initial setting		

One of the advantages of a precast slab is that its faces can be imprinted or equipped with textures for different purposes. For evaluating interface bond strength, three different types of slab bottom surface are proposed as shown in Figure 6-8: (a) flat surface, (b) with convex circular nodes, (c) with convex rectangle nodes.

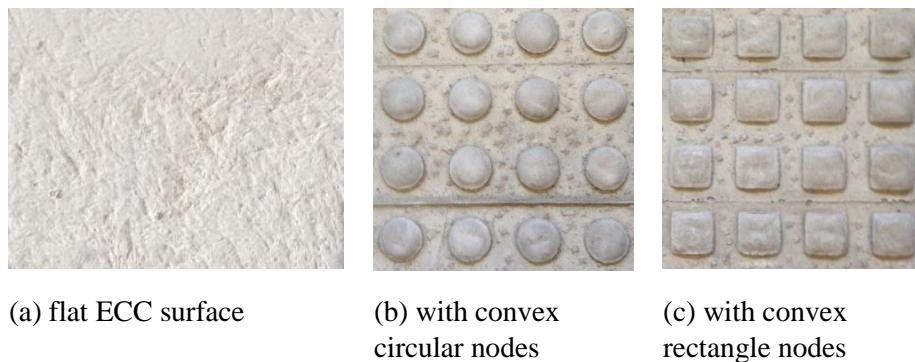


Figure 6-8: 3 types of slab bottom surface used for interface bond strength evaluation

The convex nodes are about 3-4 mm height with a diameter (or length and width) of 20-22 mm and spaced about 40 mm from each other. The purpose of the convex nodes is to create the interlock between precast slabs and grout for hopefully increasing bond strength. The convex nodes are expected to behave like anchors to keep slab in place to avoid slab drifting.

6.5.2 Testing concept

There are testing possibilities to evaluate bond strength in the layered composite. The principle of testing techniques is presented in Figure 6-9. In this research, direct shear test (e) and pull test (a) were chosen. The frames for shear test and pull-off test are shown in Figure 6-10.

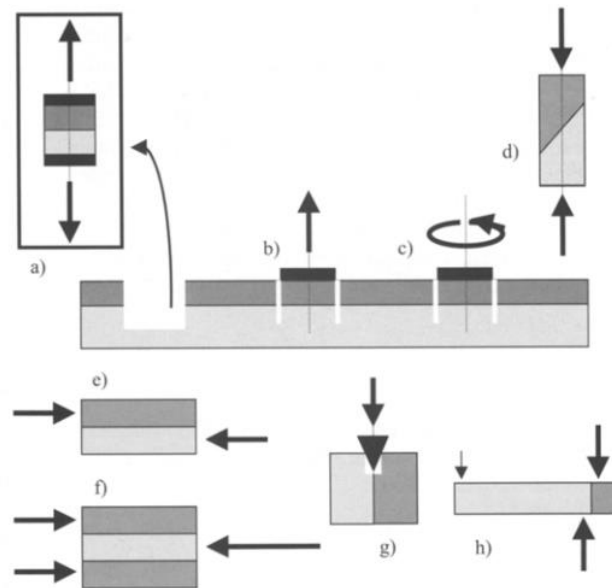
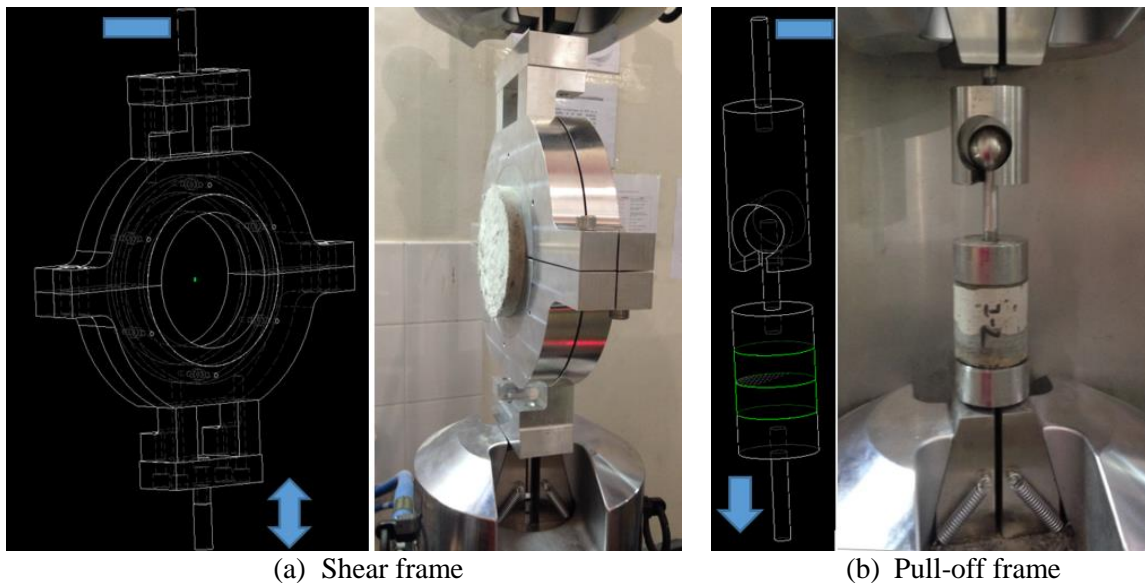


Figure 6-9: Test methods to determine bond strength: a) b) pull-off tests, c) torsion test, d) slant shear test, e) f) shear tests, g) wedge splitting test, and h) guillotine test (Silfwerbrand, 2003)



(a) Shear frame

(b) Pull-off frame

Figure 6-10: Shear frame and pull-off frame

6.5.3 Sample preparation

After mixing, ECC was poured into a 300 mm x 400 mm mould. The slabs were casted as a bottom-up method. For slabs with convex nodes, after compaction, circular or rectangle laser cut Styrofoam sheets (Figure 6-11) were placed on top of the slabs and vibrate into the ECC to create the convex nodes. The slabs were then cured at laboratory temperature for 2-3 days before de-moulding. After that, they were continued to be cured in the laboratory for a total of at least 28 days.

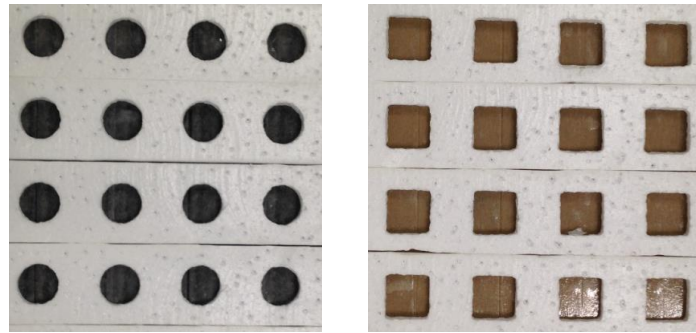


Figure 6-11: Styrofoam sheets

After curing, Styrofoam sheets were removed from the slabs to expose convex nodes. Slabs' bottom surfaces were thoroughly cleaned with low pressure water. Then the slabs were put back to the mould before pouring the grout in. After 1-2 weeks, composite slabs were removed from the formwork and core drilled using SHIBUTA M1511F/TS-160N with three different sizes of core bits. The summary of sample number is presented in Table 6-5.

Table 6-5: Summary of sample types

Slab bottom surface type	Number of slabs	Core diameter (mm)	Number of samples
smooth surface	2	143	4
		99	8
		49	10
with convex circular nodes	2	143	4
		99	8
		49	10
with convex rectangle nodes	2	143	4
		99	8
		49	10

6.5.4 Direct shear test

6.5.4.1 Test apparatus

A shear frame was designed and manufactured in-house exclusive for this research (Figure 6-10). This shear frame had interchangeable adapters to be used with different cylinder core diameters. These adapters were CNC machined to fit with the actual sample diameters after coring. The actual sample diameters here were 99 and 143 mm.

All tests were done using MTS Landmark hydraulic loading frame. The shear frame was connected to MTS loading cylinder by hydraulic wedge grip. The loading was applied from the bottom of the frame, whereas the upper part was fixed.

The limitation of this test is that there is no horizontal load (resembling the vertical traffic load) applied to the shear frame. However, this will push the shear stress results towards the safer side.

6.5.4.2 Test procedure

The shear test followed the test method Iowa 406-C (Iowa Department of Transportation, 2000). Each sample was placed in the testing jig in the manner that the bonded interface was placed in space between the main halves of the jig. The interface here was at the bottom of the PUTW slab and at the convex node foot, which was opposite to the node's tip that is imprinted in the grout.

At first, the sample was attached firmly to the fixed part of the jig. After that, the lower half of the loading part was moved up very slowly by the hydraulic loading. When it touched the sample, the upper half of the loading part is fixed to tie the sample firmly to the loading frame.

The load was applied continuously and without shock, with a constant rate within the range of 2.76-3.45 MPa per minute (400 to 500 psi per minute) (Iowa Department of Transportation, 2000). The loading was continuously applied until the specimen fails. The failure load was then recorded.

The bond strength is calculated based on the maximum load carried by the sample during the test and the sample cross area.

$$\text{Shear bond strength (MPa)} = \text{Load (N)} / \text{area of test specimen (mm}^2\text{)} \quad 6-20$$

6.5.5 Pull-off test

6.5.5.1 Test apparatus

A pull-off frame was manufactured for this test. This frame featured a swivel joint to prevent rotation force due to imperfection alignment. Using this frame the samples need to be cored completely instead of partially cut. It was designed to be used with samples that have a diameter of about 50 mm.

The tests were also done using MTS Landmark hydraulic loading frame. The pull-off frame was connected to MTS loading cylinder by hydraulic wedge grip. The tensile loading is applied from the bottom of the frame, whereas the upper part is fixed.

6.5.5.2 Test procedure

The tests were conducted base on ASTM C1583/C1583M – 13 (ASTM, 2013).

All contaminants or deteriorated material were removed from the top and bottom surfaces of samples. Two components epoxy, DEVCON 2 Ton Epoxy S-35, was used to attach the cleaned sample surfaces to steel disks of the pull-off frame.

The split frame (including sample) was attached to the hydraulic wedge grips. Then the tensile load was applied at a constant rate of 20-50 kPa/s. Failure load and failure mode were recorded.

The tensile bond strength was calculated based on the maximum load carried by the sample during the test and the sample cross area.

$$\text{Tensile bond strength (MPa)} = \text{Load (N)} / \text{area of test specimen (mm}^2\text{)} \quad 6-21$$

6.5.6 Result and discussion

In direct shear tests, the samples were failed directly at the interface, at the grout, at ECC, or the combination of those. The common failure types of samples with circular and square convex nodes were grout failure or interface failure in combination with nodes fractured. In addition, the samples with square nodes had the ECC failure as shown in Figure 6-13. Samples with flat contact to grout normally failed at the interface. However, there was one exceptional case where the failure is at ECC (see Figure 6-14).



Figure 6-12: Failure types in sample with circular convex nodes in shear test



Figure 6-13: Failure types in sample with square convex nodes in shear test



Figure 6-14: special failure type of sample with flat contact in shear test

The failures in pull-off tests were at the interface or grout. The samples with flat contact always failed at the interface. Almost all the samples with circular nodes failed at the interface in combination with nodes fractured. The exception was the interface failure, but nodes were still intact (See Figure 6-15 (b)). Some samples with square nodes had the same type of failure with the ones with circular nodes. But the majority failed at the plane where the tip of the nodes contact with the grout and grout fails (see Figure 6-15 (a))



(a) samples with square nodes

(b) samples with circular nodes

Figure 6-15: failure types of sample with convex nodes in pull-off test

The summary of test results is shown in Figure 6-16. The results clearly show that the bond strength of the samples with square convex nodes gives the highest value, and it is the most consistent. In contradiction, the samples with a flat ECC surface give the lowest bond strength and also inconsistent result. It is also worth to mention that there were two samples with flat surface failure when setting up shear test, and they are not included in the result summary. The samples with circular convex nodes also provide high bonding strength and quite consistent, the results are in between the other types of slab's bottom surface. In summary, the bond strength of all three types of samples, in general, fulfil the requirement for PUTW. However, due to the inconsistency of samples with a flat surface, the flat surface is not recommended.

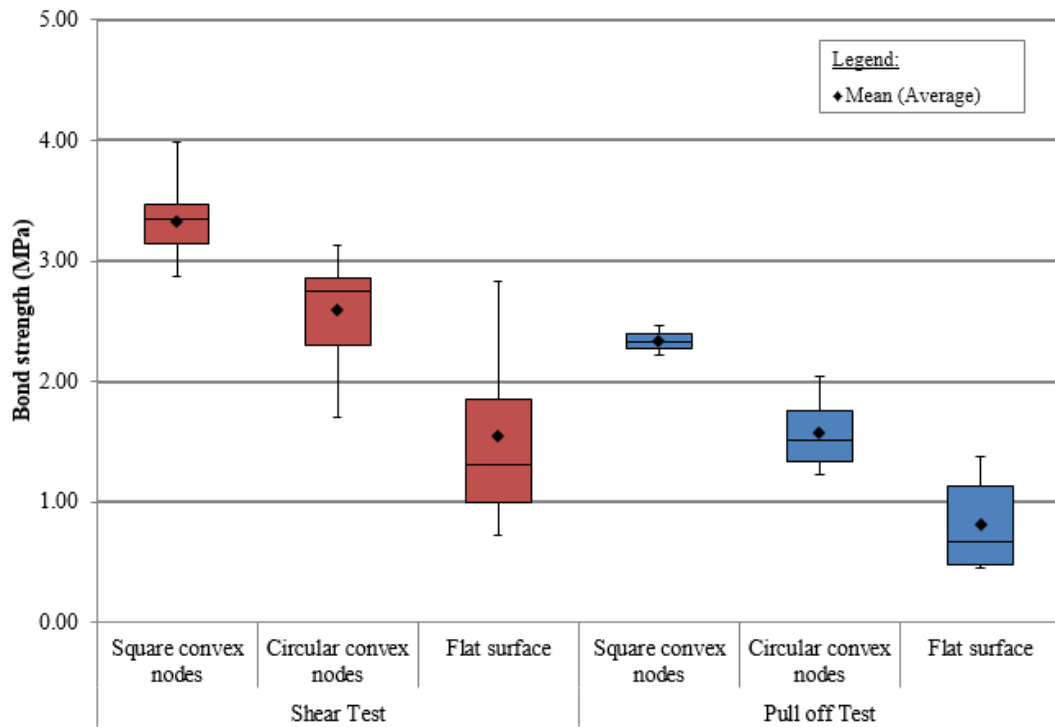


Figure 6-16: Bond test results

6.6 Conclusion

This chapter summarised the theory to calculate horizontal interface shear stresses in the composite pavement. The calculation theory together with commonly used BISAR software was used to verify the FEMs. The calibrated FEMs were later inputted with ECC non-linear material model to calculate the requirement bond strength at the interface PUTW slab–grout and grout–asphalt with all safety factor included. With a simpler approach, the vertical interface split stress in PUTW due to temperature change was also calculated, but the requirement split strength is neglectable.

Methods for improving interface bond strength were discussed. The horizontal bond strength requirement for the interface grout-asphalt is achievable in previous UTW good practice. Laboratory tests were done to test the actual bond strength between precast slab and grout layer. Three types of slab's bottom surface were proposed: (a) flat surface, (b) with convex circular nodes, (c) with convex rectangle nodes. Different sizes of cylinder samples were drill-cored from the prepared composite slabs. Direct tensile tests and pull-off tests were done using testing frames, which were in-house manufactured. The tests results indicated that there were all types of failures: directly at the interface, at the grout, at ECC, or their combinations. However, it varied depending on the type of testing and slab's surface. The summary of test results clearly showed that the bond strength of the samples with square convex nodes give the highest value, and it was the most consistent. Conversely, the samples with a flat ECC surface gave the lowest bond strength and also inconsistent result. Moreover, there were some samples with flat surface even failed during test set-up. In conclusion, the bond strength requirement for PUTW is fulfilled by any types of slab's bottom surface. However, due to the inconsistency of samples with a flat surface, it is recommended to use only the convex node types for PUTW slabs.

7 Design of Precast Ultra-Thin Whitetopping (PUTW)

7.1 Introduction

Similar to a UTW pavement, the design of PUTW includes the design of slab size (width and length) as well as the thickness of all layers in the composite pavement structure. The PUTW can inherit the stresses calculation methods of the UTW. However, due to the fact that PUTW is a precast product, construction load (slab handling during construction) is also an important factor in designing slab dimensions. The slab sizes and the long-term performance of a UTW pavement are heavily dependent on the concrete flexural strength. The flexural strength of ECC is much higher than a normal concrete. Therefore, the dimensions as well as long term performance of a PUTW with pavement slab made of ECC can be very different from a normal UTW with pavement slab made of normal concrete.

This chapter will start with summarizing the stress calculation theories that can be applied for PUTW. These theories will be used to verify FEMs that are later used for designing PUTW. All of the input for designing PUTW including traffic loading, environmental loading, pavement material properties, support layers' equivalent stiffness, overall composite stiffness as well as the interface bonding will be taken into account for pavement analysis.

7.2 Calculation of traffic-induced stress in PUTW

Eid (2012) summarized different methods to calculate the stresses and deformations under the traffic load in concrete pavement that were mentioned in (Eisenmann & Leykauf, 2003). These methods include half-space theory, multilayer theory, plate on elastic base, and models with the finite element method (FEM). In this part, Westergaad's closed-form formulas, method for calculating multilayer systems, method for calculating vertical shear stress in asphalt at joint and FEM are presented for calculation of PUTW.

7.2.1 Westergaad's closed-form formulas

Westergaad (1926) derived equations to calculate flexural stress and deformation of concrete slab on elastic foundation. He distinguished three different load cases: at slab center, slab edge and slab corner as shown in Figure 7-1.

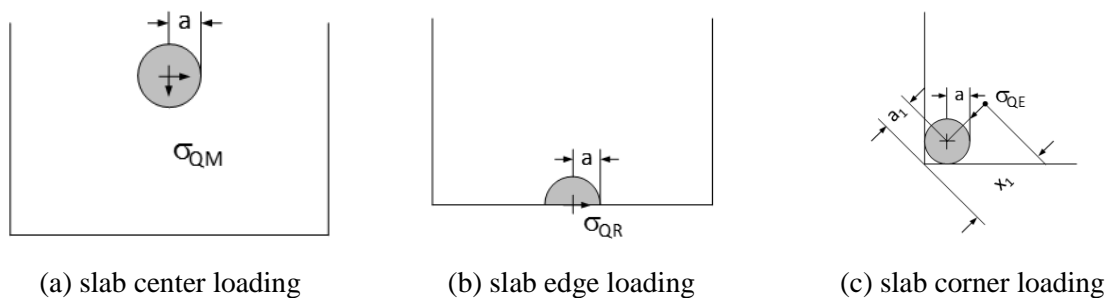


Figure 7-1: Load cases – according to Westergaad method (Eisenmann & Leykauf, 2003)

In the elastic foundation, which is described by the coefficient of subgrade reaction k [N/mm³], the half-space will be replaced by independent individual springs. The improved formulas from Westergaad (1933) are modified by empirical correction factors, where the deviations due to the impure bedding modulus between calculation results and experiments are compensated. The Westergaad's improved formulas were indicated and used in (Eisenmann & Leykauf, 2003).

The load radius a can be calculated using equation 7-1:

$$a = \sqrt{\frac{Q}{\pi \cdot p}} \quad 7-1$$

Where:

- a [mm]: radius of load distribution area
- Q [N]: load applied on the slab
- p [N/mm²]: distributed load

Westergaard (1933) introduced an equivalent radius b . The equivalent radius b depends on the actual load radius a and the slab thickness h . Thus, the influence of the stress distribution in the loading area is considered. For sufficiently thick slab, b can be determined using equation 7-2 and 7-3.

$$b = \sqrt{1,6 \cdot a^2 + h^2} - 0,675 \cdot h; \text{ when } a < 1,724 \cdot h \quad 7-2$$

$$b = a; \text{ when } a < 1,724 \cdot h \quad 7-3$$

Where:

- b [mm]: equivalent radius
- h [mm]: the slab thickness

Eisenmann (1973) proposed a method to determine the bedding modulus in a three-layer system based on the stiffness of the bonded layers, and the deformation of the subgrade. Using the Odemark's (1949) equivalence theory and the conversion of the layer thicknesses, the subgrade reaction is determined by the equations 7-4 and 7-5

$$h^* = 0,83 \cdot h_1 \cdot \sqrt[3]{\frac{E_1}{E_u}} + 0,90 \cdot h_2 \cdot \sqrt[3]{\frac{E_2}{E_u}} \quad 7-4$$

$$k = \frac{E_u}{h^*} \quad 7-5$$

Where:

- h^* [mm]: equivalent composite thickness
- h_1, h_2 [mm]: pavement slab, asphalt thickness
- E_1, E_2, E_u [MPa]: pavement slab, asphalt, support layer's equivalent elastic modulus
- k : [N/mm³]: subgrade modulus

The stress for the load cases at slab center, slab edge and slab corner can be calculated using the equations 7-6, 7-7 or 7-8 (Eisenmann & Leykauf, 2003).

$$\text{Center loading: } \sigma_{QM} = \frac{0,275 \cdot Q}{h^2} \cdot (1 + \mu) \cdot \left[\log \left(\frac{E \cdot h^3}{k \cdot b^4} \right) - 0,436 \right] \quad 7-6$$

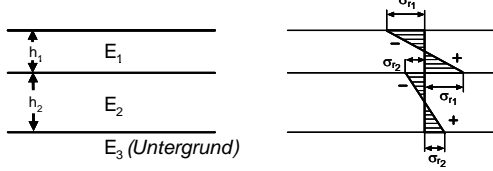
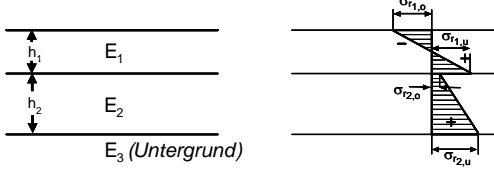
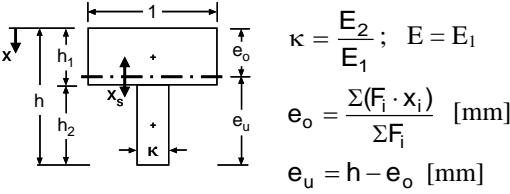
$$\text{Edge loading: } \sigma_{QR} = \frac{0,529 \cdot Q}{h^2} \cdot (1 + 0,54 \cdot \mu) \cdot \left[\log \left(\frac{E \cdot h^3}{k \cdot b^4} \right) + \log \left(\frac{b}{1 - \mu^2} \right) - 2,484 \right] \quad 7-7$$

$$\text{Corner loading: } \sigma_{QE} = \frac{3 \cdot Q}{h^2} \cdot \left[1 - \left(\frac{12 \cdot (1 - \mu^2) \cdot k}{E \cdot h^3} \right)^{0,3} \cdot (a \cdot \sqrt{2})^{1,2} \right] \quad 7-8$$

7.2.2 Calculation method for multilayer systems

The calculation procedure for multilayers systems are summarized in (Lechner & Freudenstein, 2010) which is presented in Table 7-1.

Table 7-1: Calculation method for multilayer systems (Lechner & Freudenstein, 2010)

System I: No bonding between layer 1 and 2	System II: Bonding between layer 1 and 2
<p>$\mu = \text{constant}$ $E_1 \geq E_2 \gg E_3$ [N/mm²]</p> 	<p>$\mu = \text{constant}$ $E_1 \geq E_2 \gg E_3$ [N/mm²]</p> 
<p>1) virtual bedding modulus</p> $k = \frac{E_3}{h^*} \text{ [N/mm}^3\text{]}$ $h^* = c \cdot h_1 \cdot \sqrt[3]{\frac{E_1}{E_3}} + c \cdot h_2 \cdot \sqrt[3]{\frac{E_2}{E_3}} \text{ [mm]}$ $c = \begin{cases} 0,83 & \text{for hydraulically bonded layers} \\ 0,90 & \text{for asphalt layers} \end{cases}$	
<p>2) Equivalent thickness same stiffness for $E = E_1$</p> $h_I = \sqrt[3]{\frac{E_1 \cdot h_1^3 + E_2 \cdot h_2^3}{E_1}} \text{ [mm]}$	<p>2) Equivalent thickness same stiffness for $E = E_1$</p> $h_{II} = h_1 + 0,9 \cdot h_2 \cdot \sqrt[3]{\frac{E_2}{E_1}} \text{ [mm]}$
<p>3) calculation of moment M_I for equivalent system - k, h_I and E_1 - acc. Westergaard ($M_I = \sigma_{Q,I} \cdot W_I$)</p>	<p>3) calculation of moment M_{II} for equivalent system - k, h_{II} and E_1 - acc. Westergaard ($M_{II} = \sigma_{Q,II} \cdot W_{II}$)</p>
<p>4) bending tensile stress in layer 1 and 2</p> $M_1 = M_I \cdot \frac{E_1 \cdot h_1^3}{E_1 \cdot h_1^3 + E_2 \cdot h_2^3} \text{ [N}\cdot\text{mm]}$ $M_2 = M_I \cdot \frac{E_2 \cdot h_2^3}{E_1 \cdot h_1^3 + E_2 \cdot h_2^3} \text{ [N}\cdot\text{mm]}$ $\sigma_{r1} = 6 \cdot \frac{M_1}{h_1^2}; \sigma_{r2} = 6 \cdot \frac{M_2}{h_2^2} \text{ [N/mm}^2\text{]}$	<p>4) bending tensile strains in layer 1 and 2 in a T-beam with equivalent stiffness</p>  <p>$\kappa = \frac{E_2}{E_1}; E = E_1$ $e_o = \frac{\sum(F_i \cdot x_i)}{\sum F_i} \text{ [mm]}$ $e_u = h - e_o \text{ [mm]}$</p> <p>or: $e_o = \frac{h}{2} \cdot \frac{E_2 \cdot h_2}{E_1 \cdot h_1 + E_2 \cdot h_2} + \frac{h_1}{2}$</p> <p>Moment of inertia of a T-beam [mm⁴ per mm]: $I = \sum (I_i + F_i \cdot x_{S,i}^2)$</p> $\sigma_{r1,0} = \frac{M_{II}}{I} \cdot e_o; \sigma_{r1,u} = \frac{M_{II}}{I} \cdot (h_1 - e_o) \text{ [N/mm}^2\text{]}$ $\sigma_{r2,0} = \kappa \cdot \frac{M_{II}}{I} \cdot (h_1 - e_o); \sigma_{r2,u} = \kappa \cdot \frac{M_{II}}{I} \cdot e_u \text{ [N/mm}^2\text{]}$
<p>5) elastic length (slab)</p> $L_I = 4 \sqrt{\frac{E_1 \cdot h_1^3}{12 \cdot (1 - \mu^2) \cdot k}}$	<p>5) elastic length (slab)</p> $L_{II} = 4 \sqrt{\frac{E_1 \cdot h_{II}^3}{12 \cdot (1 - \mu^2) \cdot k}}$

7.2.3 Calculation of vertical shear stress in asphalt at PUTW joint

In PUTW, the side surface of ECC slab is flat and smooth, therefore there is no load transfer from slab to slab. The load transfer is actually done by the contribution of asphalt layer and the bond between ECC slab and asphalt. Eid (2012) applied the formulas from (Leykauf, 1986) for whitetopping system to calculate shear stress in asphalt layer at joint.

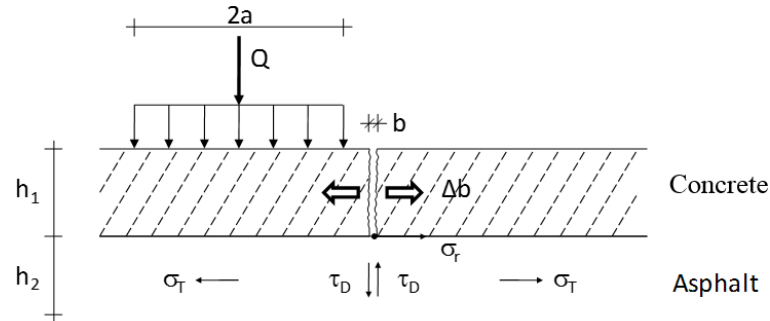


Figure 7-2: Types of stress in asphalt in the joint area of whitetopping (Eid, 2012)

Leykauf (1986) describes the relationships of reflective cracking in asphalt layer as shown in the Figure 7-2. There are 4 types of stresses presented in the Figure 7-2:

- Bending stress (σ_r)
- Vertical shear stress (τ_D)
- Tensile stress due to temperature change (σ_T)
- Asphalt expansion due to shrinkage in concrete (Δb)

The vertical shear stress in asphalt at joint of a whitetopping system can be calculated using the equation 7-9 below (Leykauf, 1986) (Eid, 2012). The assumptions are a load distributed of 45° across concrete layer and a uniform distribution of shear stress on the asphalt section.

$$\tau_D = \frac{Q}{2} \cdot \frac{1}{h_2 \cdot (2 \cdot a + 2 \cdot h_1 + h_2)} \cdot \left(1 - \frac{W}{100}\right) \quad 7-9$$

It is assumed that there is no load transfer by slabs themselves, the load transfer efficiency W here is equal to 0. The equation 7-9 is by then:

$$\tau_D = \frac{Q}{2} \cdot \frac{1}{h_2 \cdot (2 \cdot a + 2 \cdot h_1 + h_2)} \quad 7-10$$

7.2.4 Finite element models (FEMs)

Stresses calculation methods mentioned above have some limitations including: (a) effects of finite dimensions of actual pavement slabs are not considered; (b) stresses and deflections cannot be calculated correctly when slab material is working in its non-linear zone.

The three-dimensional (3D) finite element models (FEMs) are built using ANSYS Mechanical in Workbench environment to overcome the mentioned limitations. A nine (3x3) slab FEM and a seven hexagon slab FEM are created as shown in Figure 7-3 and Figure 7-4 . SOLID185 8-nodes 3D solid element is used. The ECC non-linear material model, which was verified in section 5.4, is inputted by embedding ANSYS APDL commands into ANSYS Workbench.

First layer is nine PUTW slabs or seven hexagon PUTW slabs. The slabs are assumed to have smooth side surfaces, placed 5 mm away from each other and have no connection to each other. The PUTW slabs are fully bonded into asphalt layer with the help of a very thin grout layer in between. For boundary conditions, asphalt is supported by an elastic support which is equivalent to 3 unbound material layers:

250 mm of graded granite material, 300 mm of sub base material and 500 mm of subgrade material. The value of elastic support is the bedding modulus k .

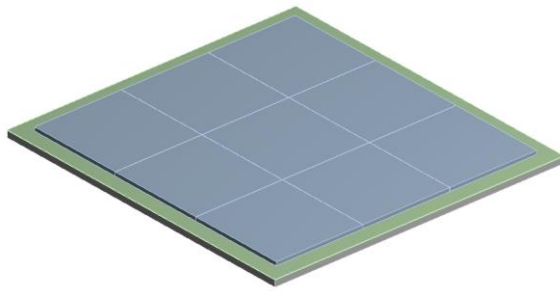


Figure 7-3: 3D 3x3 slab multilayer FEM

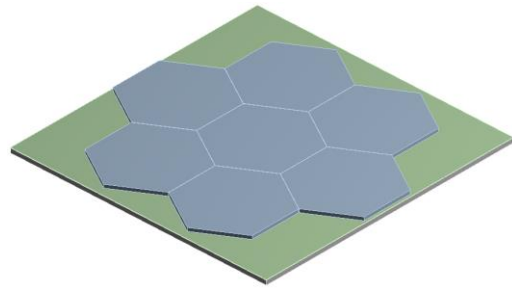


Figure 7-4: 3D seven hexagon multilayer FEM

In FEMs, loads can be applied at any locations with any amplitude on the PUTW slabs. However, there are three locations of interest: slab center, slab edge and slab corner (see Figure 7-5). According to (Lechner & Freudenstein, 2010), the stresses occurred by load acting on the slab edge and slab corner are quite similar. Moreover, the longitudinal joint layout will be arranged to avoid the regular wheel paths, therefore load cases at slab center and slab edge are of interest.

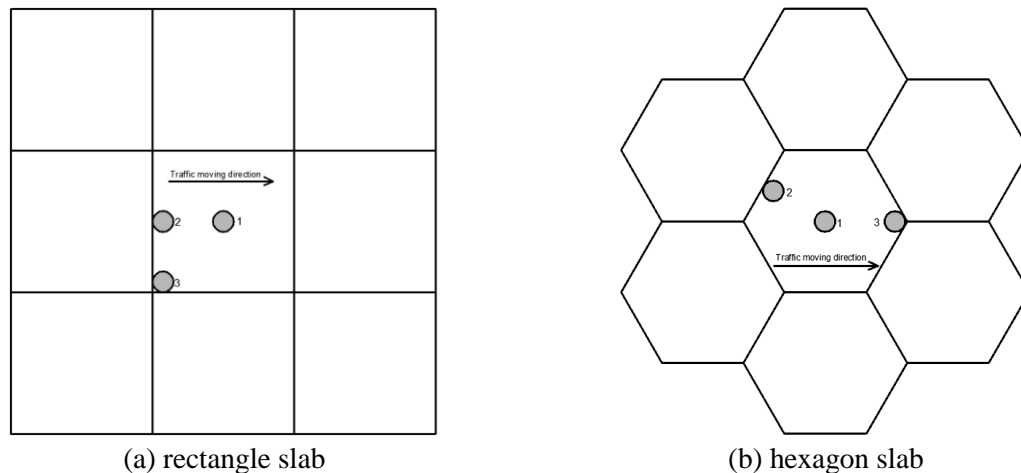


Figure 7-5: Load locations on FEMs

The FEMs are calibrated based on the formulas mentioned in section 7.2.2. For validation purpose (only), the ECC used in the FEM is assumed to be linear elastic, and the grout layer is merged with ECC to be one single layer. The calibration result of an example structure (70 mm of ECC + grout and 100 mm of asphalt and slab size of 5 m x 5 m) is shown in the Table 7-2. When asphalt elastic modulus is 2800 MPa, the difference is exceptional 13.15%, however actual stress different is just 0.12 MPa, which is very small and in a safe side. In conclusion, the FEM is calibrated. After this step, the non-linear material model of ECC is inputted to the FEM and grout layer is separated into one intermediate layer that fully bonded to ECC layer and asphalt layer for further calculation and analysis.

Table 7-2: FEM calibration result

Asphalt Elastic Modulus (MPa)	Stress at the bottom of ECC (MPa)				Stress at the bottom of Asphalt (MPa)			
	FEM	Theory	Difference (Mpa)	Difference (%)	FEM	Theory	Difference (Mpa)	Difference (%)
950	2.16	2.25	-0.09	-3.96%	0.44	0.47	-0.02	-5.31%
2800	1.03	0.91	0.12	13.15%	0.78	0.74	0.04	5.16%

7.3 Calculation of environment-induced stress in PUTW

7.3.1 Introduction

Similar to a rigid pavement, during the daily cycle of air temperature, there is an extreme temperature profile registered within the pavement composite slab. The temperature at the bottom face of the composite slab remains more or less constant due to the large extent of the soil mass beneath the pavement structure produces a reservoir effect. In the afternoon when the air temperature is highest, the temperature at the top pavement surface will be higher than the bottom of the PUTW slab. The situation is reversed at night time when the air temperature is lowest. The different in temperature at the top and bottom of the PUTW slab creates warping or curling effects (Figure 7-6) (Fwa, 2005). These effects in combination with slab self-weight and traffic load result in stresses.

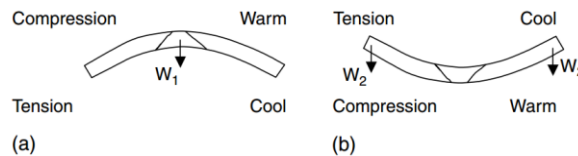


Figure 7-6: (a) daytime warping (b) night time curling (Fwa, 2005)

There are necessary assumptions for calculation of temperature-induced stresses in whitetopping pavement systems (Eid, 2012):

- The deformation of the concrete due to temperature changes slowly. When asphalt outweighs the viscous properties, it deforms to relieve stress (relaxation).
- The asphalt does not undergo elongation due to temperature changes. In the asphalt temperature gradients are not resulting any tensile or compressive stresses.
- There is a complete bond between concrete and asphalt. Therefore, the asphalt follows vertical deformations of the concrete.

In summary, asphalt has no influence on the bending moment caused by temperature gradient due to its viscous properties where it relieves stress on its own. Therefore, the bending moment is caused only by the temperature-induced deformations of the PUTW slab.

This part summarizes briefly the calculation methods for warping and curling stress in PUTW. More detail about the calculation methods are presented in Appendix A.2.

7.3.2 Warping stress

Warping stress is bending tensile stress caused by slab warping due to heating on top of the slab (positive temperature gradient). In a full restraint slab (infinite or big enough slab), all the temperature changes along the cross section (depth (z)) cause respective stresses. Stress distribution can be separated into constant σ_c , linear σ_w and residual σ_r stresses (Lechner & Freudenstein, 2010)

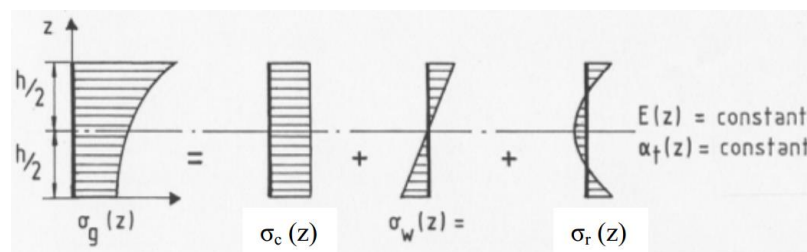


Figure 7-7: Stress distribution in a fully restraint infinite slab (Lechner & Freudenstein, 2010)

Changes within the constant part causes changes of slab-length or constant stress σ_c respectively due to obstructions by friction at the bottom interface or closing of joints during summer time. The linear

temperature gradient Δt causes slab bending and warping stress σ_w which are dependent on the slab dimensions and the support conditions. The residual stresses σ_r , caused by the non-linear part of the temperature distribution, does not translate into deformations even by complete release of restraints (Lechner & Freudenstein, 2010).

The undisturbed warping stresses on a sufficiently large slab can be calculated using equation 7-11 proposed by (Eisenmann & Leykauf, 2003) as follows:

$$\sigma_w = \frac{1}{1 - \mu} \cdot \frac{h \cdot \Delta t}{2} \cdot \alpha \cdot E \quad 7-11$$

And the disturbed warping stresses:

$$\sigma'_w = 1,2 \cdot \sigma_w \quad 7-12$$

The stress is reduced when slab length $L < 0,9 \cdot L_{crit}$ according to (Eisenmann & Leykauf, 2003)

$$\sigma''_w = \left(\frac{L - \frac{2}{3} a'}{0,9 \cdot L_{crit}} \right)^2 \cdot \sigma_w \quad 7-13$$

More information for the equation 7-13 is found in Appendix A.1.

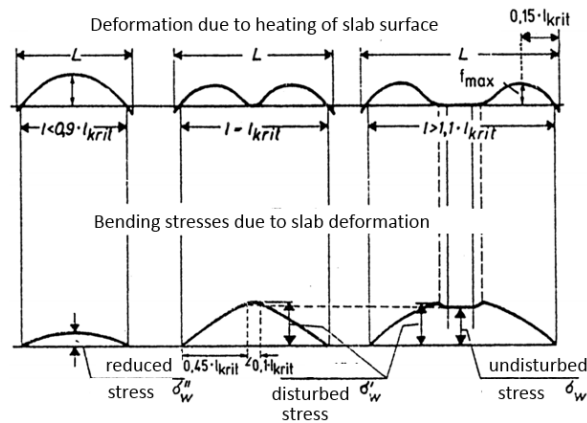


Figure 7-8: Deformation and bending stresses due to heating of slab surface (Lechner & Freudenstein, 2010)

7.3.3 Curling stress

According to (Lechner & Freudenstein, 2010), the curling stress on a sufficiently large slab $L \geq L_{crit(-)}$ can be calculated using equation 7-14 as follows:

$$\sigma_{w(-)} = \frac{1}{1 - \mu} \cdot \frac{h \cdot \Delta t}{2} \cdot \alpha \cdot E \quad 7-14$$

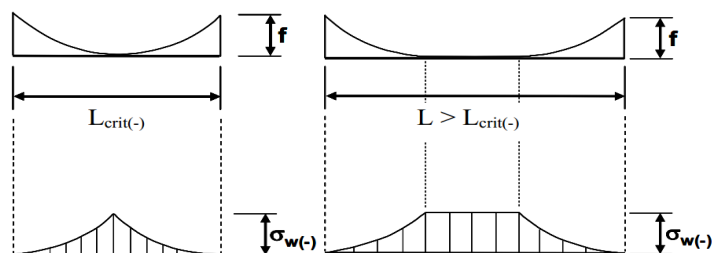


Figure 7-9: calculation of curling stress

7.4 Slab dimension design

7.4.1 Introduction

In conventional whitetopping, short joint spacing is used for slabs to deflect instead of bend to reduce slab stresses (Fwa, 2005). And moreover, short joint spacing can also reduce warping and curling stresses. The common joint spacing is from 12 to 18 times the thickness (Rasmussen & Rozycki, 2004). This factor is 12 to 15 times in (Cole et al 1998, p 206), and 12 to 24 times in (Yu & Tayabji, 2007). The factors listed above are for concrete slab, however asphalt thickness is not included. Based on the relation between slab length and elastic length, Eid (2012) concluded the maximum slab length in relation with the composite thickness (concrete + asphalt) as show in Equation 7-15.

$$l_{max} = 8,19 \cdot (h_1 + h_2) \quad 7-15$$

The slab size constraints according to literatures above are not necessarily applicable to PUTW with precast slab made of ECC, since the flexural fatigue strength of ECC is much higher compared to conventional concrete. The dimensions of PUTW are chosen based on the following criteria:

- Overall pavement system performance (under traffic load, environment load and construction load) has to be at least 25 years.
- The slabs are as big size as possible to reduce the total number of slabs which result in less total hardware for handling job (e.g. lifting and levelling devices) and labours.
- The slab width should be designed according to typical lane width.
- The longitudinal joints should not be in the wheel paths as showed in Figure 7-10.
- The slab must have one dimension (either length of width) smaller or equal to 2.4 m based on slab transport vehicle size to avoid procedure of applying permission from LTA. According to the document named “Administration of heavy vehicle movement” published by LTA, all vehicles that have the overall width of more than 2.6 m required application submissions to LTA to be allowed to use public roads. And when the overall width exceeds 3 m and/or overall height exceeds 4.5 m, the vehicles is required to have (auxiliary) police officers as escorts during the vehicle movement (LTA, 2014). 2.4 m limit is proposed based on 2.6m vehicle width limit minus assumed 0.2m of protecting vehicle side walls.
- Due to the advantages of precast product, the slabs can also be non-quadratic slabs or even hexagon slabs that are very flexible to adapt to complicated geometry. Small size hexagon paving blocks has been used for footpath for quite a long time. And recently, a bigger size of hexagon slab called urban removable pavement has been developed for normal road traffic (Larrard, et al., 2013).
- As a precast product, it is better to have the least slab types and sizes to save cost for formwork type and size. Moreover, inventory for a homogeneous slab type is much cheaper and easier.

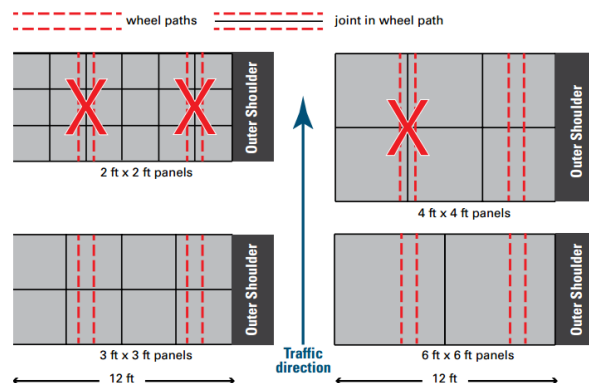
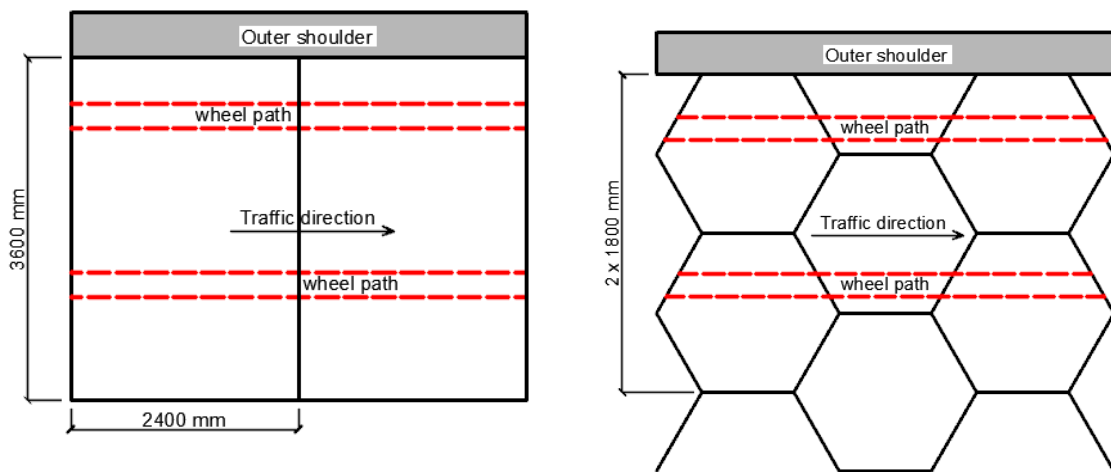


Figure 7-10: longitudinal joints should be arranged to avoid wheel paths (Harrington & Fick, 2014). Note: 1 ft = 30.48 cm

Based on the criteria mentioned, the proposed slab sizes are 3600 mm width x 2400 mm long and hexagon 1800 mm (internal diameter) for complex geometry area as shown in Figure 7-11. The PUTW using these slabs will be evaluated the long-term performance under all possible loading conditions including traffic loading, environmental loading and construction loading during installation phase. For analysis the influence of slab size to stresses in the composite pavement, slab sizes of 900 mm x 900 mm, 1800 mm x 1800mm and 3600 mm x 3600 mm are also used for comparison.

The dimension of PUTW slab for electrified roadways is proposed to be 3600 mm width x 2400 mm long. The location of the culvert should be at the center of two wheel paths. Therefore, the center of the culvert is at 1.5 m from the edge of the outer shoulder.

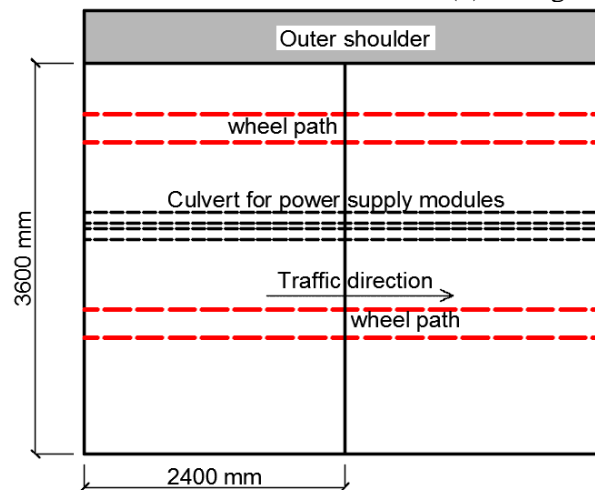
As discussed in section 4.4, the overall composite layer thickness is 170 mm. The layer in between ECC and asphalt includes slab convex nodes and grout, which is kept as thin as possible. For analysis purpose, this transition layer thickness of 10 mm is used. The equivalent support layers' elastic modulus (under asphalt layer) $E_{v2} = 80$ MPa is also chosen as a reference value. The reference values mentioned above will be directly used for all of the later calculations if there is no change to be mentioned.



*Note: Singapore uses left-hand traffic

(a) 3600 mm x 2400 mm slab

(b) Hexagon 1800 mm slab



(c) Electrified 3600 mm x 2400 mm slab

Figure 7-11: Proposed slab types and sizes.

7.4.2 Stresses and deformation of the PUTW slab in construction phase

The detailed construction procedure of PUTW is discussed in chapter 9. In this section, the stress during construction (lifting stress) and the deformation of the slabs are discussed.

During construction of a precast pavement, the slabs have to withstand their own weight as well as dynamic lifting load. Tayabji et al. (2013) recommended that with four-point lifting, the impact factor of lifting stress should be 1.5. In this research, the load applied is 2 times of the slab self-weight as a conservative approach to calculate lifting stress.

After placing and levelling, the slab rests on four-point lifting levelling devices. Due to its self-weight, the slab deforms. This deformation will permanently stay in the pavement. Therefore, the deformation is a very important factor to determine the lifting point locations. There is no more dynamic lifting load after placing and levelling slab, however factor 2 of the slab self-weight is also used to calculate slab deformation as a conservative approach.

The proposed PUTW slabs are symmetric in both longitudinal and transversal directions. Therefore, the lifting points are at 4 symmetrical locations as shown in the Figure 7-12, where X and Y are the offset to the slab edges. In terms of construction stress, the optimum locations of lifting points are the locations where maximum flexural stresses at the bottom and on top of a precast slab are approximately equal and smallest. In terms of deformation, the optimum locations of lifting (or levelling) points are the locations where total slab deformation, including upwards and downwards displacement, is the smallest.

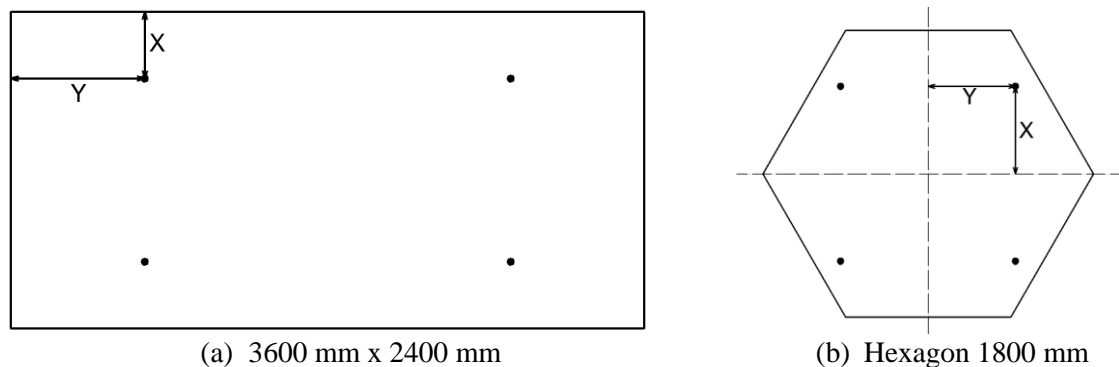


Figure 7-12: Slab lifting locations (top view)

The flexural stresses and total deformation of the slab size of 3600 mm x 2400 mm x 50 mm in construction phase are summarized in Figure 7-13 and Figure 7-14. The optimal values for X and Y are found to be 0.55 m and 0.625 m, respectively when flexural stresses are taken into account. However, when total slab deformation is of interest, values for X and Y should be 0.55 m and 0.80 m, respectively. It is clear that when Y changes from 0.60 m to 0.90 m, the total slab deformation changes greatly and the maximum flexural stress also changes. However, these stress values are far lower than the flexural strength of ECC as presented in chapter 5. Therefore, the lifting (or levelling) locations are chosen based on the total slab deformation.

The same approach is applied for hexagon slab. The reasonable lifting (or levelling) locations are 0.45 m for both X and Y .

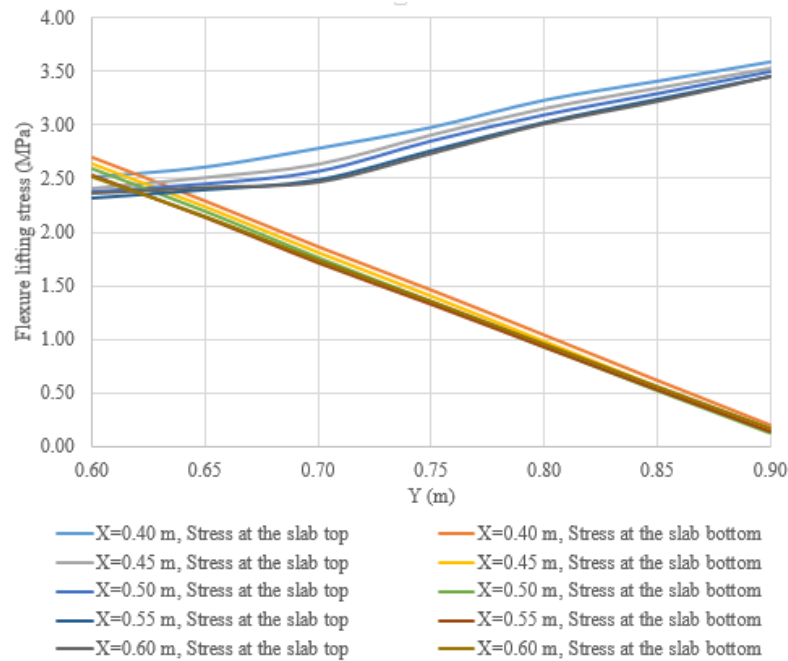


Figure 7-13: Flexural lifting stress (for slab size 3600 mm x 2400 mm x 50 mm)

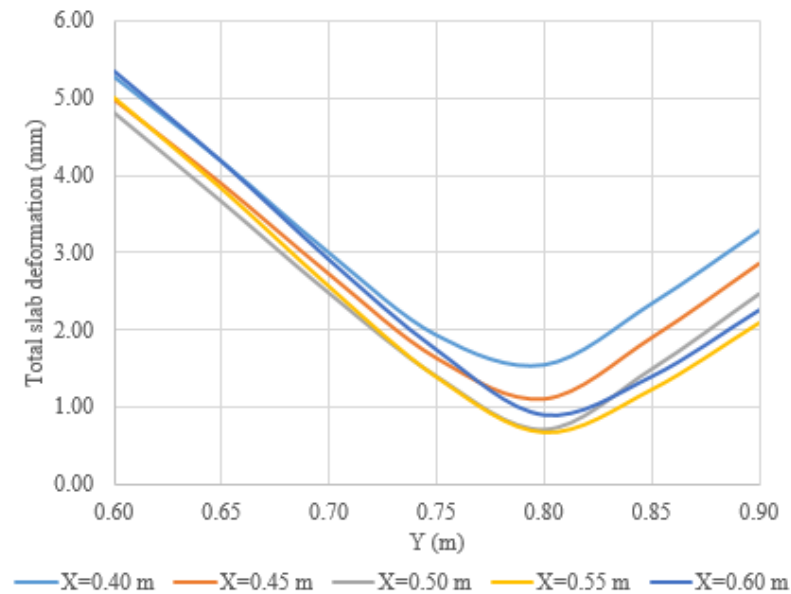


Figure 7-14: Total slab deformation (for slab size 3600 mm x 2400 mm x 50 mm)

For electrified slab 3600 mm x 2400 mm, due the asymmetric location of the culvert, there are three parameters (X, Y1, and Y2) that need to be determined (see Figure 7-15). Using the same approach above, when X, Y1, and Y2 equal to 0.55 m, 0.80 m and 0.80 m, the lowest matched flexural stresses (3.60 MPa) are found for the 50 mm thick E-PUTW. However, when total slab deformation is taken into account, optimal X, Y1, and Y2 are found to be 0.55 m, 0.95 m, and 0.90 m, respectively. The correspondent total deformation and maximum flexural stress are 0.84 mm and 4.07 MPa. At X=0.55 m and Y1=Y2=0.90 m, the total deformation increases to 1.01 mm and stress reduces to 3.89 MPa. For simplification, lifting (or levelling) locations where X=0.55 m and Y1=Y2=0.90 m are chosen.

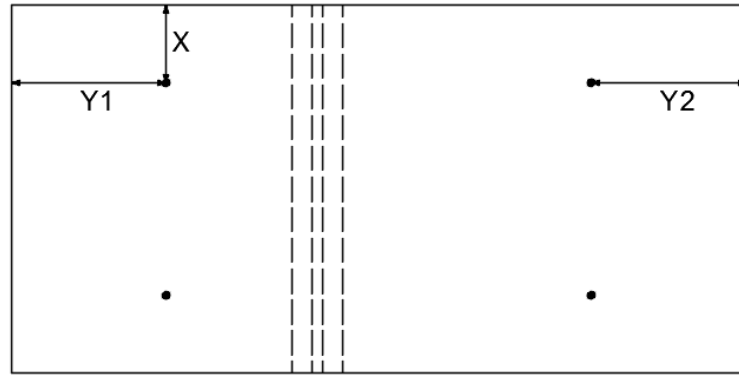


Figure 7-15: Slab lifting locations for electrified slab 3600x2400 (top view)

The lifting (or levelling) locations and the correspondent slab flexural stresses and deformation for all slab thickness are summarised in Table 7-3, Figure 7-16, Figure 7-17 and Figure 7-18.

Table 7-3: Locations of lifting points

Slab type (mm x mm)	3600x2400	Hexagon 1800	Electrified 3600x2400
X (mm)	550	450	550
Y (Y1,Y2) (mm)	800	450	900

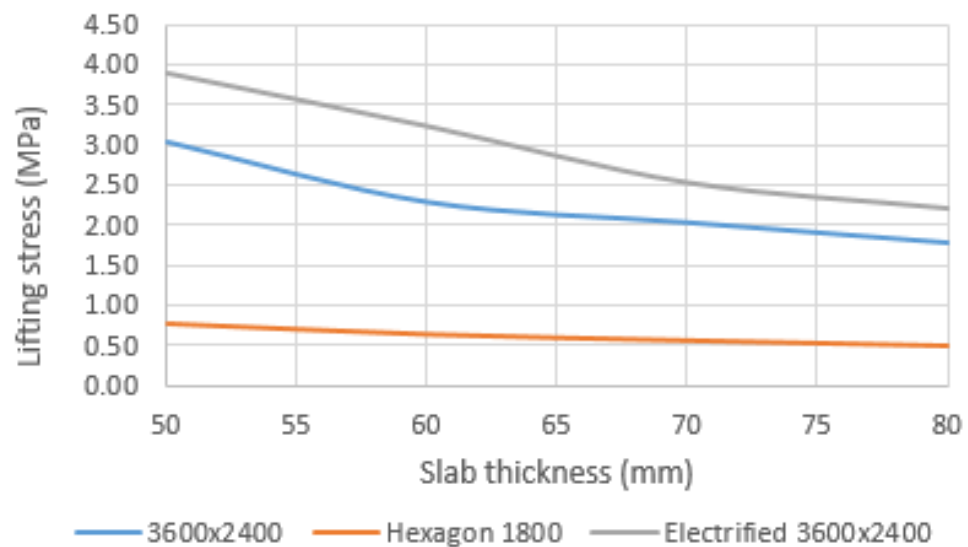


Figure 7-16: Maximum construction flexural stress

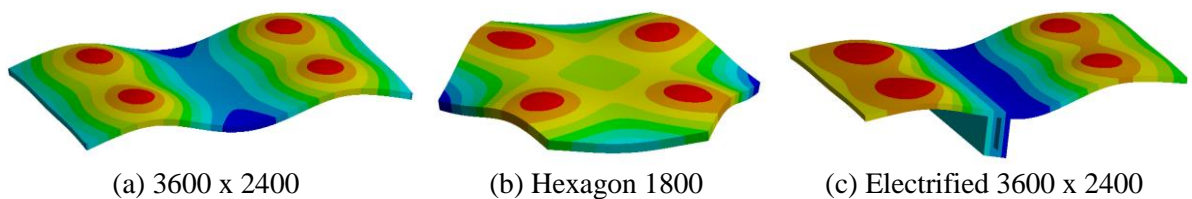


Figure 7-17: Graphical presentation of vertical slab deformation during construction

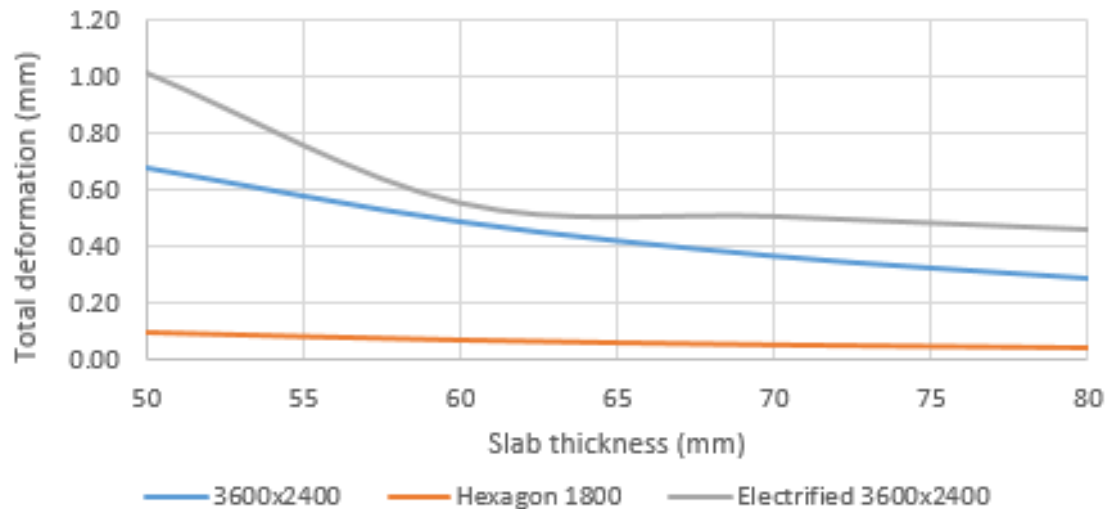


Figure 7-18: Maximum construction total deformation

The thicker the slab is, the smaller stress and deformation occur in the slab during construction. The total deformation in the worst case is 1.01 mm which is much smaller the allowable tolerant 6 mm as presented later in chapter 9. Flexural stresses occurred in precast ECC slab when lifting are very small for the proposed slab sizes with all slab thicknesses and far below the ECC flexural strength. It can be concluded that PUTW slab made of ECC is safe to be lifted during construction without any additional reinforcement mesh.

7.4.3 The influence of slab dimension on traffic and environmental induced stress

7.4.3.1 In PUTW slab

The summary of stresses in PUTW slab using the calculation methods mentioned in sections 7.2 and 7.3 with the help of calibrated non-linear 3D FEM is presented in Table 7-4, Table 7-5, Table 7-7 and Figure 7-22.

Table 7-4: The influence of slab dimension on traffic-induced stress in ECC layer (slab center loading)

Asphalt E-Modulus (MPa)	Thickness combination (mm)	Flexural stress (MPa)				
		900x900	1800x1800	Hexagon 1800	3600x2400	3600x3600
950	(50, 10, 110)	0.89	0.91	0.93	0.97	0.97
	(60, 10, 100)	1.02	1.04	1.08	1.13	1.12
	(70, 10, 90)	1.30	1.30	1.40	1.44	1.43
	(80, 10, 80)	1.29	1.28	1.40	1.44	1.43
2800	(50, 10, 110)	0.19	0.32	0.34	0.37	0.37
	(60, 10, 100)	0.38	0.39	0.38	0.42	0.41
	(70, 10, 90)	0.69	0.71	0.69	0.73	0.73
	(80, 10, 80)	0.82	0.83	0.82	0.85	0.85

Table 7-5: The influence of slab dimension on traffic-induced stress in ECC layer (slab edge loading)

Asphalt E-Modulus (MPa)	Thickness combination (mm)	Flexural stress (MPa)				
		900x900	1800x1800	Hexagon 1800	3600x2400	3600x3600
950	(50, 10, 110)	1.54	1.56	1.69	1.70	1.62
	(60, 10, 100)	1.73	1.72	1.88	1.91	1.85
	(70, 10, 90)	2.07	2.03	2.30	2.28	2.26
	(80, 10, 80)	2.07	1.99	2.31	2.26	2.27
2800	(50, 10, 110)	0.80	0.80	0.76	0.80	0.70
	(60, 10, 100)	1.08	1.07	1.00	1.07	0.96
	(70, 10, 90)	1.49	1.45	1.42	1.45	1.40
	(80, 10, 80)	1.65	1.59	1.57	1.59	1.55

Despite exceptions, the general trend is that the thinner the asphalt layer (while ECC thickness getting thicker) is, the more flexural stress in ECC layer. Stress in ECC is lower when asphalt stiffness is higher. When slab size is taking into account, the stresses change according to slab size. However, the changes are rather very small. The stresses in 3600x2400 slabs are almost identical to 3600x3600 when the load is in the slab center and slightly higher when the load is at the slab edge. Similarly, the hexagon slabs have the same stresses with 1800x1800 slabs with the center slab load case and similar to 3600x2400 with the slab edge load case.

To study the traffic-induced stress in PUTW for electrified roadways, ten locations of wheel load correspondent to ten load cases applied on the electrified PUTW slab's and the culvert's center and edges are analysed (see Figure 7-19). Similar to PUTW, the electrified PUTW pavement slab is supported by an equivalent elastic modulus $E_{v2} = 80$ MPa. The culvert rests on about 60 mm of graded granite, which is then supported by 300 mm sub-base layers then subgrade material. Therefore, the support under the culvert is assumed to have an equivalent elastic modulus of 60 MPa.

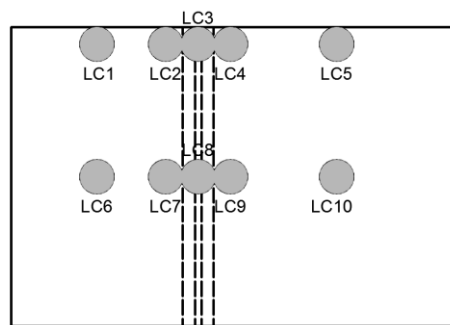


Figure 7-19: Locations of load cases applied on the electrified PUTW

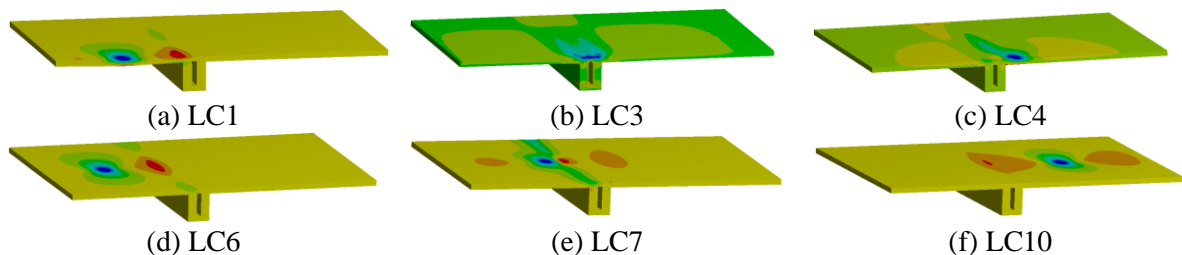


Figure 7-20: Graphical presentation of traffic-induced stresses in electrified PUTW at different load locations

In general, the traffic-induced stresses in electrified PUTW slab at different wheel load locations are relative small compared to the strength of ECC. The maximum values are found at LC3 where the wheel load is directly on top of the culvert edge. It is worth to notice that these highest values (in LC3) are at the bottom of the culvert top cover (see Figure 7-20 (b)). The maximum flexural stresses are at the top of the PUTW slab in LC1, LC6, and LC7. And for LC2, LC4, LC5, LC9, and LC10 the maximum flexural stress values are at the slab bottom. With the existing of the culvert, the flexural stresses at the bottom of the electrified PUTW slab are smaller than they are in the normal PUTW slab without the culvert (see Table 7-4, Table 7-5 and Table 7-6).

Table 7-6: Traffic-induced stress in electrified PUTW slab

Asphalt E-Modulus (MPa)	Thickness combination (mm)	Maximum flexural stress (MPa)									
		LC1	LC2	LC3	LC4	LC5	LC6	LC7	LC8	LC9	LC10
950	(50, 10, 110)	1.29	1.14	2.47	1.24	1.03	1.35	1.44	0.77	1.33	0.87
	(60, 10, 100)	1.25	1.17	2.27	1.44	1.22	1.29	1.12	0.81	1.08	1.08
	(70, 10, 90)	1.56	1.39	2.01	1.47	1.58	1.55	1.39	0.83	1.38	1.54
	(80, 10, 80)	1.59	1.39	1.77	1.43	1.62	1.56	1.36	0.85	1.35	1.55
2800	(50, 10, 110)	0.84	1.14	2.32	1.23	0.69	0.93	0.72	0.72	0.68	0.70
	(60, 10, 100)	0.85	1.23	2.14	1.43	0.65	0.93	0.63	0.78	0.69	0.65
	(70, 10, 90)	0.83	1.30	1.91	1.49	0.85	0.87	0.78	0.82	0.81	0.71
	(80, 10, 80)	0.96	1.28	1.70	1.45	0.98	0.86	0.85	0.85	0.86	0.87

To calculate the environment-induced stress, the temperature gradients in PUTW are extracted from Figure 2-8 with an additional of 10% as a conservative approach. The negative gradients (at night time) are about 0.03-0.04 K/mm, which correspond to the curling stress of about 0.5 MPa. This curling is very small compared to ECC. Therefore, this section focuses more on warping stresses. The maximum possible warping stress in PUTW calculated using analytical formulas and FEM are presented in Table 7-7. The stresses calculated using FEM is about 5-6% lower than stresses calculated using formulas. This can be explained by the fact that the length of flexible support along slab edges (see appendix A.2) is not consider in the equation 7-12 while in FEM, this length is included. Figure 7-22 illustrates warping stress of the slab size 3600x2400. It is noticed that the maximum stress is off center of the slab (see Figure 7-21)

Table 7-7: Gradients in ECC slabs (including grout) and maximum warping stress in PUTW

Thickness combination (mm)	Temperature Gradients	Maximum warping stress (MPa)		Percentage different (%)
		σ'_w (see Equation 7-12)	From FEM	
(50, 10, 110)	0.18	2.05	1.94	-5.58
(60, 10, 100)	0.17	2.26	2.14	-5.47
(70, 10, 90)	0.16	2.44	2.29	-5.96
(80, 10, 80)	0.15	2.57	2.44	-5.00

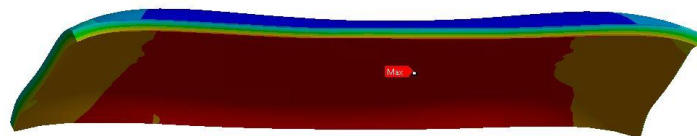


Figure 7-21: Graphical presentation of warping stress with slab size 3600x2400

The influence of slab dimensions on temperature-induced stress is presented in Figure 7-22. The figure illustrates that when slab gets longer, the warping stress at first gets bigger until a certain point then keeps relatively constant. The thicker the slab is, the lower stress it gets at shorter slab length and the higher maximum stress it gets when slab is long enough.

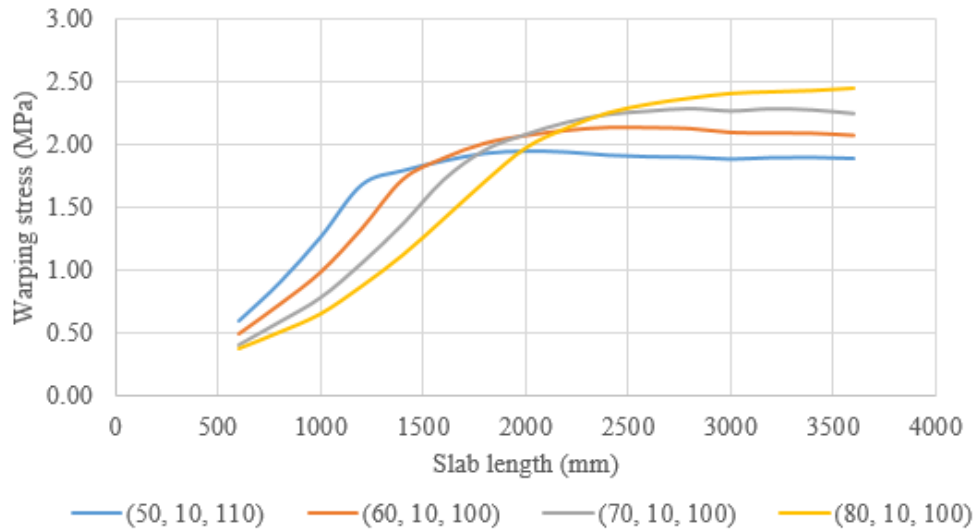


Figure 7-22: The influence of slab length and thickness on temperature-induced (warping) stress

When environment temperature gets higher, asphalt elastic modulus becomes lower which leads to higher flexural stress in ECC slab. The higher temperature registered in the pavement also increases the warping stress in ECC. The possible combination of stresses in Table 7-4 (when Asphalt elastic modulus is 950 with loading at the slab center) and Figure 7-22 is the possible highest flexural stress in ECC slab which is summarized in the Table 7-8.

Table 7-8: Maximum stress in ECC slab under traffic and environmental loading (center slab loading at midday)

Asphalt E-Modulus (MPa)	Thickness combination (mm)	Maximum flexural stress (MPa)				
		900x900	1800x1800	Hexagon 1800	3600x2400	3600x3600
950	(50, 10, 110)	1.97	2.83	2.85	2.85	2.85
	(60, 10, 100)	1.88	3.05	3.09	3.20	3.19
	(70, 10, 90)	1.99	3.26	3.36	3.69	3.68
	(80, 10, 80)	1.87	2.98	3.10	3.88	3.87

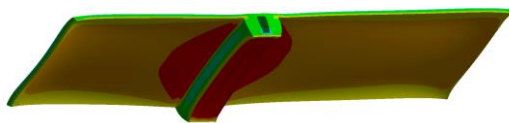
The maximum flexural stress due to temperature loads is almost 2.5 MPa, which is about 0.2MOR of ECC in Singapore. According to the way ECC fatigue test was done (Figure 5-2) and fatigue performance of ECC (Figure 5-3), it can be concluded that ECC slab will not fail under traffic and temperature loads regardless ECC slab size and thickness.

The temperature registered in the electrified PUTW is slightly different than that it in normal PUTW. There is an additional heat source coming from the power supply module to the electrified PUTW slab. As discussed in section 4.4, the saturated operating temperature can be about 50 °C in the culvert. In FEMs, both environmental temperature from pavement surface and operating temperature from the power supply module are considered to calculate temperature-induced stresses that is summarized in Table 7-9.

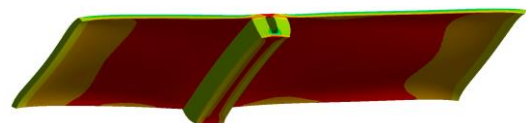
Table 7-9: Maximum temperature-induced stresses in electrified PUTW

Thickness combination (mm)	Maximum warping stress (MPa)	
	At the bottom of the slab	At the bottom of the culvert
(50, 10, 110)	2.48	3.23
(60, 10, 100)	2.41	3.14
(70, 10, 90)	2.51	3.04
(80, 10, 80)	2.56	2.86

It is interesting that the maximum stresses at the bottom of the culvert are the stresses in traffic direction and at the bottom the slab they are stresses in transversal direction (along the longer edge).



(a) stress in longitudinal direction (traffic direction / along the shorter edge)



(b) stress in transversal direction (along the longer edge)

Figure 7-23: Graphical presentation of temperature-induced stresses in electrified PUTW

The maximum possible traffic and temperature stress combination value at the bottom of the electrified slab are the maximum stress in LC2, LC4, LC5, LC9, and LC10 in Table 7-6 and the result in Table 7-9. The overall maximum value, which is $1.55 + 2.56 = 4.11$ MPa, is found at the thickness combination (80, 10, 80), with LC10.

Again, based on loading scheme of fatigue tests (Figure 5-2) and their results (Figure 5-3), electrified PUTW slab will not fail under traffic and temperature loads. In conclusion, flexural stress in ECC is not a decisive factor for choosing slab dimensions as well as performance indicator of PUTW and PUTW for electrified roadways pavement.

7.4.3.2 In asphalt layer

Because the stress in ECC slab is much lower than the fatigue strength of ECC, the fatigue performance of PUTW pavement is dependence on the fatigue strength of asphalt layer. The common fatigue performance criteria for asphalt is tensile strain as presented in section 2.4.1. Asphalt microstrain occurred in asphalt due to traffic loading at the center and edge of slab are summarized in the Table 7-10 and Table 7-11

Table 7-10: The influence of slab dimension on traffic-induced microstrain ($\mu\epsilon$) in asphalt layer (slab center loading)

Asphalt E-Modulus (MPa)	Thickness combination (mm)	Microstrain ($\mu\epsilon$)				
		900x900	1800x1800	Hexagon 1800	3600x2400	3600x3600
950	(50, 10, 110)	345.82	337.49	375.76	375.99	375.72
	(60, 10, 100)	303.69	294.03	331.96	331.37	330.99
	(70, 10, 90)	260.54	251.02	286.16	285.08	284.58
	(80, 10, 80)	223.97	215.67	249.17	246.11	245.52
2800	(50, 10, 110)	206.94	207.11	207.31	206.75	206.51
	(60, 10, 100)	194.28	194.78	195.04	194.23	193.91
	(70, 10, 90)	181.24	182.56	183.09	181.78	181.39
	(80, 10, 80)	168.82	171.10	171.80	170.02	169.57

Table 7-11: The influence of slab dimension on traffic-induced microstrain ($\mu\epsilon$) in asphalt layer (slab edge loading)

Asphalt E-Modulus (MPa)	Thickness combination (mm)	Microstrain ($\mu\epsilon$)				
		900x900	1800x1800	Hexagon 1800	3600x2400	3600x3600
950	(50, 10, 110)	353.65	344.21	376.14	385.51	389.12
	(60, 10, 100)	313.84	301.80	339.54	342.43	346.35
	(70, 10, 90)	274.56	261.42	329.95	311.00	323.60
	(80, 10, 80)	251.48	240.96	316.62	294.00	308.29
2800	(50, 10, 110)	213.01	211.82	211.25	212.28	215.10
	(60, 10, 100)	202.25	200.73	201.03	201.01	204.36
	(70, 10, 90)	201.22	194.88	203.14	191.00	195.11
	(80, 10, 80)	210.18	199.70	207.54	193.00	199.68

Load applied at the slab edge generates higher strain in asphalt. And in general, softer asphalt experiences a lot more strain than the stiffer one. When ECC lab thickness increases (while asphalt thickness decreases), the maximum strain in asphalt reduces in both asphalt's temperature with some exceptions when asphalt elastic modulus is 2800 MPa. The strains in different slab sizes are different however the differences are quite small. The slab 1800x1800 has the lowest microstrain, and the strain increase slightly when slab gets bigger.

The strain in asphalt layer of the electrified PUTW pavement correspondent to ten load cases in Figure 7-19 are listed in Table 7-12.

Table 7-12: Traffic-induced microstrain ($\mu\epsilon$) in asphalt layer of the electrified PUTW pavement

Asphalt E-Modulus (MPa)	Thickness combination (mm)	Microstrain ($\mu\epsilon$)									
		LC1	LC2	LC3	LC4	LC5	LC6	LC7	LC8	LC9	LC10
950	(50, 10, 110)	319.86	260.56	187.64	262.42	323.53	356.13	206.57	30.97	198.95	362.70
	(60, 10, 100)	302.75	239.58	187.67	241.18	307.36	313.63	177.01	30.05	170.26	321.33
	(70, 10, 90)	287.09	225.59	186.32	226.71	292.21	268.55	149.80	28.83	144.26	276.95
	(80, 10, 80)	269.22	210.84	183.56	212.69	274.25	232.03	129.28	27.57	124.58	240.54
2800	(50, 10, 110)	182.64	190.09	151.56	192.17	184.14	198.10	129.16	28.24	125.89	203.11
	(60, 10, 100)	180.83	183.08	153.40	184.72	182.41	185.30	116.04	27.32	112.94	190.88
	(70, 10, 90)	183.98	179.30	155.77	180.57	185.78	172.80	105.32	26.43	102.56	178.83
	(80, 10, 80)	184.64	173.56	156.90	175.30	186.51	161.01	96.38	25.54	93.81	167.27

The maximum asphalt microstrain value in electrified PUTW pavement and in normal PUTW with 3600x2400 slab are compared in Table 7-13. It is noticed that the strains in asphalt of the electrified PUTW pavement are only about 2.5-7% smaller than in normal PUTW with 3600x2400 slab. For simplicity, it is assumed that the electrified PUTW pavement has the same asphalt strains as normal PUTW with 3600x2400 slab.

Table 7-13: Maximum traffic-induced microstrain ($\mu\epsilon$) in asphalt layer of electrified PUTW pavement and normal PUTW pavement with 3600x2400 slab

Asphalt E-Modulus (MPa)	Thickness combination (mm)	Microstrain ($\mu\epsilon$)		difference [%]
		Electrified 3600x2400	3600x2400	
950	(50, 10, 110)	362.70	385.51	-5.92
	(60, 10, 100)	321.33	342.43	-6.16
	(70, 10, 90)	292.21	311.00	-6.04
	(80, 10, 80)	274.25	294.00	-6.72
2800	(50, 10, 110)	203.11	212.28	-4.32
	(60, 10, 100)	190.88	201.01	-5.04
	(70, 10, 90)	185.78	191.00	-2.74
	(80, 10, 80)	186.51	193.00	-3.36

Using the same approach to calculate the allowable load cycle of a pavement based on asphalt's microstrain as presented in section 2.5, the fatigue life of asphalt layer in PUTW is summarized in Table 7-14.

Table 7-14: Allowable load cycles of PUTW based on asphalt flexural performance

Thickness combination (mm)	Allowable load cycles (mil.)				
	900x900	1800x1800	Hexagon 1800	3600x2400	3600x3600
(50, 10, 110)	30.99	32.03	29.96	29.05	28.09
(60, 10, 100)	37.91	39.68	36.00	35.75	34.28
(70, 10, 90)	42.21	46.95	36.11	42.87	39.76
(80, 10, 80)	40.04	46.63	35.63	43.98	39.48

The allowable load cycles are calculated based on asphalt flexural microstrain, therefore it reflects the asphalt's strain trend. The asphalt strain in electrified PUTW are almost identical to PUTW with slab size 3600 x 2400. Therefore, the performance of electrified PUTW is similar to normal PUTW with slab size 3600 x 2400. The system performance of proposed slab sizes is not the highest however the differences are not significant. These allowable load cycles of PUTW (including electrified PUTW), even with the thinnest ECC slab of 50 mm, outweigh by approximately 25% the performance of rigid pavement in Singapore, which was calculated in section 2.5.

7.4.3.3 Influence of composite thicknesses to the vertical shear stress in asphalt at joint

The shear stress in asphalt is calculated based on the formulas presented in section 7.2.3 and FEM. The composite thicknesses combination used for calculation are (50, 10, 110), (60, 10, 100), (70, 10, 90) and (80, 10, 80).

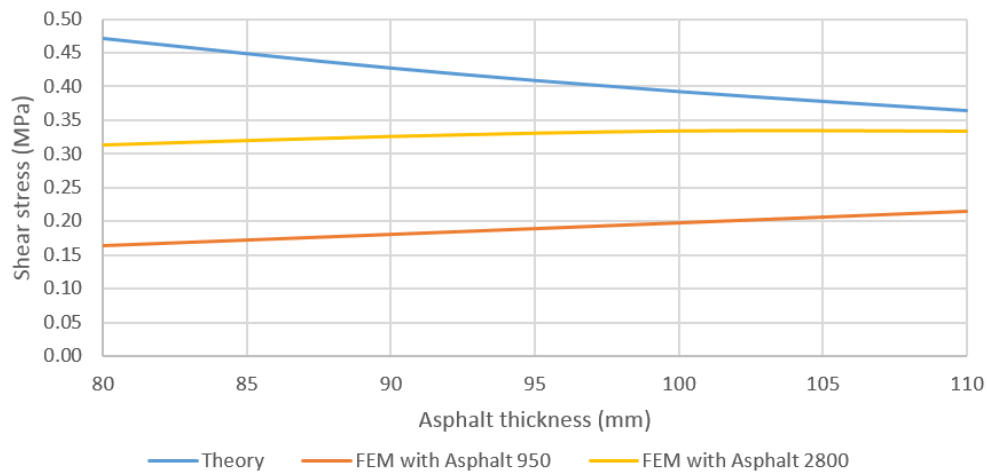


Figure 7-24: Asphalt thickness vs shear stress and joint (slab size: 3600 mm x 2400 mm)

The results from FEM are slightly smaller than the one calculated from the Equation 7-10, this can be explained by the angle of load distribution in ECC is probably more than 45° . The load might be distributed to a much larger angle thus smaller shear stress. The opposite trend of the results from FEM and from formula maybe because of the composite action.

This stress values are quite low; however, they may introduce reflective fatigue cracking in the asphalt layer which effects the overall long term performance of the PUTW. Therefore, even though it is not part of this study, further analysis and testing the joint performance of PUTW is strongly recommended for future researches.

7.5 Parameters study

7.5.1 Changing of composite thickness and support layers' equivalent modulus (E_{V2})

The intention of PUTW is to keep the composite thickness equal to asphalt layers' thickness of Type 1B pavement as listed in Table 2-3, which is 170 mm. However, in the pavement type 1A with porous asphalt the overall asphalt thickness is raised up to 190 mm (Table 2-3). In the case that construction site allows and there is no problem with connecting to other part of the pavements as well as matching the height requirements of other facilities, this total thickness can be changed. The equivalent support layers' equivalent stiffness modulus (E_{V2}) can be different from one location to others, e.g. due to construction quality, moisture, drainage or ages of the layers. The influence of both E_{V2} and overall composite thickness to the performance of overall PUTW system is analysed in this part using the calibrated non-linear FEMs. The combinations to be studied are:

- Slab type and size [mm x mm]: 3600 x 2400, Hexagon 1800
- Overall composite thickness [mm]: 170, 180, 190, 200
- ECC slab thickness [mm]: 50, 60, 70, 80
- Grout thickness [mm]: 10
- Equivalent surface modulus under asphalt layer (E_{V2}) [MPa]: 60, 80, 100, 120
- Asphalt elastic modulus [MPa]: 950, 2800

The results of all 256 combinations are summarised in Figure 7-25 and Figure 7-26. The allowable load cycles are calculated based on asphalt flexural microstrain. The general trend is that increasing slab thickness, composite thickness and E_{V2} will increase the pavement performance. However, there are some exceptions especially when $E_{V2} = 60$ MPa and hexagon slab is used. Overall, these figures can be a reference for PUTW thickness design.

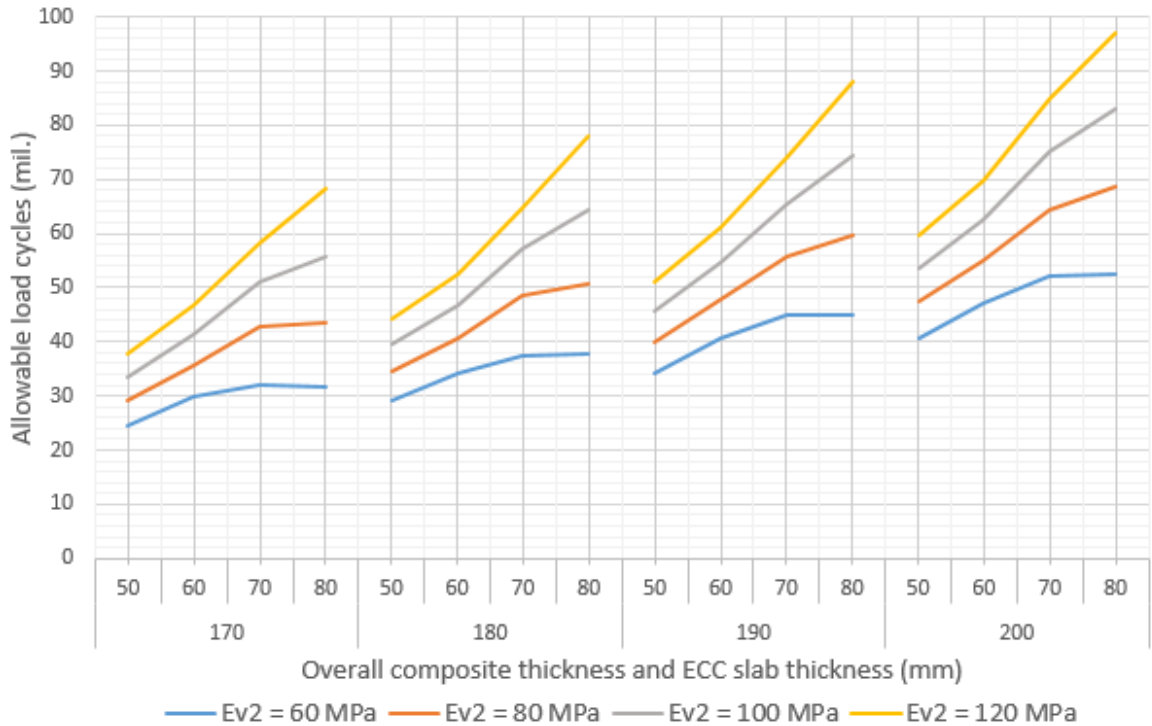


Figure 7-25: Allowable load cycles of PUTW (slab size: 3600 x 2400 and 3600 x 2400 with integrated culvert for electrified roadways) in relation with slab thickness, composite thickness and support layer's equivalent modulus

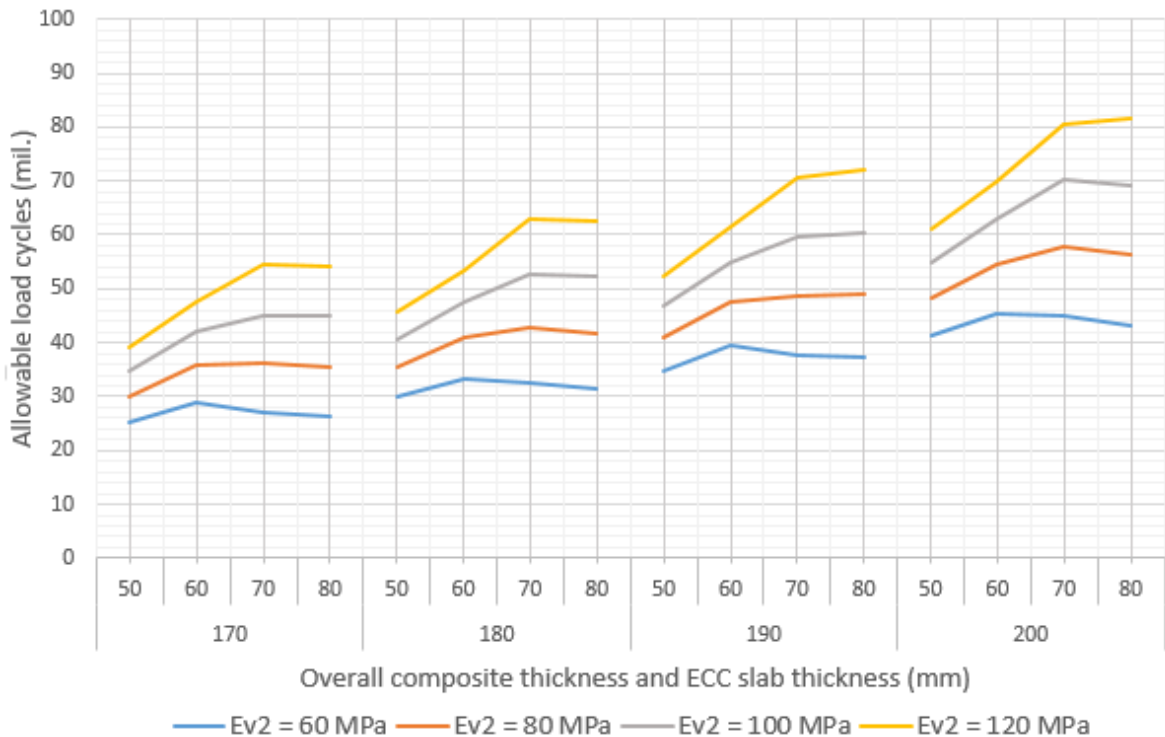


Figure 7-26: Allowable load cycles of PUTW (slab size: hexagon 1800) in relation with slab thickness, composite thickness and support layer's equivalent modulus

With the same ECC slab thickness, the allowable load cycles increase about 30-50% when overall composite thickness increases (or asphalt thickness increases) 3cm. The exceptions are with hexagon slab. There is a marginal decrease of allowable load cycles when the composite thickness increase from

190 to 200 mm at the slab thicknesses of 5 and 6 cm. The practice of rehabilitation of an old asphalt pavement with PUTW is to mill the old asphalt surface layer before installing the PUTW slab to maintain the same pavement height. However, when a construction site allows, it is recommended to keep the remaining asphalt layer as thick as possible because it will provide extra life to the PUTW. However, a special consideration about the old interface between two layers of asphalt has to be made. Because it might create additional poor bond interface in the pavement.

Similar to the increasing of composite thickness, increasing equivalent support layers' modulus gives much more life to the PUTW pavement. Changing E_{v2} in rehabilitation of asphalt pavement using PUTW is almost impossible. However, in the new construction of PUTW, the E_{v2} should be kept high to provide more life to the PUTW.

7.5.2 Changing of interface bonding condition (debonding)

This section focuses of the analysis of the PUTW pavement if debonding is occurred. In designing bonded whitetopping pavement, the common practice is to assume concrete slab is fully bonded into asphalt. However, in reality, the debonding effect may happen due to construction quality or material defects. The pavement will become partly bonded or unbonded system.

The pavement may still be partly bonded that keeps the slabs in place. However, the extreme assumption is that there is completely no bond between asphalt and ECC. When there is no bond in the pavement system, grout layer is removed from the FEM. And the thickness combination of ECC and asphalt will become: (50, 110); (60, 100); (70, 90) and (80, 80). The calibration result of the FEM is shown in Table 7-15 for the thickness combination (60, 100) as an example.

Table 7-15: FEM calibration results in the case of interface debonding (slab center)

Asphalt E-Modulus (MPa)	Flexural stress at the bottom of ECC [Mpa]				Flexural stress at the bottom of Asphalt [Mpa]			
	Ansys	Theory	diff [Mpa]	diff [%]	Ansys	Theory	diff [Mpa]	diff [%]
950	5.09	4.66	0.43	9.14%	0.39	0.37	0.02	5.01%
2800	4.14	3.89	0.25	6.42%	0.96	0.91	0.06	6.09%

Table 7-16: Traffic-induced tensile stress in ECC layer in the case of interface debonding

Asphalt E-Modulus (MPa)	Thickness combination (mm)	Flexural stress (MPa)			
		Slab size 3600 x2400		Hexagon 1800	
		Center loading	Edge loading	Center loading	Edge loading
950	(50, 110)	4.26	4.77	4.41	5.15
	(60, 100)	4.12	4.83	4.27	5.16
	(70, 90)	3.88	4.78	4.00	5.06
	(80, 80)	3.57	4.67	3.70	4.88
2800	(50, 110)	3.40	3.72	3.63	4.17
	(60, 100)	3.59	4.07	3.78	4.44
	(70, 90)	3.57	4.27	3.71	4.55
	(80, 80)	3.41	4.33	3.52	4.53

The summary of maximum equivalent flexural stresses in ECC layer is listed in Table 7-16. Without good composite (bond) action, the stress in ECC due to traffic loading increases dramatically. Such high stress is sufficient to cause slab cracking when normal concrete is used even if the thermal-induced stresses are ignored, which is the common failure mode in bonded whitetopping pavement. The high

flexural strength of ECC; however, is able to sustain the high stress caused by interfacial debonding. Therefore, fatigue performance of the pavement is not limited by ECC in this case. The performance of asphalt layer is taken into account.

The microstrains in asphalt layer with different slab sizes, slab types and location of applied load is listed in Table 7-17.

Table 7-17: Traffic-induced tensile strain in asphalt in the case of interface debonding

Asphalt E-Modulus (MPa)	Thickness combination (mm)	Tensile microstrain ($\mu\epsilon$)			
		Slab size 3600x2400		Hexagon 1800	
		Center loading	Edge loading	Center loading	Edge loading
950	(50, 110)	480.44	652.75	469.93	700.52
	(60, 100)	353.31	672.84	341.41	704.04
	(70, 90)	254.26	717.30	248.99	750.22
	(80, 80)	179.85	766.74	178.29	791.25
2800	(50, 110)	311.67	333.36	309.28	351.44
	(60, 100)	259.78	340.48	255.70	363.83
	(70, 90)	206.81	374.08	205.59	396.89
	(80, 80)	155.21	420.80	156.42	432.99

Tensile strain in asphalt is significantly high in the case of edge loading. The thinner the asphalt is, the higher tensile microstrain in the asphalt will be. These high tensile strains influence the long-term performance of the whole pavement system dramatically (see Table 7-18 and Table 7-19). When debonding happens at the slab center, the influence is quite interesting. The system with thicker ECC performs much better than the one with thinner slab. The system with ECC thickness of 70 mm has almost no influence of debonding effect at the slab center. And interestingly, when slab thickness is 8 cm, the debonding effect even increases the performance extremely significantly. If there is no bond the slab edge, the situation is very severe. The ECC is still under good working condition and forces asphalt to continue to work until end of asphalt fatigue life. However, the strains in asphalt are very high which shorten dramatically the lifetime of asphalt layer, thus whole pavement system. If the slab thickness of 6 cm is used, the extended pavement life after debonding is just about 6 million load cycles, which is about 6 years in secondary roads.

Table 7-18: Allowable load cycle of PUTW dependence on asphalt flexural performance in the case of interface debonding at the slab center

Thickness combination (mm)	Allowable load cycle (Million)	
	3600x2400	Hexagon 1800
(50, 110)	10.31	10.63
(60, 100)	19.40	20.57
(70, 90)	41.45	42.57
(80, 80)	101.56	100.47

Table 7-19: Allowable load cycle of PUTW dependence on asphalt flexural performance in the case of interface debonding at the slab edge

Thickness combination (mm)	Allowable load cycle (Million)	
	3600x2400	Hexagon 1800
(50, 110)	7.38	6.21
(60, 100)	6.88	5.68
(70, 90)	5.23	4.37
(80, 80)	3.69	3.36

Even the assumption of fully unbonding system is rather conservative, the results still give a good indication about the importance of good bonding in PUTW especially bonding at the slab edges. Therefore, joints should be always in good condition. The condition of bonding at the edge should be checked regularly and restored immediately the bond if any debonding action is found. The bond restoration at joints can be done by firstly cleaning the joint with relatively low pressure water then following by injecting the mortar. It is noticed that the pressure of water used should be low enough to not adversely destroy the bond further.

7.6 Conclusion

This part focused on the design of PUTW and PUTW for electrified roadways. As many as possible factors that might have influence on the performance of PUTW were considered. These factors included support layers' equivalent stiffness, overall composite stiffness as well as the interface bonding condition. The theories to calculate stresses in PUTW pavement due to construction load, traffic and environmental loading were summarized. FEMs were successfully calibrated using these theories. The calibrated non-linear FEMs were later used for PUTW analysis.

ECC is such a high performance material that it is not the critical factor to evaluate overall PUTW performance. The allowable load cycles of PUTW is by then dependence on asphalt layer. The graphs (See Figure 7-25 and Figure 7-26) about the relation between PUTW pavement performance and support layers' equivalent stiffness as well as overall composite stiffness were created to be used as references for PUTW thickness design. The parameters study shows that the thicker composite and the better unbound layers' stiffness will improve the service life of the PUTW significantly. Even with the thin ECC slab of 5 cm, the proposed slabs, 3600 mm x 2400 mm, 3600 mm x 2400 mm slab with culvert for electrified roadways and hexagon slab 1800 mm, provide long pavement service life, which is about 25% exceeding the Singapore conventional rigid pavement.

Further intensive laboratory and field tests about performance of asphalt at joints and interface bonding at joint are highly recommended.

8 Life Cycle Cost Analysis (LCCA) of Precast Ultra-Thin Whitetopping (PUTW)

8.1 Introduction

This chapter will focus on evaluating the life cycle cost of a PUTW to determine whether PUTW is an economical solution. Alternative pavement for comparison is Jointed Reinforced Concrete Pavement (JRCP) used in Singapore context, especially at intersection areas. The life cycle cost analysis (LCCA) considers the entire life cycle of the pavements. A well-calibrated traffic microscopic simulation for a case study area in Singapore will be used to forecast user delay cost due to pavement maintenance and rehabilitation.

8.2 Life cycle cost analysis (LCCA) of PUTW

8.2.1 Life cycle cost analysis

LCCA is an analytical tool to evaluate the economic performance of alternative pavement investments over a defined analysis period (Swei, et al., 2014). In pavement engineering, the LCCA takes into account the entire life cycle of the pavement from resource extraction, pre-fabrication, transportation, construction, maintenance, to demolition and recycling (Smith & Walls III, 1998). Since the 1960s, the LCCA has been widely used in the US (Harbuck, 2009) and it has been conducted by nearly 80% US state highway agencies to evaluate pavement alternatives (Chan, et al., 2008).

Many inputs are required in the LCCA. These values can be treated as deterministic or probabilistic in the LCCA procedure. According to (Swei, et al., 2014), the probabilistic LCCA was conducted to evaluate three alternative concrete pavements to conclude that the initial unit-cost is the main variation across all scenarios. Another study done by Scheving (2011) on the LCCA between asphalt and concrete pavement has shown that discount rate, asphalt price and concrete price have the highest impact on the whole LCCA compared to other parameters such as rehabilitation cost and user delay cost. Therefore, depending on the type of pavement investment, the purpose of the LCCA and the specific condition, the impact of each input can be verified and evaluated differently.

The main cost components could be categorized into four groups (Scheving, 2011): initial construction costs (e.g. land procurement, design, equipment costs, material costs, workers salary,), agencies costs (e.g. maintenance, rehabilitation cost, workers salary), user costs (e.g. vehicles operating cost, time delay costs, accidents costs) and environmental costs (e.g. due to pollution, noise). General LCCA methodology is to sum up the monetary value of all benefit and cost throughout the analysis period. This could be achieved by performing different economic evaluations. The most common evaluations are the Net Present Worth (NPW) or Net Present Value (NPV), Cost-Benefit Ratio (B/C), Equivalent Uniform Annual Cost (EUAC), and Internal Rate of Return (IRR) (Harbuck, 2009). The choice of appropriate method can be different depending on analysis level and the uncertainty of input parameters. For pavement alternative evaluation, NPV is considered the most suitable method (Harbuck, 2009).

The Net Present Value (NPV) of two alternative pavements can be calculated using the Equation 8-1 follows:

$$NPV = Initial_cost + \sum_{i=1}^n \frac{User_cost(i)}{(1+r)^t} + \sum_{i=1}^n \frac{Rehabilitation_cost(i)}{(1+r)^t} \quad 8-1$$

Where: t is the yearth of rehabilitation process (minor or major) after construction, i is the number of user cost, j is the number of rehabilitation and r is the discount rate (in Singapore context, discount rate $r=5\%$ (LTA, 2010))

8.2.2 Activity timing of alternative pavements

The selection of analysis period depends on pavement design life. The design life of concrete pavement in Singapore is 25 years while PUTW can last at least 25% longer (see chapter 7). However, the PUTW is chosen to be the same with conventional rigid pavement as a conservative approach. The analysis

period is longer than design life of the pavements, and it should be long enough to include at least one major rehabilitation for each alternative. Therefore, 25-year period is chosen. In the middle of their service life, minor and major maintenance are required to deal with cracking or joint damage. The activity schedule over the analysis period is shown in Figure 8-1.

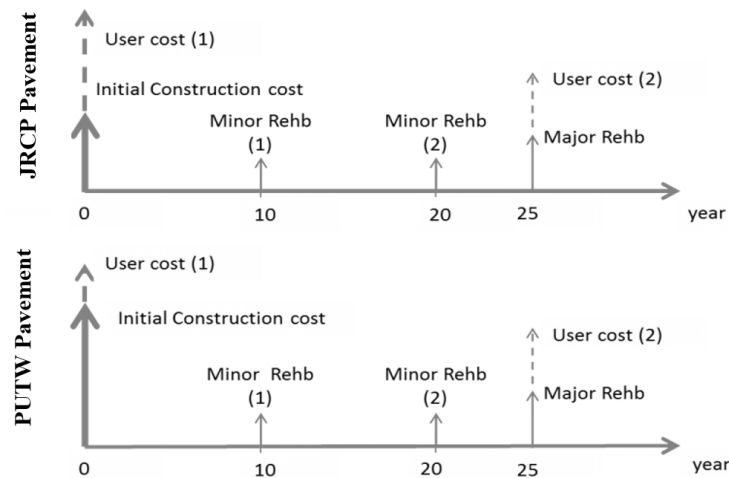


Figure 8-1: Activity schedule of alternative pavements

From the activity schedule of both pavement alternatives, all cost components are similar, in which the initial cost and user cost at the construction beginning are the most important elements to differentiate two options. The initial construction cost includes all materials, equipment, labours cost required for construction of the concrete pavement. This cost for PUTW is higher than that of conventional cast-in-place JRCP due to more complex construction procedure and more expensive ECC material. The maintenance and rehabilitation comprise similar cost components as initial construction cost, but they are much lower. JRCP requires two minor rehabilitations (e.g. renewal of joint sealing) in 10th, 20th year and one major rehabilitation in 25th year. Since there is no existing rehabilitation schedule for the new PUTW, its maintenance cost is assumed to be the same as JRCP.

8.3 User delay cost

User delay cost for the case study Clementi network was estimated in section 2.7. The summary of the results is relisted in Table 8-1 below.

Table 8-1: Travel delay cost estimation

Location	VMS=0		VMS=10%		VMS=30%	
	delay (h)	delay cost (SGD/m ²)	delay (h)	delay cost (SGD/m ²)	delay (h)	delay cost (SGD/m ²)
Int_4123	80.18	891.17	56.48	627.74	29.90	332.3
Int_4105	45.99	511.11	28.97	322.03	23.38	259.8

8.4 Initial cost and rehabilitation cost

The full replacement of 50 m short stretch concrete slab using cast-in-place method in Singapore costs roughly 185-250 SGD/m² (LTA, 2012) depending on the extent of the works, which is equal to 33,300 SGD – 45,000 SGD. In a conservative approach, 33,300 SGD is taken. Data about detail rehabilitation and maintenance costs of conventional rigid pavement in Singapore is not yet available, therefore, the CANPavTM free website tool (Cement Association of Canada, 2015) is used as a reference. With the construction site of 50 m x 3.6 m, the costs are summarized in Table 8-2.

With more complex procedures in construction, the initial construction cost of PUTW is clearly more than JRCP. The most common used Super-Slab jointed precast pavement in the USA is used as a reference for PUTW cost estimation. A Super-Slab pavement costs approximately 380 SGD/m² (270 USD/m²) which includes base preparation, precast fabrication and installation (Chang, et al., 2004).

Even ECC material is about three times more expensive than normal concrete (Li, et al., 2004), the PUTW is three times thinner, and all steel reinforcement, as well as dowel bars, tie bars and slots preparation for dowel/tie bars are completely eliminated. The cost for old slabs' removal and 19mm (3/4") stone dust base preparation for Super-Slab pavement is supposed to be higher or similar to asphalt preparation for PUTW. Grouting work is the similar to both systems. PUTW is clearly cheaper than the Super-Slab pavement. However, as a very conservative approach, the cost of PUTW is equal to the cost of the Super-Slab pavement which is 380 SGD/m² or 68,400 SGD for a construction site of 50 m x 3.6 m.

Using highly durable material, PUTW is expected to have lower maintenance and rehabilitation cost compared to conventional concrete pavement. However, this cost is to be the same as the cast-in-place method.

Table 8-2: Maintenance and rehabilitation cost of JRCP

YEARS (after construction)	Activity	Amount		Quantity		Price/Unit of Quantity (SGD)	Cost (SGD)	NPV (SGD)
12	Reseal Joints	20	% length	8	m	\$10.60	\$85	\$48
25	Partial Depth Repair	5	% area	9	m ²	\$132.50	\$1,193	\$352
25	Full Depth Repair	10	% area	18	m	\$106.00	\$1,908	\$564
25	Reseal Joints	25	% length	10	m	\$10.60	\$106	\$32
40	Partial Depth Repair	5	% area	9	m ²	\$132.50	\$1,193	\$170
40	Full Depth Repair	15	% area	27	m ²	\$106.00	\$2,862	\$407
40	Reseal Joints	25	% length	10	m	\$10.60	\$106	\$15
50	Residual Value						\$1,386	\$121
Total maintenance and rehabilitation Cost							\$6,065	\$1,450

8.5 LCCA Summary

All the costs of alternatives pavements during 25-year periods are listed in Table 8-3 - Table 8-4. The Net Present Value (NPV) of those costs are summarised in Figure 8-2 and Figure 8-3 as follows.

Table 8-3: LCCA of pavement alternative at Intersection Int_4123

	Initial construction cost (SGD)	Rehabilitation cost (SGD)	User cost (SGD)		
			VMS = 0 %	VMS = 10 %	VMS = 30 %
Cast-in-place JRCP	33,300	1,450	167,516	117,998	62,475
PUTW	68,400	1,450	23,931	16,857	8,925

Table 8-4: LCCA of pavement alternative at Intersection Int_4105

	Initial construction cost (SGD)	Rehabilitation cost (SGD)	User cost (SGD)		
			VMS = 0 %	VMS = 10 %	VMS = 30 %
Cast-in-place JRCP	33,300	1,450	96,075	60,532	48,838
PUTW	68,400	1,450	13,725	8,647	6,977

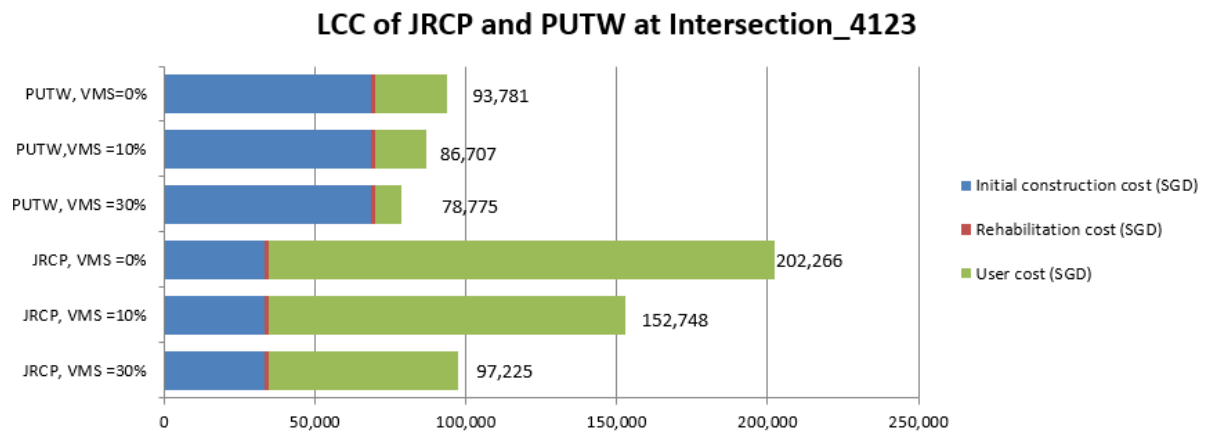


Figure 8-2: LCC of JRCP and PUTW at Intersection Int_4123

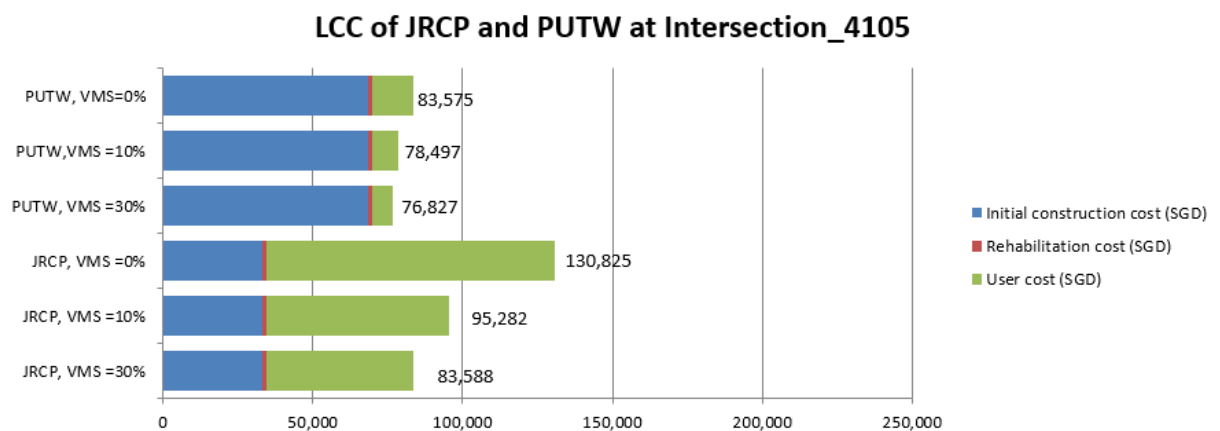


Figure 8-3: LCC of JRCP and PUTW at Intersection Int_4105

Figure 8-2 and Figure 8-3 illustrate that the initial cost contributes mainly to the total cost of PUTW whereas user cost is the most significant component in LCC of cast-in-place JRCP. The results show that LCC varies with construction site locations and traffic diversion ratio (VMS). The more VMS is, the less LCC for both alternatives is. The user cost is reduced to a half when VMS changes from 0 to 30% at the Intersection Int_4105 and this user cost deduction is about 2.7 times at another intersection. However, the PUTW alternative has much less dependence on locations and traffic condition. The travel delay cost in PUTW occupies from about 9% to 25% of total LCC while this value is 59%-83% for cast-in-place method. In general, with the construction delay of cast-in-place method of ten days, the LCC of PUTW is lower than its competitor in the study location. The difference in LCC can be as high as 2.15 times in the case of VMS=0. However, when VMS=30% the LCC of the two alternatives are quite close to balance.

8.6 The cost of electrified roadways

The cost of electrified roadways includes the cost related to the electrical components themselves, and the cost for the pavement. Electrical components related cost for S-Type power supply rail is expected to be similar to I-type power supply rail which is summarized in Table 8-5. PUTW for electrified roadways construction cost is the cost for a normal PUTW in addition to the extra material, labours and construction cost for the culvert. The initial construction cost for PUTW is about 380 SGD/m² as presented in section 8.4. It can be assumed that the cost for electrified roadway PUTW is about 400-450 SGD/m². The advantage of PUTW in minimizing user delay cost at heavy traffic corridors remains. Because the cost for electrical components are more or less fixed regardless the pavement types, PUTW

with the culvert is possibly the cheapest (life cycle cost) pavement type for electrified roadways at heavy traffic corridors.

Table 8-5: Component cost for I-type (or S-type) electrified roadway excluding road construction (Choi, et al., 2015)

Module	Components	Unit cost (USD)	Quantity	Sum (USD)
Inverter [100kW]	-	55,000	4	220,000
Cable	Supply cable	54,000	4.4	237,600
	Common cable	54,000	2	108,000
Cable protection	FRP Package	26,000	1	26,000
Core	Square type	96,000	1	96,000
Capacitor	Module type	300	500	150,000
Misc.	-	50,000	0.2	10,000
Total				847,600

8.7 Conclusion

This chapter focussed on LCCA of two pavement alternatives cast-in-place JRCP and PUTW made of ECC. Like any other PCP, PUTW has the key advantages of minimizing delay to open to traffic and reducing user delay cost, one of the most important components in LCCA. With the help of the state of the art microscopic traffic simulation tool, user delay cost was estimated for a selected case study area in Singapore. The results show that initial cost contributes mainly to the total cost of PUTW whereas user cost is the most significant component in LCC of cast-in-place JRCP. PUTW has higher initial construction cost however due to rapid installation, its user cost is far less than the cast-in-place candidate. With the longer construction delay of ten days, cast-in-place JRCP has higher LCC than PUTW in the study location. However, LCC varies with construction site locations and traffic diversion ratio, which translates to traffic volume. In summary, PUTW made of ECC can be a very economical solution, in terms of LCC for concrete pavement rehabilitation and maintenance, depending on construction site locations and traffic volume. Inhering the advantages of the PUTW, the PUTW with the culvert is arguably the cheapest pavement type for electrified roadways at heavy traffic corridors.

9 Precast Ultra-Thin Whitetopping (PUTW) Process – Guideline for PUTW Application

9.1 Introduction

The PUTW inherits the characteristics of both PCP and UTW. Therefore, the PUTW process is the combinations of the process from both PCP and UTW. However, the PUTW has very different slab dimensions and slab features (e.g. the absent of steel reinforcement, dowel bars and tie bars) to a PCP. And unlike the PCP that is normally installed unbonded on the base layer, the PUTW is installed bonded to the prepared asphalt surface. After installation, the PUTW has characteristics of a UTW pavement. However, slab sizes and the performance of the PUTW with slab made of ECC are different from a normal UTW. The mentioned differences make the process of PUTW slightly different from PCP and UTW.

This chapter focuses on the pavement process that is specifically tailored for PUTW pavement (including electrified PUTW pavement) based on the combinations of both PCP's and UTW's processes. The PUTW process involves pavement evaluation, pavement design, three-dimensional slab arrangement, slab fabrication, pavement installation and maintenance. The process should guarantee high pavement structural and functional performance. These procedures will be discussed in the following sections to be used as a guideline for PUTW and electrified PUTW application.

9.2 Pavement evaluation

Pavement evaluation is an important part of the rehabilitation process. Pavement evaluation should provide valuable information about pavement material, pavement layers, any distress (structural condition) and performance problems (functional characteristics) and their causes as well as traffic forecast data. This information is very important to determine if PUTW is a good candidate. According to (Harrington & Fick, 2014), the evaluation activities include historical data collection and future projections (desk review), on-site visual examination, core analysis, some additional tests (if needed) including FWD, analysis of material-related distress, drainage, roughness and surface friction and pavement evaluation report.

The desk review step aims to collect as much information about the existing pavement as possible. The possible information includes design data and report, construction information, layers' material properties, maintenance histories, traffic data, environment studies and pavement management reports. Determining future pavement performance (structural and functional) requirements is part of this step. The main impact factors are the required design life and forecast traffic data.

Visual examination is the most basic indication of current pavement's performance and structural condition. The types of distress in the form of visual defects or deterioration are determined primarily by occurrence and appearance. And this can give the information about the underlying causes of deterioration. Drainage condition is an important part of distress survey. Consideration should be made for vertical constraints like bridge structures, overhead clearance structures, intersection roadways, etc. when choosing overlay construction method without milling the existing pavement.

Core analyses can supplement information collected from visual inspection. Cores provide valuable information about pavement layer thickness, type and condition of layer materials, the depth of distress, the existing bond between layers.

Pavement structural capabilities are assessed using pavement deflection testing. Through back-calculate methods, elasticity modulus and subgrade reaction k are estimated base on the deflection data. Pavement functional characteristics are also assessed to give information about riding smoothness (roughness testing) and skid resistance (friction).

The last step in pavement evaluation is to summarize all the results of data collection and analyses. This report will be used for the selection of pavement repair or overlay candidate.

9.3 PUTW as a candidate

In pavement selection process, many factors have to be taken into considerations. The common factors include the projected traffic loading and volume, existing pavement condition, layer thickness, drainage, total life cycle cost including construction cost, user delay cost, vehicle operation costs, time factors involving total construction time, repair and maintenance time and frequency, corridor impact like noise level, excess pollution level, skid resistance and smoothness, material availability, and contractors availability, experience and competition (Rasmussen & Rozycki, 2004).

If the PUTW were placing over an existing asphalt pavement, the asphalt pavement has to be ensured in fair or good condition with only minor surface distresses like a pothole, rutting, bleeding, localized surface fatigue cracking, shoving, slippage (see Figure 4-10). These surface defects will then be milled off or repaired before installing the PUTW slab (Harrington & Fick, 2014). The longitudinal and transversal cracks as mentioned in (Harrington & Fick, 2014) is not recommended for PUTW to avoid potential of reflective cracking.

Owning the fast construction advantages of a PCP, PUTW is expected to be constructed in very short time windows of one to two nights. Therefore, PUTW is a good candidate for high volume traffic area because road closure for construction period influences significantly user delay cost, which is one of the main contributions of the life cycle cost (LCC). LCC is one the most important factors for pavement selection, which was discussed in detail in chapter 8. It is also important to notice that PUTW can be used not only on an existing asphalt pavement but also on a newly paved asphalt.

9.4 Pavement design

Detail design of PUTW is presented in chapter 7. Due to PUTW slab is a precast product, the slab size of 3600 mm x 2400 mm is chosen for normal application. In a more complicated geometry area (e.g. at tight curves), hexagon slabs are proposed to be used. It is also possible to use both rectangle slab of 3600 mm x 2400 mm and hexagon 1800 mm slab for one construction side. For electrified roadways, the slab size is 3600 mm x 2400 mm, which features a culvert for power supply module.

Thickness design of pavement structure can be chosen based on the designed life time of the pavement, allowed composite thickness, and unbound layers' equivalent stiffness using Figure 7-25 and Figure 7-26.

9.5 Three dimensional (3D) geometrical design for PUTW (PUTW3D)

A software tool called PUTW3D is developed for automated 3D geometrical design. PUTW3D helps to design joints layout as well as determine 3D coordination (X, Y, and Z) of every PUTW slab. The results will be used for accurately locating and installing of precast slabs. A technical drawing in AUTOCAD showing PUTW slabs on the construction site is an additional outcome of this planning tool.

The PUTW3D was programmed using MATLAB software. The respective coordinate of all slabs will be generated and, in turn, served as input to a script written in AUTOLISP to create 3D drawing in AUTOCAD.



Figure 9-1: PUTW3D development flowchart

Even though PUTW3D can be applied to any types of construction sites, it is designed specifically for potential locations of PUTW in Singapore, which are junctions and bus stops. The slab sizes for PUTW are proposed to be 3600 mm x 2400 mm and hexagon 1800 mm. However, PUTW3D can also be used with some others slab sizes (e.g. square slab 900 mm x 900 mm, rectangle slab with slab width of 1800 mm). The slab combination of rectangle slabs in the straight section of the main intersection approach and hexagon slabs in turning curve is also an option in PUTW3D.

There are several criteria used in PUTW3D:

- The alignment of rectangular slabs follows driving direction, especially in turning curve, while hexagon shapes require no geometrical constraint
- Slab corner angle: not less than 60⁰
- Small modification/adjustment of the site dimension to accommodate all full size (and half size) slabs when needed.

The user manual for PUTW3D is presented in Appendix A.3. One example of PUTW3D result is depicted in Figure 9-2.

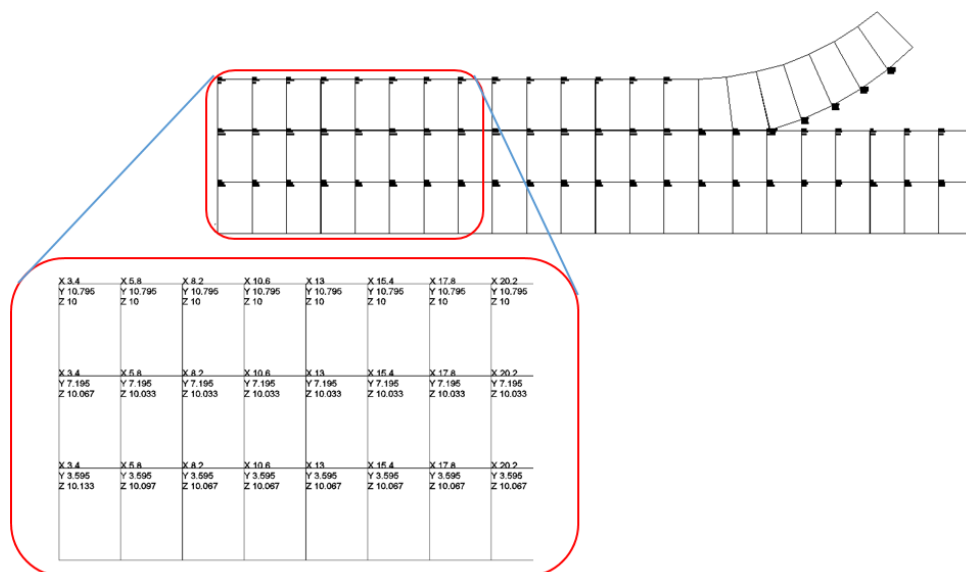


Figure 9-2: Example of joint layout and slabs' coordination in PUTW3D

9.6 Fabrication of PUTW slab

9.6.1 Introduction

The precast concrete production is very well established practice in Singapore. Since 1980s, precast technology has been implemented in Singapore in the large scale in building industry. The precast implementation level is at about 70% for Housing & Development board (HDB) projects, which involves a million HDB flats where more than 80% of Singaporeans live in (Wong, 2014). Figure 9-3 illustrates an example of highly complicated precast elements that use in building industry in Singapore made by TiongSeng group (2012). PUTW are not yet implemented, however the slab fabrication can inherit the general precast expertise, facilities and procedures.



Figure 9-3: Example of architectural precast elements in building in Singapore (TiongSeng_Group, 2012)

The PUTW slab has some features that need to be taken into consideration. It has convex nodes (circular or rectangle) designed at the bottom of the panel to increase the bonding strength between the precast slab and grout layer as presented in chapter 6. There are four lifting devices at four symmetrical locations and several grout ports for injecting grout. Following the concept of two-layer pavement slab, PUTW slab involves two layers of ECC material. The top surface of pavement slab is made of ECC with corundum in the mixture and the normal ECC for the bottom layer. The slab top surface also has grooving textures. For electrified roadways, the PUTW slab has an additional culvert.

The process for PUTW slab fabrications includes the following (Tayabji, et al., 2013):

- Setting up the formwork
- Installing the hardware (lifting devices, grout ports)
- Placing concrete
- Stripping forms
- Applying finishing details to each panels
- Curing and storing panels
- Conducting quality assurance (QA) and quality control (QC) activities.

9.6.2 Panel formwork and hardware

Formwork has to be sturdy and retain tight dimension tolerance over repeated use. And it must be checked regularly. It is recommended to have both top and bottom panels of the formwork to produce convex nodes at the bottom and surface texture on top of the PUTW slab. The flatness of the panel for the pavement surface is very important for pavement roughness (smoothness) later. Therefore, special care for these panels is needed.

One important element of precast product is the lifting devices. In PUTW, these lifting devices will be used not only for lifting the slab but also for slab levelling in construction phase. In precast concrete pavement practice, there is a product named Gracie levelling lift (Gracie Leveling Lift (TM)) (See

Figure 9-4). The Gracie levelling lift includes the body itself which casted into the slab, a lifting bolt, a levelling bolt, and a base plate. It has also plug (plastic or steel) to protect the Gracie levelling lift for panel reused.

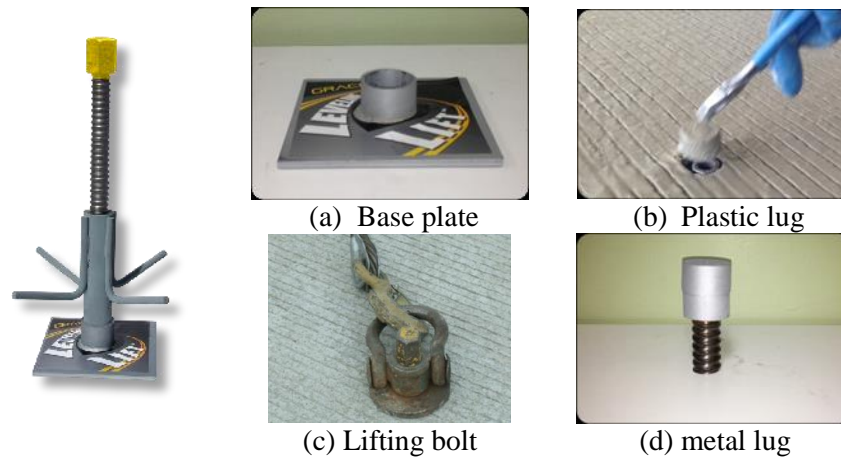


Figure 9-4: Gracie levelling lift (Gracie Levelling Lift (TM)) (Rapid Roadway Solution (TM))

The Gracie levelling lift can be used for PUTW. However, PUTW is much thinner and lighter than conventional PCP, a simpler version of the Gracie levelling lift is recommended. The purpose of the base plate is to support levelling bolts when levelling, it stops the bolts from sinking into the underneath layer. However, large base plate is not ideal for PUTW because it separates PUTW slab and asphalt creating non-bonding effect at the plate location. Moreover, PUTW is thin and light, therefore, asphalt is supposed to be stiff enough to support the levelling bolts directly. In that case, the plate can be eliminated.

The body of the lifting device has to be much shorter to match the thin PUTW slab. Moreover, if non-metallic material is required (e.g. for electrified roadways), a high quality plastic insert body can be used. The plastic body can be similar to the one in the Vossloh fastening systems W11, which is designed for ballasted track with concrete sleepers (see Figure 9-5).

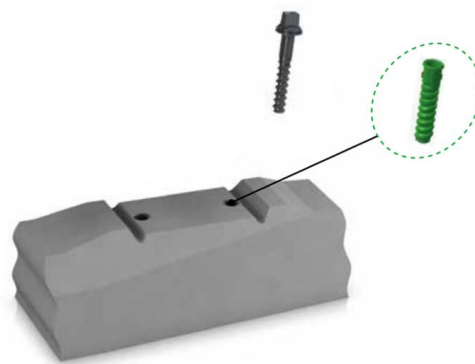


Figure 9-5: Partial of Vossloh Fastening Systems W11 (Vossloh, 2015)

Using ECC material, there is no need for any rebar mesh in PUTW slab. This is a big advantage in reducing labours and time. However, lifting devices and equipment for grout ports have to be attached to the formwork because there is no other possibility to keeps these equipment in place. The lifting devices should be kept firmly into the bottom panel of the formwork, e.g. by bolt, before placing ECC. The bolts will be removed before slab demoulding. The grout ports can be attached to the formwork similarly to the lifting devices or they can be made by drilling slab later on.

9.6.3 ECC mixtures

There are two types of ECC mixtures: normal ECC and ECC with Corundum. The mix design and mix process follow the description mentioned in chapter 5.

9.6.4 ECC placement

Before placing ECC, it is important to check the dimensions of the formwork to ensure the slab geometry tolerances. The slab is casted by placing and compacting the first layer, then followed by the second layer. Two layers of ECC are placed as fresh on fresh manner to assure the integrity of the two layers. The slab can be casted by placing normal ECC first then ECC with corundum later (called top-down method) or the other way round (ECC with corundum first then following by local ECC) (called bottom-up method).

9.6.5 Formwork stripping and panel finishing details

As soon as the ECC gains enough strength for demoulding, the formwork will be stripped and made ready for casting next slabs. It is important in this stage that the pavement slab surface should be brushed to expose the corundum on the surface before ECC becoming so stiff to work with. The slab is then checked for dimension tolerances and applied slab markings such as project name, slab specific, dimensions, and date of fabrications. After finishing jobs, the slab is moved to the storage plant for curing. In curing phase, slab may rest on some supporters (e.g. wooden beam), which tends to create permanent slab deformation due to slab self-weight. Therefore, the supporters should be placed in such the way that maintain slab surface flatness and straightness.

For PUTW with the culvert for the power supply rail modules, soft foam is glued at one specific end of the culvert. When the PUTW is placed (and gently pressed) closely to each other, the foam is compressed to prevent grout and aggregates entering the culvert.

9.6.6 QA/QC activities

One of the main advantages of the precast pavement is the high quality controlled slabs. The slab should be ensured the strict tolerance to prevent installation-related issues. Materials and equipment used in the panel fabrication processes have to meet the project specification requirements by many tests and certifications provided in QC. QA is normally provided by the highway agency's personnel or representatives of an independent third-party organization, who observe that the quality control process is in place and functioning properly, the submittals conform to the specification requirements, and the designated tests for acceptance are met. In PUTW panel fabrication, ECC quality and panel quality are the two distinct types of quality requirement and associated quality testing. ECC testing normally includes the compressive strength, flexural strength, stress-strain curve and unit weight tests. Panel quality normally includes inspecting for panel damages or any sign of early age distress, pavement slab surface quality, skid resistant tests, checking dimensional tolerances (Tayabji, et al., 2013). Slab's flatness, which contributes to pavement roughness (smoothness), is very important factor for pavement functional performance. Therefore, the slab flatness tolerances should be strictly guaranteed. According to the Code of practice for precast concrete slab and wall panels (Singapore Standards Council, 1999), the tolerances are given at ± 6 mm for slab length or width as well as the straightness (for any dimensions up to 3m). The reference geometric tolerance requirements published by PCI are illustrated in the Table 9-1. The general allowable tolerant for local slab smoothness is 6 mm, which is recommended to reduce (e.g. to 1-2 mm) for PUTW slab surface.

Table 9-1: Geometric tolerance requirements (Tayabji, et al., 2013)

Panel Feature	Tolerance
Length or width	±¼ in.
Thickness	±¼ in.
Squareness of corner in plan view	±¼ in. over 12 in.
Squareness of sides in section view	±¼ in. over the thickness
Local smoothness of any surface	¼ in. over 10 ft in any direction
Vertical location of reinforcement	±½ in.
Vertical location of pretensioning strand	±¼ in.
Blockout dimensions (if applicable)	±¼ in.
Location of lifting inserts	±½ in.

Source: PCI 2004.

9.7 Installation of PUTW pavement

9.7.1 Introduction

This guideline for PUTW installation process is designed based on the construction guidelines for jointed precast pavement (Tayabji, et al., 2013). This construction process is applied for constructing PUTW on both existing old asphalt pavement and new asphalt. The process includes:

- Panel installation staging and lane closures
- Asphalt surface preparation
- Panel placement and levelling and grouting
- QA/QC activities

9.7.2 Installation staging and lane closures

Construction of PUTW will be done at night time where the traffic movement has the least impact. The work zone required at least 2 road lanes, the rest of the road lanes are still opened for traffic. The lane closure has to comply with agency's (LTA's) work zone traffic control guidelines (LTA, 2006) (LTA, 2015).

9.7.3 Asphalt pavement preparation

9.7.3.1 New pavement construction

All the support layers of a conventional asphalt pavement are placed and compacted to requirements. Then the asphalt base course is pavement to the designed thickness as in the PUTW. The asphalt surface needs to be roughened to increase the bonding strength between the asphalt and the grout. The asphalt surface has to be kept clean before the panel is installed.

9.7.3.2 PUTW overlays over existing asphalt pavement

The existing pavement should be in a fair or good condition as mentioned in section 9.3. All the areas with potholes, localized alligator cracks or any other surface cracks, or loss of base/subgrade support will need to be repaired before milling. The milled surface will be again inspected further isolated deterioration area (Harrington & Fick, 2014). The good old asphalt should be kept as thick as possible to improve the PUTW performance as presented in section 7.5. However, if there is a need to match the existing infrastructure (e.g. road surface, curb), it is important to ensure the minimum 75 mm of remaining sound asphalt. The asphalt surface should be kept clean before the panel is installed. Figure 9-6 shows an example of asphalt surface after milling at Clementi Road, Singapore.



Figure 9-6: Asphalt surface after milling (at Clementi Road, Singapore)

9.7.3.3 Asphalt pavement preparation for electrified PUTW

After constructing new asphalt or milling the old asphalt to the designed elevation, a slot for cabling tubes and slot for the culvert are cut. The dimensions for the slots are shown in Figure 9-7 and Figure 9-8. h_c is the depth of the slot for the culvert which depends on the thickness combination chosen. It is proposed to choose h_c so that the design elevation at the bottom of the culvert has a clearance of about 5 mm to the bottom of the slot cut after compaction. For thickness combination of (60,10,100) for example, h_s is 305 mm.

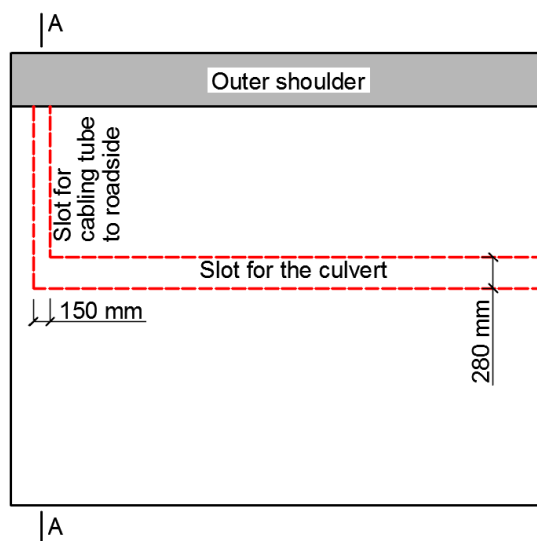


Figure 9-7: slots cut for cabling tube and precast channel (top view)

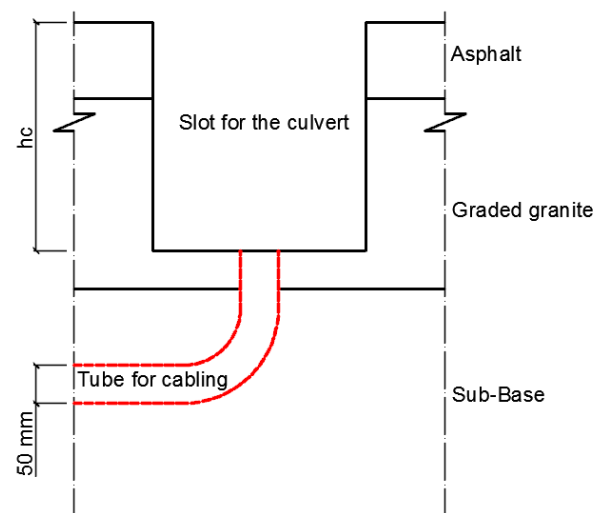


Figure 9-8: cross section A-A after installing tube for cabling and material refilled

Tube for cabling to connect power supply module with roadside equipment is installed to the slot. Slot is then refilled back the material and compacted, after that it is paved back with asphalt (or fast setting grout) and compacted (see Figure 9-8). After cutting the slot for the culvert, the culvert's base is levelled to the designed elevation.

9.7.4 Panel placement, levelling and grouting

In precast concrete pavement practice, there are four methods of panels' placement. The first method is to place the panel directly on finished base or bedding. This is the simplest method. The second method is to use strongback beams to set the panels to the desired elevation. The third method is to use threaded setting bolts to set the panels to the desired elevation. And the fourth method is to use polyurethane foam. The polyurethane foam is injected to the bottom of the slab using grout ports. Slabs are raised by expanded foam (Tayabji, et al., 2013).

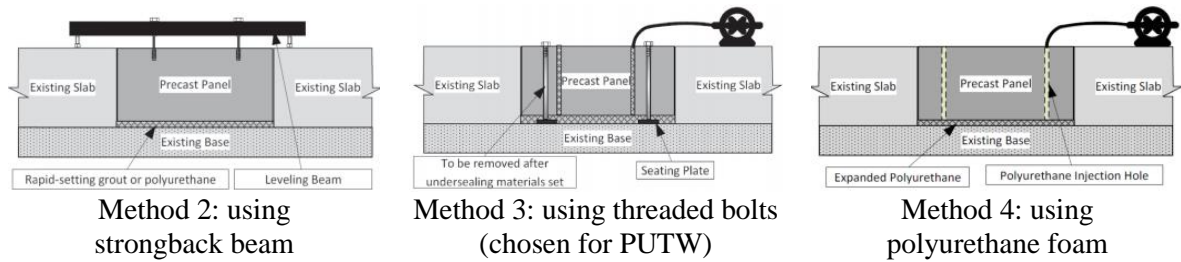


Figure 9-9: Panels placement methods used in precast concrete pavement (Tayabji, et al., 2013)

For PUTW, if the first method is used, final slabs' elevation depends totally on the prepared asphalt elevations which is very hard to achieve high accuracy. Grout injected to slab bottom is not well distributed and bond to slab and asphalt well. Moreover, grinding surface for matching the desired elevation is not an option for PUTW because the slab is already very thin and there is surface treatment embedded on PUTW slab surface as discussed in section 5.5. Therefore, this method is not suitable for PUTW. The fourth method depends very much on workers' competence and the composite bond is still unclear.

The second and the third methods are suitable for PUTW, where slabs elevations can be correctly set. The advantage of the second method is that there is no need for base plates (or seating plates) which might create localized non-bonding effect whereas the advantage of third method is that it doesn't require 2 beams for every single slab. In this research, method 3 is recommended to be used but without base plates (seating plates).

PUTW slabs have levelling bolts at four symmetric locations. When slabs are placed, the levelling bolts will be used to set the slabs to the desired elevations that were calculated in the PUTW3D software tool. The designed slab's elevation should be strictly followed to assure the pavement smoothness, which is a very important factor for the pavement functional performance. Once the slabs locations and elevations are set, the bedding grout is pumped or poured into the grout ports to fill the gaps between slabs and asphalt surface and bond these two layers together.

The recommended bedding grout is the commercially available in Singapore, the Chemilink SS-141. It is a fast setting high performance polymer modified cementitious material that is pourable and pumpable. It can produce an excellent bond strength with substrates. The technical data of the SS-141 is shown in the Table 6-4.

For placing and levelling the PUTW slab with culvert, it is important to take good care of the foam glued at the end of culvert. The foam should be gently pressed and kept at the correct position all the time during placing and levelling. The power supply modules can be inserted into the culverts before or after grouting work.

Figure 9-10 demonstrates the panel placing, levelling and grouting stages of one type of precast pavement in the United States. The construction process of PUTW is simpler than PCP due to the lack of dowel bars and tie bar. However, slabs placing, levelling and grouting works follow the same procedure.

PUTW slabs are so thin (50-80 mm) that they might be lifted by grouting works. Further field study is needed to verify whether this uplift movement of slab exists or not. However, if it happens, the problem can be overcome by putting additional weight at the lifting points.

The horizontal pavement surface gradients or slopes for drainage is about 2%. With the PUTW slab width of 3.6 m, the different in elevation of the slab is 72 mm, which might be higher than the PUTW slab thickness. If grout flows freely by its self-weight, it might soak up to the PUTW slab surface at the slab edge near the outer shoulder. This effect can be checked in future field study. However, this issue

can be solved by applying a small strip of foam at the bottom of the slab near the edge that will be places next to the outer shoulder.



(a) Panel placing (b) Panel levelling (b) grouting
 Figure 9-10: Panel placing, levelling and grouting in precast pavement (Rapid Roadway Solution (TM))

9.8 Monitoring and maintenance of PUTW

Unlike UTW, the PUTW slab made of ECC is unlikely to fail under normal traffic and environment condition. However, special care should be made for joints conditions especially interface bonding at joints. PUTW joints should be monitored or checked regularly and restored the bond immediately (by grouting) if any debonding action is found.

It is possible to use PUTW as a removable pavement in some special cases, for example: utility work underneath the PUTW pavement. There are two options for PUTW slab and asphalt removal. The first method is to remove the PUTW slab without damaging the asphalt at PUTW joints. PUTW slabs can be removed by firstly saw cutting the joints until bottom of the grout layer then lifting the slab. The bonding strength between grout and asphalt is expected to be quite high as presented in chapter 6. Therefore, directly lifting slab using four lifting bolts at once might not be possible. The slab lifting process should start from one edge of the slab using one or two lifting bolts until the slab is totally debonded from asphalt. After that, the slab is lifted using four lifting bolts. Asphalt is saw cut at the desired area for the underneath works. However, the asphalt saw cut locations must be offset from the PUTW pavement joints to avoid damage asphalt at PUTW joints. Pavement is retrofitted back until asphalt base course layer as common practice in flexible pavement. PUTW pavement process is then applied.

The second method for PUTW slab removal is to firstly saw cut the joints until the bottom of the asphalt layer. In this case, the slab is much easier to be lifted. After all other works are done, pavement will be retrofitted back until asphalt base course layer as common practice in flexible pavement. Due to the fact that asphalt was previously saw-cut, the retrofitted asphalt is unlikely to connect well with the old one to create a homogenous layer. The asphalt disruption especially exactly at PUTW joints is clearly very unfavourable to PUTW overall performance later. Therefore, method to improve to asphalt layer discontinuity should be done. Besides methods working on the asphalt layer itself, reinforced mesh or any load transfer devices can also be introduced. After restoring the continuity of asphalt layers at PUTW joints, PUTW slabs can be installed as usual.

PUTW slabs are durable therefore the slabs are expected to be reusable in the condition that lifting devices are protected with plugs after construction. However, some works should be done before slabs can be reused. Therefore, it might be not possible to reuse the slabs at the same location. Asphalt and grout are expected to bond well to the bottom of the PUTW slabs. Asphalt sticks to the bottom of slab should be removed totally. Grout might bond too well to the slab especially around the convex nodes. Therefore, totally removing of grout layer without destroying the nodes might be impossible. Partly

grout removal is recommended. However, the slab thickness might be slightly changed due to the remaining grout on slab. Therefore, when reusing these slabs, considerations of slab thickness and overall composite thickness should be made. After these steps, grout ports should be provided by drilling. Slabs are by then ready for paving.

The first method of slab removal has the advantage of maintaining the asphalt continuity at PUTW joints which is very important for overall PUTW performance. In the second method, the PUTW is easier lifted. However, method to improve the asphalt layer discontinuity at joints need to be done. The feasibility of these two method is proposed to be studied more detail in a full-scale testing.

For maintenance of power supply rail modules, the PUTW for electrified roadways is opened at one specific end of the pavement. The power supply rail modules can be taken out from there for maintenance.

For maintenance of the PUTW for electrified roadways pavement itself, the power supply rail modules also need to be taken out. Then, the process continues like a normal PUTW.

9.9 Summary

This chapter focused on the overall process of a PUTW pavement and PUTW pavement for electrified roadways. All procedures including pavement evaluation, pavement design, three-dimensional slab arrangement, slab fabrication, pavement installation and maintenance were discussed. These procedures were tailored from the combinations of both PCP's and UTW's processes based on the similarities and differences between PUTW and the other two pavements. These pavement procedures will be used as a guideline for PUTW application.

The PUTW process was presented in the way that keeps in mind the high-quality pavement in both structural and functional performance. The high pavement structural performance was considered throughout the chapter. The functional performance is guaranteed by accurately determining 3D slab coordination using the newly developed PUTW3D software tool then following by strictly controlled slab's fabrication and installation processes.

10 Conclusion

Extended road closure for rigid pavement maintenance and rehabilitation at heavy traffic road sections leads to a very expensive user delay cost. In Singapore, when a rigid pavement is used at the junctions, there is quite a complicated pavement structure at the transition area between the concrete and asphalt pavement. The supporting layers of concrete pavement, asphalt pavement and transition area pavement are also different, which interrupts the construction work for supporting layers spot by spot.

In addition, electrified roadway, which allows charging of EVs while they are in operation (moving or stationary), has good potential to be widely adopted in the near future and is an attractive approach to switch mobility from conventional fossil fuel traction to future electric traction. However, an applicable road pavement, which can help to broadly implement electrified roadways into a road management system, is not yet available.

The pavement that can overcome the mentioned issues does not yet exist in Singapore context. Therefore, this research focused on the two overall scopes:

- Identifying requirements and characteristics of the new pavement system
- Developing a pavement system that fulfils the identified requirements.

Singapore is an extremely dense country with a vehicle population of nearly 1 million. The 80 kN equivalent single axle loads (ESALS), which was calculated based on the traffic data that was collected by traffic camera and manual traffic counting, is very high throughout the network especially along highways and secondary roads which are in average 3.6 million/year and 0.9 million/year, respectively. For pavement structures, asphalt pavements are intensively used throughout the road network, whereas rigid pavements are used only at some traffic junctions and bus stops. The pavements are designed based on the Standard Details of Road Element (SDRE) published by Land Transport Authority (LTA) (LTA, 2015). The most common asphalt pavement for the heaviest roads has total asphalt thickness 170 mm, which is supported by 250 mm graded granite layers and 300 mm of sub-base material. The rigid pavement is the jointed reinforced concrete pavement that uses 225 mm thick slab. Due to some performance issues, this type of rigid pavement is becoming less popular. As a tropical country, the temperature registered in the pavement does not vary significantly all year round. The temperature on concrete pavement surface changes from 25°C at night to a maximum of 48°C in the noon time daily. Using a generous approach, the structural life time of asphalt and concrete pavement in Singapore are 15 and 25 years for heavy traffic junctions (non-expressways), respectively. User delay cost due to rigid pavement reconstruction was estimated for a selected case study area in Singapore with the help of the state of the art microscopic traffic simulation tool. The user delay cost at the study area is significantly high that is up to 5 times of the construction cost itself. An alternative pavement, which can be constructed quickly to reduce the user delay cost at heavy traffic junctions, is needed. The target design life of the alternative pavement is at least as good as the current rigid pavement, which is about 25 years.

Electrified roadways are roadways that have inductive charging components embedded inside. Therefore, they allow energy to transfer wirelessly to EVs and to charge the battery or to propel the engine when electrical vehicles (EVs) are on the move (or stationary) using Inductive Power Transfer (IPT). The locations for electrified roadways can be at taxi stands where taxis are queuing and moving slowly in a couple of minutes or up to an hour at the airport to wait for their turn to pick up passengers. For buses, these locations can be at bus terminals or bus stops. Locations at traffic lights or some key sections of roads can also be part of an electrified roadway network. If the electrified roadways are well organized and located around the city, where EVs could charge their battery whenever needed, there will be no more range limitation. In this case, the battery capacity could be reduced, that leads to the reduction of the battery weight, size and cost. Since the 1980s, the electrified roadways technology has gone through many generations with significant improvement in wireless power transfer, safety as well as road construction feasibility. However, there is still concerns about high user delay cost due to long

construction time as well as long term protection of the power supply modules and long term performance of the pavement. The requirements for an electrified roadways pavement were identified. These requirements include high performance, long lifespan, fast construction and maintenance. The power supply components should be accurately positioned and well protected inside the pavement. The pavement material should not include metallic material, i.e. steel reinforcement or metal load transfer devices. Interestingly, the possible locations for the electrified roadways are exactly the locations where PUTW shows the highest potential. The requirements of the electrified roadways also match with the characteristics of the targeted alternative pavement for rigid pavement in Singapore at the heavy traffic junctions.

Based on the identified requirements, a system called Precast Ultra-Thin Whitetopping (PUTW) is proposed. PUTW is an innovative pavement system that applies the very fast construction characteristic of precast concrete pavement (PCP) technology for Ultra-thin Whitetopping (UTW). PUTW is aimed to be an alternative for Singapore rigid pavement at heavy traffic junctions and bus stops where extended road closure is an issue and be used for electrified roadways. The pavement structures are proposed as shown in Figure 10-1.

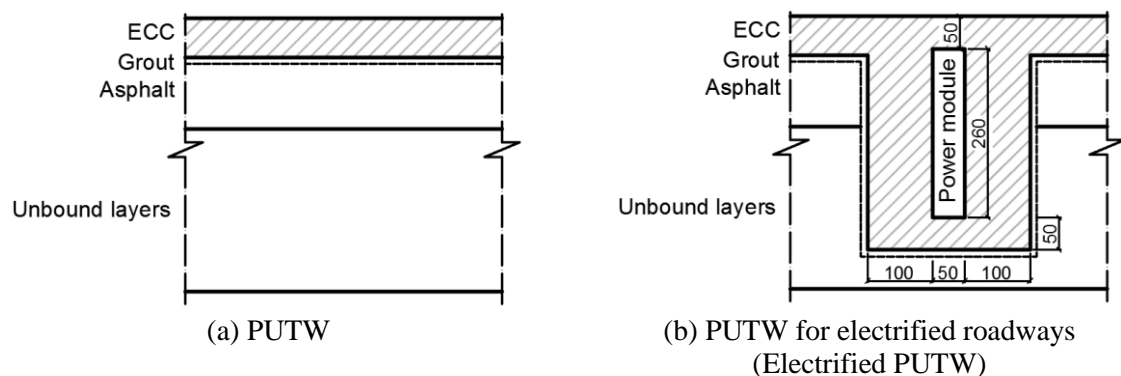


Figure 10-1: The proposed PUTW pavement structures

There are several research questions that have been answered in this study in order to develop the PUTW (including PUTW for electrified roadways) concept successfully:

- How is the structural performance of the PUTW pavement?
 - What are the pavement material's properties and performance?
 - Is there enough bond strength at the composite interface?
 - What is the design of the PUTW?
- How is the functional performance of the PUTW pavement?
- Is PUTW an economical solution?
- What are the guidelines for PUTW implementation?

The structural performance of PUTW pavement systems depends on firstly the material properties of pavement layers; secondly, interface bonding in composite layer; thirdly, PUTW slabs dimensions and lastly, joint performance.

- The PUTW pavement uses the asphalt pavement structure, which is used for the heaviest roads in Singapore, except for the pavement slab which is made of ECC. The asphalt pavement has total asphalt thickness of 170 mm supported by 250 mm graded granite layers and 300 mm of sub-base material. In PUTW, partial thickness of the asphalt (50-80 mm) is replaced by the PUTW pavement slab. The specification of asphalt layer and unbound materials for base, sub-base and sub-grade layers are according to Singapore standard specifications (LTA, 2010). Common fatigue performance criteria for asphalt is its tensile strain. A series of the fatigue functions were reviewed. The fatigue function from a recent research (Stubbs, 2011) in

combination with the factor that considers the difference in loading rate in the laboratory and reality (Lechner & Freudenstein, 2010) was used for further PUTW analysis.

- A new version of Engineered Cementitious Composite (ECC), called local ECC, was developed for the structural layer of PUTW slabs. This version of ECC uses ground granulated blast-furnace slag (GGBS) and river sand instead of micro-silica sand and coal fly ash that are used in typical ECC, because micro-silica sand and coal fly ash were initially difficult to find in Singapore. The local ECC has a very high modulus of rupture (MOR), resulting from the tensile strength (about 5 MPa), and moderate tensile ductility (above 1%). The results from fatigue tests indicated that the local ECC has superior fatigue performance. Also, its fatigue performance is even better than the typical ECC. Moreover, ECC material does not influence the electromagnetic fields. In addition, the non-linearity of ECC material model was also successfully calibrated in FEM for further application.
- The interface bonding is extremely important in PUTW pavement. There are two bonding interface in PUTW: slab-grout and grout-asphalt. The interface grout-asphalt is similar to the interface in UTW where fresh concrete is laid over a prepared asphalt. The requirements shear bond strength at the interfaces were calculated using the calibrated FEMs with all safety factor included. Methods for improving interface bond strength were discussed. The shear bond strength requirement at the interface grout–asphalt is rather small (0.6 MPa). This value is achievable in the previous UTW good practice. Laboratory tests were done to test the actual bond strength between the precast slab and grout layer. Three types of slab’s bottom surface were proposed: (a) flat surface, (b) with convex circular nodes, and (c) with convex rectangle nodes. Direct tensile tests and pull-off tests were done using testing frames, which were manufactured in-house. The test’s results indicated that there were all types of failures: directly at the interface, at the grout, at ECC, or their combinations. However, it varied depending on the type of testing and slab’s surface. The bond strength of the samples with square convex nodes gave the highest value, and it was the most consistent. In contrast, the samples with a flat ECC surface gave the lowest bond strength and inconsistent results. Moreover, some samples with flat surface failed even during the test set-up. In conclusion, the bond strength requirement for PUTW is fulfilled by any types of slab’s bottom surface. However, due to the inconsistency of samples with a flat surface, it is recommended to use only the convex nodes types for PUTW slabs.
- The dimensions of PUTW were studied considering as many as possible factors that might have influence on the performance of PUTW. These factors included support layers’ equivalent stiffness, overall composite stiffness as well as the interface bonding condition. The analysis of the PUTW was done using the calibrated non-linear FEMs. ECC material using for PUTW slab has a very high fatigue performance. Therefore, the allowable load cycles of PUTW is dependence on asphalt layer. Even with the thin ECC slab of 50 mm, the proposed slabs, 3600 mm x 2400 mm, 3600 mm x 2400 mm with integrated culvert for electrified roadways and hexagon slab with internal diameter of 1800 mm, provide long pavement service life, which is 25% exceeding the conventional rigid pavement that is commonly used in Singapore. The parameters study shows that the thicker composite and the better unbound layers’ stiffness will prolong the service life of the PUTW significantly. Moreover, reference graphs (see Figure 10-2 and Figure 10-3) were also created to be used for thickness design of PUTW.

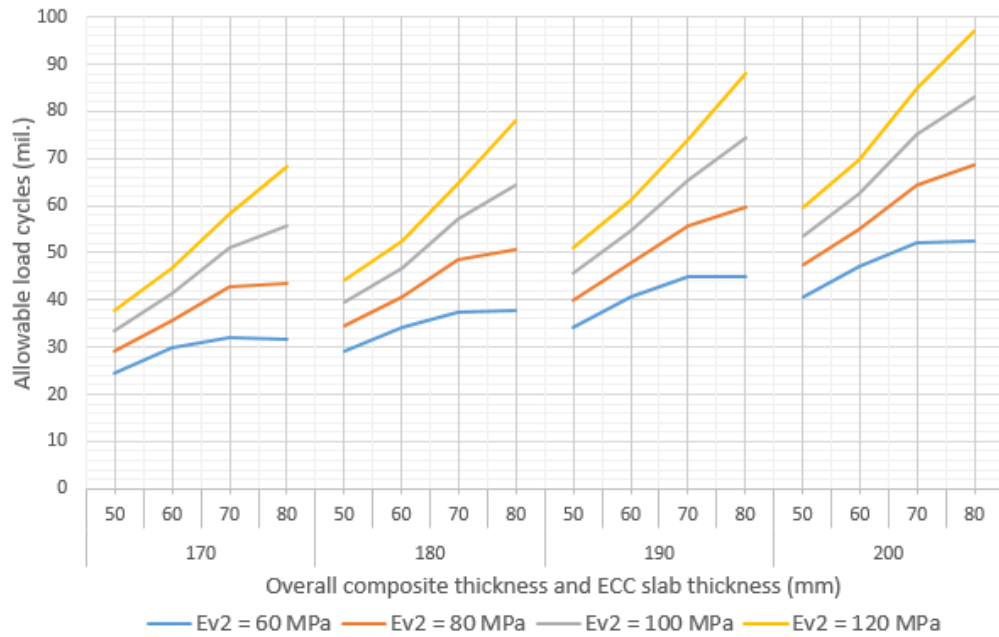


Figure 10-2: Allowable load cycles of PUTW (slab size: 3600 x 2400 and 3600 x 2400 with integrated culvert for electrified roadways) in relation with slab thickness, composite thickness and support layer's equivalent modulus

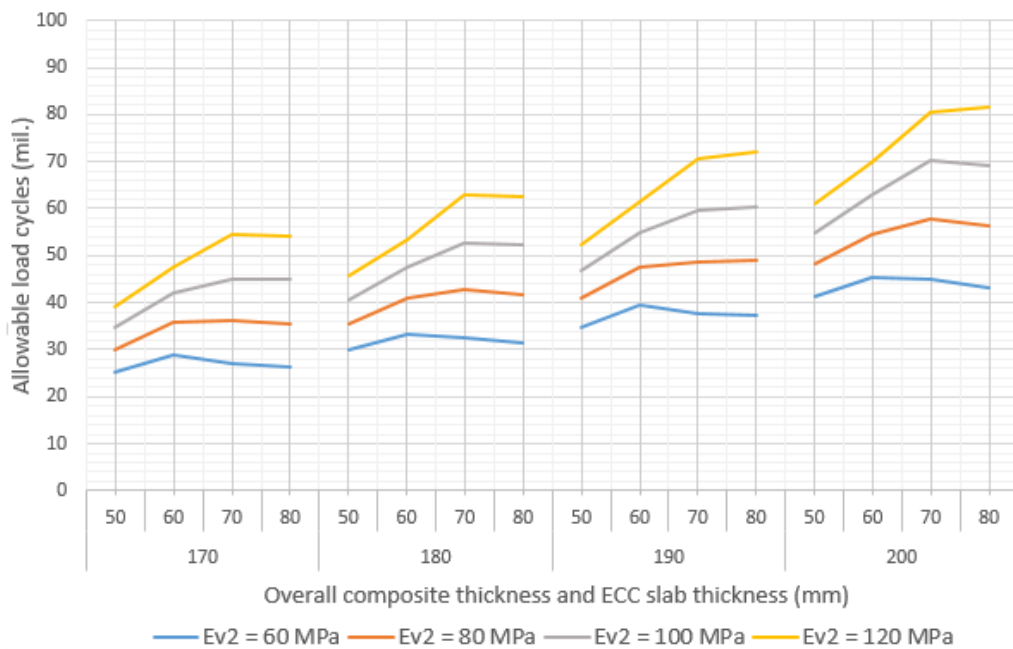


Figure 10-3: Allowable load cycles of PUTW (slab size: hexagon 1800) in relation with slab thickness, composite thickness and support layer's equivalent modulus

- Further intensive, large sized laboratory and field tests about performance of asphalt at joints and bonding at joint are highly recommended for future researches because these were not within the bounds of possibilities of this research.

The functional performance of PUTW is decided by two factors, roughness (smoothness) and skid resistance. The roughness of PUTW is decided by slab surface and the elevation correctness especially at joints. PUTW slabs are manufactured with slab surface as flat as possible. This is easily achieved by high quality formworks. With special lifting and levelling devices, the slabs can be levelled at a very high accuracy. Improving road grip of pavement made of ECC is of very high interest. Skid resistance

of pavement is a very important factor for road safety. ECC is a cementitious material with typical fine aggregates in the mix design, therefore, it does not provide enough grip on the surface. A new version of ECC was developed for the pavement surface layer. Corundum is an extremely hard material, which was successfully integrated into the ECC mixture. The new version of ECC, with a certain percentage of sand replacement by corundum (50-100%) in the mixture, still maintained very high flexural strength of a typical ECC. This new version of ECC, with exposed surface by steel brushing in one day after casting, significantly improved the skid resistance compared to the typical ECC. With corundum in the mixture, ECC gave higher skid resistance than the requirement for a new road in Singapore (65 British Pendulum number (BPN)), even after 100,000 load cycles of traffic simulation, which is equivalent to 5 to 10 years of traffic. And for the whole pavement lifetime, the skid resistance remains above 60 BPN, which is much higher than the Singapore requirement for intervention level at 45 BPN. Longitudinal grooving textures can also be used to reduce road-tyre noise with only slightly compromising the skid resistance. It can be concluded that the skid resistance is expected to last until the end of the pavement life time without any further intervention.

Life cycle cost (LCC) is one of the most important factors in pavement type selection. In this research, Life cycle cost analysis (LCCA) was done for two pavement alternatives cast-in-place JRCP and PUTW at one selected location in Singapore road network as a case study. With the help of the state of the art microscopic traffic simulation tool, which was well calibrated, user delay cost is estimated. The results showed that initial cost contributes mainly to the total cost of PUTW, whereas user cost is the most significant component in LCC of cast-in-place JRCP. PUTW has higher initial construction cost, however due to rapid installation, its user cost is far less than the cast-in-place candidate. With the longer construction delay of ten days, cast-in-place JRCP has higher LCC than PUTW in the study location. The difference in LCC can be as high as 2.15 times in the case of traffic diversion ratio 0. However, when traffic diversion ratio 30%, the LCC of the two alternatives are quite close to balance. The LCC varies with construction site locations and traffic diversion ratio, which translates to traffic volume. In conclusion, PUTW can be a very economical solution in term of LCC, depending on construction site location and traffic volume. For PUTW for electrified roadways, the cost for electrical components are more or less fixed. Inheriting the advantages of the PUTW, the PUTW with the culvert is arguably the cheapest pavement type for electrified roadways at heavy traffic corridors.

Like any other precast pavement type, PUTW process also involves pavement evaluation, pavement type selection, pavement design, geometric design, slab arrangement, slab fabrications, slab installation and maintenance. These steps were discussed in this research to be used as a guideline for PUTW. In addition, a PUTW3D software tool was also developed for 3D slab geometrical arrangement of PUTW. The process of an electrified PUTW follows the procedures of a normal PUTW with some additional works. The main additional works for electrified roadway PUTW include slot cutting for the culvert, slot cutting for cabling tube, assembling the power supply rail module to the culvert.

A wide range of theoretical simulations and laboratory testing has been done to cover as much as possible the factors that influence the performance of road sections using PUTW technique. There is still a need to study construction techniques and quality of construction work as well as other parameters such as weather conditions and their impact on pavement performance, especially bond performance and joint performance. Only a full-scale lab and in-situ testing can make it possible to evaluate these factors.

In summary, the precast ultra-thin whitetopping (PUTW) pavement system was developed in this research using Singapore local conditions such as traffic conditions, environmental condition, material availability, and pavement structures as a case study. The PUTW is a cost effective, fast constructed and durable pavement system that can help to tackle the current issues about long lane closure time at heavy traffic junctions and to implement electrified roadways into the road management system.

Bibliography

AASHTO, 1993. *AASHTO guide for design of pavement structures, 1993*. Washington, D.C.: The Association.

ACPA, 2014. *Jointed Reinforced Concrete Pavement (JRCP)*. [Online]

Available at: [http://wikipave.org/index.php?title=Jointed_Reinforced_Concrete_Pavement_\(JRCP\)](http://wikipave.org/index.php?title=Jointed_Reinforced_Concrete_Pavement_(JRCP))

Altenbach, H., Altenbach, J. & Naumenko, K., 1998. *Ebene Flächentragwerke*. Berlin, Heidelberg: Springer Berlin Heidelberg.

ASTM, 1993. *Test Method for Measuring Surface Frictional Properties Using the British Pendulum Tester*. West Conshohocken, PA: ASTM International.

ASTM, 2010. *Test Method for Flexural Properties of Unreinforced and Reinforced Plastics and Electrical Insulating Materials by Four-Point Bending*. West Conshohocken, PA: ASTM International.

ASTM, 2013. *Test Method for Tensile Strength of Concrete Surfaces and the Bond Strength or Tensile Strength of Concrete Repair and Overlay Materials by Direct Tension (Pull-off Method)*. West Conshohocken, PA: ASTM International.

ASTM, 2015. *Test Method for Measuring Pavement Macrotexture Depth Using a Volumetric Technique*. West Conshohocken, PA: ASTM International.

Birmann, D., 1981. Einfluß hydraulisch gebundener Tragschichten auf die Beanspruchung von Betondecken-Experimentelle und theoretische Untersuchungen unter besonderer Berücksichtigung der Randbelastung. *Mitt Pruefamt Landverkehrsweg TU Muenchen*, Issue 35.

Bodin, D. et al., 2010. *Effect of temperature on fatigue performance of asphalt mixes*. Nagoya, Japan, 11th International Conference on Asphalt Pavements.

Bombardier, 2015. *Primove*. [Online]

Available at: <http://primove.bombardier.com/>

[Accessed 5 5 2015].

Buch, N., Tayabji, S., Ye, D. & Brink, W., 2012. *Technical and construction consideration for jointed precast concrete pavement applications*. Quebec, Canada, International Society for Concrete Pavements.

Byung Hwan Oh, 1991. Fatigue Life Distributions of Concrete for Various Stress Levels. *Materials Journal*, 88(2).

C. A. o. C., 2015. *CANPAV*. [Online]

Available at: <http://www.canpav.ca>

[Accessed 03 08 2015].

Chan, A., Keoleian, G. & Gabler, E., 2008. Evaluation of Life-Cycle Cost Analysis Practices Used by the Michigan Department of Transportation. *J. Transp. Eng.*, 134(6), p. 236–245..

Chang, L. M., Chen, Y.-T. & Lee, S., 2004. *Using Precast Concrete Panels For Pavement Construction In Indiana*, West Lafayette: Purdue University.

Chemilink™, 2013. *High Performance Topping Compound - SS-141*. Singapore: Chemilink™ Technologies & Products.

- Chen, Z., Yang, Y. & Yao, Y., 2013. Quasi-static and dynamic compressive mechanical properties of engineered cementitious composite incorporating ground granulated blast furnace slag. *Materials & Design*, Volume 44, p. 500–508.
- Choi, S. Y., Gu, B. W., Jeong, S. Y. & Rim, C. T., 2015. Advances in Wireless Power Transfer Systems for Roadway-Powered Electric Vehicles. *IEEE Journal of Emerging and Selected Topics in Power Electronics*, 3(1), p. 18–36.
- Choi, S. Y. et al., 2015. Ultraslim S-Type Power Supply Rails for Roadway-Powered Electric Vehicles. *IEEE Transactions on Power Electronics*, 30(11), p. 6456–6468.
- Cornelissen, H., 1984. Fatigue Failure of Concrete in Tension. *Heron*, 29(4).
- Darter, M., 1977. *Design of Zero Maintenance Plain Jointed Concrete Pavement*. West Lafayette, IN, Proceedings, International Conference on Concrete Pavement Design.
- Deacon, J. A., Coplantz, J. S., Tayebali, A. A. & Monismith, C. L., 1994. Temperature considerations in asphalt-aggregate mixture analysis and design. *Transportation Research Record*, Issue 1454.
- Dowling, R., Skabardonis, A. & Alexiadis, V., 2004. *Traffic Analysis Toolbox: Guidelines for Applying Traffic Microsimulation*, Washington, D.C.: Federal Highway Administration.
- Eid, J., 2012. *Theoretische und experimentelle Untersuchungen dünner Betondecken auf Asphalt (Whitetopping)*. Munich: Lehrstuhl und Prüfamt für Verkehrswegebau.
- Eisenmann, J., 1965. Theoretische Betrachtung zur Fortentwicklung der Fahrbahndecken aus unbewehrtem Beton. *Beton*, p. 19–27..
- Eisenmann, J., 1973. *Mittragende Wirkung von verfestigten Tragschichten bei Betonfahrbahnen*. Köln: Forschungsgesellschaft für Straßen- und Verkehrswesen (FGSV).
- Eisenmann, J., 1984. Bemessung von Verkehrsflächen - Theorie und Praxis. *Straßen- und Tiefbau*, 38(6), pp. 13-17.
- Eisenmann, J. & Leykauf, G., 2003. *Betonfahrbahnen*. Berlin: Handbuch für Beton-, Stahlbeton- und Spannbetonbau.
- Eisenmann, J. & Neumann, U., 1993. *Auswirkungen von Verbundstörungen auf die Spurrinnenbildung*. München: Prüfamt für Bau von Landverkehrswegen.
- Fwa, T. F., 2005. *The Handbook of Highway Engineering*. Boca Raton: Taylor & Francis.
- Giles, C. G., B.E. Sabey & K.H.F. Cardew, 1962. Development and Performance of the Portable Skid Resistance Tester. Issue American Society for Testing and Materials (ASTM).
- Google Maps, 2013. *Google Maps*. [Online]
Available at: <https://maps.google.com.sg/>
[Accessed 24 June 2013].
- Gracie Leveling Lift (TM), n.d. *Product - Gracie Leveling Lift*. [Online]
Available at: <http://gracielevelinglift.com/index-1.html>
[Accessed 4 3 2015].
- Hall, J. W. et al., 2009. *Guide for pavement friction*. s.l.:National Cooperative Highway Research Program, Transportation Research Board of the National Academies.
- Hall, J. W. et al., 2009. *Guide for pavement friction*. National Cooperative Highway Research Program: Transportation Research Board of the National Academies.

- Harbuck, R. H., 2009. Life Cycle Cost Analysis for Transportation Projects. *AACE International's Professional Practice Guide to Life-Cycle Cost Analysis*.
- Harrington, D. S. & Fick, G., 2014. *Guide to Concrete Overlays: Sustainable Solutions for Resurfacing and Rehabilitating Existing Pavements*, American Concrete Pavement Association: National Concrete Pavement Technology Center.
- Highways England, 2015. *Feasibility study - powering electric vehicles on England's major roads*, s.l.: Highways England.
- Hoster, H., 2012. *Electromobility in Megacities*. Singapore: TUM CREATE.
- Huh, J. et al., 2011. Narrow-Width Inductive Power Transfer System for Online Electrical Vehicles. *IEEE Transactions on Power Electronics*, 26(12), p. 3666–3679.
- Huh, J. & Rim, C.-T., 2011. KAIST Wireless Electric Vehicles - OLEV. *SAE Technical Paper*, Issue 2011-39-7263, p. 7.
- Hutin, M. & Leblanc, M., 1894. *Transformer system for electric railways*. United States, Patent No. 527,857.
- IEA, 2009. *Transport, Energy and CO₂: Moving toward Sustainability*. France: International Energy Agency.
- Imam Aschuri, R. A. Y. D. H., 2003. *Temperature and Time Loading Influence on Stiffness Modulus of Asphalt Concrete Mixture and Design Life Using Analytical Method on Indonesian Tropical Conditions*. s.l., Eastern Asia Society for Transportation Studies.
- Iowa Department of Transportation, 2000. *Method of Test for Determining the Shearing Strength of Bonded Concrete. Test Method No. Iowa 406-C*. Iowa: Iowa Department of Transportation.
- Jones, E. R. & Childers, R. L., 2001. *Contemporary college physics*. 3rd ed. ed. Boston: McGraw Hill.
- Judycki, J., 1997. *Comparison of fatigue criteria for flexible and semi-rigid pavements*. Seattle, Washington, Eighth International Conference on Asphalt Pavements.
- Júlio, E. N., Branco, F. A. & Silva, V. D., 2004. Concrete-to-concrete bond strength. Influence of the roughness of the substrate surface. *Construction and Building Materials*, 18(9), p. 675–681.
- Kim, J.-K., Kim, J.-S., Ha, G. J. & Kim, Y. Y., 2007. Tensile and fiber dispersion performance of ECC (engineered cementitious composites) produced with ground granulated blast furnace slag. *Cement and Concrete Research*, 37(7), p. 1096–1105.
- Kim, J. et al., 2013. Coil Design and Shielding Methods for a Magnetic Resonant Wireless Power Transfer System. *Proceedings of the IEEE*, 101(6), p. 1332–1342.
- Kitaguchi, W., Nishizawa, T. & Mizukura, K., 2006. Structural Design Method Of Precast Reinforced Concrete Pavement Based On Fatigue Analysis. *Journal Of Pavement Engineering, JSCE*, Volume 11, p. 115–122.
- KITAGUCHI, W., Nishizawa, T. & Mizukura, K., 2006. Structural design method of precast reinforced concrete pavement based on fatigue analysis. *Journal Of Pavement Engineering, JSCE*, Volume 11, p. 115–122.
- Koh, S. & Chin, H., 2007. *Traffic Simulation Modeling: VISSIM*, Singapore: National University of Singapore.

- Larrard, F., Sedran, T. & Balay, J.-M., 2013. Removable urban pavements. *International Journal of Pavement Engineering*, 14(1), p. 1–11.
- Lau, C., Fwa, T. & Paramasivam, P., 1994. Interface shear stress in overlaid concrete pavements. *Journal of Transportation Engineering*, Issue 2, p. 163.
- Lau, C. M., Fwa, T. F. & Paramasivam, P., 1994. *Interface Shear Stress in Overlaid Concrete Pavements*. [Online]
Available at: [http://ascelibrary.org/doi/abs/10.1061/\(ASCE\)0733-947X\(1994\)120:2\(163\)](http://ascelibrary.org/doi/abs/10.1061/(ASCE)0733-947X(1994)120:2(163))
- Lechner, B. & Freudenstein, S., 2010. *Road design lecture notes (Technische Universität München)*. Munich: Lehrstuhl und Prüfamnt für Verkehrswegebau - Technische Universität München.
- Leykauf, G., 1986. Reflexionsrisse bei Asphaltstraßen. *Straßen- und Tiefbau*, 40(4).
- Liu, X., 2013. *Adaptive Network Control with Traffic Lights Modeled in Microscopic Traffic Simulation*, Singapore: Technical University of Munich.
- Li, V. C., 2007. Engineered cementitious composites (ECC) material, structural, and durability performance.
- Li, V. C., Fischer, G. & Lepech, M., 2004. Crack Resistant Concrete Material for Transportation Construction. *Transportation Research Board 83rd Annual Meeting*.
- LTA, 2006. *Code of practice Traffic control at work zone*. Singapore: LTA.
- LTA, 2010. *Civil design criteria for road and rail transit systems*, Singapore: LTA.
- LTA, 2010. *Materials and Workmanship Specifications*. A1 ed. Singapore: s.n.
- LTA, 2012. *Information for developing precast concrete pavement*. Singapore: LTA.
- LTA, 2014. *Code of Practice: Street Work Proposals Relating to Development Works*. 1.1 ed. Singapore: LTA.
- LTA, 2014. *One Motoring - Administration Of Oversized Heavy Vehicle Movement*, Singapore: LTA.
- LTA, 2015. *Code of practice for works on public street*. Singapore: LTA.
- LTA, 2015. *Publications & Research*. Singapore: LTA.
- LTA, 2015. *Singapore Land Transport Statistics in Brief*. Singapore: LTA.
- LTA, 2015. *Standard Details Of Road Elements (SDRE)*. Singapore: LTA.
- LTA, 2015. *Standard Details Of Road Elements (SDRE)*. s.l.:s.n.
- Márkus, G. & Otto, J., 1978. *Theorie und Berechnung rotationssymmetrischer Bauwerke*. 3. Aufl. Düsseldorf: Werner..
- Martin, P. T., Chaudhuri, P., Tasic, I. & Zlatkovic, M., 2011. *Freeway incidents: Simulation and analysis*, Utah: University of Utah.
- Menon, G. & Kuang, L. C., 2006. *Lessons from Bus Operations*, Singapore: Land Transport Authority.
- Ministry of Public Work Indonesia, 2012. *Manual Design of Road Pavement*. s.l.:Ministry of Public Work Indonesia.

- Mirzadeh, I., Butt, A. A., Toller, S. & Birgisson, B., 2014. Life cycle cost analysis based on the fundamental cost contributors for asphalt pavements. *Structure and Infrastructure Engineering: Maintenance, Management, Life-Cycle Design and Performance*, p. 10:12.
- MOM, 2014. *Labour Force in Singapore, 2014*, Singapore: Ministry of Manpower.
- Nawy, E. G., 2008. *Concrete Construction Engineering Handbook*. Boca Raton: CRC Press.
- NCHRP, 2004. *Thin and Ultra-thin Whitetopping*, Washington: Transportation Research Board.
- NEA, 2015. *Weather Statistics*. Singapore: National Environment Agency.
- Neville, A. M., 2011. *Properties of concrete*. 5th ed. ed. Harlow: Prentice Hall.
- NguyenDinh, N. & Lechner, B., 2013. *Suitable Pavement Systems for Electrified Roadway*. Singapore, Architecture and Civil Engineering (ACE 2013) - Global Science 38 - Technology Forum (GSTF).
- NguyenDinh, N., Yang, E.-H. & Lechner, B., 2014. *Precast electrified roadway pavement systems using engineered cementitious composite*. Prague, Czech Republic, 12th International Symposium on Concrete Roads.
- Nishizawa, T., Mizukura, K. & Tamura, K., 2006. Structural design method of precast reinforced concrete pavement with consideration of concrete and steel fatigues. *Journal of Pavement Engineering, JSCE*, Volume 11, pp. 115-122.
- NZ Transport Agency, 2013. *Specification for state highway skid resistance management*. s.l.:NZ Transport Agency.
- Obata, H., Nishizawa, T., Sasaki, I. & Kokubu, K., 2007. Effect Of Improved Interfacial Bond On White Topping Using Ultra High Strength Fiber Reinforced Concrete. *Journal Of Pavement Engineering, JSCE*, Volume 12, p. 183-188.
- Odemark, N., 1949. Undersökning av elasticitetsegenskaperna hos olika jordarter samt teori för beräkning av beläggningar enligt elasticitetsteorin.
- OLEV Tech, 2015. *OLEV Technology - FAQ*. [Online] Available at: <http://olevtech.com/faq-category/safety/>
- Pawitra, E., 2002. *A Program to Estimate User Cost due to Road works*, Singapore: Nanyang Technological University.
- Pentland, W., 2013. Korea Constructs Road That Wirelessly Charges Moving Electric Buses. *Forbes*.
- Pereira, D. D. S., Balbo, J. T. & Khazanovich, L., 2006. Theoretical and field evaluation of interaction between ultra-thin whitetopping and existing asphalt pavement. *International Journal of Pavement Engineering*, 7(4), p. 251-260.
- Priest, A. L. & Timm, D. H., 2006. *Methodology and calibration of fatigue transfer functions for mechanistic-empirical flexible pavement design*, Auburn, Alabama: NCAT - Auburn University.
- Qian, S. Z., Li, V. C., Zhang, H. & Keoleian, G. A., 2013. Life cycle analysis of pavement overlays made with Engineered Cementitious Composites. *Cement and Concrete Composites*, 35(1), p. 78-88.
- Quing, C., 2013. *Analysis of bus priority schemes in Singapore*, Singapore: Nanyang Technological University.
- Rao, S. & Roesler, J. R., 2004. *Cumulative fatigue damage analysis of concrete pavement using accelerated pavement testing results*. Urbana, University of Illinois at Urbana-Champaign.

- Rapid Roadway Solution (TM), n.d. *Rapid Roadway*. [Online] Available at: <http://www.rapidroadwaysolutions.com> [Accessed 7 6 2015].
- Rasmussen, R. O. & Rozycki, D. K., 2004. *Thin and Ultra-Thin Whitetopping, A Synthesis of Highway Practice*, Washington, D.C: NCHRP Synthesis 338, Transport Research Board.
- Risch, F., 2011. *Kontaktlose Energieübertragung in Elektro-fahrzeuge im Stand und in der Bewegung (EROAD)*. s.l.:s.n.
- Rolf Werner, Martin Peck & Johannes Steigenberger, 2010. Kreisverkehrsflächen in Beton: Erfahrungen in der Schweiz, Deutschland und Österreich.
- Sahmaran, M. et al., 2009. Influence of aggregate type and size on ductility and mechanical properties of engineered cementitious composites. 106(3).
- Salem, O., Deshpande, A., Genaidy, A. & Geara, T., 2013. User costs in pavement construction and rehabilitation alternative evaluation. *Structure and Infrastructure Engineering: Maintenance, Management, Life-Cycle Design and Performance*, pp. 285-294.
- Scheving, A. G., 2011. *Life Cycle Cost Analysis of Asphalt and Concrete Pavements*, s.l.: Reykjavík University, Iceland .
- Sharma, A., 2013. Guidelines for the Design and Construction of Ultra Thin Whitetopping. *The International Journal of Engineering and Science (IJES)*, 2(01), pp. 269-274.
- Shell International Oil Products B.V., 1998. *BISAR 3.0. User Manual..* The Hague: Bitumen Structures Analysis in Roads.
- Shell International Petroleum Co. Ltd., 1978. *Shell pavement design manual*. London: Shell International Petroleum Co..
- Shladover, S. E., 1992. Highway Electrification And Automation. *California Partners for Advanced Transit and Highways (PATH)*.
- Shladover, S. E., 2006. PATH at 20 - History and Major Milestones. *IEEE Transactions on intelligent transportation systems*, 8(4), pp. 584-592.
- Shook, J., Finn, F., Witzczak, M. & Monismith, C., 1982. *Thickness Design of Asphalt Pavements – The Asphalt Institute Methods*. Delft, Fifth International Conference on Structural Design of Asphalt Pavement.
- Silfwerbrand, J., 2003. Shear bond strength in repaired concrete structures. *Materials and Structures*, 36(6), p. 419–424.
- Singapore Standards Council, 1999. *Code of practice for precast concrete slab and wall panels*. Singapore: SPRING Singapore.
- Smith, M. R. & Walls III, J., 1998. *Life-Cycle Cost Analysis in Pavement Design — Interim Technical Bulletin*, Washington, DC: Federal Highway Administration.
- Steigenberger, J., 1998. *Verbunddecke für Staubereiche*. Wien: Bundesministerium für wirtschaftliche Angelegenheiten .
- Stubbs, A. P., 2011. *Fatigue Behaviour of Hot Mix Asphalt for New Zealand Pavement Design*, Christchurch, New Zealand: University of Canterbury.

- Suh, I.-S., 2011. *Application of Shaped Magnetic Field in Resonance (SMFIR) Technology to Future Urban Transportation*. Korea Advanced Institute of Science and Technology, Korea, CIRP design conference.
- Swei, O., Gregory, J. & Kirchain, R., 2014. *Probabilistic Life-Cycle Cost of Pavements: Characterization and Application of Parameter Input Variation for Scenarios*. Czech Republic, 12th International Symposium On Concrete Roads 2014.
- Systems Control Technology, I., 1994. *Roadway Powered Electric Vehicle Project Track Construction And Testing Program Phase 3D*, California: California PATH Research Paper.
- Tan, S.-A. & Fwa, T.-F., 1992. Influence of pavement materials on the thermal environment of outdoor spaces. *Building and Environment*, 27(3), p. 289–295.
- Tayabji, S., 2011. *International Precast Concrete Pavement Applications: A Summary of Practice*.
- Tayabji, S., Ye, D. & Buch, N., 2013. *Precast Concrete Pavement Technology. SHRP 2 Report*, Issue S2-R05-RR-1.
- Tayebali, A. A., Deacon, J. A., Coplantz, J. S. & Monismith, C. L., 1993. Modeling Fatigue Response of Asphalt-Aggregate Mixtures (with Discussion). *Journal of the Association of Asphalt Paving Technologists*, Volume 62.
- Tepfers, R., Hedberg, B. & Szczekocki, G., 1984. Absorption of energy in fatigue loading of plain concrete. *Mat. Constr.*, 17(1), pp. 59-64.
- TiongSeng_Group, 2012. *Our Projects - Parkroyal @ Upper Pickering Street*. [Online] Available at: <http://www.tiongseng.com.sg/portfolio-items/parkroyal-upper-pickering-street/>
- Tschegg, E., Macht, J., Jamek, M. & Steigenberger, J., 2007. Mechanical and Fracture-Mechanical Properties of Asphalt-Concrete Interfaces. *ACI Materials Journal*, 104(5), p. 474–480.
- Tubey, L. W. & Hosking, J. R., 1972. *Synthetic aggregates of high resistance to polishing: Part 2 - corundum-rich aggregates*. Crowthorne, Berkshire: Transport and Road Research Laboratory.
- UK Highway Agency, 2004. *Design manual for roads and bridges: skid resistance*. s.l.:s.n.
- Villagra, J., d'Andréa-Novel, B., Fliess, M. & Mounier, H., 2011. A diagnosis-based approach for tire-road forces and maximum friction estimation. *Control Engineering Practice*, 19(2), p. 174–184.
- Vossloh, 2015. *Vossloh fastening systems - W 21*. [Online] Available at: <http://www.vossloh-fastening-systems.com/>
- Walker, N., 2011. *Primovecity - e-Mobility for all Vehicles*. Munich: s.n.
- Wallman, C.-G. & Astrom, H., 2001. Friction measurement methods and the correlation between road friction and traffic safety. Volume 911.
- Weng, J. & Meng, Q., 2013. Estimating capacity and traffic delay in work zones: An overview. *Transportation Research Part C*, Volume 35, pp. 34-45.
- Westergaard, H. M., 1926. Stresses in concrete pavements computed by theoretical analysis. *Public Roads*.
- Westergaard, H. M., 1933. Analytical tools for judging results of structural tests of concrete pavements. *Public Roads*, 14(10), p. 185–188.
- Wikipedia contributors, 2012. Nissan Leaf. *Wikipedia, the free encyclopedia*.

-
- Wong, S. K., 2014. *HDB's Productivity Journey & Research In Precast & Prefabrication*. Singapore: HDB.
- Woodward, D., Orr, S. & Dillon, M., 2013. *Predicting the skid resistance of concrete*. São Paulo, International Journal of Pavements Conference.
- Wu, D. Q. & Zhang, Y., 2011. *The semi-rigid pavement with higher performances*. Brunei Darussalam, CAFEO 29, Sustainable Urbanization – Engineering Challenges and Opportunities.
- Wu, H. H. et al., 2011. *A review on inductive charging for electric vehicles*. Niagara Falls, ON, IEEE, p. 143–147.
- www.heise.de, n.d. *Bild 3 / 8 - Technik - Korea testet das berührungslose Laden von Elektroautos Autos*. [Online]
Available at: <http://www.heise.de/autos/artikel/Korea-testet-das-beruehrungslose-Laden-von-Elektroautos-957228.html?bild=2;view=bildergalerie>
[Accessed 2012].
- Xian, C. L., 2014. *Traffic light control for multi-junctions*, 2014: Nanyang Technological University.
- Yang, E.-H., Yang, Y. & C. Li, V., 2007. Use of High Volumes of Fly Ash to Improve ECC Mechanical Properties and Material Greenness. *ACI materials journal*, 104(6), p. 620.
- Yilmaz, M. & Krein, P. T., 2013. Review of Battery Charger Topologies, Charging Power Levels, and Infrastructure for Plug-In Electric and Hybrid Vehicles. *IEEE Transactions on Power Electronics*, 28(5), p. 2151–2169.
- Yu, H. T. & Tayabji, S., 2007. *Thin Whitetopping—the Colorado Experience*. U.S. Department of Transportation: Federal Highway Administration.
- Yurong, L., Fwa, T. F., Kapilan, S. & Choo, Y. S., 2001. Effect of aggregate properties of pavement skid resistance. Volume 4.

List of figures

Figure 1-1: Typical section of rigid pavement at junction in Singapore (LTA, 2015)	1
Figure 1-2: Rigid pavement structure at junctions and the connection with flexible pavement (LTA, 2015).....	1
Figure 1-3: Electrified Roadway concept (Wu, et al., 2011)	2
Figure 2-1: Deflectograph (LTA, 2012)	3
Figure 2-2: Sideway-force coefficient routine investigation machine (SCRIM) (LTA, 2012)	3
Figure 2-3: Multifunction road monitor (LTA, 2012)/Traffic loading and environment loading	3
Figure 2-4: Total motor vehicle population (LTA, 2015).....	4
Figure 2-5: Locations for manual video recording (Google Maps, 2013).....	4
Figure 2-6: Flexible ESALS (80 kN or 18 kips) in design lane around Singapore road network	5
Figure 2-7: Mean surface temperatures of pavements in morning, midday and evening for 6/11/90 (Tan & Fwa, 1992).....	5
Figure 2-8: Day and night thermal gradients for concrete pavement in Singapore (Lau, et al., 1994)...	5
Figure 2-9: Flexible pavement structure (LTA, 2015).....	6
Figure 2-10: Rigid pavement structure at junctions and the connection with flexible pavement (LTA, 2015).....	7
Figure 2-11: Rigid pavement structure at bus stops and the connection with flexible pavement (LTA, 2015).....	7
Figure 2-12: Summary of fatigue functions (Eid, 2012).....	9
Figure 2-13: Allowable load cycles of asphalt pavement versus asphalt layers' thickness.....	11
Figure 2-14: 3D FEM of rigid pavement	11
Figure 2-15: Clementi network and detail simulation of the roadwork at the intersection.....	13
Figure 2-16: Define reduced speed road segment for construction simulation	14
Figure 2-17: Travel time lost due to construction at intersections Int_4123 and Int_4105	14
Figure 3-1: Electrified Roadway concept (Wu, et al., 2011)	19
Figure 3-2: Battery state of charge of an electric vehicle using electrified roadways	19
Figure 3-3: Potential locations of electrified roadways for bus application	20
Figure 3-4: Inductive energy transfer for Tram (Hutin and Leblanc, 1894).....	21
Figure 3-5: PATH Test track. Source: PATH.....	22
Figure 3-6: Test track layout (Systems Control Technology, 1994).....	22
Figure 3-7: Demonstration projects with SMFIR technology (Suh, 2011).....	23
Figure 3-8: Application of reactive resonant current loop for an OLEV.....	23
Figure 3-9: OLEV system at a bus stop in Gumi (Pentland, 2013)	24
Figure 3-10: Demonstration project for tramway in Augsburg trade fair site (Walker, 2011).....	24
Figure 3-11: Demonstration project for bus in Lommel (Bombardier, 2011)	24
Figure 3-12: Cross section of U-type (2G) power supply rail	28
Figure 3-13: Cross section of W-type (3G) power supply rail	28
Figure 3-14: Cross section of I-type (4G) power supply rail.....	28
Figure 3-15: Cross section of S-type (5G) power supply rail.....	28
Figure 3-16: The pavement for the W-type power supply rail (3G) (www.heise.de).....	28
Figure 3-17: Deployment of I-type (4G) modules at 24 m test side. (a) Prototype module. (b) Deployed module (Choi, et al., 2015)	29
Figure 3-18: Foldable S-type power supply modules: (a) fully deployed case, (b) one-third folded case, (c) two-thirds folded case, (d) completely folded case (Choi, et al., 2015).....	29
Figure 3-19: Measured the highest temperatures of the S-type power supply rail after 50 min operation in thermal equilibrium state (Choi, et al., 2015).....	30
Figure 4-1: Types of Prestressed precast concrete pavement (PPCP) (Tayabji, et al., 2013).....	33
Figure 4-2: Welded lift loop connection (Tayabji, 2011)	34
Figure 4-3: The "Horn" Load Transfer Device (Tayabji, 2011).....	34

Figure 4-4: Compression Joint Unit (Tayabji, 2011).....	34
Figure 4-5: Dowel bar slot at the bottom of the slab (Buch, et al., 2012).....	34
Figure 4-6: Installing dowel bars using DBR method (Buch, et al., 2012)	34
Figure 4-7: Kwik Slab joint interlocking system (Buch, et al., 2012)	34
Figure 4-8: Michigan method (Buch, et al., 2012)	34
Figure 4-9: Narrow mouth surface dowel slot (Buch, et al., 2012)	34
Figure 4-10: UTW on a fair or better asphalt pavement (still in good structural performance) with only minor surface distresses (Harrington & Fick, 2014).....	35
Figure 4-11: Effects of interface bonding (Fwa, 2005)	36
Figure 4-12: The proposed PUTW pavement structures	37
Figure 5-1: Typical uniaxial tensile stress-strain curve and crack width development of ECC material (Li et al., 2004)	39
Figure 5-2: Loading scheme of fatigue test	42
Figure 5-3: Fatigue response of ECC and normal concrete under four-point bending.....	43
Figure 5-4: Four-point bending test setup (Courtesy of Mr. Jishen Qiu, NTU)	43
Figure 5-5: 3D FEM of Four-point bending test.....	43
Figure 5-6: The verification of ECC material model for FEM.....	44
Figure 5-7: Type of pavement surface textures (Hall, et al., 2009)	44
Figure 5-8: (a) Expected grooving on slab surface. (b) Mould with grooving plate. (c) Final slabs	47
Figure 5-9: Flexural strength of ECC with corundum at 28 days.....	47
Figure 5-10: British Pendulum Tester (BPT).....	48
Figure 5-11: Sand Patch Method (SPM).....	48
Figure 5-12: Wheel Tracking Machine.....	48
Figure 5-13: Skid resistance of exposed ECC with corundum versus typical ECC (M45)	49
Figure 5-14: The influence of traversal and longitudinal grooving textures on skid resistance	49
Figure 5-15: Long-term performance of ECC with corundum regarding skid resistance	50
Figure 5-16: small scale testing of the transparency of ECC material to magnetic field.....	51
Figure 6-1 Reference PUTW system for interface shear stresses.....	52
Figure 6-2: Equivalent model for calculating horizontal shear stress at different pavement depths	54
Figure 6-3: Horizontal shear stress under vertical load at the interface ECC-grout (at $h_1 = 5$ cm)....	55
Figure 6-4: Horizontal shear stress under vertical load at the interface grout-asphalt (at $h_1 = 6$ cm).55	
Figure 6-5: Horizontal shear stress under vertical and horizontal load at the interface ECC-grout (at $h_1 = 5$ cm).....	57
Figure 6-6: Horizontal shear stress under vertical and horizontal load at the interface grout-asphalt (at $h_1 = 6$ cm)	57
Figure 6-7: The influence of grout layer thickness to the maximum horizontal interface shear stresses (slab size: 900x900x50)	59
Figure 6-8: 3 types of slab bottom surface used for interface bond strength evaluation	61
Figure 6-9: Test methods to determine bond strength: a) b) pull-off tests, c) torsion test, d) slant shear test, e) f) shear tests, g) wedge splitting test, and h) guillotine test (Silfwerbrand, 2003).....	62
Figure 6-10: Shear frame and pull-off frame	62
Figure 6-11: Styrofoam sheets	63
Figure 6-12: Failure types in sample with circular convex nodes in shear test	64
Figure 6-13: Failure types in sample with square convex nodes in shear test	65
Figure 6-14: special failure type of sample with flat contact in shear test.....	65
Figure 6-15: failure types of sample with convex nodes in pull-off test	65
Figure 6-16: Bond test results.....	66
Figure 7-1: Load cases – according to Westergaard method (Eisenmann & Leykauf, 2003)	67
Figure 7-2: Types of stress in asphalt in the joint area of whitetopping (Eid, 2012).....	70
Figure 7-3: 3D 3x3 slab multilayer FEM.....	71
Figure 7-4: 3D seven hexagon multilayer FEM	71

Figure 7-5: Load locations on FEMs	71
Figure 7-6: (a) daytime warping (b) night time curling (Fwa, 2005)	72
Figure 7-7: Stress distribution in a fully restraint infinite slab (Lechner & Freudenstein, 2010).....	72
Figure 7-8: Deformation and bending stresses due to heating of slab surface (Lechner & Freudenstein, 2010).....	73
Figure 7-9: calculation of curling stress	73
Figure 7-10: longitudinal joints should be arranged to avoid wheel paths (Harrington & Fick, 2014). Note: 1 ft = 30.48 cm.....	74
Figure 7-11: Proposed slab types and sizes.	75
Figure 7-12: Slab lifting locations (top view).....	76
Figure 7-13: Flexural lifting stress (for slab size 3600 mm x 2400 mm x 50 mm)	77
Figure 7-14: Total slab deformation (for slab size 3600 mm x 2400 mm x 50 mm).....	77
Figure 7-15: Slab lifting locations for electrified slab 3600x2400 (top view).....	78
Figure 7-16: Maximum construction flexural stress	78
Figure 7-17: Graphical presentation of vertical slab deformation during construction	78
Figure 7-18: Maximum construction total deformation.....	79
Figure 7-19: Locations of load cases applied on the electrified PUTW	80
Figure 7-20: Graphical presentation of traffic-induced stresses in electrified PUTW at different load locations.....	80
Figure 7-21: Graphical presentation of warping stress with slab size 3600x2400	81
Figure 7-22: The influence of slab length and thickness on temperature-induced (warping) stress.....	82
Figure 7-23: Graphical presentation of temperature-induced stresses in electrified PUTW	83
Figure 7-24: Asphalt thickness vs shear stress and joint (slab size: 3600 mm x 2400 mm).....	86
Figure 7-25: Allowable load cycles of PUTW (slab size: 3600 x 2400 and 3600 x 2400 with integrated culvert for electrified roadways) in relation with slab thickness, composite thickness and support layer's equivalent modulus.....	87
Figure 7-26: Allowable load cycles of PUTW (slab size: hexagon 1800) in relation with slab thickness, composite thickness and support layer's equivalent modulus	87
Figure 8-1: Activity schedule of alternative pavements	92
Figure 8-2: LCC of JRCP and PUTW at Intersection Int_4123	94
Figure 8-3: LCC of JRCP and PUTW at Intersection Int_4105	94
Figure 9-1: PUTW3D development flowchart	97
Figure 9-2: Example of joint layout and slabs' coordination in PUTW3D	98
Figure 9-3: Example of architectural precast elements in building in Singapore (TiongSeng_Group, 2012).....	99
Figure 9-4: Gracie levelling lift (Gracie Leveling Lift (TM)) (Rapid Roadway Solution (TM)).....	100
Figure 9-5: Partial of Vossloh Fastening Systems W11 (Vossloh, 2015)	100
Figure 9-6: Asphalt surface after milling (at Clementi Road, Singapore)	103
Figure 9-7: slots cut for cabling tube and precast channel (top view)	103
Figure 9-8: cross section A-A after installing tube for cabling and material refilled	103
Figure 9-9: Panels placement methods used in precast concrete pavement (Tayabji, et al., 2013)....	104
Figure 9-10: Panel placing, levelling and grouting in precast pavement (Rapid Roadway Solution (TM))	105
Figure 10-1: The proposed PUTW pavement structures	108
Figure 10-2: Allowable load cycles of PUTW (slab size: 3600 x 2400 and 3600 x 2400 with integrated culvert for electrified roadways) in relation with slab thickness, composite thickness and support layer's equivalent modulus.....	110
Figure 10-3: Allowable load cycles of PUTW (slab size: hexagon 1800) in relation with slab thickness, composite thickness and support layer's equivalent modulus	110

List of tables

Table 2-1 Structural Numbers and Terminal Serviceability assigned for different pavements	5
Table 2-2: Paved road length in Singapore.....	6
Table 2-3: Thickness of flexible pavement layers (LTA, 2015).....	6
Table 2-4: Microstrain in asphalt pavement under traffic loading.....	10
Table 2-5: Load cases applied on Singapore rigid pavement	12
Table 2-6: Maximum flexural stresses in Singapore rigid pavement with different load cases	12
Table 2-7: The value of travel time from different time and location worldwide	15
Table 2-8: Mean Gross Wage and number of employment of each occupation.....	16
Table 2-9: Average delay cost of each type of vehicle per hour.....	16
Table 2-10: Travel delay cost estimation.....	16
Table 3-1: Example of electrified roadways' locations along a bus line and the energy collected by one bus during its daily operation.....	20
Table 3-2: Overview of WPT system (Highways England, 2015)	25
Table 3-3: Summary of the performance of electrified roadway.....	26
Table 3-4: TRL and MRL of DWPT systems (Highways England, 2015).....	27
Table 3-5: Five generations of KAIST OLEV (Huh & Rim, 2011) (Choi, et al., 2015)	27
Table 5-1: Proportions of mix design in current study	41
Table 5-2: Summary of monotonic test results	42
Table 5-3: Input parameters to the materials model in ANSYS	43
Table 5-4: Standards of skid resistance for new road of many countries in BPN scale	45
Table 5-5: Standards of skid resistance for the intervention level (in BPN scale) of major and minor roads.....	45
Table 5-6: Chemical specification of Corundum.....	46
Table 5-7: Mixture design of ECC and surface treatment of ECC mixed with Corundum	46
Table 6-1: Maximum horizontal shear stress at the interface ECC slab-grout	58
Table 6-2: Maximum horizontal shear stress at the interface grout-asphalt.....	58
Table 6-3: Maximum vertical interface split stress in PUTW due to temperature change	60
Table 6-4: Chemilink™ SS-141 technical data (Chemilink™, 2013).....	61
Table 6-5: Summary of sample types	63
Table 7-1: Calculation method for multilayer systems (Lechner & Freudenstein, 2010)	69
Table 7-2: FEM calibration result.....	71
Table 7-3: Locations of lifting points	78
Table 7-4: The influence of slab dimension on traffic-induced stress in ECC layer (slab center loading)	79
Table 7-5: The influence of slab dimension on traffic-induced stress in ECC layer (slab edge loading)	80
Table 7-6: Traffic-induced stress in electrified PUTW slab	81
Table 7-7: Gradients in ECC slabs (including grout) and maximum warping stress in PUTW	81
Table 7-8: Maximum stress in ECC slab under traffic and environmental loading (center slab loading at midday)	82
Table 7-9: Maximum temperate-induced stresses in electrified PUTW	83
Table 7-10: The influence of slab dimension on traffic-induced microstrain ($\mu\epsilon$) in asphalt layer (slab center loading)	83
Table 7-11: The influence of slab dimension on traffic-induced microstrain ($\mu\epsilon$) in asphalt layer (slab edge loading)	84
Table 7-12: Traffic-induced microstrain ($\mu\epsilon$) in asphalt layer of the electrified PUTW pavement	84
Table 7-13: Maximum traffic-induced microstrain ($\mu\epsilon$) in asphalt layer of electrified PUTW pavement and normal PUTW pavement with 3600x2400 slab	85
Table 7-14: Allowable load cycles of PUTW based on asphalt flexural performance	85

Table 7-15: FEM calibration results in the case of interface debonding (slab center)	88
Table 7-16: Traffic-induced tensile stress in ECC layer in the case of interface debonding	88
Table 7-17: Traffic-induced tensile strain in asphalt in the case of interface debonding	89
Table 7-18: Allowable load cycle of PUTW dependence on asphalt flexural performance in the case of interface debonding at the slab center.....	89
Table 7-19: Allowable load cycle of PUTW dependence on asphalt flexural performance in the case of interface debonding at the slab edge	90
Table 8-1: Travel delay cost estimation.....	92
Table 8-2: Maintenance and rehabilitation cost of JRCP	93
Table 8-3: LCCA of pavement alternative at Intersection Int_4123	93
Table 8-4: LCCA of pavement alternative at Intersection Int_4105	93
Table 8-5: Component cost for I-type (or S-type) electrified roadway excluding road construction (Choi, et al., 2015)	95
Table 9-1: Geometric tolerance requirements (Tayabji, et al., 2013)	102

List of Abbreviations

3D	Three-dimensional
AASHTO	American association of state highway and transportation officials
AC	Alternating current
ACPA	American concrete pavement association
ADT	Average daily traffic
ANSYS	A software tool
APDL	ANSYS parametric design language guide
ASTM	American society for testing and materials
B/C	Cost-benefit ratio
BISAR	A software tool
BPN	British pendulum number
BPT	British pendulum tester
BS	British standard
CBR	California bearing ratio
CEM	Cement
CIP	Cast-in-place
CNC	Computer numerically controlled
DBR	Dowel bar retrofit
DC	Direct current
DOT	Department of transportation
DWPT	Dynamic wireless power transfer
ECC	Engineered cementitious composite
EMF	Electro-magnetic field
ESALS	Equivalent single axle loads
EUAC	Equivalent uniform annual cost
EVs	Electric vehicles
FEM	Finite element method, finite element model
FN	Friction number
GGBS	Ground granulated blast-furnace slag
HGV	Heavy goods vehicle
HMA	Hot mix asphalt
HRWRA	High-range water-reducing admixture
ICNIRP	International commission on non-ionizing radiation protection
ICS	Inductive coupling system
IPT	Inductive power transfer
ITS	Intelligent transportation system
JRCP	Jointed reinforced concrete pavement
JPrCP	Jointed precast concrete pavement
KAIST	Korea advanced institute of science and technology
LCC	Life cycle cost
LCCA	Life cycle cost analysis
LGV	Light good vehicle
LTA	Land transportation authority
LTE	Load transfer efficiency
LVDT	Linear variable displacement transducer
MOR	Modulus of rupture
MRL	Manufacturing readiness level
MTD	Mean texture depth
NEA	National environment agency
NPV	Net present value
NPW	Net present worth
NTU	Nanyang technological university
OLEV	On-line electric vehicle

OPC	Ordinary Portland cement
PATH	California partners for advanced transit and highways
PCP	Precast concrete pavement
PIARC	Permanent international association of road congresses
PMS	(Singapore) pavement management system
PPCP	Prestressed precast concrete pavement
PUTW	Precast ultra-thin whitetopping
PVA	Polyvinyl alcohol
QA	Quality assurance
QC	Quality control
RPEV	Roadway powered electric vehicle project
SCATS	A software tool
SCRIM	Sideway-force coefficient routine investigation machine
SDM	Stopping distance measurement
SDRE	Standard details of road element
SFC	Sideway force coefficient
SMA	Stone matrix asphalt
SMFIR	Shaped magnetic field in resonance
SN	Structural number
SN	Skid number
S-N	Cyclic stress (s) - cycles to failure (n)
SP	Superplasticizer
SPM	Sand patch method
TRL	Technology readiness level
TRRL	Transport and road research laboratory
USA	United states of America
UTW	Ultra-thin whitetopping
VDC	Volt direct current
VISSIM	A software tool
VMS	Traffic diversion ratio
vph	Vehicle per hour
WPT	Wireless power transfer
WTM	Wheel tracking machine

List of Symbols

Symbols in Chapter 2: Pavement system

<i>Symbol</i>	<i>Explanation</i>	<i>unit</i>
N, N_f	Allowable loading cycles	cycles
$\varepsilon_t, \mu\varepsilon$	Tensile strain in asphalt	$\mu\varepsilon$
E^*	Dynamic modulus of asphalt mix	MPa , N/mm ²
C	Function of volume of voids and volume of bitumen in the mix	-
V_B	Volume of bitumen	%
V_v	Volume of voids	%
S_{mix}	Stiffness modulus of asphalt mix	MPa , N/mm ²
D	Total damage of the pavement	-
T	Asphalt temperature	°C
σ	Flexural stress in concrete	MPa , N/mm ²
MOR	Modulus of Rupture	MPa , N/mm ²
E_1, E_2	Asphalt elastic modulus	MPa , N/mm ²
E_{GG}	Graded granite elastic modulus	MPa , N/mm ²
E_{SB}	Subbase elastic modulus	MPa , N/mm ²
E_{GG}	Subgrade elastic modulus	MPa , N/mm ²
h_1, h_2	Asphalt wearing course, base course thickness	mm
μ_1, μ_2	Asphalt Poisson's ratio	-
μ_2	Asphalt Poisson's ratio	-

Symbols in Chapter 5: Engineered Cementitious Composite (ECC) material for Precast Ultra-Thin Whitetopping (PUTW)

<i>Symbol</i>	<i>Explanation</i>	<i>unit</i>
M	Bending moment at the middle span	Nmm
b	Coupon's width	mm
h	Coupon's thickness	mm
ε	Strain	mm/mm
σ	Stress	MPa , N/mm ²

Symbols in Chapter 6: Interface bonding in Precast Ultra-Thin Whitetopping (PUTW)

<i>Symbol</i>	<i>Explanation</i>	<i>unit</i>
Q	Load	N
p	Distributed load (contact pressure)	MPa , N/mm ²
a	Load radius	mm
E_1	ECC elastic modulus	MPa , N/mm ²
E_2	Asphalt elastic modulus	MPa , N/mm ²
E_{GG}	Graded granite elastic modulus	MPa , N/mm ²
E_{SB}	Subbase elastic modulus	MPa , N/mm ²
E_{GG}	Subgrade elastic modulus	MPa , N/mm ²
h_1, h_{ECC}	ECC thickness	mm
h_{grout}	Grout thickness	mm
h_{GG}	Graded granite thickness	mm
h_{SB}	Subbase thickness	mm
h_{GG}	Subgrade thickness	mm
h_2	Asphalt thickness	mm
μ_1	ECC Poisson's ratio	-
μ_2	Asphalt Poisson's ratio	-

τ_{xz}, τ_{zx}	Shear stress	MPa , N/mm ²
$S_y(z)$	First moment of area (Static moment)	mm ³
$q(x)$	Transversal force	N
I_y	Moment of inertia	mm ⁴
κ	Asphalt elastic modulus : ECC elastic modulus	-
β	Asphalt thickness : ECC thickness	-
e_0	Position of neutral axis	mm
z	Position of interface	mm
z_c	Distance from center of calculated area to neutral axis	mm
F	Calculated area	mm ²
$T(\kappa, \beta)$	Shear flow	N/mm
V	Load distributed factor	-
ν	Poisson's ratio	-
μ	shear stiffness	MPa , N/mm ²
u, v, w	displacement in x -, y -, and z - directions	mm
S	magnitude of the braking load	N

Symbols in Chapter 7: Design of Precast Ultra-Thin Whitetopping (PUTW)

<i>Symbol</i>	<i>Explanation</i>	<i>unit</i>
Q	Load applied on the slab	N
p	Distributed load (contact pressure)	MPa , N/mm ²
a	Radius of load distribution area	mm
b	Equivalent radius	mm
h^*, h_I, h_{II}	Equivalent composite thickness	mm
h_1, h_2	Pavement slab, asphalt thickness	mm
E_1, E_2, E_u	Pavement slab, asphalt, support layer's equivalent elastic modulus	MPa , N/mm ²
k	Subgrade modulus	MPa , N/mm ²
$\sigma_{QM}, \sigma_{QR}, \sigma_{QE}$	Stresses at slab center, slab edge, slab corner	MPa , N/mm ²
σ_{r1}, σ_{r2}	Bending tensile stress in layer 1 and 2	MPa , N/mm ²
$\sigma_{r1u}, \sigma_{r2u}$	Bending tensile stress at the bottom of layer 1 and 2	MPa , N/mm ²
$\sigma_{r1o}, \sigma_{r2o}$	Bending tensile stress at the top of layer 1 and 2	MPa , N/mm ²
L_I, L_{II}	Elastic length	mm

A. Appendix

A. 1. Summary of skid resistance measurement and improvement methods

Summary of Skid resistance measurement methods

Testing Method	In lab	In situ	Advantages	Disadvantages	Type / Results	Associated Code	Illustration
Micro Texture							
<ul style="list-style-type: none"> British Pendulum Tester This test method utilizes a measurement representing the steady-state friction force on a locked test wheel as it is dragged over a wetted pavement surface under constant load and at a constant speed while its major plane is parallel to its direction of motion and perpendicular to the pavement. 	√	√	<ul style="list-style-type: none"> The BPT is used worldwide. The BPT can be used to measure both longitudinal and lateral friction. 	<ul style="list-style-type: none"> BPN variability is large and can be affected by operator procedures and wind effects. Traffic control is required It does not always simulate pavement-tire characteristics. 	Locked wheel test / BPN, Skid Resistance Value (SRV)	ASTM E 303	 <p>Source: Munro Group</p>
<ul style="list-style-type: none"> Dynamic Friction Tester This test method provides a measure of surface friction as a function of sliding speed. This test method may be used to determine the relative effects of various polishing techniques on materials or material combinations. (E17 Committee 2009a) 	√	√	The DFT provides good repeatability and reproducibility and is unaffected by operators or wind. It also provides friction coefficients that are representative of high-speed values.	<ul style="list-style-type: none"> Traffic control is required It does not always simulate pavement-tire characteristics. 	Slider / DFT numbers. This device also reports the peak friction, IFI, designated by F(60) and SP.	ASTM E 1911	 <p>Source: Google image</p>

Testing Method	In lab	In situ	Advantages	Disadvantages	Type / Results	Associated Code	Illustration
<p>▪ California Portable Skid Tester</p> <p>A test with towed trailer skid testers that provide skid numbers. They are obtained with a locked wheel. Friction is reduced to a low uniform value with three roller bearings fitted at 120° points to bear against the guide rod at each corner of the carriage.</p>		√	<ul style="list-style-type: none"> • Relatively easy to use • Low cost of operation and maintenance 	<ul style="list-style-type: none"> • Traffic control is required • Less accuracy for testing in temperature less than 40°F due to the glycerin will become viscose and yield. 	Locked Wheel Test / μ , Skid Number (SN)	CTM 342	 <p>Source: Hall et al., (2009)</p>
<p>▪ SCRIM (Sideway Force Coefficient Routine Investigation Machine)</p> <p>The normal testing speed for the machine is 50km/h and skidding resistance values for the nearside wheel track only.</p> <p>The principle of the machine is that a test wheel, mounted mid-machine in line with the nearside wheel track and angled at 20° to the direction of travel, and is applied to the road surface under a known load.</p>		√	<ul style="list-style-type: none"> • Ability for continuous friction measurement throughout a test section • Commonly used in UK 	<ul style="list-style-type: none"> • Less traffic control is required 	Side Force Test / side-force coefficient (SFC)	Road Research Laboratory Road Note 27	 <p>Source: Hall et al., (2009)</p>

Testing Method	In lab	In situ	Advantages	Disadvantages	Type / Results	Associated Code	Illustration
Macro Texture							
<ul style="list-style-type: none"> Circular Texture Meter The Circular Texture Meter (CT Meter), also known as the Circular Track Meter uses a charge coupled device (CCD) laser-displacement sensor to measure the vertical profile of a pavement surface. 	√	√	<ul style="list-style-type: none"> Repeatable, reproducible, and independent of operators Correlates well with MTD. Measures positive and negative texture. Is small (29 lb [13 kg]) and portable. Setup time is short (less than 1 minute) 	<ul style="list-style-type: none"> The method is slow (about 45 seconds to complete) and requires lane closure. Represents a small surface area. 	Mean Profile Depth (MPD) and Root Mean Square (RMS) statistics that characterize profile macrotexture.	ASTM E 2157	 <p>Source: Hanson & Prowell</p>
<ul style="list-style-type: none"> Sand Patch (Texture Depth) This volumetric-based spot test method provides the mean depth of pavement surface macrotexture. The operator spreads a known volume of glass beads in a circle onto a cleaned surface and determines the diameter and subsequently mean texture depth (MTD). 		√	<ul style="list-style-type: none"> Simple and inexpensive methods and equipment. When combined with other data, can provide friction information. Widely used method. 	<ul style="list-style-type: none"> Method is slow and requires lane closure. Only represents a small area. Only macrotexture is evaluated. Sensitive to operator variability. (Poor repeatability) Labor intensive activity. 	Mean texture depth (MTD)	ASTM E 965 / ISO 10844	 <p>Source: Google image</p>

Testing Method	In lab	In situ	Advantages	Disadvantages	Type / Results	Associated Code	Illustration
<p>▪ Outflow Meter</p> <p>This test method is suitable as a field test to evaluate the surface drainage, and in some cases, the internal drainage of the surface course of a pavement. When used with other tests, the outflow time may be used to evaluate the texture produced by an asphalt concrete mix, a finishing method used on Portland cement concrete pavement, and refinishing operations on an old pavement surface.</p>		√	<ul style="list-style-type: none"> • Simple methods and relatively inexpensive equipment. • Provides an indication of hydroplaning potential in wet weather. • Test can be conducted when pavement is wet 	<ul style="list-style-type: none"> • Method is slow and requires lane closure. • Only represents a small area of the pavement surface. • For very rough textures, a large quantity of water is required. 	Outflow time (OFT) is the time in milliseconds for outflow of specified volume of water.	ASTM E 2380	 <p>Source: Google image</p>
<p>▪ Grip Tester</p> <p>The Grip Tester is a fixed slip device. The test wheel rotates with a constant slip, i.e., the wheel is lightly braked to provide a difference in velocity between the test wheel and the speed of the tester. The slip ratio is usually between 10 and 20 percent.</p>		√	<ul style="list-style-type: none"> • Commonly used in Europe, UK and New Zealand • Operating and maintenance costs are low 	<ul style="list-style-type: none"> • requires lane closure • The reproducibility of the GripTester was not as good as that of SCRIM. 	Fixed Slip Device / Grip Number	ASTM E 1844	 <p>Source: Hall et al., (2009)</p>

Testing Method	In lab	In situ	Advantages	Disadvantages	Type / Results	Associated Code	Illustration
<ul style="list-style-type: none"> ▪ Electro-optic method (EOM) (laser) Non-contact very high-speed lasers are used to collect pavement surface elevations at intervals of 0.01 in (0.25 mm) or less. This type of system, therefore, is capable of measuring pavement surface macrotexture (0.5 to 50 mm) profiles and indices. 	√	√	<ul style="list-style-type: none"> • Collects continuous data at high speeds. • Correlates well with MTD. • Can be used to provide a speed constant to accompany friction data. 	<ul style="list-style-type: none"> • Equipment is very expensive. • Skilled operators are required for collection and data processing. 	Mean Profile Depth	ASTM E 1845 ISO 13473-1 ISO 13473-2 ISO 13473-3	 <p>Source: Hall et al., (2009)</p>
Mega Texture							
<ul style="list-style-type: none"> ▪ Response Type Devices Response type devices were the first type of device used to measure road roughness. These types of devices almost always consist of an instrument installed in a vehicle or trailer to record the up-and-down movement of the suspension (called the suspension stroke). 		√	<ul style="list-style-type: none"> • Response type devices have been used in many parts of the world for many years. • Relatively inexpensive. 	<ul style="list-style-type: none"> • The precision and repeatability is low • In response type devices, the transformation of the road profile to an IRI value is completely dependent on the properties of the vehicle suspension system. • Require calibration at least on an periodical basis. 	International Roughness Index (IRI) [m/km]	ASTM E1926 - 08	 <p>Source: COTO, 2007</p>

Testing Method	In lab	In situ	Advantages	Disadvantages	Type / Results	Associated Code	Illustration
<p>▪ High-Speed Profiling Devices</p> <p>High-speed profiling devices are capable of measuring a precision profile of one or more wheel paths while moving at speeds more than 100 km/h. This device equipped with height sensor (transducer), accelerometer and distance sensor.</p>		√	<ul style="list-style-type: none"> • Capable of measuring the surface profile very precisely. • Capable of measuring the longitudinal and transverse profile at the same time, thereby providing a roughness and rutting assessment simultaneously. • A high-resolution video of the pavement surface. 	<ul style="list-style-type: none"> • Inertial profiling devices using laser height sensors are not successful for profiling gravel roads. • Relatively expensive • Extensive validation testing and control procedures are still needed to ensure that the measured profile is accurate. 	International Roughness Index (IRI) [m/km]	ASTM E1926 - 08	 <p>Source: (COTO, 2007)</p>
<p>▪ Static or Slow Moving Devices (ARRB Walking Profiler)</p> <p>The ARRB Walking Profiler was developed by the Australian Road Research Board Ltd. and is roughly the size of a lawnmower. A built-in data acquisition system captures and stores profile data while measurements take place.</p>		√	<ul style="list-style-type: none"> • Equipment is very cheap • Easy to use • The ARRB Walking Profiler outputs include distance, grade and IRI. • High accuracy (The profile accuracy is $\pm 1,0$ mm/50 m and the IRI accuracy is $\pm 0,1$ m/km). 	<ul style="list-style-type: none"> • Low speed of measurement. It performed at walking pace or roughly 800 meters per hour, with a practical production rate of approximately 4 km per day. 	International Roughness Index (IRI) [m/km]	ASTM E1926 - 08	 <p>(Source: ARRB Group)</p>

Methods to improving skid resistance of concrete pavement surface (Hall, et al., 2009)

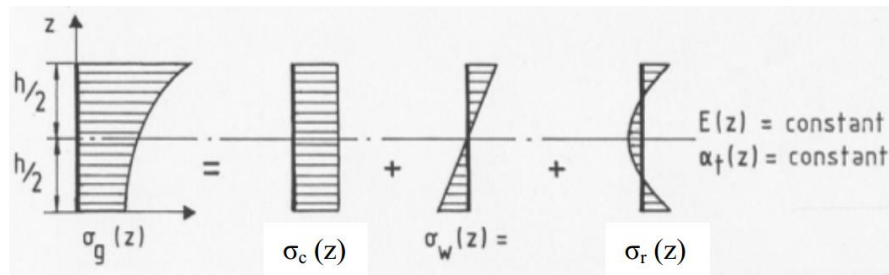
Application	Mix/Texture Type	Description
New PCC or PCC Overlay	Broom Drag (longitudinal or transverse)	A long-bristled broom is mechanically or manually dragged over the concrete surface in either the longitudinal or transverse direction. Texture properties are controlled by adjusting the broom angle, bristle properties (length, strength, density), and delay behind the paver. Uniform striations approximately 1.5 to 3.0 mm deep are produced by this method.
	Artificial Turf Drag (longitudinal)	An inverted section of artificial turf is dragged longitudinally over a concrete surface following placement. Texture properties are controlled by raising/lowering the support boom, adding weight to the turf, and delaying application to allow surface hardening. This method produces uniform 1.5 to 3.0 mm deep surface striations. Typically ranges from 0.2 to 0.4 mm, but a deep texture (min depth of 1.0 mm) has been specified.
	Burlap Drag (longitudinal)	One or two layers of moistened coarse burlap sheeting are dragged over the concrete surface following placement. Texture properties are controlled by raising/lowering the support boom and adjusting the delay following concrete placement. Typically ranges from 0.2 to 0.4 mm
	Longitudinal Tine	A mechanical assembly drags a wire comb of tines (~127 mm long and 3 m wide) behind the paver (and usually following a burlap or turf drag). Texture properties are controlled by the tine angle, tine length, tine spacing, and delay for surface curing. Grooves from 3 to 6 mm deep and 3 mm wide are produced by this method, typically spaced at 19 mm. Typically ranges from 0.4 to 1.0 mm.
	Transverse Tine	Accomplished using methods similar to longitudinal tining, however, the mechanical assembly drags the wire comb perpendicular to the paving direction. Variations include skewing the tines 9 to 14° from perpendicular and using random or uniform tine spacing from 12 to 38 mm. Ranges from 0.4 to 1.0 mm.
	Diamond Grinding (longitudinal)	A self-propelled grinding machine with a grinding head of gang-mounted diamond sawing blades removes 3 to 19 mm of cured concrete surface, leaving a corduroy type surface. Blades are typically 2 to 4 mm wide and spaced 4.5 to 6 mm apart, leaving 2 to 4 mm high ridges. This method is most commonly used to restore surface characteristics of existing pavements. Typically ranges from 0.7 to 1.2 mm.
	Porous PCC	Gap-graded, small-diameter aggregate are combined with cement, polymers, and water to form a drainable surface layer (typically 200 mm thick). That surface layer is bonded to the underlying wet or dry dense concrete layer.
	Exposed Aggregate PCC	A set retarder is applied to the wet concrete surface and the surface is protected for curing. After 12 to 24 hours, the unset mortar is removed to a depth of 1 to 2 mm using a power broom. Typically exceeds 0.9 mm.
Friction Restoration of Existing PCC Pavement	HMA Overlay	See HMA surface mixes above.
	TyreGrip	TyreGrip® is a resurfacing system that consists of a two part epoxy resin top dressed with calcined bauxite aggregate. The aggregate is fractured 100 percent and is approximately No. 10 (2 mm) size material.
	White topping, Thin White Topping (TWT) and	According to (Rasmussen et al., 2004), white topping is a PCC layer constructed atop an existing HMA pavement structure. White topping differs from other concrete overlay types, which include bonded and unbounded concrete layer.

	Ultra white topping (UTW)	<ul style="list-style-type: none"> • Conventional whitetopping—a concrete overlay of 200 mm or more, designed and constructed without consideration of a bond between the concrete and underlying HMA. • TWT—an overlay of greater than 100 mm and less than 200 mm in thickness. • UTW—with a thickness equal to or less than 100 mm (4 in.), this overlay requires a bond to the underlying HMA to perform well.
Retexturing of Existing PCC Pavement	Diamond Grinding (longitudinal)	See diamond grinding above.
	Longitudinal Diamond Grooving	A self-propelled grooving machine saws longitudinal groove in the road surface about 3 to 6 mm deep and spaced 13 to 38 mm apart. This method adds macrotexture for drainage but relies on the original surface for microtexture. Typically ranges from 0.9 to 1.4 mm.
	Transverse Diamond Grooving	Completed in a manner similar to longitudinal diamond grooving, except the grooves are sawn transverse to the travel direction. Typically ranges from 0.9 to 1.4 mm.
	Shot Abrading	An automated machine hurls recycled round steel abrasive material at the pavement surface, abrading the surface and/or removing the mortar and sand particles surrounding the coarse aggregate to a depth of up to 6 mm. Texture properties are controlled by adjusting the steel abrasive material velocity and approach angle and by modifying the forward equipment speed. Typically ranges from 0.6 to 1.2 mm.

A. 2. Calculation of environment-induced stress in PUTW

1. Warping stress

Warping stress is bending tensile stress caused by slab warping due to heating on top of the slab (positive temperature gradient). In a full restraint slab (infinite or big enough slab), all the temperature changes along the cross section (depth (z)) cause respective stresses. Stress distribution can be separated into constant σ_c , linear σ_w and residual σ_r stresses (Lechner & Freudenstein, 2010)



Stress distribution in a fully restraint infinite slab (Lechner & Freudenstein, 2010)

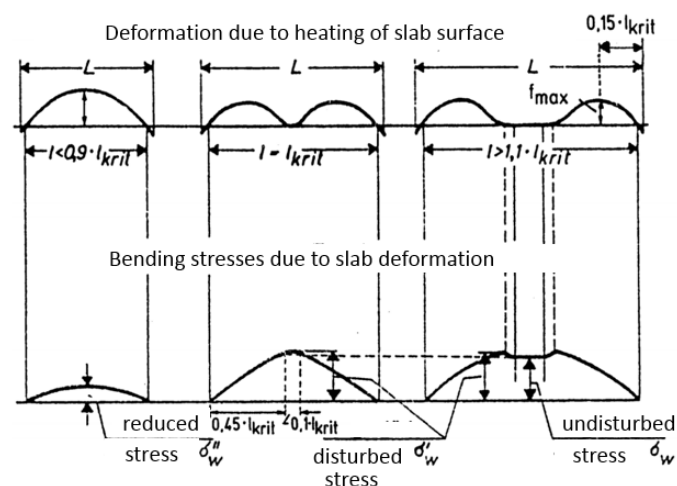
Changes within the constant part causes changes of slab-length or constant stress σ_c respectively due to obstructions by friction at the bottom interface or closing of joints during summer time. The linear temperature gradient Δt causes slab bending and warping stress σ_w which are dependence on the slab dimensions and the support conditions. The residual stresses σ_r , caused by the non-linear part of the temperature distribution, does not translate into deformations even by complete release of restraints (Lechner & Freudenstein, 2010).

The undisturbed warping stresses on a sufficiently large slab can be calculated using equation 0-1 proposed by (Eisenmann & Leykauf, 2003) as follows:

$$\sigma_w = \frac{1}{1-\mu} \cdot \frac{h \cdot \Delta t}{2} \cdot \alpha \cdot E \quad 0-1$$

The stress is reduced when slab length $L < 0.9 \cdot L_{crit}$ according to (Eisenmann & Leykauf, 2003)

$$\sigma_w'' = \left(\frac{L - \frac{2}{3} a'}{0,9 \cdot L_{crit}} \right)^2 \cdot \sigma_w \quad 0-2$$



Deformation and bending stresses due to heating of slab surface (Lechner & Freudenstein, 2010)

Determination of L_{crit} using Δt and self-weight g (Eid, 2012):

According to (Eisenmann, 1965) the deformation in the middle of the slab by a temperature gradient Δt :

$$w_{\Delta t} = \frac{1}{8} \cdot l^2 \cdot \alpha_t \cdot \Delta t \quad 0-3$$

The deformation in the middle of the slab by slab self-weight (Márkus & Otto, 1978)

$$w_g = \frac{g \cdot \left(\frac{l}{2}\right)^4}{64 \cdot K} \cdot \left(\frac{5 + \mu}{1 + \mu}\right) \quad 0-4$$

With the slab stiffness (Altenbach, et al., 1998)

$$K = \frac{E \cdot I}{(1 - \mu^2)} \quad 0-5$$

The critical length of a circular plate is obtained by (Eisenmann, 1965) by equating the deformations:

$$w_{\Delta t} = w_g \quad 0-6$$

$$L_{crit} = \sqrt{\frac{128 \cdot \alpha_t \cdot \Delta t \cdot E \cdot I}{g \cdot (5 + \mu) \cdot (1 - \mu)}} \quad 0-7$$

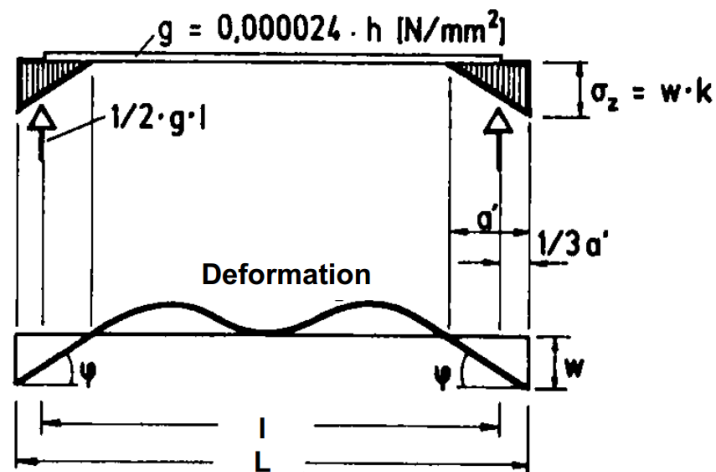
For square slab:

$$l_{qP} = \frac{1}{\sqrt{2}} \cdot l_o \quad 0-8$$

The critical length for square slab:

$$L_{crit_qP} = \sqrt{\frac{64 \cdot \alpha_t \cdot \Delta t \cdot E \cdot I}{g \cdot (5 + \mu) \cdot (1 - \mu)}} \quad 0-9$$

Determination of effective slab span (length) l ; assuming $L = L_{crit}$ (Eid, 2012) (Lechner & Freudenstein, 2010):



Calculation of effective slab span

Where:

- σ_z = vertical pressure [N/mm²]
- w = vertical deflection [mm]
- k = bedding modulus [N/mm³]
- a' = length of flexible support along slab edge [mm]
- L_{crit} = critical slab length assuming rigid support along slab edges
- $l = L - 2/3a'$ = reduced slab length assuming flexible support along slab edges

The vertical deflection w at the edge can be described:

$$w = a' \cdot \varphi \quad 0-10$$

According to (Eisenmann & Leykauf, 2003):

$$\frac{g \cdot l}{2} = a' \cdot \frac{w}{2} \cdot k \quad 0-11$$

From equations 0-10 and 0-11 we obtain a' as follows:

$$a' = \sqrt{\frac{g \cdot l}{\varphi \cdot k}} \quad 0-12$$

The rotation φ caused by temperature gradient and self-weight can be determined at the supports. The curvature caused by temperature Δt is constant. The angle φ is obtained as the integral of the curvature. Since the rotation in the center of the slab is equal to zero, the angle at the edge is:

$$\varphi_{\Delta t}(0) = 0,5 \cdot l \cdot \alpha_t \cdot \Delta t \quad 0-13$$

The opposite rotation caused by self-weight is given by the derivative of the bending line of the beam:

$$\varphi_g(x) = w'(x) = \frac{g}{24 \cdot E \cdot I} (4 \cdot x^3 - 6 \cdot l \cdot x^2 + l^3) \quad 0-14$$

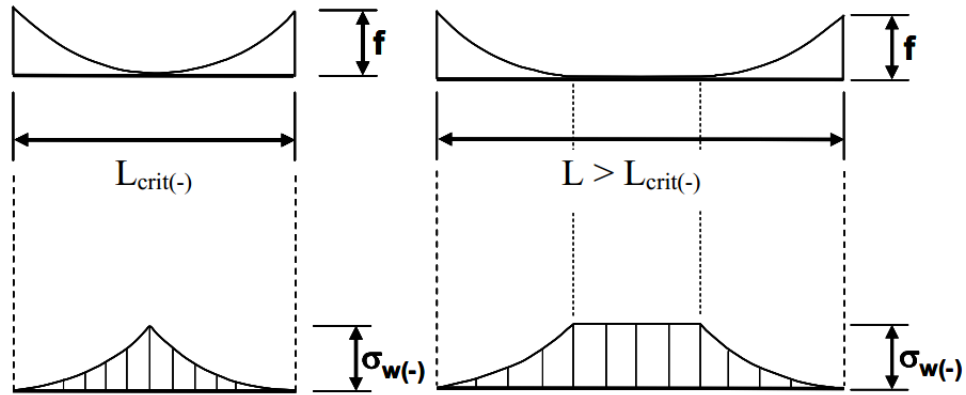
At support ($x = 0$), the rotation due to the dead weight is obtained:

$$\varphi_g(0) = \frac{g \cdot l^3}{24 \cdot E \cdot I} \quad 0-15$$

Based on (Eisenmann & Leykauf, 2003), the resulting rotation at the supports is then:

$$\varphi = \varphi_{\Delta t} - \varphi_g = 0,5 \cdot l \cdot \alpha_t \cdot \Delta t - \frac{g \cdot l^3}{24 \cdot E \cdot I} \quad 0-16$$

2. Curling stress



Calculation of curling stress

According to (Lechner & Freudenstein, 2010), the curling stress on a sufficiently large slab $L \geq L_{crit(-)}$ can be calculated using equation 0-17 as follows:

$$\sigma_{w(-)} = \frac{1}{1 - \mu} \cdot \frac{h \cdot \Delta t}{2} \cdot \alpha \cdot E \quad 0-17$$

The critical length of the circular slab $L_{crit(-)}$ can be calculated based on the equating of moments:

$$M_{\Delta t} = M_g \quad 0-18$$

According to (Lechner & Freudenstein, 2010), the curling moment of a fully movement constrain slab is:

$$M_{\Delta T} = \frac{1}{1 - \mu} \cdot \alpha_t \cdot \Delta t \cdot E \cdot I \quad 0-19$$

And the self-weight moment is:

$$M_g = \frac{g \cdot l^2}{8} \quad 0-20$$

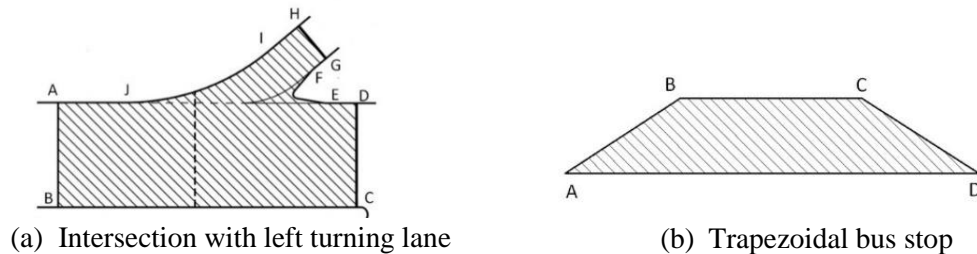
Therefore, $L_{crit(-)}$ is determined based on equations 0-18, 0-19, and 0-20:

$$L_{crit(-)} = \sqrt{\frac{8 \cdot \alpha_t \cdot \Delta t \cdot E \cdot I}{g \cdot (1 - \mu)}} \quad 0-21$$

A. 3. PUTW3D - User manual

1. PUTW3D input parameters

Essential input for PUTW3D are the geometry of the construction area and other additional points (e.g. water collecting inlet points). The figure below illustrates examples for site geometry at intersection and bus stop. Detailed input parameters for PUTW3D are listed in the following



Site geometry at intersection and bus stop

Input for calculation of PUTW slabs in PUTW3D

Input parameter		Specific points/parameters	Input method
Site geometry	Intersection leg (no left turning) or Bus top	A, B, C, D	Manual or from text file
	Intersection leg (with left turning)	A, B, C, D, E, F, G, H, J	
Water collection inlet / additional points	Other points needed	W1, W2, W3, W4, W5	
Curve radius	Only for left turning lane	r	
Number of lanes	Lane number including widened left-turning lane	n	
Slab type	Rectangle, Hexagon or combination		Select suitable option
Slab size	Optimal size generated by the program or user input can be defined	Length and width	

2. PUTW3D output

The output of PUTW3D is the summary of required slabs that includes the number of full size slabs, and other size slabs as well as slab arrangement and their coordination as in Figure 9-2.

Definitions of slab size

Size	Percentage of full size slab	Note
Full size	100%	
Almost full	80%-100%	
Partial	10%-80%	
Slab on curve		in left turning curve
Half size	50%	in the case of hexagon slabs
The rest spaces	< 10%	to be filled with additional filling matter

3. Tool execution

- Run *MCRInstaller.exe* file to establish the program running environment;
- Run *PUTW3D.exe*;

4. Detail steps

- Select one site geometry among 4 options from the user interface;
- Input the site boundary manually or through a text file;
- Input water collector inlet / additional points, the check button help to evaluate the plausibility of these additional input by limit the inclination of each point to others not exceeding 5% and also to ensure there is no same point having different coordinates;
- Plot the site with all points and boundary, z-coordinate will be shown in the plot;
- Select the slab type: rectangle, hexagon or combination;
- Confirm the slab type to generate the most suitable slab size;
- Select the slab size, in which slabs can be arranged longitudinally or transversally to driving direction (in case of having rectangle slabs);
- After calculation, the number of slabs will be shown in the right panel as well as small modification of construction site to accommodate as most full size slabs as possible.

5. Working with AutoCAD

- The output data will be stored in *PUTW3D_coordinate.txt* file, which will be used for generating a technical drawing in AutoCAD;
- Open AutoCAD → run “*apload*” command → load “*PUTW3D*” script;
- Change to 3D view → run “*PUTW3D*” command and browse to the text file for the drawing.

This following figure is showing detail steps when using PUTW3D tool.



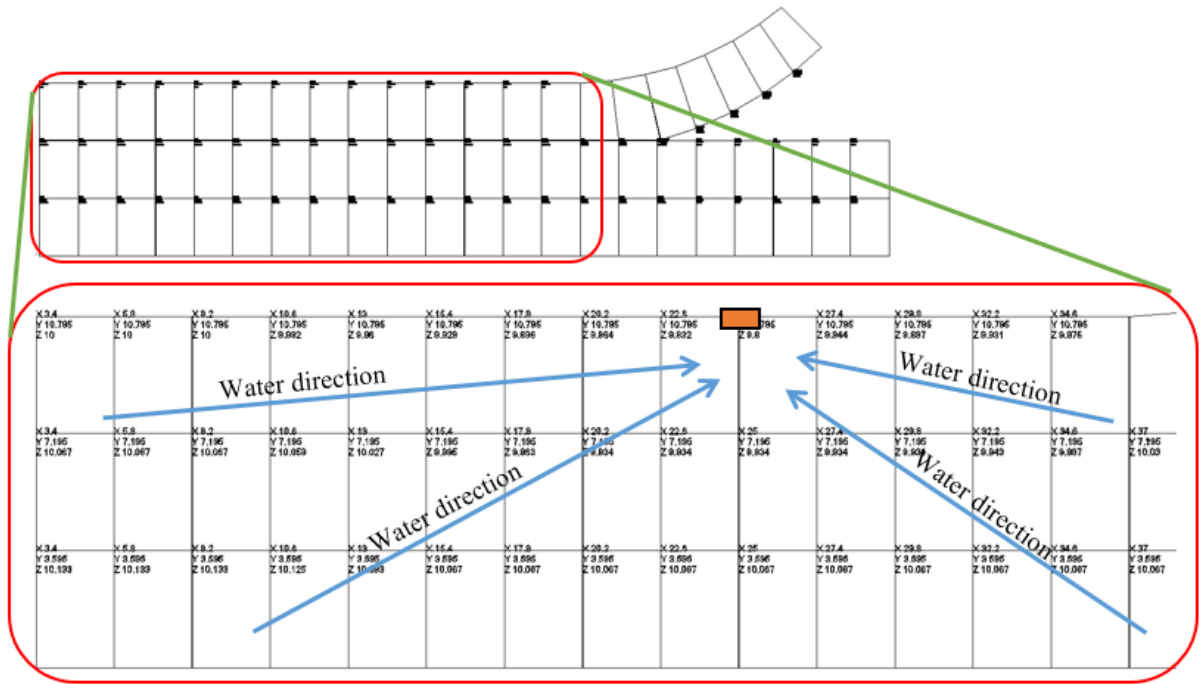
Example: Calculation of PUTW slabs for an intersection with widened left-turning lane (3 lanes, 10.8 m width, 52 m length) with boundary co-ordinates of construction site stored in text file; additional points are collected later then input manually. Details are showing as below table:

Input	Site geometry (input from text file)	
	Additional points (manually input)	W1 (10, 10.8, 10), W2 (10, 0, 10.2), W3 (45, 0, 10.2), W4 (36, 10.8, 10), W5 (25, 10.8, 9.8)

The slab layout is calculated based on the slab type and size, therefore different selection results in various output as following table. The slab size generated by PUTW3D is the optimized option.

Output	Slab type and size	PUTW slab number		Slabs arrangement
		Full size	Total	
Rectangle (2.4m x 3.6m)		Full size	58	
		Slabs on curve	7	
		Total	65	
Hexagon (2.4m by self-input)		Full size	105	
		Almost full	2	
		Partial	14	
		Half size	29	
		Total	190	
Combination (2.4m x 3.6m)		Full size	58+10	
		Almost full	5	
		Partial	12	
		Half size	2	
		Slabs on curve	32	
		Total	87	

The technical drawing in AutoCAD has clearly shows all co-ordinates of installed PUTW slabs, which take into account additional points. From this example, the water collector inlet (lower z co-ordinate) can be illustrated together with water direction from other areas as following figure.



Example of joint layout and slabs' coordination in PUTW3D